NUCLEAR ENERGY LEVELS OF ^{31}S AND ^{33}Cl

Thesis by

Calvin Elroy Moss

In Partial Fulfillment of the Requirements

For the Degree of

Doctor of Philosophy

California Institute of Technology

Pasadena, California

1968

(Submitted December 6, 1967)

Acknowledgments

Abstract

The reaction $^{32}S(^{3}He, \alpha)^{31}S$ has been used to locate 42 levels in ^{31}S. For 11 of the first 17 levels ℓ_n-values have been determined. The first 6 excited states of ^{31}S have been studied by applying the particle-gamma correlation method of Litherland and Ferguson (their Method II) to the reaction $^{32}S(^{3}He, \alpha\gamma)^{31}S$. The resulting spins and parities are: E_x, J^{π} = 1.25 MeV, $3/2^+$; 2.23 MeV, $5/2^+$; 3.08 MeV, $1/2^+$; 3.29 MeV, $5/2^+$, $3/2^+$; 3.35 MeV, $7/2$, $3/2$; 3.44 MeV, $3/2^+$. Mixing and branching ratios have also been determined. The ground state Q-value for the reaction $^{32}S(^{3}He, \alpha)^{31}S$ has been measured to be 5.538 ± 0.006 MeV. Analysis of the spectra of the reaction $^{32}S(^{3}He, d)^{33}Cl$ which were obtained as a by-product of the spectra of the reaction $^{32}S(^{3}He, \alpha)^{31}S$ located levels in ^{33}Cl at the following excitation energies: 0, 810 ± 9, (1978 ± 14), 2351 ± 9, 2686 ± 8, 2848 ± 9 (a known doublet), 2980 ± 9, and 4119 ± 10 keV. The 2.0 MeV level was only weakly populated, and to confirm its existence the reaction $^{36}Ar(p, \alpha)^{33}Cl$ has been studied. In this reaction the 2.0 MeV level was strongly populated and the measured excitation energy was 1999 ± 20 keV. The experimental results for ^{31}S and ^{33}Cl are compared with their analogs and with nuclear model predictions.

TABLE OF CONTENTS

I. INTRODUCTION

A. Justification for This Experiment

Relative to the nuclei with $A \leq 28$ there has been little work reported on the nuclei with $28 < A \leq 40$. The nuclear models, some of which are discussed in Section IV. B., have in general not been very successful in describing the observed properties of these nuclei. Probably the main reason for this is that the models are too simple. With the computers now available it appears feasible to study more realistic models. In particular, a generalization of the shell model calculation of Glaudemans et al. (1964) seems promising. More experimental information is needed so that the parameters in the theories can be determined and the predictions can be checked. The nucleus ^{31}S was chosen for study in the present experiment because it was the lightest nucleus in this mass region which could be studied with the CIT-ONR tandem accelerator and for which there was little experimental information (see below). The primary objective was to study ^{31}S, but fragmentary information about ^{33}Cl was also obtained.

The information on ^{31}P and ^{31}S available at the start of present investigation was essentially that contained in the compilation by Endt and van der Leun (1962) and is summarized in Figure 1. The shell model calculation by Glaudemans et al.(1964) predicted a low-lying $1/2^+$ level and a $7/2^+$ level, neither of which had been identified (see Figure 2). An earlier Nilsson model calculation by Broude et al.(1958) also predicted these two levels.

The information on ^{33}S and ^{33}Cl available at the start of the present investigation was also essentially the same as that contained in the compilation by Endt and van der Leun (1962) and is summarized in Figure 3. On the basis of the level scheme shown here for ^{33}S, two unreported levels were expected at an excitation energy of 3 MeV in ^{33}Cl. The shell model calculation by Glaudemans et al.(1964) predicted the levels shown in Figure 4.

B. Outline of Present Experiment

The present experiment may be divided into seven parts as follows:

1) The ground state Q-value of the reaction ^{32}S(^{3}He, α)^{31}S was measured. This work is described in Section II. A., pages 4 through 13 .

2) Alpha particle spectra from the reaction ^{32}S(^{3}He, α)^{31}S were measured to locate levels in ^{31}S below 7.8 MeV excitation energy. This work is described in Section II. B., pages 13 through 23 .

3) Angular distributions of the alpha particles from the reaction ^{32}S(^{3}He, α)^{31}S were measured for 14 of the first 21 levels in ^{31}S and compared with DWBA distributions to determine ℓ_n-values. This work is described in Section II. C., pages 23 through 31 .

4) Angular correlations for the first six excited states populated in the reaction ^{32}S(^{3}He, $\alpha\gamma$)^{31}S were measured to determine the spins of these states. This work is

described in Section III, pages 32 through 60 .

5) Deuteron spectra from the reaction $^{32}S(^3He, d)^{33}Cl$
which were obtained as a by-product of the alpha particle
spectra from the reaction $^{32}S(^3He, \alpha)^{31}S$ were analyzed
to locate levels in ^{33}Cl below 4.2 MeV excitation energy.
This work is described in Section V.A., pages 69
through 78 .

6) Angular distributions of the deuterons from the reaction
$^{32}S(^3He, d)^{33}Cl$ were analyzed for three of the levels in
^{33}Cl and compared with DWBA distributions to determine
ℓ_p-values. This work is described in Section V.B.,
pages 78 through 81 .

7) Alpha particle spectra from the reaction $^{36}Ar(p, \alpha)^{33}Cl$
were measured to confirm the existence of a level in
^{33}Cl near 2.0 MeV which was only weakly populated in the
reaction $^{32}S(^3He, d)^{33}Cl$. This work is described in
Section VI, pages 82 through 85 .

II. $^{32}S(^3He, \alpha)^{31}S$

A. Mass of ^{31}S

1. Introduction

The 1964 Mass Table of Mattauch et al.(1965) gives
-18992 ± 11 keV for the mass excess of ^{31}S. When we discovered
that the mass excess calculated from the ground state Q-value for
the reaction $^{32}S(^3He, \alpha)^{31}S$ derived from our spectra described in
II. B. lay well outside of the 11 keV error quoted here, a careful
measurement of this Q-value was made with the 61-cm magnetic
spectrometer. This instrument has been described by Groce (1963)
and McNally (1966), and this thesis assumes familarity with either
of these theses or the operation of the spectrometer.

2. Targets

A thin target was used to check for possible contributions
from other $(^3He, \alpha)$ reactions near the peak from $^{32}S(^3He, \alpha)^{31}S$
(G. S.), and a spectrum is shown in Figure 5(a). This target was
made by evaporating ZnS containing natural sulfur from a tantalum
boat onto tungsten of 0.178 mm thickness which had been carefully
cleaned with a solution recommended by Misch and Ruther (1953)
consisting of one part by volume of concentrated HF and three parts
of concentrated HNO_3, and then thoroughly rinsed with distilled
water.

A thick target was made in a similar manner, and a
spectrum is shown in Figure 5(b). The backing in this case was
0.254 mm thick.

No deterioration of this kind of target was observed provided the beam was kept below 0.3 μA on a .5 mm^2 area. No evidence was observed for (^{3}He, α) reactions with the zinc isotopes at $E_{3_{He}}$ = 8.5 MeV.

For both the thin target spectrum and the thick target spectrum the 61-cm spectrometer was placed at 150° to the incident beam. The normal to the target bisected the angle between the incoming beam and the spectrometer. The thin target spectrum shows no interference from other groups. The thick target spectrum has been used to compute Q, since the analysis of a thick target spectrum (after the method of Bardin, 1961) is not subject to errors introduced by an uncertain target thickness.

3. Spectra Collection Details

The thin target spectrum was obtained with the 16-detector array with a 3.18 mm (FW perpendicular to the mean orbit) slit in front of each detector which accepted a momentum interval $\Delta p = p/720$. No foil was placed in front of the detectors. Details of the operation of the array are discussed in Appendix F. Two slightly different settings of the magnetic field of the spectrometer were made in such a way that alternate points shown in Figure 5(a) correspond to the same field setting. An electron suppressor upstream from the target was placed at -300 volts, and the target and beam catcher were placed at +300 volts relative to the chamber walls. These voltages were used for all of the spectra described below. The spectrometer angular acceptance was 1.50° (FW) in the θ direction and 11.6° (FW) in the ϕ direction. The slits in front of the target chamber were 2.03 mm (FW) in both the vertical

direction and the horizontal direction. The widths of the image slit and the object slit of the beam analyzing magnet were both 3.81 mm (FW).

The thick target spectrum was obtained with a single surface barrier detector in the focal plane of the spectrometer. A slit 0.794 mm (FW) was placed in front of the detector ($\Delta p/p$ = 1/2800), and again no detector foil was used. A block diagram of the electronics is shown in Figure 6. The window of the single channel analyzer was set so that only the alpha particles were counted (deuterons and protons were also present), and the RIDL 400-channel analyzer was used as a monitor. The spectrometer current was cycled from 0 to 700 amperes to 0 to the current for the lowest point on the spectrum, and then always increased between data points so that the shift due to hysteresis would be reproduced. The beam analyzing magnet was also cycled. The spectrometer angular acceptance was 2.0$^\text{o}$ (FW) in the θ direction and 9.0$^\text{o}$ (FW) in the ϕ direction. The slits in front of the target chamber were 0.508 mm (FW) in the vertical direction and 1.016 mm (FW) in the horizontal direction. The widths of the image slit and the object slit of the beam analyzing magnet were both 1.916 mm (FW).

The slit settings and detector foil thickness for the thin and thick target spectra are tabulated in Table I, columns a and b, respectively. In the discussions below of other spectra, only a tabulation will be given.

4. Analysis of the Thick Target Spectrum

To determine the Q-value, the true momentum position of the thick target step shown in Figure 5(b) must be determined

by unfolding the various experimental resolution functions from the spectrum. The step profile depends on the following:

1) The vertical dimension of the beam spot, $\delta r_{s,sp}$. The maximum energy (frequency) spread of the alpha particles geometrically allowed by $\delta r_{s,sp} = 0.508$ mm FW was 3.7 keV FW (5.4 kc/sec, $\Delta p/p = 1/5500$) and is shown in Figure 5(b).

2) The variation of the beam intensity across the beam analyzer slits. The maximum energy spread in the beam allowed by $\delta r_{s,a} = \delta r_{c,a} = 1.016$ mm FW was 19.7 keV FW ($\Delta f_{sp} = 28.6$ kc/sec, $\Delta p_{sp}/p_{sp} = 1/1000$). However, because Pearson (1963) and Groce (1963) reported that the beam energy resolution was much smaller ($\leq 10\%$) than this maximum beam energy spread, it is estimated that the variation of the beam intensity across the beam analyzer slits caused an energy spread in the beam of ≤ 2.0 keV ($\Delta f_{sp} \leq 2.9$ kc/sec, $\Delta p_{sp}/p_{sp} = 1/10000$).

3) The variation of the beam analyzing magnet current. On the basis of the stability of the signal observed on the scope monitoring the NMR magnetometer in the beam analyzing magnet, it is estimated that this current variation caused an energy spread in the beam of 1 keV FW ($\Delta f_{sp} = 1.5$ kc/sec, $\Delta p_{sp}/p_{sp} = 1/20000$).

4) The energy dependence of the reaction cross section. Since the compound state lies at 20 MeV excitation in

^{35}Ar, it is assumed that the cross section does not
change significantly over the energy range of the step.

5) Surface contaminants. A fresh target was used to take
the thick target spectrum shown in Figure 5(b) so as to
minimize surface contaminants which sometimes build
up during long runs, and it is assumed that effects
from surface contaminants are negligible.

6) The energy dependence of the stopping cross section
in the target. Because the stopping powers for the
incident and emergent particles change < 0.5% in the
energy range of the step (Demirlioglu and Whaling,
1962), the spread in the alpha particle energy caused
by this energy dependence is ignored.

7) Aberrations in the spectrometer. An accurate measure
of this contribution is not available, but Groce (1963)
found that the aberrations round the upper step edge
and decrease the absolute value of the slope of the
step. On the basis of his data this latter effect shifts
the location of the midpoint by ≤ 1.3 keV (≤ 1.9 kc/sec,
$\Delta p/p = 1/15000$) in the present measurement. This
uncertainty is included in the error assigned to the
true momentum position of the thick target step (see
below).

8) The angular acceptance $\delta\theta$ of the spectrometer and the
variation of $d\sigma/d\Omega$ over this angular acceptance range.
The spread in the alpha particle energy (frequency)
from the kinematic shift within $\delta\theta = 2.0^\circ$ FW was 29

keV (42 kc/sec, $\Delta p/p = 1/1000$) and is shown in Figure 5(b). On the basis of the known variation of angular distributions from direct reactions (see Section II.C.), it is assumed that cross section $d\sigma/d\Omega$ is constant over $\delta\theta$.

9) The variation of the magnetic spectrometer current. On the basis of the stability of the signal observed on the scope monitoring the NMR magnetometer in the magnetic spectrometer it is estimated that this current variation caused an energy (frequency) spread in the alpha particle energy of ≤ 2 keV FW (≤ 2.9 kc/sec, $\Delta p/p = 1/10000$).

10) The detector slit width $\delta r_{c,sp}$. The slit width $\delta r_{c,sp} = 0.794$ mm FW contributes 7 keV FW (10.2 kc/sec, $\Delta p/p = 1/2900$) to the step width and is shown in Figure 5(b).

In summary, it is assumed that the step width is determined predominantly by $\delta r_{s,sp}$, $\delta\theta$, and $\delta r_{c,sp}$ with small contributions from the variation of the beam intensity across the beam analyzer slits, the variations of the magnet currents, and the aberrations. The contributions from all of these except the aberrations are symmetric in momentum and when folded into the ideal step, the midpoint of the resulting curve should quite accurately represent the momentum of the alpha particles emitted from the surface. The midpoint frequency shown in Figure 5(b) is 29694 ± 4 kc/sec (= ± 2.8 keV; $\Delta p/p = \pm 1/7400$) where the error includes the statistical uncertainty and the uncertainty due to the aberrations.

5. Calibrations

The calibration procedure was similar to the one used by McNally (1966). A standard ^{212}Po source with a 0.795 mm horizontal slit in front of it was placed at the target position 7.925 cm from the bottom of the lucite lid on the target chamber (see Groce, 1963) with the aid of a height gauge and a magnifying glass. That the target position was 7.925 cm from the lucite was checked by sighting down the beam tube with a telescope from the switching magnet. The spectrometer current was cycled as described in Section II. A. 3. above. The calibration spectrum shown in Figure 7(a) was taken with the same electronics shown in Figure 6 and the same detector slit (.794 mm FW) and the same spectrometer slit settings (θ = 2.0^O, ϕ = 9.0^O FW) used to observe the thick target spectrum described above. The peak frequency of 27689 ± 1 is taken as the calibration point as recommended by Groce (1963). This same number was also obtained when this calibration was repeated three weeks later.

To calibrate the beam analyzing magnet a carefully drilled 0.203 mm diameter hole in a 0.127 mm thick sheet of tantalum was placed at the target position and the spectrometer was placed at 0°. After cycling the beam analyzing magnet current, it was set to a current corresponding to an NMR magnetometer frequency of 20935 kc/sec. The slit settings are given in Column c of Table I. Figure 7(b) shows the spectrum of ^{4}He^{++} particles passing through the hole. This spectrum was obtained by varying the spectrometer current after cycling the spectrometer current as described above. The peak frequency was 27672 ± 1 kc/sec and was reproducible provided the steering and focusing controls of the tandem were set at approximately the same values.

The calibration "constant" k_s for the magnetic spectrometer is defined by the formula

$$k_s = \frac{E}{f^2 Z^2} \frac{M}{M_P} (1 + \frac{E}{2M})$$

substituting $E = 8785.0 \pm 0.8$ keV (Wapstra, 1964) and $f_{s\alpha} = 27689 \pm 1$ kc/sec into this formula yields $k_{s\alpha} = 0.0113934 \pm 0.0000013$ MeV/(Mc/sec)^2. The ratio of k_s at other frequencies to $k_{s\alpha}$ has been accurately measured by McNally (1966). This curve is a function of the geometry and the permeabilities of the materials in the spectrometer and is assumed to be constant with time.

The calibration constant k_a for the beam analyzing magnet is defined by an analogous formula. Since the analyzing magnet has a uniform field, k_a may be assumed to be constant for the purposes of this experiment. This assumption was checked by Fisher and Whaling (1964) to 1 part in 3000. The ratio curve indicates that $k_s(f_s = 27672)$ equals $k_{s\alpha}$ to better than 0.001%. Hence

$$k_a = k_{s\alpha} \frac{f^2_{s\ beam}}{f^2_a}$$

gives $k_a = 0.0199062 \pm 0.0000033$ MeV/(Mc/sec)^2 (measured July 14, 1966). Miller (1966) quotes 0.019905 ± 0.000012 MeV/(Mc/sec)^2 (measured October 30, 1965) from a ^{6}Li$(\alpha, n)^9$B threshold measurement, and McNally (1966) quotes 0.019881 ± 0.000005 from a measurement similar to the present one (measured May 12, 1964).

6. Calculation of the Q-value

A relativistic Q-value and excitation energy program which calculates the errors has been written and is described in detail in Appendix A. The program was intended for transmission targets, but by setting all of the input target thicknesses equal to zero, it may be used for thick targets in a reflection geometry. Table III lists the inputs, the assumed errors, and the results. The spectrometer track reading of 150° was not used but rather a value obtained by averaging over the angular acceptance of the spectrometer with a program listed in Appendix B. Except at 90° this observation angle will differ from the track reading because of $\delta\phi$. The error of $.05^O$ in the spectrometer angle is based on the uncertainty in the track protractor readings described by Groce (1963).

The result for the Q-value is:

$$^{32}S(^{3}He, \alpha)^{31}S \quad Q = 5.538 \pm 0.006 \text{ MeV} .$$

Other measurements of this Q-value were obtained in the transmission target spectra discussed in Section II. B., and the results are given in Table IX. As a further check, transmission target spectra from the reaction $^{34}S(^{3}He, \alpha)^{33}S$ (see Section II. B. 8.) and the reactions $^{32}S(^{3}He, d)^{33}Cl$ and $^{34}S(^{3}He, d)^{35}Cl$ (see Section V. A. 2. (iv)) which were observed simultaneously with the spectra from the reaction $^{32}S(^{3}He, \alpha)^{31}S$ were used to compute the Q-values for those levels which corresponded to emitted particles of approximately the same momentum as that of the alphas corresponding to the ground state of ^{31}S, and the results were compared with previously reported measurements.

Using Q = 5. 538 ± 0. 006 and the 1964 Mass Table (Mattauch et al. ,1965) for the mass excesses

$$^{32}S \quad -26012.7 \quad \pm \quad 0.9$$

$$^{3}He \quad 14931.34 \quad \pm \quad .21$$

$$^{4}He \quad 2424.75 \quad \pm \quad .39$$

yields

$$^{31}S \quad -19045 \quad \pm \quad 6 \quad .$$

This disagrees with the mass excess quoted for ^{31}S in the 1964 Mass Table:

$$-18992 \quad \pm \quad 11 \quad .$$

The mass links shown in the schematic diagram of the input data which is given with the 1964 Mass Table indicate that this number is based on a measurement of the threshold of the reaction $^{28}Si(\alpha, n)^{31}S$ and on either a measurement of the threshold of the reaction $^{31}P(p, n)^{31}S$ or a measurement of the end-point energy of the β-decay of ^{31}S or both.

B. Excitation Energies of Levels in ^{31}S

1. Introduction

The purpose of the work described in this section was to locate energy levels in ^{31}S. The reactions which can provide information about ^{31}S are listed (Endt and van der Leun, 1962):

1) $^{28}Si(\alpha, n)^{31}S$ $\qquad Q = -8.149$ MeV

2) $^{31}P(p, n)^{31}S$ $\qquad -6.232$

3) $^{32}S(\gamma, n)^{31}S$ $\qquad -15.095$

4) $^{29}Si(^3He, n)^{31}S$ $\qquad 3.951$

5) $^{31}P(^3He, t)^{31}S$ $\qquad -5.468$

6) $^{32}S(p, d)^{31}S$ $\qquad -12.870$

7) $^{32}S(d, t)^{31}S$ $\qquad -8.837$

8) $^{32}S(^3He, \alpha)^{31}S$ $\qquad 5.483$

9) $^{33}S(p, t)^{31}S$ $\qquad -15.254$.

Only (8) was suitable. Reactions (1) - (4) emit neutrons and were therefore unsuitable because closely spaced levels were expected. Reactions (5), (6), (7), and (9) have large negative Q-values.

2. Targets

Several kinds of sulfur targets were tested. Elemental sulfur was not tried because it melts at 113°C. A target of Sb_2S_3 on thin gold foil was made by evaporating $BaCl_2$, gold, and Sb_2S_3 onto a glass slide and then floating off the gold and Sb_2S_3 combination on distilled water and mounting it on tantalum sheet over a hole 9 mm in diameter. This combination was abandoned when it was discovered that the Sb_2S_3 slowly evaporated with 0.3 μA of 12.0 MeV $^3He^{++}$ on a 0.8 mm^2 area. The compound MoS_2 was tried but it appeared to

decompose during the evaporation from the boat. The combination of ZnS on a nickel foil was made by mounting 5000 $\overset{o}{A}$ nickel foils (obtained from the Chromium Corporation of America) on a tantalum frame and then evaporating ZnS onto it. Even though this combination was durable under bombardment, it was abandoned because it was feared that at $E_{3_{He}}$ = 12.0 MeV weak reactions from the zinc and nickel would be seen. Carbon foils with Sb_2S_3 or ZnS were tried but repeatedly broke when the beam hit them. However, Ajzenberg-Selove and Wiza (1966) have recently reported success with Sb_2S_3 on a carbon foil.

The combination used for this experiment was CdS on a gold foil. The procedure used to prepare the Sb_2S_3 targets was used to prepare the CdS targets. No evaporation was observed for beams of less than 0.3 μA of 12.0 MeV $^3He^{++}$ on a 0.8 mm^2 area. The Coulomb barrier for cadmium (Z = 48) is so high that no significant reactions were expected and none were observed. Targets were made from CdS containing natural sulfur (95.0% ^{32}S, 0.76% ^{33}S, 4.22% ^{34}S, 0.014% ^{36}S) and from CdS containing sulfur enriched in ^{32}S which was obtained from the Oak Ridge National Laboratory. The isotopic analysis supplied with the material gave 98.1% ^{32}S, 0.1% ^{33}S, 1.5% ^{34}S, and 0.1% ^{36}S.

In all of the target making operations great care was taken to avoid contaminants. The tantalum frames and glass slides were boiled in cleaning solution, rinsed several times in distilled water, blotted dry with tissue, and wiped with lens paper to remove lint and dust. The bell jar was thoroughly cleaned before each evaporation even though the user before had already cleaned it once. The boats were heated to a temperature well above that required to evaporate CdS before anything was placed in them and before the

glass slides were placed in the bell jar. This precaution degassed the evaporation area and evaporated any contaminants that might have been present. After the foils were floated off, they were allowed to float on the water for several minutes to dissolve and disperse the trace of $BaCl_2$ present. The targets, including the frames, were never handled with the fingers because close observation has shown that perspiration will condense on a cold target several millimeters from the point of contact with the skin. The targets were never left in the target chamber when the cold trap in the target chamber was not cold because it has been observed that under these conditions the target will pick up traces of diffusion pump oil.

The thicknesses of the gold and CdS deposited on the glass slide were monitored by a Sloan Deposit Thickness Monitor (Model 2a) during the evaporation. This device measures the change in frequency of a resonating quartz crystal as a deposit condenses on its surface. The change in frequency is proportional to the mass of the deposit. Because the spatial distribution of material coming from the boat was not isotropic, the thickness monitor did not receive the same amount of material as the glass slide. Typically the thicknesses calculated from the thickness monitor differed by 15% from those measured by elastic scattering as described below. The largest observed difference was 40% which occurred when the glass slide and the resonating crystal were close to the boat ($\sim$ 6 cm) for the evaporation of the CdS containing enriched sulfur.

In order to determine the target thickness more accurately, the loss in energy of 10-MeV $^3He^{++}$ scattered from the target was measured with the spectrometer and the 16-detector array. It was assumed that sulfur was still in the form of CdS on the target, which

was convenient because cadmium has a much larger Rutherford scattering cross section than does sulfur. With the target turned to present the gold foil to the incident beam the peak due to scattering from cadmium was shifted down by the energy lost in passing twice through the gold. Similarly, with the target turned to present the CdS to the incident beam, the peak due to scattering from gold was shifted down by the energy lost in passing twice through the CdS (see Figure 8). The target thicknesses were calculated with the aid of the stopping power curves of Demirlioglu and Whaling (1962) and the results are given in Table IV.

3. Supplementary Data

The calibration constant of the spectrometer for detector 8 in the array with the 1.84 mm (measured perpendicular to the mean orbit) detector slits was determined in the same way as described in Section II.A.5 for the single detector. The array preamplifier and amplifier were not used but rather the detector was connected to a Tennelec preamplifier and a double delay line amplifier as shown in Figure 6. The spectrum is shown in Figure 9 and the peak frequency was 27703 ± 1 kc/sec. The result was $k_{s\alpha} = 0.0113819 \pm 0.0000012$ MeV/(Mc/sec)^2.

At a given magnetic field setting, McNally (1966) showed that the ratio of the momentum corresponding to any one detector to the momentum corresponding to detector 8 is a constant, independent of the magnetic field. Equivalently, a frequency can be associated with each detector, and the ratios of these frequencies have the same values as the ratios of momenta. Table II lists the frequency ratios as measured by McNally (1966) and used in this analysis. To calculate the frequency associated with detector x,

it is only necessary to multiply the frequency for detector 8 by the ratio for detector x.

The procedure described by McNally (1966) was used to measure the yield factors. A beam of 12.0 MeV ^{3}He^{++} particles was scattered from a clean sheet of tantalum of thickness 0.127 mm. The spectrometer was set at 150°, and the same slit settings used for the reaction spectra described in Section II. B. 4. (see Table I, column d) were used here for $\delta z_{s, sp}$, $\delta r_{s, sp}$, $\delta \theta$, $\delta \phi$, and $\delta r_{c, sp}$. A region of the spectrum well below the maximum energy of the elastically scattered ^{3}He^{++} particles was scanned with detector 8 and the spectrum is shown in Figure 10 (open circles). The straight line is an approximation to this spectrum. Then the region was observed with the array (solid circles). Dividing the yields observed by the array into the yields given by the line at the frequencies corresponding to the detectors in the array gives the yield factors listed in Table II, column a. To calculate the corrected yield for detector x, it is only necessary to multiply the yield recorded in detector x by yield factor x. In effect, the frequency factors and yield factors transform the data to a single detector spectrum.

4. ^{32}S(^{3}He, α)^{31}S Spectra Collection Details

A beam of from 0.1 to 0.3 μA of 12 MeV ^{3}He^{++} particles bombarded the target. The beam analyzing magnet was cycled (as described in Section II. A. 3) at the beginning of the data collection. The slit settings and detector foil used are given in Table I, column d. With 20 volts bias on the detectors the alpha particles and deuterons were completely stopped in the depleted region whereas the protons were not and produced smaller pulses than the deuterons. Because

the detectors were separated by 5.79 mm as measured perpendicular to the central orbit, four (or five) steps of the magnetic field corresponding to a displacement of approximately 1.4 (or 1.2) mm of the spectrum relative to the detectors were made for each of the regions of the spectrum. As a check the ends of adjacent regions were overlapped. The data were read out on the Nuclear Data Optikon (Model ND307).

5. Reduction of Data to Spectra

The 16 alpha particle groups were summed with a desk calculator, and then these sums were punched on cards along with the frequency of detector 8. Near the end of this work, 100 runs with little background could be processed in 8 hours. From these data along with the frequency factors and yield factors the program given in Appendix C calculated the frequency and corrected yield for each detector and plotted the resulting spectra, which are shown in Figure 11.

An attempt to read the data directly into the CIT IBM 7094 computer through a data link for immediate analysis was abandoned because graphical output could not be obtained immediately. Typically there was a 30 minute wait for a plot. The system was inconvenient to use because the ranges of channels to sum had to be fed into the computer remote console and because approximately ten switches had to be set each time data were read into the computer. More serious difficulties were the fact that the computer sometimes lost the data and the fact that the computer did not operate 24 hours a day. A CRT with a light pen, a data storage facility such as a magnetic tape unit, and full-time computer service would expedite the analysis of spectrometer data.

6. Discussion of Spectra

The contributions to the resolution of peak (9) in Figure 11(b), which is typical of all of the peaks shown in Figure 11, are listed in Table V. This list includes all of the factors that determine the thick target profile as well as variations in the energy loss in the target and the straggle. If the resolution function for each of these contributions were known, then they could be convoluted to obtain the total resolution function. The observed resolution is 31 keV (FWHM) for peak (9) in Figure 11(b).

The peaks in Figure 11 were first identified by a non-relativistic kinematics program. The input consisted of the incident beam energy, the thicknesses of the CdS and gold, the spectrometer frequencies of a group at two or more angles, the corresponding spectrometer angles, and the corresponding angles between the beam and the normal to the target. The program calculated the energies of the emerging alphas from the spectrometer frequencies, and then corrected these energies and the energy of the incident beam for the target thickness in a manner similar to that used in the program described in Appendix A. The resulting alpha particle energies at two or more angles and the beam energy were used to calculate the mass of the target nucleus and the Q-value. The mass was typically determined to ±1 AMU and never worse than ±3 AMU.

The identifications given by the non-relativistic program were checked by calculating the spectrometer frequencies with a relativistically correct program. For ^{31}S the mass of the ground state was taken from Section II. A. 6 and the excitation energies were taken from II. B. 7. For other nuclei the compilations of Lauritsen and Ajzenberg-Selove (1962) and Endt and van der Leun (1962) were used. Since some levels were seen at only two angles,

the spectra were carefully checked for groups from the target nuclei ^{12}C, ^{13}C, ^{16}O, ^{28}Si, ^{33}S, and ^{34}S. Peaks from ^{12}C are labeled in Figure 11. The identification of the peaks from ^{16}O was facilitated by some spectra taken by David Hensley with a ^{16}O target under similar conditions. Note in particular the strong peak from the 6.18 MeV level in ^{15}O at f = 30100 in Figure 11(b) for example. The identification of the peaks from ^{34}S was facilitated by some spectra taken by Dr. J. Dubois with a ^{34}S target under similar conditions. No groups were observed from ^{13}C, ^{28}Si, or ^{33}S. As a further check on these identifications the yields in the natural spectra and in the enriched spectra were compared.

7. Calculations of Excitation Energies and Q-values

For each spectrum shown in Figure 11 the program described in Appendix A was used to calculate the excitation energies and Q-values for levels in ^{31}S. A final excitation energy was calculated by averaging the excitation energies calculated from selected peaks. The criteria for selection were that the peaks be symmetric and not confused by a large background. The results are shown in Tables VI and IX.

The excitation energies and Q-values for the reaction ^{34}S(^{3}He, α)^{33}S were also calculated with this program after setting M_2 and M_4 equal to the masses of ^{34}S and ^{33}S, respectively. The results are listed in Table VII.

8. Results

The last two columns of Table VI compare the present results for ^{31}S with those reported by Ajzenberg-Selove and Wiza

(1966). The correspondence between the levels is based more on the relative excitation energies and strengths than on the absolute excitation energies. The third excited state was located at an excitation energy of 3.075 ± .010 MeV in the present experiment but was not reported by Ajzenberg-Selove and Wiza (1966). A group which is tentatively attributed to a weakly populated level at an excitation energy of (5.026 ± .016) MeV in ^{31}S was found in the present experiment but was not reported by Ajzenberg-Selove and Wiza (1966). Levels forming closely spaced doublet which were not resolved by Ajzenberg-Selove and Wiza (1966) were found at excitation energies of 5.407 ± .010 and 5.440 ± .010, 6.540 ± .012 and (6.593 ± .015), (6.711 ± .013) and 6.743 ± .013, and 7.161 ± .011 and 7.199 ± .013 MeV in the present experiment.

The strong group seen at θ_{lab} = 15° by Ajzenberg-Selove and Wiza (1966) and attributed to a level in ^{31}S at an excitation energy of 6.896 ± .025 was also seen in the present experiment (at f = 30100 in Figures 11(b) and (c)) but attributed to a strong group from the 6.180 MeV level in ^{15}O. The "group" seen at θ_{lab} = 15° and 45° by Ajzenberg-Selove and Wiza (1966) and attributed by them to a level in ^{31}S at an excitation energy of 7.522 ± .020 MeV, was also attributed to ^{15}O in the present experiment. At θ_{lab} = 15° this "group" was attributed to the 6.792 MeV level in ^{15}O and at θ_{lab} = 45° to the 6.180 MeV level. The group seen at θ_{lab} = 15° by Ajzenberg-Selove and Wiza (1966) and attributed by them to a level in ^{31}S at an excitation energy of 7.60 ± .030 MeV was attributed to the 6.860 MeV level in ^{15}O in the present experiment. No evidence was seen in the present experiment for levels at 6.99 ± .030 and 7.66 ± .030 MeV.

The last two columns of Table VII compare the present results for ^{33}S with those reported by Endt and Paris (1958). The good agreement of the excitation energies for the 3.83 MeV level is a check on the ground state Q-value for the reaction ^{32}S(^{3}He, α)^{31}S (see Section II. A. 6) because the group from the 3.83 MeV level in ^{33}S is close to the group from the ground state of ^{31}S (see Figure 11).

C. Angular Distributions of ^{31}S States

1. Introduction

The purpose of the work described in this section was to measure the angular distributions from the reaction ^{32}S(^{3}He, ^{4}He)^{31}S. The experimental distributions were fitted with the angular distributions computed from direct reaction theory to determine the angular momentum ℓ_n of the neutron extracted from the target nucleus. J-dependence was used to make tentative spin assignments for some levels in ^{31}S.

2. Experimental Procedure

A target of 97 ± 29 μg/cm^2 of CdS containing enriched sulfur (98.1% ^{32}S, 0.1% ^{33}S, 1.5% ^{34}S, and 0.1% ^{36}S) on 289 ± 87 μg/cm^2 gold foil was used for all of the distributions except those for levels 3, 4, and 6 for which a target of 289 ± 87 μg/cm^2 of Sb$_2$S$_3$ containing natural sulfur on 289 ± 87 μg/cm^2 of gold was used, because CdS had not been tried when these distributions were measured. Evaporation was not a problem with a beam of no more than 0.3 μA of 12.0 MeV ^{3}He^{++} on the CdS target and no more than 0.1 μA on the Sb$_2$S$_3$ target. Because of the severe elastic scattering

from the gold, an attempt to monitor the elastic scattering from
the sulfur with a solid state counter in the target chamber was
unsuccessful. Instead, equal amounts of charge as measured by
the Eldorado Electronics (Model Cl-110) current integrator were
allowed to strike the target at each angle, and the measurement
at 20° was repeated several times during the measurement of a
distribution to check for target deterioration. In the one case
where a change was noted, the measurements were repeated.
The alpha particles were detected with the 16 detector array.

The slit settings and detector foil thickness listed in
Table I, column f, were used for all of the distributions except
those from levels 3, 4, and 6. For these three, which were
measured nine months earlier, the slit settings and detector foil
thickness listed in Table I, column g, were used. The energy
resolution (typically 35 keV) was comparable to that shown in
Figure 11 except for levels 3, 4, and 6 which was not as good
(typically 50 keV).

The same yield factors used for the spectra from the
reaction $^{32}S(^{3}He, \alpha)^{31}S$ described in Section II. B., and listed in
Table II, column a, were used for all of the distributions except
those from levels 3, 4, and 6. For these three, another set
measured by the procedure described in Section II. B. 3 and given
in Table II, column b, was used.

Angular distributions for levels in one span of the array
were measured simultaneously. Other spectra collection details
are similar to those described in Section II. B. 4.

3. Analysis of Experimental Data

The data were reduced to spectra by the procedure described in Section II. B. 5. Suppose N is the number of particles striking the focal plane, f is the frequency, and Y is the number of counts in a peak. Then it was assumed that

$$Y = \int_{peak} \frac{dN}{df} \, df \approx \frac{1}{\overline{\Delta f}} \text{ (area of peak)}$$

where $\overline{\Delta f}$ is the collector slit width. The area was estimated by drawing a triangle through the experimental points as shown in Figure 11. The resulting yields were corrected for target angle, converted to center-of-mass yields, and normalized so that the maximum value was unity. The center-of-mass distributions were then plotted (Figures 13-26) along with the DWBA distributions (see Section II. C. 4 below).

4. DWBA Distributions

For these calculations it was assumed that the reaction mechanism was simple pick-up. The zero-range approximation was used and spin-orbit coupling was neglected.

The optical model parameters used here for the reaction $^{32}S(^3He, \alpha)^{31}S$ were those used by Blau et al. (1965) for the reaction $^{39}K(^3He, \alpha)^{38}K$ and are given as Set I in Table X. Woods-Saxon shapes were used for the real and imaginary parts of the optical potential

$$U(r) = -\frac{V}{e^x + 1} - i\frac{W}{e^{x'} + 1}$$

$$x = \frac{r - R}{a} \qquad x' = \frac{r - R'}{a'}$$

$$R = r_o(M)^{1/3} \qquad R' = r'_o(M)^{1/3} \;.$$

The ^{3}He parameters were found by Blau et al.(1965) by fitting the elastic scattering of ^{3}He by ^{39}K at $E_{3_{He}}$ = 9.00 MeV with the search code HUNTER. The alpha parameters were derived by Blau et al.(1965) from an optical model analysis by Bassel et al. (1962) of measurements of elastic scattering of 18 MeV alpha particles from ^{40}Ar by Seidlitz et al.(1958). Variations of the parameters for the reaction ^{32}S(^{3}He, α)^{31}S by up to 50% caused only small variations in the predicted distributions, and the distributions were never shifted by more than 3° in the range θ_{CM} = 0° to 40°. No case was found where the distribution for one ℓ_n-value and one set of parameters could be confused with the distribution for another ℓ_n-value and a different set of parameters. Because of these findings, and because it is well known that these parameters are insensitive to the mass and energy, (Hodgson, 1963a) it was assumed that the parameters used for the ^{39}K(^{3}He, α)^{38}K reaction were appropriate for the ^{32}S(^{3}He, α)^{31}S reaction.

Another set of parameters, labeled Set II in Table X, was obtained by interpolating the values of Hodgson (1963b) for nuclei in this mass region. The predicted distributions are very

similar to those with Set I parameters.

The parameters labeled Set III in Table X were used by Fou and Zurmuhle (1966) for the reaction $^{32}S(^{3}He, \alpha)^{31}S$ at $E_{3_{He}} = 15.0$ MeV. These parameters were obtained from the analysis of elastic scattering of ^{3}He from ^{40}Ca at 15 MeV and elastic scattering of alphas from ^{40}Ca at 24 MeV. The predicted distributions are very similar to those for Set I and again the distributions are very insensitive to variations in these parameters.

The distributions for these three sets of parameters were calculated with the code TSALLY which uses the zero-range approximation and was written by Bassel, Drisko, and Satchler (1962). This is not a search code and only calculates the distributions for given sets of input parameters. The distributions calculated by TSALLY were manually punched on cards and then normalized and plotted along with the experimental distributions by the computer. Figure 12 shows a typical comparison of the angular distributions predicted by Sets I, II, and III. Attempts to improve the fits by varying the parameters met with little success, and it was decided to use Set I parameters for all of the levels. Figures 13 - 26 show the results.

5. Discussion

Figure 13 shows the angular distribution for $^{31}S(G.S.)$ which must have $\ell_n = 0$ because for this state $J^{\pi} = 1/2^{+}$ (Endt and van der Leun, 1962). The second peak is larger relative to the first peak than the theory predicts but the edge of the forward peak is correctly positioned. The theoretical distributions for $\ell_n = 0, 1, 2, 3,$ and 4 are shown. These distributions are similar for different excitation energies.

The angular distributions for $^{31}S(1.25)$ and $^{31}S(2.23)$ were not measured because they had already been measured by Fou and Zurmuhle (1966).

Figure 14 shows the angular distribution for $^{31}S(3.08)$. The theoretical distribution for $\ell_n = 0$ fits the data best. The second peak is larger relative to the first peak than the theory predicts, just as it was for the ground state. Level $^{31}S(3.08)$ is assigned $\ell_n = 0$ and therefore $J^\pi = 1/2^+$.

Figure 15 shows the angular distribution for $^{31}S(3.29)$. The theoretical distribution for $\ell_n = 2$ fits the data quite well. Fou and Zurmuhle (1966) found a J-dependence in $\ell_n = 2$ angular distributions from the reaction $^{32}S(^3He, \alpha)^{31}S$. They found that the main peak in the $\ell_n = 2$ angular distribution to the $3/2^+$ level at an excitation energy of 1.25 MeV was shifted to a more forward angle by a few degrees relative to the forward peak for the $5/2^+$ level at 2.23 MeV (see Section III. C. for the spin assignments). Glashausser and Rickey (1967) observed a similar J-dependent shift for these same levels in the reaction $^{32}S(p, d)^{31}S$, and they discuss other reactions which show that J-dependence in neutron pickup reactions is a widely occurring phenomenon. In the present experiment the angular distribution for $^{31}S(3.44)$ (discussed below) which has $J = 3/2$ (see Section III. C. for the spin assignment) falls between the theoretical distributions for $\ell_n = 1$ and 2 (see Figure 16). Because of J-dependence level $^{31}S(6)$ is assigned $\ell_n = (2)$ and $J^\pi = (3/2^+)$ (parentheses mean the assignment is tentative) and level $^{31}S(3.29)$ which falls closer to the theoretical distribution for $\ell_n = 2$ is assigned $\ell_n = 2$ and $J^\pi = (5/2)^+$.

No attempt was made to obtain the angular distribution for $^{31}S(3.35)$ because this weak group was not well resolved from the strong $^{31}S(3.29)$.

Figure 16 shows the angular distribution for ^{31}S(3.44).
As mentioned above, the distribution falls between the theoretical
distributions for ℓ_n = 1 and 2, and because of J-dependence
^{31}S(3.44) is assigned ℓ_n = (2) and J^π = (3/2$^+$).

Figure 17 shows the angular distribution for ^{31}S(4.08).
For $\theta_{lab} \leq 20^\circ$, ^{31}S(4.08) was obscured by ^{11}C(G.S.). The
theoretical distribution for ℓ_n = 2 is consistent with the measured
distribution, and because the measured distribution is not shifted
forward relative to the theoretical distribution, J^π = (5/2$^+$) is
suggested. Level ^{31}S(4.08) is assigned ℓ_n = (2) and J^π = (5/2$^+$).

No attempt was made to obtain the angular distribution
for ^{31}S(4.21) because this group was obscured by ^{11}C(G.S.).

Figure 18 shows the angular distribution for ^{31}S(4.45).
The gap in the distribution was caused by ^{11}C(G.S.). Level
^{31}S(4.45) is assigned ℓ_n = 3.

Figure 19 shows the angular distribution for ^{31}S(4.52).
The gap in the distribution was caused by ^{11}C(G.S.). Level
^{31}S(4.52) is assigned ℓ_n = 2.

Figure 20 shows the angular distribution for ^{31}S(4.58).
The gap in the distribution was caused by ^{11}C(G.S.). No assign-
ment is made for level ^{31}S(4.58) because the fit is poor.

Figure 21 shows the angular distribution for ^{31}S(4.72).
The gap in the distribution was caused by ^{11}C(G.S.). Level
^{31}S(4.72) is assigned ℓ_n = 2, (3). The fact that the experimental
distribution is shifted to a greater angle than the theoretical distri-
bution is attributed to J-dependence, and J = (5/2) is assigned to
this level.

Figure 22 shows the angular distribution for ^{31}S(4.87).
For this level and all higher levels discussed below, the point at

$\theta_{CM} = 6^O$ was obscured by elastic scattering of $^3He^{++}$ particles. The minimum at $\theta_{CM} = 28^O$ is best fitted by the theoretical distribution for $\ell_n = 1$, but since a point was not obtained near enough to $\theta_{CM} = 0^O$ to confirm the predicted decrease in $d\sigma/d\Omega$ there, this level is assigned $\ell_n = (1)$.

Figure 23 shows the angular distribution for $^{31}S(4.97)$. The minimum at $\theta_{CM} = 28^O$ is best fitted by the theoretical distribution for $\ell_n = 1$, and therefore this level is assigned $\ell_n = 1$.

No attempt was made to obtain the angular distribution of $^{31}S(5.03)$ because this group was not resolved from $^{31}S(4.97)$.

Figure 24 shows the angular distribution for $^{31}S(5.15)$. This level is assigned $\ell_n = 0$ and therefore $J^\pi = 1/2^+$.

Figure 25 shows the angular distribution for $^{31}S(5.30)$. The lack of structure suggests that this level is not populated by a pick-up reaction, and no assignment is made.

No attempt was made to obtain the angular distribution for $^{31}S(5.41)$ and $^{31}S(5.44)$ because these groups were not resolved.

Figure 26 shows the angular distribution for $^{31}S(5.52)$. No assignment is made.

6. Results

Table XI summarizes the results of this and previous work. The present assignment of $\ell_n = 3$ to $^{31}S(4.45)$ disagrees with the assignment of $\ell_n = 2$ to this level by Fou and Zurmuhle (1966). However, there is a $7/2^-$ level in the mirror nucleus ^{31}P at 4.43 MeV excitation energy (Harris et al., 1964). Furthermore, Fou

and Zurmuhle (1966) did not resolve the 4.45 MeV level from the 4.52 MeV level which has $\ell_n = 2$.

The assignment of $\ell_n = 2$ to ^{31}S(3.29) disagrees with the assignment of $\ell_n = 1$ to this level by Kavaloski (1963) but agrees with Fou and Zurmuhle (1966) and Glashausser and Rickey (1967).

III. ^{32}S(^{3}He, ^{4}Heγ)^{31}S ANGULAR CORRELATIONS

A. Introduction

This section describes the application of a correlation technique called Method II by Litherland and Ferguson (1961) to the reaction ^{32}S(^{3}He, ^{4}Heγ)^{31}S. This method, which gives information about the spin, parity, and mixing ratio for levels in the residual nucleus, was first mentioned by Newton (1952), but its power was not widely recognized until Litherland and Ferguson (1961) again pointed it out. One of the first applications that illustrated its power was a study of the reaction ^{16}O(^{3}He, pγ)^{18}F by Poletti and Warburton (1965). Following this study, numerous other studies employing this technique were published.

What is new in the present application is a refinement in the experimental technique. Most previous applications have used an annular solid-state detector at 180° and studied only the well separated low-lying states of the residual nucleus. For high-lying levels information about the spin, parities, and mixing ratios has usually been obtained by resonance experiments. The present technique serves well in the intermediate region. Because the levels are closely spaced, high resolution is needed for either the particles or the gammas. The former was chosen. A magnetic spectrometer was placed at 0° to detect the particles, and the gammas in coincidence were detected with a NaI(Tl) crystal. The main disadvantage is the small solid angle of the spectrometer. This disadvantage can be overcome with an array of detectors in the focal plane of spectrometer and with an array of NaI(Tl) crystals, but this was not done in the present experiment. Similar

experiments employing magnetic spectrometers are in progress at Chalk River and MIT.

B. Theory

The formulas which will be discussed here are similar to those given by Poletti and Warburton (1965). Derivations of them will not be given (see Ferguson, 1965).

The essential feature of Method II is that it limits the gamma rays which are observed to those from aligned states with a small number of magnetic substates populated. Consider the reaction:

$$a \quad + \quad b \rightarrow c \quad + \quad d$$

Spins	J_a		J_b	J_c	J_d	

Orbital Angular Momentum $\quad L_{ab} \qquad L_{cd}$

Magnetic Quantum Number $\quad M_a \; M_{ab} \; M_b \quad M_c \; M_{cd} \; M_d$

Since the beam direction is the z axis, $M_{ab} = 0$. Suppose c is detected at 0° (or 180°). Then for these particles $M_{cd} = 0$. By conservation of angular momentum

$$M_a + M_b = M_c + M_d$$

and therefore

$$M_d \leq |\vec{J}_a| + |\vec{J}_b| + |\vec{J}_c| \quad .$$

If the gamma rays from the decay of d are detected in coincidence with the particles c observed at 0° (or 180°) and if the beam and target are unpolarized, then the angular distribution of the gamma rays can be expressed by

$$W(\theta) = \sum_k a_k P_k(\cos \theta) = \sum_k \rho_k(J_d) F_k(J_d J_e) Q_k P_k(\cos \theta) \qquad (1)$$

where θ is the angle between the direction of the gamma-ray detector and the axis of alignment. The $P_k(\cos \theta)$ are Legendre polynomials and k takes on even values from 0 to $2J_d$. The Q_k are the standard attenuation coefficients for the gamma-ray detector, the $\rho_k(J_d)$ are statistical tensors which describe the alignment of the state d, and the $F_k(J_d J_e)$ depend specifically on the gamma-ray transition.

In more detail, the statistical tensors are given by

$$\rho_k(J_d) = \sum_{M_d \geq 0} \rho_k(J_d, M_d) P(M_d) \qquad (2)$$

where $P(M_d)$ is the normalized population parameter for the magnetic substate M_d and

$$\rho_k(J_d, M_d) = (2 - \delta_{M_d 0}) \frac{(J_d M_d J_d - M_d | k\ 0)}{(J_d M_d J_d - M_d | 0\ 0)} . \qquad (3)$$

The $F_k(J_dJ_e)$ are given by the following if no more than two multipolarities L and L' = L + 1 are involved in the gamma-ray transition.

$$F_k(J_dJ_e) = \frac{F_k(LLJ_dJ_e) - (-)^\sigma 2xF(LL'J_dJ_e) + x^2F_k(L'L'J_dJ_e)}{1 + x^2} \quad (4)$$

where

$$F_k(LL'J_eJ_d) = (-)^{J_e-J_d-1}[(2L+1)(2L'+1)(2J_d+1)]^{1/2}(L\,1L'\,-1\,|\,k\,0)$$

$$\times W(J_dJ_dLL', kJ_e) \quad . \quad (5)$$

In formula (5), $W(J_dJ_dLL', kJ_e)$ is the Racah coefficient, and the mixing parameter x is given by $x = \langle e\|L{+}1\|d\rangle/\langle e\|L\|d\rangle$. The exponent σ is 0 for an ML, EL + 1 mixture, and 1 for an EL, ML + 1 mixture. In the following analysis, it was assumed initially that σ = 0 regardless of the suspected nature of the transition.

For comparison with experiment it is more convenient to rewrite formula (1) in the form

$$W(\theta) = \sum_{M_d \geq 0} I(M_d)[\sum_{\substack{k \\ even}} \rho_k(J_d, M_d)F_k(J_dJ_e)Q_kP_k(\cos\theta)] \quad (6)$$

where $\rho_k(J_dM_d)$ is given by formula (3), and $I(M_d)$ is the un-normalized population parameter, that is,

$$P(M_d) = \frac{I(M_d)}{\sum\limits_{M_d' \geq 0} (\delta_{0\,M_d'} \, I(M_d') + 2I(M_d'))} . \qquad (7)$$

Formula (6) clearly shows that $W(\theta)$ is linear in $I(M_d)$ and nonlinear in x. The best fit to the data corresponds to the lowest value of Q^2, where Q^2 is given by

$$Q^2 = \frac{1}{n} \sum_i \left[\frac{Y(\theta_i) - W(\theta_i)}{E(\theta_i)} \right]^2 \qquad (8)$$

where $E(\theta_i)$ is the uncertainty in the gamma-ray yield $Y(\theta_i)$ at θ_i and n is the number of degrees of freedom.

In the reaction $^{32}S(^3He, \, ^4He\gamma)^{31}S$, $M_d = \pm 1/2$, and formula (6) becomes

$$W(\theta) = I(1/2) \sum_k \rho_k(J_d, 1/2) F_k(J_d J_e) Q_k P_k(\cos\theta) . \qquad (9)$$

Only the two parameters $I(1/2)$ and x must be fitted.

C. Correlations in the Reaction $^{32}S(^3He, \, ^4He\gamma)^{31}S$

1. Excitation Functions

To maximize the yield of alphas at 0° in the correlation and branching ratio measurements it was necessary to measure

rough excitation functions for the groups of interest. These excitation functions were measured at $\theta_{lab} = 10^O$ with the array, and the various slit settings are given in Table I, column e. The target consisted of ZnS containing natural sulfur on a 2500 $\overset{O}{A}$ Ni foil.

Figure 27 shows the results. Measurements were made at every 200 keV from 8 to 12.2 MeV. The arrows indicate the beam energies selected for the correlation and branching ratio measurements. For $^{31}S(2)$ the correlation and branching ratio were measured before the excitation function was measured, and the beam energies were not optimum.

2. Experimental Setup for the Correlations

A schematic diagram of the setup is shown in Figure 28. The alpha particles were detected in the magnetic spectrometer at 0° with a silicon surface barrier detector. The detector was masked by a slit (1.27 cm wide for $^{31}S(1.25)$, $^{31}S(2.23)$, and $^{31}S(3.08)$ and .635 cm wide for $^{31}S(3.29)$, $^{31}S(3.35)$, and $^{31}S(3.44)$) and covered with an aluminum foil which presented a thickness 1.7 mg/cm^2 to the particles passing through the spectrometer. For the correlations of the levels at 3.29 and 3.35 MeV excitation, the beam was caught in a cup of diameter 0.635 cm placed at a distance of 25 cm from the target. The half-angle subtended by this cup was 0.72^O. The outer aperture was a hole of 1.676 cm diameter also placed at a distance of 25 cm from the target. The half-angle subtended by this aperture was 1.85^O. For the correlations of the other levels an older, dirtier beam catcher which produced more gamma-ray background was used because completion of the newer beam catcher was unexpectedly delayed on three occasions by other experiments

immediately before scheduled runs. The cup in the old system was 48 cm from the target and subtended a half-angle of 1.1^O. The entrance slits to the spectrometer defined the outer aperture and subtended a half-angle of 2.0^O. The correlation from the 2.23 MeV level was measured with both systems and the results agreed within the experimental uncertainties.

The gamma rays were detected in a 12.70 cm diameter x 10.16 cm long NaI(Tl) crystal which could be moved from 90° to 150°. The distance from the target to the front face of the crystal was 13.7 cm. This spacing could easily be reproduced by means of a spacer between the crystal and the outside of the target chamber. The crystal was supported on a wooden table clamped to a target chamber support. The angles were set by means of lines drawn on this table.

A diagram of the electronics is shown in Figure 29. The internal lower level discriminator gate in the RIDL 400-channel analyzer was disconnected from the input and the gating pulses from the diodes were fed to this gate rather than to the coincidence gate supplied by the company. This modification suggested by Dr. R. W. Kavanagh greatly reduced the dead time in the analyzer when there was a high count rate at the input. The two diodes prevented cross-talk between the two coincidence units (RIDL 32-3). The high voltage stabilizer sampled the counting rates in two windows--one on each side of a peak-- and adjusted the high voltage to keep these two counting rates equal. The rest of the circuit is standard.

Due to the complexity of the setup and the fact that most of the equipment was used for other experiments, it was difficult to set up the experiment quickly enough so that there was enough

time remaining in the 24-hour run to measure the correlation. A standard arrangement for everything used in this experiment was developed, and special length cables reserved for this experiment were made for connecting the electronics. Careful scheduling of the day for the run was necessary in order that all of the required equipment be available. In spite of this diligence, on several days the correlation was not completed even though the beam was available most of the day.

After the equipment was assembled, the next step was to set the gains and the single channel analyzer (S. C. A.) windows. The gain for the gamma rays was set by lowering the coincidence level in one of the coincidence units so that it triggered on singles. The gain could then be adjusted so that the spectrum was spread over the desired number of channels. The gain for the alpha particles was set so the pulses reaching the S. C. A. were between 5 and 10 volts because this was the best operating region for the S. C. A. The gamma-ray S. C. A. was used in the integral mode and set to discriminate against low energy gamma rays. Raising this discriminator decreased the number of randoms. The S. C. A. window for the particles was set on the alpha particles after identifying them with the usual techniques of placing foils in front of the detector and changing the bias. This procedure was complicated by the fact that there were some ^{3}He particles scattered around the spectrometer, but their energy was always lower than the energy of the alphas. The magnetic field was varied to find the setting at which the peak was centered on the slit in front of the detector.

The next step was to set the various pulse widths and delays. Groce (1963) gives the formula

$$t(\text{nanoseconds}) = 202.0 \sqrt{A/E}$$

for the time required for a particle to travel the distance from the target along the mean orbit to the detector, where A is the atomic weight and E is the energy in MeV. The times for the extreme outer and inner orbits are approximately 10% longer and shorter, respectively. For an alpha with E = 14 MeV, t = 108 ± 11 ns. Because of this time spread, because of the walk in the S.C.A.'s, and because it was difficult to set the rather coarse delay controls accurately, a resolving time of 2τ = 120 ns was used, that is, the widths of the logic pulses to the coincidence circuit were 60 ns. To set the appropriate delays for these logic pulses, a measurement of the counting rate versus delay was made and the delay with the maximum counting rate was selected for the "reals" channel. An additional 2 μs was added to the "randoms" channel. The delay on the linear gamma-ray pulses was set by calculating the required delay from the other delays in the circuit and then checked by observing whether every coincidence was stored in the RIDL 400-channel analyzer.

3. Spectra

^{31}S(1.25)

Figure 30 shows the gamma-ray spectrum at $\theta_\gamma = 120^\circ$ from the decay of the level at 1.25 MeV excitation energy in ^{31}S. The gamma-ray S.C.A. was set so that pulses were stored only above channel 34. In Figure 30 the randoms spectrum multiplied by the ratio $\dfrac{\text{number of reals}}{\text{number of randoms}}$ has already been subtracted. This ratio was measured by feeding uncorrelated pulses into both channels

and counting the number of coincidences in both the real and random
channels. This ratio was approximately one for the spectra from
all of the levels. In the spectra from the 1.25 MeV level, the
randoms spectrum typically contained one-third as many counts
as the reals spectrum with most of the counts in channels below
the photopeak. The resolution (FWHM) of the photopeak was 10%
or 130 keV. The gamma-ray singles rate was approximately 50K
per sec and the alpha particles singles rate was approximately 75
per sec. A gamma ray was detected in coincidence with about 2%
of the alpha particles detected. Each angle required about three
hours with a beam of 0.15 μA of 11.2 MeV ^{3}He^{++}.

Figure 31 shows the angular correlation of the gamma
rays in the photopeak normalized to the number of alpha particles
detected. The error bars represent the statistical uncertainties.

^{31}S(2.23)

Figure 32 shows the gamma-ray spectrum at $\theta_\gamma = 135^O$
from the decay of the level at 2.23 MeV excitation energy in ^{31}S.
The randoms spectrum which have already been subtracted in
Figure 32 contained approximately one-third as many counts as
the real spectrum with most of the counts in channels below the
photopeak. The resolution (FWHM) of the photopeak was 8% or 180
keV. The gamma-ray singles rate was approximately 42K per sec
and the alpha particles singles rate was approximately 80 counts
per sec. A gamma ray was detected in coincidence with about 2.6%
of the alphas. Each angle required about three hours with a beam
of 0.18 μA of 8.5 MeV ^{3}He^{++}. The gamma-ray energy calibration
was established with gamma-ray sources.

Figure 33 shows the angular correlation of the gamma rays in the photopeak normalized to the number of alpha particles detected. The error bars represent the statistical uncertainties.

^{31}S(3.08)

Figure 34 shows the sum of the gamma-ray spectra at all angles from the decay of the level at 3.08 MeV excitation energy in ^{31}S. The random spectra which have already been subtracted in Figure 34 contained approximately one-third as many counts as the reals spectra with most of the counts in channels below the photopeak. The resolution (FWHM) of the photopeak was 6% or 190 keV. The gamma-ray singles rate was approximately 50K per sec and the alpha particle singles rate was approximately 6 counts per sec. A gamma ray was detected in coincidence with about 3.2% of the alphas detected. Each angle required about four hours with a beam of 0.2 μA of 8.4 MeV ^{3}He^{++}. The gamma-ray energy calibration was established with gamma-ray sources.

Figure 35 shows the angular correlation of the gamma rays in the photopeak normalized to the number of alpha particles detected. The error bars represent the statistical uncertainties.

^{31}S(3.29)

Figure 36 shows the gamma-ray spectrum from the decay of the level at 3.29 MeV excitation energy in ^{31}S at $\theta_\gamma = 90^\circ$. The random spectrum which has already been subtracted in Figure 36 contained approximately one-fifth as many counts as the reals spectra with most of the counts in channels below channel 60. The

gamma-ray singles rate was approximately 65K per sec and the alpha particle singles rate was approximately 1 count per sec. A gamma ray was detected in coincidence with about 5.3% of the alpha particles detected. Each angle required about six hours with a beam of 75 nA of the 12.0 MeV ^{3}He^{++}. The gamma-ray energy calibration was established with gamma-ray sources.

Figure 37 shows the angular correlation of the photopeak of the 2.04 MeV gamma ray. The error bars represent the statistical uncertainties.

^{31}S(3.35)

Figure 38 shows the sum of the gamma-ray spectra at all angles from the decay of the level at 3.35 MeV excitation energy in ^{31}S. The random spectra which have already been subtracted in Figure 38 contained approximately one-fifth as many counts as the reals spectra with most of the counts in channels below channel 30. The gamma-ray singles rate was approximately 60K per sec and the alpha particles singles rate was approximately 0.5 counts per sec. A gamma ray was detected in coincidence with about 4.5% of the alphas detected. Each angle required about four hours with a beam of 80 nA of 9.0 MeV ^{3}He^{++}. The gamma-ray energy calibration was established with gamma-ray sources.

Figure 39 shows the angular correlation of the photopeak of the 2.11 MeV gamma ray. The error bars represent the statistical uncertainties.

^{31}S(3.44)

Figure 40 shows the sum of the gamma-ray spectra at all angles from the decay of the level at 3.44 MeV excitation energy in ^{31}S. The random spectra which have already been subtracted in Figure 40 contained approximately one-third as many counts as the reals spectra with most of the counts in channels below channel 80. The gamma-ray singles rate was approximately 50K per sec and the alpha particle singles rate was approximately 3 counts per sec. A gamma ray was detected in coincidence with about 3.1% of the alphas detected. Each angle required about five hours with a beam of 70 nA of 12.2 MeV ^{3}He^{++}. The gamma-ray energy calibration was established with gamma-ray sources.

Figure 41 shows the angular correlation of the photopeak of the 3.44 MeV gamma ray. The error bars represent the statistical uncertainties.

4. Analysis of the Data

The attenuation factors Q_k in Formula (6), Section III. B., were calculated with the formulas

$$Q_k = \frac{J_k}{J_o}$$

$$J_k = 2\pi \int_o^\gamma \sin \beta \, d\beta \, P_k(\cos \theta)(1 - e^{-\tau X(\beta)})$$

where

β = angle with respect to the crystal axis

$X(\beta)$ = the distance through the crystal

τ = gamma attenuation coefficient
(from Grodstein, 1957).

(See Figure 42 for the notation as given by Rose (1953)).

These results are given in Table XII.

With $\sigma = 0$ in Formula (4), Section III. B., Q^2 was minimized with respect to $I(1/2)$ for all possible combinations of J_d and J_e and a discrete set of values for x. Then for each combination of J_d and J_e a plot was made of these minima versus arctan x as shown in Figure 43 for example. The dips in these plots correspond to possible solutions. The probability that a given dip is the correct one can be found by referring to χ^2 - probability tables (see Nijgh et al.,1959). The 0.1% confidence limit is shown and only points on these curves which lie below this limit are assumed to be possible solutions.

The values of the mixing ratio x and its error at the minimum were found with an adaptation of a procedure given by Smith (1964) for the analysis of triple correlations. Let x_2 be the value of the mixing ratio near a minimum. Let

$$x_1 = x_2 - d$$

$$x_3 = x_2 + d$$

where d is much less than the width (FWHM) of the dip. Then to a good approximation the center of the dip is $x_2 + \Delta x$ where

$$\Delta x = \frac{Ad}{2B}$$

$$A = Q^2(x_1) - Q^2(x_3)$$

$$B = Q^2(x_1) + Q^2(x_3) - 2Q^2(x_2)$$

furthermore, Q^2 at the minimum is

$$Q^2(x_2) - \frac{A^2}{8B} \,.$$

This process was iterated and found to converge very rapidly. The uncertainty in the mixing ratio is given by

$$\sigma_x = \sqrt{\frac{2d^2}{B(H - P - 1)}}$$

where   H = number of angles

              P = number of magnetic substates with $m_z \geq 0$.

The program for these calculations is given in Appendix D.

^{31}S(1.25)

Level ^{31}S(1.25) decays only to the $1/2^+$ ground state (see Section III.C.5) and therefore only $J_e^\pi = 1/2^+$ must be considered. The coincidence requirement limits the possible lifetime of the level ^{31}S(1.25) to $\tau_\gamma \lesssim 1$ μs and therefore $\Gamma_\gamma \gtrsim 7 \times 10^{-10}$ ev. This limit on Γ_γ limits the possible values of J_d which must be considered in the analysis. The general surveys by Wilkinson (1960) and Skorka et al.(1966) of the measured transition strengths in light nuclei give some guide to the maximum transition strengths for various values of J_d. For electric transitions, which are usually stronger than magnetic transitions, the limits on Γ_γ for various values of J_d are:

J_d	Transition	Γ_γ(ev)
1/2	E1	$\lesssim 10^{-2}$
3/2	E1	$\lesssim 10^{-2}$
5/2	E2	$\lesssim 10^{-4}$
7/2	E3	$\lesssim 10^{-9}$
9/2	E4	$\lesssim 10^{-17}$

Since for this level $\Gamma_\gamma \geq 7 \times 10^{-10}$ ev , only values of $J_d \leq 7/2$ must be considered.

Figure 43 shows the minimum of Q^2 with respect to I(1/2) as a function of arctan x for all allowed combinations of J_d and J_e. All of these curves were calculated with $\sigma = 0$ in Formula (4), Section III.B. Only $J_d = 3/2$ gives a fit and x is restricted to two values. Fou and Zurmuhle (1966) found $\ell_n = 2$ for this level and

therefore the parity is positive and the gamma-ray transition is an M1, E2 mixture which is consistent with $\sigma = 0$. The results are given in Table XII. The fit to the correlation data is shown in Figure 31.

^{31}S(2. 23)

Level ^{31}S(2. 23) decays only to the $1/2^+$ ground state (see Section III. C. 5) and therefore only $J_e^{\pi} = 1/2^+$ must be considered. The limits on Γ_γ for various values of J_d are:

J_d	Transition	Γ_γ(ev)
1/2	E1	$\lesssim 10^{-1}$
3/2	E1	$\lesssim 10^{-1}$
5/2	E2	$\lesssim 10^{-2}$
7/2	E3	$\lesssim 10^{-7}$
9/2	E4	$\lesssim 10^{-14}$

Since the coincidence requires $\Gamma_\gamma \geq 7 \times 10^{-10}$ ev , only values of $J_d \leq 7/2$ must be considered.

Figure 44 shows the minimum of Q^2 with respect to $I(1/2)$ as a function of arctan x for all allowed combinations of J_d and J_e. All of these curves were calculated with $\sigma = 0$ in Formula (4), Section III. B. Only $J_d = 5/2$ gives a fit and x is restricted to two values. Fou and Zurmuhle (1966) found $\ell_n = 2$ for this level and therefore the parity is positive and the gamma-ray transition is an E2, M3 mixture which is inconsistent with $\sigma = 0$. To correct this,

it is only necessary to change the signs of the mixing ratios calcu-
lated from Figure 44. Thus, the values are x = -.053 ± .036 and
-2.411 ± .243. The results are given in Table XII. The fit to the
correlation data is shown in Figure 33.

$^{31}S(3.08)$

Level $^{31}S(3.08)$ decays only to the $1/2^+$ ground state (see
Section III.C.5) and therefore only $J_e^{\pi} = 1/2^+$ must be considered.
The limits on Γ_γ for various values of J_d are:

J_d	Transition	Γ_γ(ev)
1/2	E1	$\lesssim 10^{-1}$
3/2	E1	$\lesssim 10^{-1}$
5/2	E2	$\lesssim 10^{-2}$
7/2	E3	$\lesssim 10^{-6}$
9/2	E4	$\lesssim 10^{-13}$

Since the coincidence requires $\Gamma_\gamma \gtrsim .7 \times 10^{-10}$ ev , only values of
$J_d \leq 7/2$ must be considered.

Figure 45 shows the minimum of Q^2 with respect to
I(1/2) as a function of arctan x for all allowed combinations of
J_d and J_e. All of these curves were calculated with $\sigma = 0$ in
Formula (4), Section III.B. Both $J_d = 1/2$ and $J_d = 3/2$ give fits.
It was found that $\ell_n = 0$ for this level (see Section II.C.) and therefore
$J_d^{\pi} = 1/2^+$. The results are given in Table XII. The fit to the
correlation data is shown in Figure 35.

^{31}S(3.29)

Level ^{31}S(3.29) decays to both the $3/2^+$ level at 1.25 MeV and the $5/2^+$ level at 2.23 MeV (see Section III.C.5). For the transition to the $3/2^+$ level at 1.25 MeV, $J_e = 3/2^+$. The limits on Γ_γ for this transition are:

J_d	Transition	Γ_γ(ev)
1/2	E1	$\lesssim 10^{-1}$
3/2	E1	$\lesssim 10^{-1}$
5/2	E1	$\lesssim 10^{-1}$
7/2	E2	$\lesssim 10^{-3}$
9/2	E3	$\lesssim 10^{-8}$
11/2	E4	$\lesssim 10^{-14}$

Since the coincidence requires $\Gamma_\gamma \gtrsim 7 \times 10^{-10}$ ev , only values of $J_d \leq 9/2$ must be considered.

Figure 46 shows the minimum of Q^2 with respect to $I(1/2)$ as a function of arctan x for all allowed combinations of J_d and J_e. All of these curves were calculated with $\sigma = 0$ in Formula (4), Section III. B. Both $J_d = 3/2$ and $J_d = 5/2$ give fits, but $J_d = 5/2$ is favored. It was found that $\ell_n = 2$ for this level (see Section II.C.) and therefore the parity is positive and the gamma-ray transition is an M1, E2 mixture which is consistent with $\sigma = 0$ for both $J_d^\pi = 3/2^+$ and $J_d^\pi = 5/2^+$. The results are given in Table XII. The fits to the correlation data are shown in Figure 37.

For the transition to the $5/2^+$ level at 2.23 MeV the statistical uncertainties in the data were so large that nothing useful was found from the correlation analysis.

For both the cascade through the $3/2^+$ level at 1.25 MeV and the cascade through the $5/2^+$ level at 2.23 MeV, an extension of the analysis was made to analyze the angular correlation of the second gamma-ray transition. The parameters in these cases were very insensitive to the present data, and nothing useful was found.

^{31}S(3.35)

Level ^{31}S(3.35) decays only to the $3/2^+$ level at 1.25 MeV (see Section III. C. 5) and therefore only $J_e^\pi = 3/2^+$ must be considered. The limits on Γ_γ for various values of J_d are:

J_d	Transition	Γ_γ(ev)
1/2	E1	$\lesssim 10^{-1}$
3/2	E1	$\lesssim 10^{-1}$
5/2	E1	$\lesssim 10^{-1}$
7/2	E2	$\lesssim 10^{-3}$
9/2	E3	$\lesssim 10^{-7}$
11/2	E4	$\lesssim 10^{-14}$

Since the coincidence requires $\Gamma_\gamma \gtrsim 7 \times 10^{-10}$ ev , only values of $J_d \leq 9/2$ must be considered.

Figure 47 shows the minimum of Q^2 with respect to $I(1/2)$ as a function of arctan x for all allowed combinations of J_d and J_e. All of these curves were calculated with $\sigma = 0$ in Formula (4), Section III. B. Fits were obtained for $J_d = 7/2$, $3/2$, $9/2$, and $5/2$ in the order of preference. Since there is only a 1% probability that $J_d = 9/2$ is a fit and only a 0.3% probability that $J_d = 5/2$ is a fit, these two values are not considered further. The parity is assumed positive because the parities of all of the levels in the analog ^{31}P up to 4.3 MeV excitation energy are positive (see Section IV. A). For $J_d^\pi = 7/2^+$, the gamma-ray transition is an E2, M3 mixture which is inconsistent with $\sigma = 0$. To correct this it is only necessary to change the signs of the mixing ratios calculated from Figure 47. Thus, the values are x = -.467 ± .521 and -2.204 ± 2.920 for $J_d^\pi = 7/2^+$. For $J_d^\pi = 3/2^+$, the gamma-ray transition is an M1, E2 mixture which is consistent with $\sigma = 0$ and no correction is necessary. The results are given in Table XII. The fits to the correlation data are shown in Figure 39.

The second gamma-ray transition of the cascade through the $3/2^+$ level at 1.25 MeV was analyzed, but again the parameters were insensitive and nothing useful was found.

$^{31}S(3.44)$

Level $^{31}S(3.44)$ decays to the $1/2^+$ ground state and to either the $3/2^+$ level at 1.25 MeV or the $5/2^+$ level at 2.23 MeV or both (see Section III. C. 5). For the decay to the ground state, $J_e^\pi = 1/2^+$. The limits on Γ_γ for various values of J_d are:

J_d	Transition	Γ_γ(ev)
1/2	E1	$\lesssim 10^{-1}$
3/2	E1	$\lesssim 10^{-1}$
5/2	E1	$\lesssim 10^{-2}$
7/2	E2	$\lesssim 10^{-6}$
9/2	E3	$\lesssim 10^{-13}$

Since the coincidence requires $\Gamma_\gamma \gtrsim 7 \times 10^{-10}$ ev , only values of $J_d \leq 7/2$ must be considered.

Figure 48 shows the minimum of Q^2 with respect to $I(1/2)$ as a function of arctan x for all allowed combinations of J_d and J_e. All of these curves were calculated with $\sigma = 0$ in Formula (4), Section III. B. Only the curve for $J_d = 3/2$ fits. It was found that $\ell_n = (2)$ for this level (see Section II. C) and therefore the parity is tentatively positive and the gamma-ray transition is tentatively an M1, E2 mixture which is consistent with $\sigma = 0$. The results are given in Table XII. The fit to the correlation data is shown in Figure 41.

The photopeak yields were also fitted with a series of Legendre polynomials

$$\sum_{k \text{ even}} a_k Q_k P_k(\cos \theta)$$

where $k \leq 2J_d$ for simple decay or $k \leq \min (2J_d, 2J_e)$ for the second gamma ray in a cascade. The uncertainties were assigned in the standard manner as described in Nijgh et al. (1959). The normalized coefficients, that is a_k/a_o, and their uncertainties are given in Table XII.

5. Branching Ratios

To measure branching ratios, the lucite target chamber top was replaced with an aluminum cup covered with tantalum into which a 10.16 cm × 10.16 cm NaI(Tl) crystal could be inserted (see Figure 49). This allowed the front face to be placed at 3.556 cm from the center of the beam spot and thus increased the efficiency. It was necessary to make separate runs for the branching ratios because there was not enough electronic equipment available to measure the branching ratios and the correlations simultaneously. In some cases, runs with the aluminum cup were not taken and only the correlation spectra were used to determine the branching ratios. Except for the aluminum cup the setup was the same as that used for the correlation measurements.

^{31}S(2.23)

The gamma-ray decay spectrum taken with the aluminum cup of the level at an excitation energy of 2.23 MeV in ^{31}S is shown in Figure 50(a). Figure 50(c) shows a standard gamma-ray line shape obtained by observing the reaction ^{12}C(^{3}He, p)^{14}N to the level at 2.311 MeV excitation in ^{14}N and observing the gamma rays from the decay of this level in coincidence with the protons. Figure

50(b) shows a line shape for a 1.25 MeV gamma ray obtained by observing the reaction $^{32}S(^{3}He, \alpha)^{31}S$ to the level at 1.25 MeV excitation energy in ^{31}S and observing the gamma rays from the decay of this level in coincidence with the alphas.

To calculate a branching ratio limit to the state at 1.25 it was assumed that the line shape for a 2.23 MeV gamma ray was well approximated by the line shape for the 2.311 MeV gamma ray. The gain and normalization of the 2.31 MeV line shape spectrum were adjusted with the computer so that the 2.31 MeV photopeak matched the 2.23. Then various amounts of the 1.25 MeV line shape with appropriate gain were added to the 2.31 line shape until the composite just exceeded the statistical uncertainties in the region of the 1.25 MeV photopeak in the spectrum from the decay of the 2.23 MeV level. In this mixture if $Y(90^{O})_{1.25 \text{ photopeak}}$ is the number of counts in the 1.25 MeV gamma-ray peak and $Y(90^{O})_{2.23 \text{ photopeak}}$ is the number of counts in the 2.31 MeV gamma-ray peak, then

$$\frac{N_{1.25}}{N_{2.23}} \leq \frac{Y(90^{O})_{1.25 \text{ photopeak}}}{Y(90^{O})_{2.23 \text{ photopeak}}} \frac{PF_{2.23}}{PF_{1.25}} \frac{J_{o}^{2.23}}{J_{o}^{1.25}}$$

$$\frac{(a_{o}^{2.23} + a_{2}^{2.23} Q_{2}^{2.23} P_{2}(\cos 90^{O}))}{(a_{o}^{1.25} + a_{2}^{1.25} Q_{2}^{1.25} P_{2}(\cos 90^{O}))_{\min}} \qquad (10)$$

where

$N_{1.25}$ = number of events in which the 2.23 MeV level cascaded through the 1.25 MeV level and an α was detected.

$N_{2.23}$ = number of events in which the 2.23 MeV level decayed directly to the ground state and an α was detected.

$PF_{2.23}$ = photofraction for a 2.23 MeV gamma ray (from Weitkamp, 1963).

$PF_{1.25}$ = photofraction for a 1.25 MeV gamma ray (from Weitkamp, 1963).

$J_O^{2.23}$ = total efficiency for a 2.23 MeV gamma ray.

$J_O^{1.25}$ = total efficiency for a 1.25 MeV gamma ray.

$(a_O^{2.23} + \ldots)$ = relative angular correlation yield ($a_O = 1$) of 2.23 MeV gamma ray for the parameters found with the χ^2 analysis.

$(a_O^{1.25} + \ldots)$ = minimum with respect to $x_{2.23 \to 1.25}$ of the relative angular correlation yield ($a_O = 1$) for the 1.25 MeV gamma ray in the cascade.

This formula yields $\dfrac{N_{1.25}}{N_{2.23}} \leq .029$ and therefore

$$\text{branching to 1.25 MeV level} = \frac{\dfrac{N_{1.25}}{N_{2.23}}}{1 + \dfrac{N_{1.25}}{N_{2.23}}} \leq 3\% \, ,$$

to ground state $\geq 97\%$. (See Figure 53.)

^{31}S(3.08)

The analysis of branching of the decay of the 3.08 MeV level was very similar. The line shape of a 3.08 MeV gamma ray was obtained by observing the gamma rays from the decay of ^{11}B(^{3}He, p)^{13}C(3.09). The 2.311 MeV line shape was used as an approximation to the line shape of a 2.23 MeV gamma ray in the 3.08 → 2.23 → 0 cascade. The 1.25 MeV line shape was used for the 1.25 MeV gamma ray in the 3.09 → 1.25 → 0 cascade. Using a formula similar to Formula (10) above yields

$$\frac{N_{2.23}}{N_{3.08}} \leq .09$$

$$\frac{N_{1.25}}{N_{3.08}} \leq .15$$

and therefore

branching to 2.23 level	$\leq$	8%
to 1.25 level	$\leq$	13%
to ground state	$\geq$	85% .

^{31}S(3.29)

The branching ratios for the decay of the 3.29 MeV level were extracted from the correlation spectra because no spectrum with the aluminum cup was taken. To calculate a limit on a possible branch to the ground state the counts in

channels 170 through 180 corresponding to the photopeak of a 3.29 gamma ray were summed at each angle. The yields were normalized to the number of particles detected in coincidence. The resulting correlation was fitted with an expansion in Legendre polynomials.

$$\sum_{k \text{ even}} a_k P_k(\cos \theta)$$

where $k \leq 4$ because the spin of the 3.29 level was found to be $5/2^+$ (see Section III.C.4). Similarly, the angular correlation of the 2.04 MeV gamma ray after subtracting the contribution from the 2.23 MeV gamma ray, emitted in the cascade of the 3.29 to 1.25 MeV level was fitted with an expansion in Legendre polynomials. Then

$$\frac{N_{3.29}}{N_{2.04}} = \frac{PF_{2.04}}{PF_{3.29}} \frac{J_o^{2.04}}{J_o^{3.29}} \frac{a_o^{3.29}}{a_o^{2.04}}$$

where

$N_{3.29}$ = number of events in which the 3.29 MeV level decays directly to the ground state and an α was detected.

$N_{2.04}$ = number of events in which the 3.29 MeV level cascades through the 1.25 MeV level and an α was detected.

$PF_{2.04}$ = photofraction for a 2.04 MeV gamma ray (from Weitkamp, 1963).

$PF_{3.29}$ = photofraction for a 3.29 MeV gamma ray (from Weitkamp, 1963).

$J_o^{2.04}$ = total efficiency for a 2.04 MeV gamma ray.

$J_o^{3.29}$ = total efficiency for a 3.29 MeV gamma ray.

This gives

$$\frac{N_{3.29}}{N_{2.04}} \leq .184.$$

Similar analyses were done to obtain branching ratios for branches to the level at 3.08 MeV and the level at 2.23. These gave

$$\frac{N_{3.08}}{N_{2.04}} \leq .227$$

$$\frac{N_{2.23}}{N_{2.04}} = .326 \pm .049.$$

These results were combined to give

branching to ground state $\qquad \leq \quad 12\%$

$\qquad$ to 1.25 MeV level $\quad = 75^{+3}_{-12}\%$

$\qquad$ to 2.23 MeV level $\quad = 25^{+3}_{-6}\%$

$\qquad$ to 3.08 MeV level $\quad \leq \quad 15\%$.

^{31}S(3.35)

Figure 51 shows the gamma-ray spectrum for the decay of the level at 3.35 MeV excitation obtained with the aluminum cup. The analysis was similar to that for ^{31}S(2.23). The results were

branching to ground state $\qquad \leq \quad 6\%$

$\qquad$ to 1.25 MeV level $\quad \geq \quad 78\%$

$\qquad$ to 2.23 MeV level $\quad \leq \quad 21\%$

$\qquad$ to 3.08 MeV level $\quad \leq \quad 6\%$.

^{31}S(3.44)

The branching ratios for the decay of the level at 3.44 MeV were extracted from the correlation spectra because no spectrum was taken with the aluminum cup. The analysis was similar to that for the level at 3.29. The results were

branching to ground state $\qquad = 46^{+3}_{-4}$

$\left.\begin{array}{l}\text{to 1.25 MeV level} \\ \text{to 2.23 MeV level}\end{array}\right\} = 54^{+3}_{-4}\%$

$\qquad$ to 3.08 MeV level $\quad \leq \quad 2\%$.

IV. DISCUSSION OF ^{31}S LEVELS

A. Comparison with ^{31}P

Figure 52 shows the energy level diagrams for ^{31}S and ^{31}P.
All of the information on ^{31}S was determined in the present experi-
ment except the ℓ_n-values for the levels at 1.25, 2.23 and 7.04
(see Section II. C. 6). The information on ^{31}P published since the
compilation by Endt and van der Leun (1962) was completed comes
from studies of the reactions ^{30}Si(p, γ)^{31}P (Harris and Seagondollar,
1962; Harris and Seagondollar, 1963; Harris and Hennecke, 1964;
van Rinsvelt and Smith, 1964; Harris and Breitenbecher, 1966;
van Rinsvelt and Endt, 1966; Willmes and Harris, 1967), and
^{30}Si(d, n)^{31}P (Cujec et al., 1965; Davies et al., 1965). Figure 53
shows the gamma-ray decay schemes and Table XIII compares the
mixing ratios. A comparison of the signs of the mixing ratios for
^{31}S and ^{31}P is meaningless because different phase conventions
were used for the mixing ratios in ^{31}P. These phase conventions
are given in the references cited in the footnotes to Table XIII.

The levels at 1.25, 2.23, and 3.08 MeV in ^{31}S have,
respectively, the same spin, parity, and decay scheme as the
levels at 1.25, 2.23, and 3.13 MeV in ^{31}P. These levels are
assumed to be isobaric analogs.

For the 5/2$^+$ level at 3.29 MeV in ^{31}P, the only possibilities
for an analog are the 5/2$^+$ (3/2)$^+$ level at 3.29 MeV and the (7/2,
3/2) level at 3.35 MeV in ^{31}S. The decay scheme of the 3.29 MeV
level in ^{31}P matches the decay scheme of the 3.29 MeV level in
^{31}S but does not match the decay scheme of the 3.35 MeV level.
Therefore the 3.29 MeV level in ^{31}P is assumed to be the isobaric
analog of the 3.29 MeV level in ^{31}S.

For the $7/2^+$ level at 3.41 MeV in ^{31}P the only possible analog is the $(7/2, 3/2)$ level at 3.35 MeV in ^{31}S because this is the only level in this excitation region which can be fitted with $J = 7/2$. Furthermore, the decay schemes match.

For the $3/2^+$ level at 3.51 MeV in ^{31}P the only remaining possibility is the $3/2^{(+)}$ level in ^{31}S at 3.44 MeV. Again the decay schemes match.

For the higher levels one can only speculate on which levels are analogs on the basis of the present information. If the order of levels is the same in ^{31}P and ^{31}S, then one might propose the following analogs.

^{31}P		^{31}S	
4.19 MeV,	$5/2^+$	4.08 MeV,	$(5/2^+)$
4.26 ,	$3/2^+$	4.21	
4.43 ,	$7/2^-$	4.46	, $\ell_n = 3$
4.59 ,	$5/2^+$	4.52	, $\ell_n = 2$
4.63 ,	$3/2$	4.58	
4.78 ,	$5/2, (7/2)$	4.72	, $\ell_n = 2, (3)$
5.01 ,	$3/2^-$	4.87	, $\ell_n = 1$
5.12		4.97	, $\ell_n = 1$
5.25 ,	$(1/2)$	5.15	, $1/2^+$

The only inconsistency is the lack of an analog for the (5.03) MeV level in ^{31}S. This is not unexpected since the experiments with the reaction ^{30}Si(d, n)^{31}P may not have resolved this level and the experiments with the reaction ^{30}Si(p, γ)^{31}P may not have populated it.

B. Comparison with Models

The low-lying $1/2^+$ level and $7/2^+$ level in ^{31}P and ^{31}S predicted by Broude et al. (1958) and Glaudemans et al. (1964) (see Figure 2) and mentioned in the Introduction (Section I. A.) have been located. In ^{31}P van Rinsvelt and Endt (1964) located the $1/2^+$ level at 3.13 MeV excitation and van Rinsvelt and Smith (1964) located the $7/2^+$ level at 3.41 MeV excitation. In ^{31}S the $1/2^+$ level has been located in the present experiment at 3.08 MeV excitation and the $7/2^+$ tentatively at 3.35 MeV.

The Nilsson model calculation by Broude et al. (1958) was based on the incorrect assignment of $J^\pi = 3/2^+$ to the level at 3.13 MeV excitation in ^{31}P. Broude et al. (1958) assumed that the level was the second member of a rotational band based on Nilsson orbit number 9 ($1/2^+$, ground state; $3/2^+$, 3.13 MeV; $5/2^+$, 2.23 MeV) while the other low-lying levels were obtained by coupling two bands based on orbits 8 and 11. Subsequently, Kossanyi-Demay et al. (1965) found that $\frac{BE2(0 \to 2.23 \text{ MeV})}{BE2(0 \to 3.13 \text{ MeV})} \sim 9$ from inelastic electron scattering which disagrees with the expected value of 3/2 for levels of the same band. Also van Rinsvelt and Endt (1964) assigned $J^\pi = 1/2^+$ to the 3.13 MeV level in ^{31}P by means of a polarization measurement, and the analog at 3.08 MeV in ^{31}S was assigned $J^\pi = 1/2^+$ in the present experiment. On the basis of the information for ^{31}P, Bishop et al. (1965) identified the 3.13 MeV level with Nilsson orbit number 11 and repeated the calculations. Couplings between the three rotational bands based on the Nilsson orbits 8, 9, and 11 were allowed. A range of values for the parameters μ, $\varkappa$, and η (standard notation) were chosen from considerations of neighboring nuclei. Figure 54, column 1, shows

the results for $\mu = 0.167$, $\varkappa = 0.05$, and $\eta = -3$. There is a serious disagreement with experiment, and similar disagreements were obtained for other choices of these parameters. No computed electromagnetic properties were reported. Bishop et al. (1965) concluded that it was rather difficult to explain the level scheme of ^{31}P with the Nilsson model.

Kamavataram (1966) generalized the Nilsson model for ^{31}P to take into account three nucleons outside of a ^{28}Si core. The ground state of ^{31}P has two neutrons and a proton in Nilsson orbit 9. For the low-lying $1/2^+$, $3/2^+$, and $5/2^+$ excited states, Kamavataram considered the excitation of one of these three nucleons into higher Nilsson orbits of positive parity and the different possible parent states of the other two nucleons in constructing properly anti-symmetrized $T = 1/2$ wave functions. Kamavataram (1966) tabulated the configurations of three particle states of ^{31}P. The Hamiltonian consisted of a collective part and a part which took into account two-body residual interaction (see Brink and Kerman, 1959). The parameters were selected from a consideration of neighboring nuclei. Calculating the matrix elements of this Hamiltonian with the wave functions described above and diagonalizing yielded the results shown in Figure 54, column 2. Here $\eta = -2$ and $\mu = 0.3$ and the residual interaction is 0.5 MeV. No computed electromagnetic properties were reported. This more complicated model is in better agreement with experiment than the simple Nilsson model is, but it fails to predict a low-lying $7/2^+$ level.

Chi and Davidson (1963) proposed a modification of the Nilsson model in which the extra nucleon was coupled to an asymmetric core rather than the usual symmetric core. The Hamiltonian consisted of

two parts: H_R, the Hamiltonian for a rotating core of fixed shape
with quadrupole moments of inertia, and H_P, the Hamiltonian for
the single particle moving in an asymmetric oscillator potential
with $\vec{\imath} \cdot \vec{s}$ and $\vec{\imath}^2$ terms. The energy eigenvalues were obtained
by an exact diagonalization of this Hamiltonian using an appropriate
core-particle basis. The model was applied throughout the 2s-1d
shell, and for all nuclei for which there was sufficient experimental
information, the three model parameters (P, a core strength
parameter, and the usual β and γ parameters) were determined.
For ^{31}P, P = 0.180, β = 0.205, and γ = 31.0°, and the predicted
energy levels are shown in Figure 54, column 3. This model also
is in better agreement with experiment than the simple Nilsson
model is, but it fails to predict a $1/2^+$ level other than the ground
state below 5 MeV. The computed mean life of the 1.27 MeV state
in ^{31}P is 11.1 ps which disagrees with the value of 0.5 ps
measured by Levesque et al. (1962).

Glaudemans et al. (1964) assumed an inert ^{28}Si core and
performed a shell-model calculation for the nucleons outside of
this core. Fifteen interaction energies and two binding energies of
$2s_{1/2}$ and $1d_{3/2}$ nucleons to a ^{28}Si core were determined by a
least-squares fit to 50 well established levels in the nuclei from
^{29}Si to ^{40}Ca. From the best values of the 17 parameters thereby
obtained, the energies and wave functions of 377 levels in this
mass region were calculated. The results for A = 31 are shown
in Figure 54, column 4. The agreement with experiment is fairly
good except that the $5/2^+$ level at 2.23 MeV is not reproduced.
The authors concluded, therefore, that it probably arises from
excitation of the ^{28}Si core. Wiechers and Brussaard (1965), using
the wave functions obtained with this model, calculated the level

widths for M1 transitions to the ground state of ^{31}P from the 1.27 and 3.13 MeV levels and to the ground state of ^{31}S from the 1.25 MeV level. For the 1.27 MeV level in ^{31}P the calculated width $\Gamma(M1) = 0.0460 \times 10^{-3}$ ev is too small compared to the experimental width $\Gamma(M1) = 2.8 \times 10^{-3}$ ev, (Booth and Wright, 1962). For the 2.23 MeV level in ^{31}P the calculated width $\Gamma(M1) = 86.0 \times 10^{-3}$ ev is in good agreement with the experimental width $\Gamma(M1) \simeq 60.0 \times 10^{-3}$ ev, (Booth and Wright, 1962). For the 1.25 MeV level in ^{31}S the calculated width $\Gamma(M1) = 0.0589 \times 10^{-3}$ ev has not been checked experimentally.

Thankappan (1962) proposed a model for ^{31}P in which the odd proton was coupled to a vibrating ^{30}Si core. Core vibration modes through three phonons were included. The first excited state of ^{30}Si at 2.24 MeV was interpreted as the first excited state of the core, which gives $\hbar\omega = 2.24$ MeV. Two other parameters of the model, namely, the separation energy Δ of the single particle states $2s_{1/2}$ and $1d_{3/2}$ and the constant q indicating the strength of the coupling of the odd particle to the collective oscillation of the core, were considered as free parameters and adjusted to obtain the best agreement of the calculated and the observed energy levels. The level spectrum, shown in Figure 54, column 5, is in fairly good agreement with experiment. A fourth parameter k was introduced in the calculations of the electromagnetic transition probabilities. For k = 10 MeV, Thankappan calculated that the second $3/2^+$ level in ^{31}P which was thought to be the 3.13 MeV level, decays in the ratios 55; 18; 27 to the 0, 1.27, and 2.23 MeV levels, respectively. However, experimentally the 3.13 MeV level decays by at least 99% to the ground state (van Rinsvelt and Endt, 1966). Subsequent to these calculations, it was shown, as mentioned above, that the

3. 13 MeV level has $J^{\pi} = 1/2^+$, and therefore the second $3/2^+$ level in ^{31}P should be identified with the 3. 51 MeV level. The experiment branching ratios from the 3. 51 MeV level to the 0, 1. 27, and 2. 23 levels are 64: 20: 16, respectively (Harris and Breitenbecher, 1966) in good agreement with the calculated ratios. The calculated mixing ratios for these transitions are also in good agreement with experiment. For k = 10 MeV, Thankappan calculated that the $5/2^+$ level at 2. 23 in ^{31}P decays in the ratios 47: 53 to the 0 and 1. 27 MeV levels, respectively. However, experimentally the 2. 23 MeV level decays by at least 97% to the ground state (Endt and van der Leun, 1962). For k = 10 MeV the mixing ratio for the decay of the 1. 27 MeV level is x = 7. 8 which disagrees with the experimental value of 0. 28 (van Rinsvelt and Smith, 1964).

Crawley (1965) proposed a model for ^{31}P in which a $2s_{1/2}$ hole was coupled to ^{32}S core excitations. The dashed lines in Figure 54 indicate the proposed coupling scheme. This was based on the inelastic scattering of 17. 5 MeV protons from ^{31}P and ^{32}S. Strongly excited levels with similar angular distributions were assumed to correspond. This model incorporates the $7/2^-$ level at 4. 43 MeV and predicts a $5/2^-$ level at 5. 66 MeV. The model also predicts a $5/2^+$ and $9/2^+$ for levels at 4. 78 and 5. 34 MeV, respectively. Subsequently Cujec et al. (1965) found $J^{\pi} = 1/2^+$ for the 5. 25 MeV level which is probably the 5. 34 MeV level of Crawley. No electromagnetic properties were reported for this model. This model had been proposed earlier by Clegg and Foley (1961) but there was not enough experimental information available at that time for meaningful conclusions.

Of the several models summarized here Thankappan's model with the vibrating core seems to give the best fit to experiment.

The well established rotational structure near A = 25 (see Litherland et al., 1958) gives way to a vibrational structure near A = 30. Many more measurements are needed to test this. In particular, if ^{30}Si and its analog ^{30}S have a vibrational structure, there should be an approximately degenerate 0^+, 2^+, 4^+ triplet near 4 MeV excitation. There are three levels in ^{30}Si at 3.51, 3.77, and 3.79 MeV. For the 3.51 MeV level $J^\pi = 2^+$, but for the 3.77 and 3.79 MeV levels, values for J^π have not been determined. In ^{30}S two levels have been located at 3.43 and 3.71 MeV excitation (McMurray et al., 1967) but values for J^π for these levels have not been determined.

V. $^{32}S(^3He, d)^{33}Cl$

A. Excitation Energies of Levels in ^{33}Cl

1. Introduction

This section describes the results from the deuteron spectra from the reaction $^{32}S(^3He, d)^{33}Cl$ which were obtained as a by-product of the alpha particle spectra from the reaction $^{32}S(^3He, \alpha)^{31}S$ described in Section II. B. In addition, some information obtained by extensions of the deuteron spectra to higher excitation energies in ^{33}Cl is presented.

It was useful to analyze the deuteron spectra because, of the reactions listed by Endt and van der Leun (1962)

1)	$^{32}S(p, \gamma)^{33}Cl$	Q = 2.285
2)	$^{32}S(p, p')^{32}S$	2.285
3)	$^{32}S(d, n)^{33}Cl$	.060
4)	$^{33}S(p, n)^{33}Cl$	-6.358
5)	$^{31}P(^3He, n)^{33}Cl$	3.430
6)	$^{32}S(^3He, d)^{33}Cl$	-3.208
7)	$^{32}S(\alpha, t)^{33}Cl$	-17.528
8)	$^{33}S(^3He, t)^{33}Cl$	-5.593
9)	$^{35}Cl(p, t)^{33}Cl$	-15.663
10)	$^{36}Ar(p, \alpha)^{33}Cl$	-4.355

reaction 6) is the most suitable for locating low-lying levels in ^{33}Cl. In previous studies of reaction 1) (see Endt and van der Leun, 1962) not all of the low-lying levels predicted from the mirror nucleus ^{33}S were populated. Reaction 2) does not populate low-lying levels. Reactions 3), 4), and 5) emit neutrons. Reactions 7) and 9) have large negative Q-values and reaction 8) is not suitable because it is difficult to distinguish between low-energy tritons and ^{3}He^{+} particles in the spectrometer. Reaction 10) is also suitable, and a study of the reaction is described in Section VI.

The description is divided as follows: Section 2 describes the deuteron spectra from the reaction ^{32}S(^{3}He, d)^{33}Cl obtained as a by-product of the alpha particle spectra from the reaction ^{32}S(^{3}He, α)^{31}S. Sections 2 and 3 describe, respectively, single detector spectra and four detector array spectra corresponding to higher excitations in ^{33}Cl.

The single detector, and later a four detector array, was used when it was discovered that the sixteen detector was temporarily unusable for deuterons of energy $\leq$ 5 MeV.

2. Sixteen Detector Array Spectra

(i) Experimental details

Since the deuteron spectra from the reaction ^{32}S(^{3}He, d)^{33}Cl were taken simultaneously with the alpha spectra from the reaction ^{32}S(^{3}He, α)^{31}S described in Section II. B., the experimental details were identical. With a bias of 20 volts on the detectors the pulses from the protons were smaller than those

from the deuterons. The same program described in Appendix C was used to reduce the data to spectra.

(ii) Discussion of spectra

The deuteron spectra are shown in Figure 55. As before, the peaks were first identified by a non-relativistic kinematics program which calculated the mass of the target nucleus and the Q-value of the reaction from the frequencies at two or more angles after correcting for the target thickness. Masses were typically determined to ± 1 AMU. Then a relativistically correct program was used to check the identification. Since some levels were seen at only two angles, the spectra were carefully checked for levels from the expected contaminants ^{12}C, ^{13}C, ^{16}O, ^{28}Si, ^{33}S, and ^{34}S. Peaks from the reaction $^{12}C(^3He, d)^{13}N$ and $^{16}O(^3He, d)^{17}F$ are labeled in Figure 55. The identifications of the peaks from the reaction $^{34}S(^3He, d)^{35}Cl$ were facilitated by some spectra of this reaction taken by Dr. J. Dubois under similar conditions with ^{34}S targets. No levels from ^{13}C, ^{28}Si, or ^{33}S were observed. As a further check on these identifications the yields from natural and enriched targets were compared.

Levels (2) and (7) are only weakly populated in this reaction. Level (2), most readily seen in Figure 50(e), was tentatively located in these spectra by calculating its position from its excitation energy measured in the reaction $^{36}Ar(p, \alpha)^{33}Cl$ (see Section VI) and by comparing the natural and enriched target spectra at 45°. The identification was made more difficult by the fact that one or more peaks from the reaction $^{34}S(^3He, d)^{35}Cl$ were not resolved from level (2).

The known doublet (Endt and van der Leun, 1962) at 2.848 - 2.856 MeV excitation energy was not resolved and no attempt has been made to determine the relative intensities of these levels. The contributions to the resolution of a typical peak in the spectra shown in Figure 55 are listed in Table XIV, and the observed resolution was 10 keV (FWHM).

(iii) Calculations of excitation energies

The excitation energies and Q-values for levels in ^{33}Cl were calculated with the program described in Appendix A after suitable modification to account for the fact that deuterons and not alpha particles were being emitted. Table XV lists the results for the excitation energies for the spectra shown in Figure 55. As before, to obtain final excitation energies, an average of the excitation energies calculated from selected peaks was taken and the results are shown. Q-values for the ground state of ^{33}Cl are given in Table XVI.

Q-values for the reaction ^{34}S(^{3}He, d)^{35}Cl were also calculated with this program and then combined with Q_{GS} = .8764 ± .0030 (Maples et al., 1966) to find the excitation energies which are listed in Table XVII.

(iv) Results

Table XV compares the present results for ^{33}Cl with those reported previously. The present experiment obtained accurate excitation energies for levels (2) and (3) and located levels (4) and (7). For the ground state, the present experiment found

$$Q_{GS} = -3.217 \pm 5 \ .$$

Using this value and the 1964 Mass Table (Mattauch et al., 1965) for the mass excesses

^{32}S	-26012.7 ± 0.9 keV
^{3}He	$14931.34 \pm .21$
D	$13135.91 \pm .13$

yields

^{33}Cl	$-21000. \pm 5 \ .$

This is to be compared with the mass excess quoted for ^{33}Cl in the 1964 Mass Table;

$$-21014 \pm 12 \ .$$

Table XVII compares the present results for ^{35}Cl with those reported previously. The Q-value for the ground state of ^{35}Cl is known to $\pm$ 3 keV (Maples et al., 1966) and the excitation energies of the levels in ^{35}Cl at 4.058 and 4.174 MeV are known to $\pm$ 5 keV (Endt and van der Leun, 1962). The good agreement of the excitation energies found in the present experiment for these levels with the excitation energies given by Endt and van der Leun (1962) is a check on the ground state Q-value for the reaction ^{32}S(^{3}He, d)^{33}Cl and a further check on the ground state Q-value

for the reaction $^{32}S(^3He, \alpha)^{31}S$, because all of these groups occur at approximately the same frequency (see Figures 11 and 55).

3. Single Detector Spectra

(i) Experimental details

The target consisted of 579 ± 174 $\mu g/cm^2$ of Sb_2S_3 on 1255 ± 377 $\mu gm/cm^2$ of gold. The beam of 0.2 μA of 12.0 MeV $^3He^{++}$ was incident on the Sb_2S_3 side. The normal to the target always bisected the angle between the beam direction and the spectrometer. Previous experience with this kind of target showed that with this beam current, the target depletion was slow ($\leq 5\%$ in six hours). This target was used rather than a CdS target because it was the thickest available at the time of these measurements. A high yield was needed to compensate for the low efficiency of the single detector.

The pulses from the silicon surface barrier detector were fed to a Tennelec (Model 100A) preamplifier and then into the internal amplifier of a RIDL 400-channel analyzer. The spectra were read out on punch tape and then read back into another RIDL 400-channel analyzer, which was equipped with a device for integrating peaks. One run could be analyzed while the next run was in progress. Background subtractions, dead time corrections, and plotting were done manually during the experiment.

The same calibrations used for the measurement of the ground state Q-value of the reaction $^{32}S(^3He, \alpha)^{31}S$ (Section II.A. 5) was used for the beam analyzing magnet ($k_a = .0199062 \pm .0000033$ MeV/(Mc/sec)^2) and for the spectrometer ($k_{s\alpha} = .0113934 \pm .0000013$ MeV/(Mc/sec)^2).

The slit settings are given in Table I, column h.

(ii) Discussion of spectra

Figure 56 shows the deuteron spectra at 20° and 45°. The gaps in the spectra correspond to regions of severe elastic scattering from the gold foil. The observed resolution of 83 keV (FW) is due mainly to the target thickness and the collector slit width. The alpha particle spectra and proton spectra obtained simultaneously were of little interest because of the poor resolutions and the high level densities.

The peaks were again first tentatively identified from the shifts with angle. Levels (5) and (6) were expected from the sixteen counter array spectra (see Section V. A. 2) and from previous work (see Endt and van der Leun, 1962). The level from ^{13}N(2. 367) was uniquely identified from its kinematic shift. The identification of the ^{35}Cl(7. 56) was confirmed by a deuteron spectrum from the reaction ^{34}S(^{3}He, d)^{35}Cl taken under similar conditions by Dr. J. Dubois which showed that this level is strongly populated. Level (9) was attributed to ^{33}Cl on the basis of its kinematic shift and intensity. The spectra of J. Dubois do not show the region containing this level.

(iii) Calculation of excitation energies

The Q-values at 20° and 45° for levels (5) + (6) and (9) were calculated with a modified version of the program given in Appendix A. For each group Q-values at the two angles were averaged and then combined with Q_{GS} = -3. 217 ± 5 (see Section V. A. 2) to find the excitation energies. The results are given in Table XV.

The Q-value to the level in ^{35}Cl was also calculated with a suitably modified version of the program given in Appendix A. Again the Q-values at the two angles were averaged and then combined with $Q_{GS} = .8764 \pm .0030$ (Maples et al., 1966) to find the excitation energy. These results are also given in Table XVII.

(iv) Results

Table XV compares these results for ^{33}Cl to the previously reported results. The agreement for the level at 4.12 MeV excitation energy is quite good. The level at 3.986 ± 12 which has been seen in the reaction ^{32}S$(p, \gamma)^{33}$Cl (Lonsjo, 1962; and Prosser and Gordon, 1967) was not seen here.

The level in ^{35}Cl at 7.559 MeV excitation energy is probably the level reported at 7.559 from the reaction ^{34}S$(p,\gamma)^{35}$Cl (see Table XVII).

4. Four Detector Spectra

(i) Experimental details

The target consisted of 97 ± 29 μg/cm^2 of CdS containing sulfur enriched to 98.1% ^{32}S on 287 ± 86 μg/cm^2 of gold. The beam of 0.2 μA of 12.0 MeV ^{3}He^{++} was incident on the CdS side. The target was oriented so that the angle between the incident particles and the target normal was equal to the angle between the emerging particles and the target normal.

Four adjacent detector (9 through 12) in the 16
detector were used. The others were masked off. The pulses
from each counter were fed into a Tennelec (Model 100A) pre-
amplifier, then to a RIDL single delay line amplifier (Model
RIDL 30-23), and then into the routing system of a RIDL 400-
channel analyzer. There was little dead time (typically $\leq 5\%$)
with this system. The peaks were integrated with the integrating
device on the analyzer, and then read out on punch paper tape for
a permanent record. Background subtractions, dead time
corrections, and plotting was done manually.

The same calibrations used for the spectra from
the reaction $^{36}Ar(p, \alpha)^{33}Cl$ (see Section VI. C.) were used for the
beam analyzing magnet (k_a = .0199062 ± .0000033 MeV/(Mc/sec)^2)
and for the spectrometer (k_s = .0113844 ± .0000013 MeV/(Mc/sec)^2).

The slit settings are given in Table I, column i.

(ii) Discussion of spectra

Only the regions about the peaks found in the single
detector spectra were re-investigated with the four detector array.
This re-investigation was made because narrower detector slits
$\delta r_{c, sp}$ were feasible with the four detector array than with the
single detector and therefore better resolution could be obtained.
The peaks were again identified from the shifts with angle, and the
results confirm the single detector results.

(iii) Calculation of excitation energies

The Q-values and excitation energies for the levels
in ^{33}Cl and ^{35}Cl observed in these spectra were calculated in the

same way as were those for the single detector spectra and the results are given in Tables XV and XVII.

(iv) Results

The results are compared with other measurements in Tables XV and XVII.

B. Angular Distributions of ^{33}Cl States

1. Introduction

This section describes the results from the deuteron angular distributions from the reaction ^{32}S(^{3}He, d)^{33}Cl which were obtained as a by-product of the alpha particle distributions from the reaction ^{32}S(^{3}He, α)^{31}S described in Section II. C. Only the distributions from the levels at 0, 2.35, and 2.69 MeV excitation in ^{33}Cl were obtained as by-products. The distributions from the 2.35- and 2.69-MeV levels were interesting because the spins and parities for these levels were not known. It was hoped that comparisons with theoretical predictions would determine ℓ_p-values for these levels. Measurements of the distributions from the levels at 0.81, 2.85, 2.86 and 4.12 MeV excitation were not made because the spins and parities of these levels were known. Measurements of the distributions from the levels at 1.98 and 2.98 MeV were not made because these levels were so weakly populated that measurements of their distributions would have required an excessive amount of machine time. An extensive study of the reaction ^{32}S(p, γ)^{33}Cl in progress at the University of Kansas with higher proton energies

than used previously should yield the spins, parities, mixing ratios, and branching ratios for the low-lying levels in ^{33}Cl.

2. Experimental Details

Because these deuteron angular distributions were measured simultaneously with the alpha particle angular distributions, the experimental conditions were identical to those described in Section II. C. 2. Exactly the same procedure described in Section II. C. 3 was used to analyze these distributions.

3. DWBA Predictions

For these calculations it was assumed that the reaction mechanism was simple stripping. The zero-range approximation was used and spin-orbit coupling was neglected.

The three sets of optical model parameters for the ^{3}He particles described in Section II. C. 4 and listed in Table XVIII were also tried for this reaction. Again the predicted distribution for each set were very similar and the Set I parameters of Table XVIII were selected.

The optical model parameters used for the deuterons were those found by Perey and Perey (1963) at Oak Ridge for the elastic scattering of deuterons from aluminum at 11. 8 MeV and are given as Set IV in Table XVIII. The shape of the potential is given by

$$U(r) = -\frac{V}{e^x + 1} + iW' \frac{d}{dx'} \left(\frac{1}{e^{x'} + 1}\right)$$

$$x = \frac{r - R}{a} \qquad x' = \frac{r - R'}{a'}$$

$$R = r_o(M)^{1/3} \qquad R' = r_o'(M)^{1/3} .$$

The distributions were again calculated with the code TSALLY. The same procedure described in Section II. C. 4 was used to plot the results. Attempts to improve the fits by varying the parameters met with little success.

4. Discussion

Figure 57 shows four points on the angular distribution for ^{33}Cl(G. S.) which must have $\ell_p = 2$ because for this state $J^\pi = 3/2^+$. The theoretical prediction for $\ell_p = 2$ is consistent with the data.

Figure 58 shows the angular distribution for ^{33}Cl(2. 35). The points at $\theta_{CM} = 6^O$ and 11° were obscured by ^{17}F(. 500). Since ^{33}Cl(2. 35) is unbound by approximately 60 keV and since the TSALLY code is not suitable for unbound levels, it was assumed that the level was bound by 100 keV. Varying this binding energy by less than 1 MeV had little effect, a result in agreement with Goosman's observation (1967) for a similar case in the reaction ^{36}Ar(^{3}He, d)^{37}K. Level ^{33}Cl(2. 35) is assigned $\ell_p = (2)$ which implies $J^\pi = (3/2^+)$ or $(5/2^+)$.

Figure 59 shows the angular distribution for ^{33}Cl(2.68). This level was also assumed bound by 100 keV. The theoretical distributions for $\ell_p \geq 2$ fail to dip as much as the experimental distribution near $\theta_{CM} = 0^O$. The theoretical distribution for $\ell_p = 3$ agrees best with the experimental distributions, but no assignment is made.

5. Results

Table XIX summarizes the results of this and previous work. The values listed in columns b and c are for the reaction ^{32}S(d, n)^{33}Cl. Column d gives the known values of J^{π} or the values of J^{π} implied by these ℓ_p-values.

VI. $^{36}Ar(p, \alpha)^{33}Cl$

1. Introduction

Since an initial analysis of the data from the reaction $^{32}S(^3He, d)^{33}Cl$ failed to locate the second excited state in ^{33}Cl predicted from the mirror nucleus ^{33}S the second most suitable reaction $^{36}Ar(p, \alpha)^{33}Cl$ (Q = -4.355) was studied with the magnetic spectrometer to find this level as described in this section.

2. Target

A diagram of the gas cell used in this experiment is shown in Figure 60. This cell was designed by Dr. D. R. Goosman. The beam was first collimated by the slits (1.016 mm (FW)) in both the horizontal and vertical directions immediately in front of the target chamber. Following this, the beam was collimated by a hole 4.8 mm in diameter in a sheet of tantalum of 0.38 mm thickness at a distance of 3.8 mm in front of foil A. This second collimator, which was attached to the gas cell but electrically insulated from it, was aligned by moving the gas cell to find a minimum in the beam striking the collimator. An optical alignment procedure using the target chamber protractors gave the same result to better than 30'.

The first exit aperture was 1.59 mm (FW) in the θ direction by 3.81 mm (FW) in the θ direction. At the center of the target it subtended 3.73° (FW) in the θ direction and 8.95° (FW) in the ϕ direction. The second exit aperture was 1.59 mm (FW) (= 2.43°) in the θ direction by 4.57 mm (FW) (= 7.01°) in the

ϕ direction. By placing the spectrometer at 0° it was also possible to align these apertures with the beam by measuring the beam striking them. Again this setting agreed with a setting made with the target chamber protractors.

Because the reaction was observed only at 20°, 40°, and 60°, the beam entered through foil A and the α particles emerged through foil C as shown. Foil A was a 5000 $\overset{o}{A}$ nickel foil. Both were supplied by the Chromium Corporation of America. They were glued to the stainless steel walls with epoxy.

The target gas obtained from Monsanto Research Corporation by Dr. David Goosman contained 99.94% ^{36}Ar and .06% ^{38}Ar. The cell was pumped for 24 hours before it was filled with argon to a pressure of 14.0 cm of mercury.

3. Supplementary Data

The calibration constant for detector eight in the array with the 3.18 mm detector slits was determined in the same way as the constant for the single detector was determined as described in Section II. A. 5. Again the electronics shown in Figure 6 were used. The result was $k_{s\alpha}$ = 0.0113844 ± 0.0000013 MeV/(Mc/sec)^2, (f = 27700 ± 1 kc/sec).

The yield factors were again measured with the procedure described by McNally (1966). The same slit settings used for the alpha spectra from the reaction ^{36}Ar(p, α)^{33}Cl described in Section VI. 5 were used for the slits immediately in front of the target chamber (vertical, 1.02 mm (FW); horizontal, 1.02 mm (FW)), the angular acceptance slits of the spectrometer (θ = 2^O (FW), ϕ = 6.6^O (FW)), and the detector slits ($\delta r_{c, sp}$ = 3.18 mm (FW)). The exit

apertures were not used in the measurements of the yield factors, and furthermore the elastic scattering was from a sheet of tantalum rather than from a column of gas. However, since only peak positions and not absolute yields were required from the spectra, these two differences were unimportant. Table II, column c, lists the yield factors.

4. $^{36}Ar(p, \alpha)^{33}Cl$ Spectra Collection Details

A beam of 0.2 μA of 12.011 ± .014 MeV (f_a = 24643 kc/sec) protons bombarded the target. Neither the beam analyzing magnet nor the magnetic spectrometer were cycled because low accuracy was expected because of the energy losses in the gas cell. The slit settings not associated with the gas cell and detector foil thickness are given in Table I, column j. An electron suppressor upstream from the target was placed at -300 v, and the gas cell and the Faraday cup were placed at +300v relative to the chamber walls. With 55 volts bias, most of the detectors completely stopped the alphas and the protons. In those cases where the protons were not stopped, the data were not analyzed. At 20° two steps of the magnetic field corresponding to a displacement of approximately 2.90 mm of the spectrum relative to the detectors were made for each of the regions of the spectrum. As a check the ends of adjacent regions were overlapped. At 40° and 60° only one setting of the magnetic field was made in each region because of a lack of machine time. The data were read out on the Nuclear Data Optikon (Model ND 307), and reduced to spectra in exactly the same way as described in Section II. B. 5.

5. Discussion of Spectra

Figure 61 shows the spectra. Only a small range excitation (< 3 MeV) was scanned because of the unfavorable Q-value (Q = -4.355). The peaks here from levels in ^{33}Cl at 0, .810, and 2.351 MeV excitation (see Section V. A) and from ^{13}N(G.S.) (Ajzenberg-Selove and Lauritsen, 1959) were identified from their positions predicted by a relativistic kinematics program after appropriate corrections for the various energy losses. Level number (2) was identified by its kinematic shift with angle. Checks were made for contributions from the reactions ^{12}C(p, α)^{9}B, ^{13}C(p, α)^{10}B, ^{14}N(p, α)^{11}C, and ^{14}N(p, ^{3}He)^{12}C.

6. Calculation of Excitation Energy

The spectra shown in Figure 61 were used to calculate the excitation of level (2) in ^{33}Cl. Table XX gives the various energy losses for a typical peak. Since only a nominal value of 10000 $\overset{O}{A}$ for the thickness of the exit foil was available and since the alpha particles lost approximately 400 keV in this foil, it was necessary to determine the thickness more accurately. At each angle the stopping power curves of Demiolioglu and Whaling (1962), the excitation energies in ^{33}Cl from the reaction ^{32}S(^{3}He, d)^{33}Cl (see Section V), and the mass excesses for ^{33}Cl (see Section V), ^{36}Ar, protons, and alpha particles (Mattauch et al., 1965) were used to calculate the exit foil thickness for each peak except those from level (2). The average of the resulting exit foil thickness at each angle (typically 11400 $\overset{O}{A}$) was used to calculate the excitation energy of level (2). The excitations at the three angles were then averaged to obtain the final excitation energy of 1.999±.020 MeV for level (2) in ^{33}Cl.

VII. DISCUSSION OF ^{33}Cl STATES

A. Comparison with ^{33}S

Figure 62 shows the isobaric level diagram for ^{33}S and ^{33}Cl. The information summarized here for ^{33}S was taken from the compilation of Endt and van der Leun (1962) as well as from more recent work by Becker et al.(1966), O'Dell et al.(1966), and Moss (1967) (see Appendix G). The information for ^{33}Cl was taken from Endt and van der Leun (1962) and the present work.

The levels in ^{33}Cl at 0, .810, 1.978, and 2.351 MeV correspond quite well in excitation energies to the levels in ^{33}S at 0, .841, 1.965, and 2.313 MeV, respectively. Furthermore, if it is assumed that the reactions ^{32}S(d, p)^{33}S and ^{32}S(^{3}He, d)^{33}Cl are simple stripping reactions, then the relative reduced widths to corresponding levels should be similar. Table XXI gives the values of $(2J + 1) \, \theta_n^2$ quoted by Endt and van der Leun (1962) for the reaction ^{32}S(d, p)^{33}S, and the relative intensities at $\theta_{Lab} = 45^O$ of the deuteron groups corresponding to the levels in ^{33}Cl. For the first four levels these two quantities are qualitatively similar. In particular, the level at 2.0 MeV excitation is weakly populated in both. It is highly probable that these levels are isobaric analogs.

On the basis of the present information one can only speculate on the correspondences of the next four higher lying levels in ^{33}S and ^{33}Cl. We suggest the following correspondences:

$$^{33}S \qquad\qquad\qquad ^{33}Cl$$

2.869 MeV, $\ell_n = 2$	2.848 MeV, $5/2^+$
2.937 , $7/2^-$	2.686
2.970	2.980
3.224 , $3/2^-$	2.856 , $3/2^-$

These correspondences are consistent with the values of $(2J + 1)$ θ_n^2 and the intensities given in Table XXI. In particular, the level at 2.970 MeV in ^{33}S and the level at 2.980 in ^{33}Cl are weakly populated. As pointed out in Section V.B.5, the theoretical angular distribution for $\ell_p = 3$ agreed best with the experimental distribution for $^{33}Cl(2.686)$. However, the agreement was not good enough to make an assignment.

B. Comparison with Theory

A refinement of the Nilsson Model for ^{33}S and ^{33}Cl has been discussed by Bishop (1959). He assumed that the $3/2^+$ ground state and the $5/2^{(+)}$ level at 2.0 MeV formed the first two members of a $K = 3/2$ band. Then the formula

$$E_{J,K} = \epsilon_K + \frac{\hbar^2}{2I} [J(J+1) - 2K^2 + \delta_{K,(1/2)} a(-)^{J+(1/2)}(J+1/2)]$$

(see Preston, 1962) gives $\frac{\hbar^2}{2I} = +396$ keV and predicts a $7/2^+$ level at 4.8 MeV. He further assumed that the $1/2^+$ level at 0.8 and the $3/2^+$ level at ~ 2.3 MeV formed the first two members of a $K = 1/2$

band. If it is assumed that $\frac{\hbar^2}{2I}$ = 396 keV for this band also, then the formula gives a = 0.30 and predicts a $5/2^+$ level at 3.74 (see Figure 63, column 1). Experimentally if one assumed the isobaric correspondence suggested in Section VII.A., then the second $5/2^+$ level is at 2.848 MeV in ^{33}Cl. The location of the first $7/2^+$ level is not known.

The results for ^{33}Cl of the shell model calculation by Glaudemans et al.(1964) which was described in Section IV.B. are shown in Figure 63, column 2. If the isobaric correspondence suggested in Section VII.A. is again assumed, then the predicted sequence $3/2^+$, $1/2^+$, $5/2^+$, and $3/2^+$ agrees with experiment. However, the excitation energies do not agree very well with experiment. The second $5/2^+$ level is predicted to lie at 3.8 MeV which is well above the second experimentally observed $5/2^+$ at 2.848 MeV in ^{33}Cl. This model predicts a $7/2^+$ level at 2.9 MeV which suggests the possible identification of this level with the experimentally observed level at 2.980 MeV in ^{33}Cl. The fact that the wave function given by Glaudemans et al.(1964) for the first $5/2^+$ state does not look like the wave function for the ground state of ^{32}S plus a proton could explain the weak population of this level in the stripping reaction ^{32}S(^{3}He, d)^{33}Cl.

A similar shell model calculation for odd-parity levels of nuclei in the region $33 \le A \le 41$ has been done by Erné (1966). An inert ^{32}S core was assumed and one nucleon was considered to be in the $1f_{7/2}$ shell while the others were in the $1d_{3/2}$ shell. Values for the twelve two-particle interaction energies and the binding energies to the ^{32}S core of $1d_{3/2}$ and $1f_{7/2}$ nucleons were determined by a least-squares fit of the computed energies to the energies of sixty states in the region $33 \le A \le 41$ with known spin

and isospins. Then from these fourteen parameters, the energies and wave functions of 240 states in this region were calculated. For A = 33 only a $7/2^-$ level at 2.94 MeV is predicted. This is shown in Figure 63, column 3. Experimentally there is a $7/2^-$ level in ^{33}S at 2.937 MeV. The suggested analog in ^{33}Cl occurs at 2.686 MeV (see Section VII. A). The good agreement of the predicted excitation with the observed excitation in ^{33}S is not surprising since this $7/2^-$ level in ^{33}S was one of the levels fitted. The $3/2^-$ level at 2.856 in ^{33}Cl is not predicted.

APPENDIX A: PROGRAM FOR CALCULATING THE Q-VALUES
AND EXCITATION ENERGIES OF LEVELS IN ^{31}S

The Q-value for the ground state is given by the relativistically correct formula

$$Q_{GS} = M_1 + M_2 - M_3 - \left\{ [M_1 + M_2 + E_{1GS} - M_3 - E_{2GS}]^2 \right.$$

$$\left. - P_{1GS}^2 - P_{3GS}^2 + 2P_{1GS}P_{3GS} \cos\theta_3 \right\}^{1/2}$$

where

$$P_{1GS}^2 = E_{1GS}(E_{1GS} + 2M_1)$$

$$P_{3GS}^2 = E_{3GS}(E_{3GS} + 2M_3)$$

M_1, M_2, M_3 = nuclear masses not including the electron masses

E_{1GS}, E_{3GS} = kinetic energies after corrections for the target thickness

$$E_{1GS} = (1 + \frac{X_{GS90}}{R_{90}})[(M_1^2 + 2M_p Z_1^2 K_1 F_{1GS}^2)^2 - M_1]$$

$$- (1 + C_{CDSHE3}) \frac{C_{AVO}}{W_{CDS}} \frac{T_{TGT}}{2\cos\theta_{in}} Z_1^2 \epsilon_{CDS} (\frac{M_p}{M_1} E_{1GS}) \ .$$

(The beam is assumed incident on the side with the CdS.)

X_{GS90} = position of the beam in the beam analyzing magnet slits, normally 0.

R_{90} = radius of the orbit in the beam analyzing magnet.

M_p = mass of the proton.

K_1 = calibration constant of the beam analyzing magnet.

F_{1GS} = beam analyzing magnet frequency.

C_{CDSHE3} = fractional error in the stopping power for ^{3}He particles in CdS, normally 0.

C_{AVO} = Avogadro constant.

W_{CDS} = atomic weight of CdS.

T_{TGT} = thickness of CdS in a direction normal to the target.

θ_{in} = THIN = angle between the beam and the normal to the target.

ϵ_{CDS} = stopping power of CdS for protons, a function of energy.

$$E''_{3GS} = (1 + C_{FACTOR} \times Y_{GSTGT}) \left\{ [M_3^2 + 2M_p Z_3^2 \right.$$

$$\left. (1 + R_{EK3GS}) K_{3GS}(F_{3GS}, K_{30}) F_{3GS}^2]^{1/2} - M_3 \right\}$$

$$E'_{3GS} = E''_{3GS} + (1 + C_{AUHE4}) \frac{C_{AVD}}{W_{AU}} \frac{T_{BACK}}{\cos \theta_{out}} Z_3^2 \, \epsilon_{AU} \left(\frac{M_p}{M_3} E''_{3GS} \right)$$

$$E_{3GS} = E'_{3GS} + (1 + C_{CDSHE4}) \frac{C_{AVO}}{W_{CDS}} \frac{T_{TGT}}{2 \cos \theta_{out}} Z_3^2 \, \epsilon_{AU} \left(\frac{M_p}{M_3} E'_{3GS} \right)$$

C_{FACTOR}	=	magnification of the spectrometer times $\Delta E/E$ per unit length perpendicular to the mean orbit.
Y_{GSTGT}	=	vertical position of the beam spot, normally 0.
R_{EK3GS}	=	fractional error in the ratio K_{3GS}/K_{30}, normally 0.
K_{3GS}	=	calibration "constant" for the spectrometer, a function of F_{3GS} and K_{30}.
F_{3GS}	=	magnetic spectrometer frequency.
K_{30}	=	calibration "constant" for the spectrometer at a frequency corresponding to the energy of the alpha particles (8785.0 ± 0.8 keV (Wapstra,1964)) from a 212_{Po} source.
C_{AUHE4}	=	fractional error in the stopping power for alpha particles in Au, normally 0.
W_{AU}	=	atomic weight of gold.
TBACK	=	thickness of gold in a direction normal to the target.
θ_{out}	=	THOUT = angle between the emerging particles and the normal to the target.
ϵ_{AU}	=	stopping power of gold for protons, a function of energy.
C_{CDSHE4}	=	fractional error in the stopping power for alpha particles in gold, normally 0.

The Q-value for the N-th excited state is given by a similar set of equations and definitions with "GS" replaced by "N".

The excitation energy for the N-th excited state is given by

$$EX = Q_{GS} - Q_N .$$

To calculate the error in a Q-value, errors are assigned to the arguments of Q which have a significant error. Let Q be a function of the arguments x_i and suppose the error in x_i is Δx_i. Then the error in Q due to this error in x_i is

$$\Delta Q_i = Q(x_1, x_2 \ldots x_i + \Delta x_i \ldots) - Q(x_1, x_2 \ldots x_i \ldots)$$

and the total error in Q due to all of the x_i is

$$\Delta Q_{TOTAL} = \sqrt{\sum_i (\Delta Q_i)^2} .$$

Table VIII gives the values of the arguments, their errors, and the errors introduced in Q for two typical cases.

The error in the excitation energy is calculated in a similar way. Since the ground state and the N-th excited state are not observed simultaneously, there are separate arguments for the ground state and the N-th excited state in some cases. This is the reason for the subscripts "GS" and "N" above. Table VIII also gives the errors introduced in the excitation energy for the same two cases.

The input for this program consists of the following cards:

	Argument	Error
Card 1	K1,	ERR(1)
Card 2	FIGS,	EKK(2)
3	XGS90	3
4	TTGT	4
5	CDSHE3	.
6	CDSHE4	.
7	AUHE4	.
8	THIN	.
9	THOUT	.
10	FIN	.
11	XN90	.
12	K30	.
13	EK3GS	.
14	EK3N	.
15	F3GS	.
16	YGSTGT	.
17	TBACK	.
18	YNTGT	.
19	TH3	.
20	F3N	20

.

.

.

blank card

Card 20 may be repeated indefinitely to analyze other levels observed under identical conditions.

If the conditions are not identical, a blank card is placed after the last card in this first group which has F3N and ERR(20) and cards 1 through 20 are repeated. This procedure may also be repeated indefinitely.

A listing of the program is given below.

```
$IBFTC DAT      DECK
C
C       DATA FOR S32(HF3,HE4)S31, CDS
C
        BLOCK DATA
        COMMON/TEX/M1,M2,M3,M4,Z1,Z2,Z3,Z4,NPART1,NPART3,NMAT1,NMAT2
        DOUBLE PRECISION M1,M2,M3,M4
        DATA M1,M2,M3,M4,Z1,Z2,Z3,Z4,NPART1,NPART3,NMAT1,NMAT2/
      1 2808.3433D0,29773.1073D0,3727.3147D0,28848.650D0,2.,16.,2.,16.,5,
      2 4,1,2/
        END
$IBFTC MEX      DECK
C
C       MAIN PROGRAM
C       PROGRAM FOR THE ERRORS IN THE EXCITATION ENERGIES AND Q-VALUES
C            OF LEVELS IN S31
C
        DIMENSION X(20),ERRX(20),SERREX(20),ERRQGS(20),ERRQN(20),A(20)
        REAL K1,K30,K3GS,K3N
        DOUBLE PRECISION M1,M2,M3,M4,QGS,QN
        EQUIVALENCE (K1,X(1))
        COMMON/TEX/M1,M2,M3,M4,Z1,Z2,Z3,Z4,NPART1,NPART3,NMAT1,NMAT2
        COMMON/ARG/K1,F1GS,XGS90,TTGT,CDSHE3,CDSHE4,AUHE4,THIN,THOUT,F1N,
      1 XN90,K30,FK3GS,EK3N,F3GS,YGSTGT,TBACK,YNTGT,TH3,F3N,QGS,QN,EX
   10   READ(5,20) (X(I),ERRX(I),I=1,19)
   20   FORMAT(2F10.0)
        DATA(A(I),I=1,19)/2HK1,4HF1GS,5HXGS90,4HTTGT,6HCDSHE3,6HCDSHE4,
      1 5HAUHE4,4HTHIN,5HTHOUT,3HF1N,4HXN90,3HK30,5HEK3GS,4HEK3N,4HF3GS,
      2 6HYGSTGT,5HTBACK,5HYNTGT,3HTH3/
        WRITE(6,30)
   30   FORMAT(1H1)
        WRITE(6,40) (A(I),X(I),ERRX(I),I=1,19)
   40   FORMAT(A6,4X,2F15.8)
   45   READ(5,20)F3N,ERRX(20)
        IF(F3N.EQ.0.) GO TO 10
C       INSERT BLANK CARD IF ANYTHING BUT F3N CHANGES
        CALL QEX
        EX0=EX
        QGS0=QGS
        QN0=QN
        DO 60 I=1,20
        X(I)=X(I)+ERRX(I)
        CALL QEX
        SERREX(I)=EX-EX0
        ERRQGS(I)=QGS-QGS0
        ERRQN(I)=QN-QN0
        X(I)=X(I)-ERRX(I)
   60   CONTINUE
        SUMEX=0.
        SUMQGS=0.
        SUMQN=0.
        DO 70 I=1,20
        SUMEX=SUMEX+(SERREX(I))*(SERREX(I))
        SUMQGS=SUMQGS+(ERRQGS(I))*(ERRQGS(I))
        SUMQN=SUMQN+(ERRQN(I))*(ERRQN(I))
   70   CONTINUE
        TEX=SQRT(SUMEX)
        TQGS=SQRT(SUMQGS)
        TQN=SQRT(SUMQN)
        WRITE(6,80)
   80   FORMAT(1H1,66X,36HERRORS IN EX INTRODUCED BY ERRORS IN)
```

```
      WRITE(6,90) F3N,ERRX(20),EXO,(SERREX(I),I=1,20),TEX
   90 FORMAT(1H0,2X,3HF3N,4X,6HERRF3N,5X,2HEX,13X,2HK1,7X,4HF1GS,6X,
     1 5HXGS90,5X,4HTTGT,5X,6HCDSHE3,4X,6HCDSHE4,5X,5HAUHE4,5X,4HTHIN,
     2 6X,5HTHOUT,6X,3HF1N/1X,F7.3,F9.4,F10.6,5X,10F10.6/1H0,34X,
     3 4HXN90,7X,3HK30,6X,5HEK3GS,5X,4HEK3N,6X,4HF3GS,5X,6HYGSTGT,5X,
     4 5HTBACK,5X,5HYNTGT,6X,3HTH3,7X,3HF3N/32X,10F10.6/1H0,35X,3HTEX/
     5 32X,F10.6///)
      WRITE(6,100)
  100 FORMAT(1H0,66X,37HERRORS IN QGS INTRODUCED BY ERRORS IN)
      WRITE(6,110) F3N,ERRX(20),QGSO,(ERRQGS(I),I=1,20),TQGS
  110 FORMAT(1H0,2X,3HF3N,4X,6HERRF3N,4X,3HQGS,13X,2HK1,7X,4HF1GS,6X,
     1 5HXGS90,5X,4HTTGT,5X,6HCDSHE3,4X,6HCDSHE4,5X,5HAUHE4,5X,4HTHIN,
     2 6X,5HTHOUT,6X,3HF1N/1X,F7.3,F9.4,F10.6,5X,10F10.6/1H0,34X,
     3 4HXN90,7X,3HK30,6X,5HEK3GS,5X,4HEK3N,6X,4HF3GS,5X,6HYGSTGT,5X,
     4 5HTBACK,5X,5HYNTGT,6X,3HTH3,7X,3HF3N/32X,10F10.6/1H0,35X,4HTQGS/
     5 32X,F10.6///)
      WRITE(6,120)
  120 FORMAT(1H0,66X,36HERRORS IN QN INTRODUCED BY ERRORS IN)
      WRITE(6,130) F3N,ERRX(20),QNO,(ERRQN(I),I=1,20),TQN
  130 FORMAT(1H0,2X,3HF3N,4X,6HERRF3N,5X,2HQN,13X,2HK1,7X,4HF1GS,6X,
     1 5HXGS90,5X,4HTTGT,5X,6HCDSHE3,4X,6HCDSHE4,5X,5HAUHE4,5X,4HTHIN,
     2 6X,5HTHOUT,6X,3HF1N/1X,F7.3,F9.4,F10.6,5X,10F10.6/1H0,34X,
     3 4HXN90,7X,3HK30,6X,5HEK3GS,5X,4HEK3N,6X,4HF3GS,5X,6HYGSTGT,5X,
     4 5HTBACK,5X,5HYNTGT,6X,3HTH3,7X,3HF3N/32X,10F10.6/1H0,35X,3HTQN/
     5 32X,F10.6///)
      GO TO 45
      END
$IBFTC QEX      DECK
      SUBROUTINE QEX
C
C     K1=CALIBRATION CONSTANT FOR 90 DEGREE ANALYZER IN MEV*(SEC/MC)**2
C     F1GS=INCIDENT BEAM FREQUENCY FOR GROUND STATE PEAK IN MC/SEC
C     XGS90=BEAM POSITION IN 90 DEGREE ANALYZER SLITS IN MILS FOR GS.
C           ENTRANCE AND EXIT SLITS ARE ASSUMED EQUAL. + OR - SLIT
C           SETTING ARE TREATED AS ERRORS. ERROR CALCULATED=1/2 MAX
C           POSSIBLE ERROR.
C     TTGT=TARGET THICKNESS IN MICROGRAMS/(CM)**2.  BEAM IS ASSUMED
C     INCIDENT ON TARGET SIDE.
C     CDSHE3=FRACTIONAL ERROR IN THE STOPPING POWER FOR HE3 IN THE
C           TARGET MATERIAL, NORMALLY 0
C     CDSHE4=FRACTIONAL ERROR IN THE STOPPING POWER FOR HE4 IN THE
C           TARGET MATERIAL, NORMALLY 0
C     AUHE4=FRACTIONAL ERROR IN THE STOPPING POWER FOR HE4 IN THE
C       .   BACKING
C     F1N=FREQUENCY FOR NTH EXCITED STATE IN MC/SEC
C     XN90=BEAM POSITION IN 90 DEGREE ANALYZER SLITS IN MILS FOR NTH
C             EXCITED STATE.
C     K30=CALIBRATION CONSTANT FOR MAGNETIC SPECTROMETER IN MEV*(SEC/
C           MC)**2 AT THE ALPHA SOURCE ENERGY 8.785 MEV
C     K3GS=CALIBRATION CONSTANT FOR MAGNETIC SPECTROMETER IN MEV*(SEC/
C           MC)**2 AT F3GS
C     F3GS=MAGNETIC SPECTROMETER FREQUENCY FOR GROUND STATE PEAK IN
C           MC/SEC
C     YGSTGT=BEAM POSITION IN VERTICAL TGT SLITS IN MILS FOR GS.
C             ERROR CALCULATED =1/2 MAXIMUM POSSIBLE ERROR.
C     YNTGT=BEAM POSITION IN VERTICAL TGT SLITS IN MILS FOR NTH EXCITED
C             STATE.  ERROR CALCULATED = 1/2 MAXIMUM POSSIBLE ERROR
C     TBACK=BACKING THICKNESS IN MICROGRAMS/(CM)**2
C     F3N=MAGNETIC SPECTROMETER FREQUENCY FOR NTH EXCITED STATE PEAK IN
C           MC/SEC
C     TH3=SPECTROMETER ANGLE IN DEGREES
```

```
C      K3N=CALIBRATION CONSTANT FOR MAGNETIC SPECTROMETER IN MEV*(SEC/
C          MC)**2 AT F3N
C      THIN=ANGLE BETWEEN NORMAL TO TARGET AND INCIDENT BEAM IN DEGREES
C      THOUT=ANGLE BETWEEN NORMAL TO TARGET AND EMERGENT PARTICLES IN
C          DEGREES
C
       REAL K1,K30,K3GS,K3N
       DOUBLE PRECISION M1,M2,M3,M4
       DOUBLE PRECISION E1PGS,E1PN,DE1GS,DE1N,DE2GS,DE2N,DE3GS,DE3N,
     1 E1GS,E1N,E3PPGS,E3PGS,E3PPN,E3GS,E3N,EM4,ETGS,ETN,P1SQGS,
     2 P1SQN,COSTH,P1GS,P1N,P3GS,P3N,W,WW,XGS,XN,QGS,QN,P3SQGS,P3SQN
       COMMON/TEX/M1,M2,M3,M4,Z1,Z2,Z3,Z4,NPART1,NPART3,NMAT1,NMAT2
       COMMON/ARG/K1,F1GS,XGS90,TTGT,CDSHE3,CDSHE4,AUHE4,THIN,THOUT,F1N,
     1 XN90,K30,EK3GS,EK3N,F3GS,YGSTGT,TBACK,YNTGT,TH3,F3N,QGS,QN,EX
       DATA RAD,R/57.2957795,34000./
C      M'S ARE NUCLEAR MASSES NOT INCLUDING ELECTRON MASSES
       E1PGS=DSQRT(M1*M1+2.*938.256*Z1*Z1*K1*F1GS*F1GS)-M1
       E1PN=DSQRT(M1*M1+2.*938.256*Z1*Z1*K1*F1N*F1N)-M1
       TKNSS1=TTGT/(2.*COS(THIN/RAD))
       DE1GS=(1.+CDSHE3)*ENLOSS(NPART1,E1PGS,NMAT1,TKNSS1,1,3)
       DE1N=(1.+CDSHE3)*ENLOSS(NPART1,E1PN,NMAT1,TKNSS1,1,3)
       E1GS=F1PGS*(1.+XGS90/R)-DE1GS
       E1N=E1PN*(1.+XN90/R)-DE1N
       K3GS=(1.+EK3GS)*CK3(F3GS,K30)
       K3N=(1.+EK3N)*CK3(F3N,K30)
       E3PPGS=(1.+FACTOR*YGSTGT)*(DSQRT(M3*M3+2.*938.256*Z3*Z3*K3GS*
     1 F3GS*F3GS)-M3)
       E3PPN=(1.+FACTOR*YNTGT)*(DSQRT(M3*M3+2.*938.256*Z3*Z3*K3N*
     1 F3N*F3N)-M3)
       TKNSS3=TBACK/COS(THOUT/RAD)
       DE3GS=(1.+AUHE4)*ENLOSS(NPART3,E3PPGS,NMAT2,TKNSS3,1,3)
       DE3N=(1.+AUHE4)*ENLOSS(NPART3,E3PPN,NMAT2,TKNSS3,1,3)
       E3PGS=E3PPGS+DE3GS
       E3PN=E3PPN+DE3N
       TKNSS2=TTGT/(2.*COS(THOUT/RAD))
       DE2GS=(1.+CDSHE4)*ENLOSS(NPART3,E3PGS,NMAT1,TKNSS2,1,3)
       DE2N=(1.+CDSHE4)*ENLOSS(NPART3,E3PN,NMAT1,TKNSS2,1,3)
       FACTOR=.84/(125.*360.*2.)
       E3GS=E3PGS+DE2GS
       E3N=E3PN+DE2N
       EM4=M1+M2-M3
       ETGS=M1+M2+E1GS
       ETN=M1+M2+E1N
       P1SQGS=E1GS*(E1GS+2.0D0*M1)
       P1SQN=E1N*(E1N+2.0D0*M1)
       P3SQGS=E3GS*(E3GS+2.0D0*M3)
       P3SQN=E3N*(E3N+2.0D0*M3)
       COSTH=DCOS(TH3/RAD)
       P1GS=DSQRT(P1SQGS)
       P1N=DSQRT(P1SQN)
       P3GS=DSQRT(P3SQGS)
       P3N=DSQRT(P3SQN)
       W=ETGS-M3-E3GS
       WW=ETN-M3-E3N
       XGS=W*W-P1SQGS-P3SQGS+2.0D0*COSTH*P1GS*P3GS
       XN=WW*WW-P1SQN-P3SQN+2.0D0*COSTH*P1N*P3N
       QGS=EM4-DSQRT(XGS)
       QN=EM4-DSQRT(XN)
       EX=QGS-QN
       RETURN
       END
```

```
$IBFTC LOS      DECK
      FUNCTION ENLOSS(NPART,ENERGY,NMAT,TKNESS,NUTSTK,NUTSES)
C
C     THIS PROGRAM CALCULATES THE ENERGY LOSS OF PARTICLES IN CDS OR AU
C     NPART=PARTICLE OPTION NUMBER
C     1=PROTON
C     2=DEUTERON
C     3=TRITON
C     4=HELIUM 4
C     5=HELIUM 3
C
C     NMAT=MATERIAL OPTION NUMBER
C     1=CDS
C     2=AU
C
C     TKNESS=THICKNESS
C
C     NUTSTK=THICKNESS UNITS OPTION NUMBER
C     1=MICROGRAMS/CM**2
C     2=MILLIGRAMS/CM**2
C     3=CM
C     4=ANGSTROMS
C     5=MILS
C     6=INCHES
C
C     NUTSES=ENERGY LOSS UNITS OPTION NUMBER
C     1=EV
C     2=KEV
C     3=MEV
C
      DIMENSION ATWT(2),RHO(2),UEV(3)
      DATA AVO/.602252E 24/
      DATA (ATWT(I),I=1,2)/72.24,196.967/
      DATA (RHO(I),I=1,2)/4.82,19.3/
      DATA (UEV(I),I=1,3)/1.,.1E-02,.1E-05/
      A=AVO/ATWT(NMAT)
      GO TO (10,20,30,40,50,60), NUTSTK
   10 B=0.1E-05*TKNESS
      GO TO 70
   20 B=0.1E-02*TKNESS
      GO TO 70
   30 B=RHO(NMAT)*TKNESS
      GO TO 70
   40 B=0.1E-07*RHO(NMAT)*TKNESS
      GO TO 70
   50 B=0.254E-02*RHO(NMAT)*TKNESS
      GO TO 70
   60 B=2.54*RHO(NMAT)*TKNESS
   70 GO TO (110,120,130,140,150), NPART
  110 EP=ENERGY
      ZSQ=1.
      GO TO 160
  120 EP=ENERGY/2.
      ZSQ=1.
      GO TO 160
  130 EP=ENERGY/3.
      ZSQ=1.
      GO TO 160
  140 EP=ENERGY/4.
      ZSQ=4.
      GO TO 160
```

```
   150  EP=ENERGY/3.
         ZSQ=4.
   160  GO TO (210,220), NMAT
   210  C=ZSQ*ECDS(EP)
         GO TO 230
   220  C=ZSQ*EAU(FP)
   230  D=UEV(NUTSES)
         ENLOSS=A*B*C*D
         RETURN
         END
$IBFTC CECDS    DECK
         FUNCTION ECDS(EP)
         DIMENSION F(29),DEL(29)
         DATA F/22.1,19.8,17.8,16.2,14.9,13.93,13.10,12.38,11.74,12.38,
        1 9.78,8.27,7.19,6.40,5.81,5.34,4.93,4.58,4.29,4.04,3.83,3.65,3.48,
        2 3.32,3.17,3.04,2.93,2.83,2.72/
         DATA DEL/-0.2,0.3,0.4,0.3,0.33,0.14,0.11,0.08,0.07,2.82,1.09,0.43,
        1 0.29,0.20,0.12,0.06,0.06,0.04,0.04,0.03,0.01,0.01,0.01,0.02,
        2 0.02,0.01,-0.01,-0.01/
         IF(EP.LT.0.3) GO TO 44
         IF(FP.GT.1.0) GO TO 27
         DO 26 I=1,9
         TRY = 0.1*FLOAT(I+2)
         IF(EP.LT.TRY) GO TO 32
    26 CONTINUE
    27 IF(EP.GE.5.0) GO TO 29
         DO 30 I=10,18
         TRY = 0.5*FLOAT(I-8)
         IF(EP.LT.TRY) GO TO 33
    30 CONTINUE
    32 BOT = 0.1
         X0 = 0.1*FLOAT(I+1)
         GO TO 28
    29 DO 31 I=19,29
         TRY = 0.5*FLOAT(I-8)
         IF(EP.LT.TRY) GO TO 33
    31 CONTINUE
    33 BOT = 0.5
         X0 = 0.5*FLOAT(I-9)
    28 P = (EP-X0)/BOT
         E2 = -P*(P-1.)*(P-2.)/6.
         F2 = -(1.-P)*P*(P+1.)/6.
         FCDS= (1.-P)*F(I-1) + P*F(I) + E2*DEL(I-1) + F2*DEL(I)
         FCDS = ECDS*1.0E-15
         RETURN
    44 ECDS = 22.1*1.0E-15
         RETURN
         END
$IBFTC CEAU     DECK
         FUNCTION EAU(EP)
         DIMENSION F(29),DEL(29)
         DATA F/36.3,32.4,29.5,27.1,25.1,23.5,22.1,20.9,19.9,20.9,17.0
        1 ,14.7,13.26,12.12,11.16,10.35,9.67,9.09,8.58,8.13,7.73,7.37,
        2 7.04,6.75,6.50,6.28,6.07,5.88,5.71/
         DATA DEL/-1.3,1.0,0.5,0.4,0.4,0.2,0.2,0.2,0.2,4.7,1.6,0.86,0.30,
        1 0.18,0.15,0.13,0.10,0.07,0.06,0.05,0.04,0.03,0.04,0.04,0.03,0.01,
        2 0.02,0.02,0.02/
         IF(EP.LT.0.3) GO TO 44
         IF(EP.GT.1.0) GO TO 27
         DO 26 I=1,9
         TRY = 0.1*FLOAT(I+2)
```

```
      IF(EP.LT.TRY) GO TO 32
   26 CONTINUE
   27 IF(EP.GE.5.0) GO TO 29
      DO 30 I=10,18
      TRY = 0.5*FLOAT(I-8)
      IF(EP.LT.TRY) GO TO 33
   30 CONTINUE
   32 BOT = 0.1
      X0 = 0.1*FLOAT(I+1)
      GO TO 28
   29 DO 31 I=19,29
      TRY = 0.5*FLOAT(I-8)
      IF(EP.LT.TRY) GO TO 33
   31 CONTINUE
   33 BOT = 0.5
      X0 = 0.5*FLOAT(I-9)
   28 P = (EP-X0)/BOT
      F2 = -P*(P-1.)*(P-2.)/6.
      F2 = -(1.-P)*P*(P+1.)/6.
      FAU = (1.-P)*F(I-1) + P*F(I) + E2*DEL(I-1) + F2*DEL(I)
      EAU = EAU*1.0E-15
      RETURN
   44 EAU = 36.3*1.0E-15
      RETURN
      END
SIBFTC CK3      DECK
      FUNCTION CK3(F,CK30)
C
C     CK3 AS A FUNCTION OF FREQUENCY IN MC/SEC
C     THE FUNCTION INTERPOLATES OR EXTRAPOLATES THE EXPERIMENTAL POINTS
C
      DIMENSION XX(16),YY(16),XXP(3),YYP(3)
      DATA XX/14.0,16.0,18.0,20.0,22.0,24.0,26.0,28.0,30.0,32.0,34.0,
     1 36.0,38.0,40.0,42.0,44.0/
      DATA YY/1.00025,1.00000,.99975,.99950,.99938,.99945,.99969,
     1 1.00002,1.00063,1.00130,1.00204,1.00291,1.00376,1.00478,1.00590,
     1 1.00700/
      DO 100 I=1,14
      II=I
      IF(XX(I).GE.F) GO TO 200
  100 CONTINUE
      KMIN=14
      GO TO 300
  200 KMIN=II-1
      IF(KMIN.LE.0) KMIN=1
  300 KMAX=KMIN+2
      DO 400 J=KMIN,KMAX
      N=J-KMIN+1
      XXP(N)=XX(J)
      YYP(N)=YY(J)
  400 CONTINUE
      N=2
      CK3=CK30*AITKEN(XXP,YYP,F,N)
      RETURN
      END
SIBLDR*MGHAIT
```

APPENDIX B.   PROGRAM FOR $\theta_{\text{Effective}}$

Let

θ = THETA = the spectrometer angle (track reading).

$\Delta\theta$ = DTHT = the half angle of the spectrometer aperature in the θ direction.

$\Delta\phi$ = DPHI = the half angle of the spectrometer aperature in the ϕ direction.

Figure 64 shows the notation.

Then

$$\theta_{\text{effective}} = \text{TEFF}$$

$$= \frac{1}{4\,\text{Tan}\,\Delta\theta\,\,\text{Tan}\,\Delta\phi} \int_{\eta = -\text{Tan}\,\Delta\phi}^{\eta = \text{Tan}\,\Delta\phi} \int_{\xi = -\text{Tan}\,\Delta\theta}^{\xi = \text{Tan}\,\Delta\theta}$$

$$\text{Tan}^{-1}\left(\frac{((\sin\theta + \xi\cos\theta)^2 + \eta^2)^{1/2}}{\cos\theta - \xi\sin\theta}\right)\,d\xi\,d\eta \ .$$

The program listed below calculates this integral from THETA = TMIN to THETA = TMAX in steps of DTHT. In all of the present work NSTEPS = 51.

```
$IBFTC TEF      DECK
C
C         COMPUTES THETA EFFECTIVE
C
          DIMENSION T1(101),T2(101)
     6    READ(5,101)TMIN,DELT,TMAX,DTHT,DPHI,NSTEPS
    101   FORMAT(5F10.0,I5)
C
C           NOTATION
C                 TMIN = THETA MIN
C                 DELT = STEP FOR THETA
C                 TMAX = THETA MAX
C                 DTHT = DELTA THETA
C                 DPHI = DELTA PHI
C                 NSTEPS = NUMBER OF TABULATED VALUES FOR INTEGRAND
C           INTEGRATION WILL BE DONE BY SIMPSONS RULE
C
          WRITE(6,200)DTHT,DPHI,NSTEPS
    200   FORMAT(35H1THETA EFFECTIVE FOR DELTA THETA = F4.2,
        1 14H, DELTA PHI = F4.2, /
        246H0THE NUMBER OF POINTS TAKEN FOR INTEGRATION = I5, /
        3  1H0 15X 5HTHETA 3X 9HTHETA EFF )
          TDTHT = TAN(DTHT/57.295779)
          TDPHI = TAN(DPHI/57.295779)
          DENOM = 4.*TDTHT*TDPHI
          DXI = 2.*TDTHT/FLOAT(NSTEPS-1)
          DETA = 2.*TDPHI/FLOAT(NSTEPS-1)
          NN = (NSTEPS-1)/2 - 1
          THETA = TMIN
     5    TRAD = THETA/57.295779
          CT = COS(TRAD)
          ST = SIN(TRAD)
          FTA = -TDPHI
          DO 1 I = 1,NSTEPS
          XI = -TDTHT
          DO 2 J = 1,NSTEPS
          ARG = SQRT((ST+XI*CT)*(ST+XI*CT)+ETA*ETA)/(CT-XI*ST)
          T1(J) = ATAN(ARG)
          IF(T1(J).LT.0.)T1(J)= T1(J) + 3.1415927
     2    XI = XI + DXI
          SUM = 0.
          DO 3 J = 1,NN
     3    SUM = SUM + 4.*T1(2*J) + 2.*T1(2*J+1)
          T2(I) = DXI/3.*(SUM+T1(1)+4.*T1(NSTEPS-1)+T1(NSTEPS))
     1    ETA = ETA + DETA
          SUM = 0.
          DO 4 J = 1,NN
     4    SUM = SUM + 4.*T2(2*J) + 2.*T2(2*J+1)
          TEFFR  =DETA/3.*(SUM+T2(1)+4.*T2(NSTEPS-1)+T2(NSTEPS))
          TEFF = TEFFR*57.295779
          TEFF = TEFF/DENOM
          WRITE(6,201)THETA,TEFF
    201   FORMAT(1H 10X F10.0,F12.4)
          THETA = THETA + DELT
          IF(THETA.LE.TMAX)GO TO 5
          GO TO 6
          END
```

APPENDIX C.   ARRAY DATA REDUCTION PROGRAM

For each run the frequencies for the detectors are calculated from the frequency for detector eight. The sixteen sums corresponding to the yields in the sixteen detectors are multiplied by the sixteen yield factors. The resulting corrected yields are then plotted against frequency. Other runs may be plotted on the same sheet(s) of graph paper.

The input consists of the following cards:

Card 1	DD
Card 2	NPLOTS, YMAX
Card 3	(XMN(I), I = 1, NPLOTS)
Card 4	(XMX(I), I = 1, NPLOTS)
Card 5	RUN, F8
Card 6	SUM
Card 7	RUN, F8
Card 8	SUM

.

.

.

Blank Card

.

where

DD   =   title of $\leq$ 12 characters

NPLOTS = number of sheets of graph paper

YMAX = number of counts at the top edge of the graph
paper

XMN = array of frequencies at the left edge of the
NPLOTS sheets of graph paper.

XMX = array of frequencies at the right edge of
the NPLOTS sheets of graph paper.

RUN = arbitrary run number

F8 = frequency of detector 8

SUM = array of 16 sums corresponding to the
yields in the 16 detectors.

Cards 5 and 6 contain the data for one run. Cards for
other runs which are to be plotted on the same sheet(s) of graph
paper are placed after card 6 as illustrated by cards 7 and 8. A
blank card must be placed after the last run for this plot. This
sequence of cards may be repeated indefinitely.

A listing of the program is given below.

```
$IBFTC CMD        DECK
C
C        ARRAY DATA REDUCTION
C
         DIMENSION DD(12),INN(3)
          INTEGER RUN,ABCD
         DATA INN /1H(, 6H          , 6HF10.0) /
         DIMENSION CORR(16),FREQ(16),X(1000),Y(1000),Z(1000),E(1000)
       DIMENSION TIT1(2)
       DATA TIT1/9HFREQUENCY/
       DATA TIT2/5HYIELD/
         DIMENSION XMN(8),XMX(8),SUM(16)
C
C        NOTATION
C              X IS AN  ARRAY OF FREQUENCIES
C              Y IS AN ARRAY OF SUMS FROM THE 16 COUNTER ARRAY
C              E IS AN ARRAY OF FREQUENCIES TO BE PLOTTED
C              Z IS AN ARRAY OF SUMS TO BE PLOTTED
C
         DATA(FREQ(I),I=1,16)/.98149,.98416,.98689,.98961,.99230,
     1 .99494,.99749,1.,1.00257,1.00502,1.00749,1.00984,1.01222,1.01453,
     2 1.01692,1.01912/
         DATA(CORR(I),I=1,16)/.879,1.018,.950,.954,.949,.995,1.033,1.000,
     1 1.124,1.005,1.109,1.160,1.171,1.232,1.254,1.279/
     12  CONTINUE
         READ(5,500)DD
     500 FORMAT(12A6)
         READ(5,102)NPLOTS,YMAX
     102 FORMAT(I2,F10.0)
          INN(2) = ABCD(NPLOTS)
         READ(5,INN)(XMN(I),I=1,NPLOTS)
         READ(5,INN)(XMX(I),I=1,NPLOTS)
          WRITE(6,210)(XMN(I),XMX(I),I=1,NPLOTS)
     210 FORMAT(1H02F10.0)
         L = 0
     3   READ(5,100)RUN,F8
     100 FORMAT(I2,F10.0)
         IF(F8.EQ.0.)GO TO 4
         WRITE(6,201)RUN,F8
     201 FORMAT(5H1RUN I2, 7H, F8 = F10.0 /
     1 1H0 16X 4HFREQ 7X 8HCORR SUM 12X 3HSUM      )
         L = L + 16
         READ(5,103)SUM
     103 FORMAT(16F5.0)
         DO 1 J = 1,16
         F = F8*FREQ(J)
         S = SUM(J)*CORR(J)
         N = (L-16) + J
         X(N) = F
         Y(N) = S
         WRITE(6,200)J,X(N),Y(N),SUM(J)
     200 FORMAT(1H I10,F10.3,F15.3,F15.3)
     1   CONTINUE
         GO TO 3
     4   CONTINUE
         WRITE(6,204)
     204 FORMAT(1H1)
         DO 10 J = 1,NPLOTS
          XMIN = XMN(J)
         XMAX = XMX(J)
         K = 0
```

```
      DO 11 I = 1,N
      IF(X(I).LT.XMIN.OR.X(I).GT.XMAX)GO TO 11
      K = K + 1
      E(K) = X(I)
      Z(K) = Y(I)
11    CONTINUE
      WRITE(6,203)J,XMIN,XMAX,YMAX,K
203   FORMAT(6HOPLOT I1, 9H, XMIN = F6.0, 9H, XMAX = F6.0,
     1 9H, YMAX = F6.0, 2H, I3, 7H POINTS )
      CALL LABEL(0.0,0.0,0.0,YMAX,10.0,10,TIT2,5,1)
      CALL LABEL(0.0,0.0,XMIN,XMAX,15.0,15,TIT1,9,0)
      CALL XYPLT(K,E,Z,XMIN,XMAX,0.,YMAX,DD,1,3)
10    CONTINUE
      GO TO 12
      END
$IBLDR*MLLLBL
$IBLDR*MLLXYP
```

APPENDIX D. PROGRAM FOR THE ANALYSIS OF PARTICLE-GAMMA CORRELATIONS

The analysis is carried out in the manner described in Sections III. B and III. C. 4. Only one gamma ray is considered, but only a simple modification is necessary to analyze any member of a gamma-ray cascade (see Appendix E and Poletti and Warburton, 1965). The program can handle one or two non-negative magnetic substates, that is M_d = 0; 1/2; 0, 1; or 1/2, 3/2. Admixtures of the first magnetic substate which is not allowed may be added to observe a possible effect from the finite size of the particle detector. These admixtures are specified as a fraction of the population of the last allowed magnetic substate. Then Formula (9) of Section III. B. becomes

$$W(\theta) = \sum_{M_{dMAX} \geq M_d \geq 0} I(M_d)[\sum_{k \text{ even}} \rho_k(J_d, M_d)F_k(J_dJ_e)Q_kP_k(\cos \theta)]$$

$$+ (ADM) \times I(M_{dMAX})[\sum_k \rho_k(J_d, M_{dMAX} + 1)F_k(J_dJ_e)Q_kP_k(\cos \theta)]$$

where M_{dMAX} is the maximum allowed magnetic substate and ADM is the admixture of the magnetic substate $M_{dMAX} + 1$.

The input consists of the following:

Card 1		Q(5)
Card 2	K,	A(K)
Card 3	L,	B(L)
Card 4	H,	P

Card 5	THT(H)
Card 6	Y(H)
Card 7	ERR(H)
Card 8	MAXADM, ADM(MAXADM)

where

Q(5)	=	attenuation coefficients Q_0, Q_2, Q_4, Q_6, Q_8
K	=	number of values of the spin of the initial state ($K \leq 6$)
A(K)	=	spins of the initial state
L	=	number of values of the spin of the final state ($L \leq 6$)
B(L)	=	spins of the final state
H	=	number of angles
P	=	number of non-negative magnetic substates allowed
THT(H)	=	angles
Y(H)	=	yields
ERR(H)	=	uncertainties in the yields
MAXADM	=	number of values for the admixture ADM. ($MAXADM \leq 3$)
ADM(MADADM)	=	admixtures

A listing of the program is given below.

```
$IBFTC PGC      DECK
C
C        PARTICLE-GAMMA CORRELATION ANALYSIS
C
         DIMENSION A(6),B(6),PHI(37),QSQR(37,3),PPR(37,3,2),PHIMIN(6,3),
       1 EPMIN(6,3),EPMAX(6,3),XMIN(6,3),ERRX(6,3),CHISQ(6,3),
       2 PPMINR(6,3,2),DXR(6,3),PHISTP(6,3,11),QSQSTP(6,3,11),XTRIAL(6),
       3 NMIN(3),DUMMY(2)
         COMMON/LSQ/P,H,ITHT,KMAX,THT(16),KADM,ALPHA,AP,ADM(3),I3,Q(5),BP,
       1 SIGMA,X,ATANX,KARG,KCALC,ERR(16),Y(16),PP(2),QSQ,NDEG
         INTEGER P,H,SIGMA
      5  READ(5,10)Q
     10  FORMAT(5F10.3)
         READ(5,20) K,(A(I),I=1,K)
         READ(5,20) L,(B(I),I=1,L)
     20  FORMAT(I2,3X,6F5.2)
         READ(5,30)H,P
C        H=NUMBER OF ANGLES, H.LE.8
C        P=NUMBER OF MAGNETIC SUBSTATES, P.LE.2
     30  FORMAT(2I2)
         READ(5,40) (THT(I),I=1,H)
     40  FORMAT(8F10.3)
         READ(5,40) (Y(I),I=1,H)
         READ(5,40) (ERP(I),I=1,H)
         READ(5,50) MAXADM,(ADM(I),I=1,MAXADM)
C        MAXADM.LE.3
     50  FORMAT(I2,3X,6F5.2)
         SIGMA=0
C        IN THE REMAINDER OF THIS PROGRAM, SIGMA HAS BEEN ASSUMED TO
C        BE ARBITRARY.
         NDEG=H-P-1
C
C        THIS SECTION PRINTS OUT INPUT
C
         WRITE(6,100)H,P,NDEG
    100  FORMAT(5H1H = I2,4X,4HP = I2,4X,7HNDEG = I2)
         WRITE(6,110)
    110  FORMAT(//1H0,9X,26HQ0     Q2     Q4     Q6     Q8)
         WRITE(6,120)Q
    120  FORMAT(8X,5F6.3)
         WRITE(6,130) (THT(I),I=1,H)
    130  FORMAT(//9H0ANGLES  8F13.2/9X,8F13.2/9X,8F13.2)
         WRITE(6,140) (Y(I),I=1,H)
    140  FORMAT(//9H0YIELDS  8F13.6/9X,8F13.6/9X,8F13.6)
         WRITE(6,150) (ERR(I),I=1,H)
    150  FORMAT(//9H0ERRORS  8F13.6/9X,8F13.6/9X,8F13.6)
C
C        THIS SECTION BEGINS THE CALCULATIONS
C
         PHI(1)=-90.
         DO 210 I=2,37
    210  PHI(I)=PHI(I-1)+5.
         ITHT=0
         DO 760 I1=1,K
         AP=A(I1)
         DO 760 I2=1,L
         TWOA=2.*AP
         IAP=TWOA/2.
         FLIAP=IAP
         IF(FLIAP*2.-TWOA)205,206,205
    205  KMAX=TWOA-1.
```

```
          ALPHA=.5
          GO TO 207
   206    KMAX=TWOA
          ALPHA=.0
   207    KCALC=0
          BP=B(I2)
          DO 520 I3=1,MAXADM
          KARG=2
          KADM=0
          GO TO (230,250),P
   230    DO 240 I4=1,37
          ATANX=PHI(I4)
          CALL QSPP
          QSQR(I4,I3)=QSQ
   240    PPR(I4,I3,1)=PP(1)
          GO TO 265
   250    IF(AP-1.0)255,256,256
   255    P=1
          GO TO 257
   256    P=2
   257    DO 260 I4=1,37
          ATANX=PHI(I4)
          CALL QSPP
          QSQR(I4,I3)=QSQ
          PPR(I4,I3,1)=PP(1)
   260    PPR(I4,I3,2)=PP(2)
C
C
C         FINDS MINIMA OF QSQ-S AS A FUNCTION OF X
C
   265    IF(AP-1.)520,270,270
   270    IXMIN=1
          KSTART=1
          IF(QSQR(1,I3).GT.15.) GO TO 340
          IF(QSQR(1,I3)-QSQR(2,I3))280,340,340
   280    ATANX=-89.9
          CALL QSPP
          IF(QSQ-QSQR(1,I3))290,300,300
   290    XTRIAL(IXMIN)=ATAN(-89.9/57.295779)
          IXMIN=2
          GO TO 340
   300    PHIMIN(1,I3)=-90.
C         FIRST INDEX=MINIMUM INDEX
C         SECOND INDEX=ADM INDEX
          EPMIN(1,I3)=0.
          EPMAX(1,I3)=0.
          XMIN(1,I3)=0.
          ERRX(1,I3)=0.
          CHISQ(1,I3)=QSQR(1,I3)
          DO 310 I7=1,P
   310    PPMINR(1,I3,I7)=PPR(1,I3,I7)
C         FIRST INDEX OF PPMINR=MINIMUM INDEX
C         SECOND INDEX OF PPMINR=ADM INDEX
C         THIRD INDEX=POPULATION PARAMETER INDEX
          DXR(1,I3)=0.
          DO 330 I=1,11
          RI1=I-1
          PHISTP(1,I3,I)=-89.9+.5*RI1
C         FIRST INDFX=MINIMUM INDEX
C         SECOND INDFX=ADM INDEX
C         THIRD INDFX=STEP INDFX
          ATANX=PHISTP(1,I3,I)
```

```
          CALL QSPP
   330    QSQSTP(1,I3,I)=QSQ
          IXMIN=2
          KSTART=2
   340    DO 360 I5=2,36
          IF(QSQR(I5,I3).GT.15.) GO TO 360
          IF(QSQR(I5,I3).LT.QSQR(I5-1,I3).AND.QSQR(I5,I3).LT.QSQR(I5+1,
         1 I3)) GO TO 350
          GO TO 360
   350    XTRIAL(IXMIN)=TAN(PHI(I5)/57.295779)
          IXMIN=IXMIN+1
   360    CONTINUE
          IF(QSQR(37,I3).GT.15.) GO TO 430
          IF(QSQR(37,I3)-QSQR(36,I3)) 370,430,430
   370    ATANX=89.9
          CALL QSPP
          IF(QSQ-QSQR(37,I3)) 380,390,390
   380    XTRIAL(IXMIN)=ATAN(89.9/57.295779)
          IXMIN=IXMIN+1
          GO TO 430
   390    PHIMIN(IXMIN,I3)=90.
          EPMIN(IXMIN,I3)=0.
          EPMAX(IXMIN,I3)=0.
          XMIN(IXMIN,I3)=0.
          ERRX(IXMIN,I3)=0.
          CHISQ(IXMIN,I3)=QSQR(37,I3)
          DO 400 I7=1,P
   400    PPMINR(IXMIN,I3,I7)=PPR(37,I3,I7)
          DXR(IXMIN,I3)=0.
          DO 420 I=1,11
          RI1=I-1
          PHISTP(IXMIN,I3,I)=84.9+.5*RI1
          ATANX=PHISTP(IXMIN,I3,I)
          CALL QSPP
   420    QSQSTP(IXMIN,I3,I)=QSQ
          KSTOP=IXMIN-1
          IXMIN=IXMIN+1
          GO TO 440
   430    KSTOP=IXMIN-1
   440    NMIN(I3)=IXMIN-1
          IF(KSTART.GT.KSTOP) GO TO 520
C         WILL OCCUR WITH ONLY A MINIMUM AT -90 OR +90
C         OR NO MINIMUM
          DO 515 I8=KSTART,KSTOP
          KARG=1
          X2=XTRIAL(I8)
          DX=0.
          DO 490 I=1,10
          X2=X2+DX
          DP=ABS(X2)/100.
          IF(DP-.01)450,450,460
   450    D=.01
          GO TO 470
   460    D=DP
   470    X1=X2-D
          X3=X2+D
          X=X1
          CALL QSPP
          QX1=QSQ
          X=X2
          CALL QSPP
```

```
        QX2=QSQ
        X=X3
        CALL QSPP
        QX3=QSQ
        AE=QX1-QX3
        BE=QX1+QX3-2.*QX2
        DX=AE*D/(2.*BE)
        IF(ABS(X2).LT..001) GO TO 490
        PERC=ABS(DX/X2)
        IF(PERC.LT..001) GO TO 500
  490   CONTINUE
  500   XMIN(I8,I3)=X2+DX
        ERRX(I8,I3)=SQRT(2.*D**2/(BE*FLOAT(H-P-1)))
        CHISQ(I8,I3)=QX2-AE**2/(8.*BE)
        PHIMIN(I8,I3)=ATAN(XMIN(I8,I3))*57.295779
        EPMIN(I8,I3)=ATAN(XMIN(I8,I3)-ERRX(I8,I3))*57.295779
        EPMAX(I8,I3)=ATAN(XMIN(I8,I3)+ERRX(I8,I3))*57.295779
        DXR(I8,I3)=DX
        DO 510 I7=1,P
  510   PPMINR(I8,I3,I7)=PP(I7)
        PSMIN=ATAN(XMIN(I8,I3))*57.295779-2.5
        IF(PSMIN.LT.-89.9) PSMIN=-89.9
        IF(PSMIN.GT.84.9) PSMIN=84.9
        KARG=2
        DO 515 I=1,11
        RI1=I-1
        PHISTP(I8,I3,I)=PSMIN+RI1*.5
        ATANX=PHISTP(I8,I3,I)
        CALL QSPP
        QSQSTP(I8,I3,I)=QSQ
  515   CONTINUE
  520   CONTINUE
C
C       THIS SECTION WRITES THE OUTPUT
C
        WRITE(6,220) A(I1),B(I2)
  220   FORMAT(5H1A = F4.1,3X,4HB = F4.1)
        WRITE(6,600) (ADM(I),I=1,MAXADM)
  600   FORMAT(12H0ADMIXTURE =,13X,F10.3,30X,F10.3,30X,F10.3)
        WRITE(6,610)
  610   FORMAT(4H0PHI,16X,3HQSQ,7X,4HP(1),6X,4HP(2),16X,3HQSQ,7X,4HP(1),
       1 6X,4HP(2),16X,3HQSQ,7X,4HP(1),6X,4HP(2)//)
        GO TO (620,640),P
  620   DO 630 I=1,37
  630   WRITE(6,635) PHI(I),(QSQR(I,J),PPR(I,J,1),J=1,MAXADM)
        GO TO 661
  635   FORMAT(1H ,F4.0,10X,2F10.3,20X,2F10.3,20X,2F10.3)
  640   DO 650 I=1,37
  650   WRITE(6,660)PHI(I),(QSQR(I,J),PPR(I,J,1),PPR(I,J,2),J=1,MAXADM)
  660   FORMAT(1H ,F4.0,10X,3F10.3,10X,3F10.3,10X,3F10.3)
  661   DO 750 I3=1,MAXADM
        IF(AP-1.)665,669,669
  665   WRITE(6,666) ADM(I3)
  666   FORMAT(16H0FOR ADMIXTURE =,F6.3)
        WRITE(6,668)
  668   FORMAT(1H0,14X,4HP(1),6X,4HP(2))
        WRITE(6,667)(PPR(1,I3,I),I=1,P)
  667   FORMAT(11X,2F10.3)
        GO TO 750
  669   NMINP=NMIN(I3)
        IF(NMINP-0) 750,750,670
```

```
  670    WRITE(6,671) ADM(I3)
  671    FORMAT(16HOFOR ADMIXTURE =,F6.3,18H    MINIMA OCCUR AT)
         DO 745 I8=1,NMINP
         WRITE(6,680)
  680    FORMAT(1H0,10X,4X,6HPHIMIN,5X,5HEPMIN,5X,5HEPMAX,8X,4HXMIN,16X,
        1 4HERRX,15X,5HCHISQ,17X,3HDXR)
         WRITE(6,690) PHIMIN(I8,I3),EPMIN(I8,I3),EPMAX(I8,I3),XMIN(I8,I3),
        1 ERRX(I8,I3),CHISQ(I8,I3),DXR(I8,I3)
  690    FORMAT(1H ,10X,3F10.3,4E20.8)
         WRITE(6,700)
  700    FORMAT(1H0,14X,4HP(1),6X,4HP(2))
         DO 702 K=1,P
         DUMMY(K)=PPMINR(I8,I3,K)
  702    CONTINUE
         WRITE(6,710) (DUMMY(K),K=1,P)
  710    FORMAT(11X,2F10.3)
         WRITE(6,720)
  720    FORMAT(1H0,7X,6HPHISTP,4X,6HQSQSTP)
         DO 730 I=1,11
  730    WRITE(6,740) PHISTP(I8,I3,I),QSQSTP(I8,I3,I)
  740    FORMAT(7X,F7.3,3X,F8.3)
  745    CONTINUE
  750    CONTINUE
  760    CONTINUE
         GO TO 5
         END
$IBFTC QPP        DECK
C
C        A SUBROUTINE FOR QSQ AND PP
C        THIS SUBROUTINE USES THE FOLLOWING PROGRAMS
C            RK,FAK
C
         SUBROUTINE QSPP
         COMMON/LSQ/P,H,ITHT,KMAX,THT(16),KADM,ALPHA,AP,ADM(3),I3,Q(5),BP,
        1 SIGMA,X,ATANX,KARG,KCALC,ERR(16),Y(16),PP(2),QSQ,NDEG
         DIMENSION PLR(5,16),RKQADR(5,2),SUMK(16,2),D(2),C(2,2)
         REAL NUM(2)
         INTEGER P,H,SIGMA
         KMAXP=KMAX/2+1
         IF(ITHT-0) 35,20,35
C        IF ITHT.EQ.0, CALCULATES A NEW LEGENDRE POLYNOMIAL ARRAY
C            AND SETS ITHT=1
C        IF ITHT.NE.0, USES STORED ARRAY
   20    RNDEG=NDEG
         DO 30 J1=1,H
         COSTHT=COS(THT(J1)/57.295779)
         DO 30 J2=1,5
         J2P=2*(J2-1)
   30    PLR(J2,J1)=PL(J2P,COSTHT)
C        FIRST INDEX = K INDEX
C        SECOND INDEX = ANGLE INDEX
         ITHT=1
   35    GO TO (40,240),P
   40    IF(KADM-0) 70,50,70
C        IF KADM.EQ.0, CALCULATES NEW RKQADR-S AND SETS KADM=1
C        IF KADM.NE.0, USES STORED RKQADR-S
   50    ALPHA1=ALPHA+1.
         DO 60 J1=1,KMAXP
         RJ1=2*(J1-1)
         RKQADR(J1,1)=(RHOK(RJ1,AP,ALPHA)+ADM(I3)*RHOK(RJ1,AP,ALPHA1))
        1 *Q(J1)
```

```
      60  CONTINUE
C         FIRST INDEX = K INDEX
C         SECOND INDEX = PP INDEX
          KADM=1
      70  DO 80 J1=1,H
          SUMK(J1,1)=0.
          DO 80 J2=1,KMAXP
          AK = 2*(J2-1)
          SUMK(J1,1)=SUMK(J1,1)+RKQADR(J2,1)*F(AK,AP,BP,SIGMA,X,ATANX,
         1 KARG,KCALC)*PLR(J2,J1)
      80  CONTINUE
C         FIRST INDEX = ANGLE INDEX
C         SECOND INDEX = PP INDEX
          KCALC=1
          D(1)=0.
          C(1,1)=0.
          DO 90 J1=1,H
          ERRSQ = ERR(J1)*ERR(J1)
          D(1)=D(1)+Y(J1)*SUMK(J1,1)/ERRSQ
          C(1,1)=C(1,1)+SUMK(J1,1)*SUMK(J1,1)/ERRSQ
      90  CONTINUE
          PP(1)=D(1)/C(1,1)
          IF(.0001-C(1,1)) 120,120,100
     100  GO TO (105,115), KARG
     105  WRITE(6,110)X,D(1),C(1,1),PP(1)
     110  FORMAT(20HOWARNING      FOR X = ,F10.4,2H ,,13H NUMERATOR =,E12.4,
         1 15H DENOMINATOR = ,E12.4,8H PP(1) = ,F12.4)
          GO TO 120
     115  WRITE(6,116) ATANX,D(1),C(1,1),PP(1)
     116  FORMAT(28HOWARNING      FOR ARCTAN X  = ,F10.4,2H ,,
         1 13H NUMERATOR = E12.4,15H DENOMINATOR = ,E12.4,8H PP(1) = ,F12.4)
     120  SUMQSQ=0.
          DO 130 J1=1,H
          TERM=(Y(J1)-PP(1)*SUMK(J1,1))/ERR(J1)
     130  SUMQSQ=SUMQSQ+TERM*TERM
          QSQ=SUMQSQ/RNDEG
          GO TO 380
     240  IF(KADM-0)270,250,270
     250  ALPHA1=ALPHA+1.
          ALPHA2=ALPHA+2.
          DO 260 J1=1,KMAXP
          RJ1=2*(J1-1)
          RKQADR(J1,1)=RHOK(RJ1,AP,ALPHA)*Q(J1)
          RKQADR(J1,2)=(RHOK(RJ1,AP,ALPHA1)+ADM(I3)*RHOK(RJ1,AP,ALPHA2))*
         1 Q(J1)
     260  CONTINUE
C         FIRST INDEX = K INDEX
C         SECOND INDEX = PP INDEX
          KADM=1
     270  DO 280 J1=1,H
          DO 280 J2=1,2
          SUMK(J1,J2)=0.
          DO 280 J3=1,KMAXP
          AK = 2*(J3-1)
          SUMK(J1,J2)=SUMK(J1,J2)+RKQADR(J3,J2)*F(AK,AP,BP,SIGMA,X,ATANX,
         1 KARG,KCALC)*PLR(J3,J1)
     280  CONTINUE
C         FIRST INDEX = ANGLE INDEX
C         SFCOND INDEX = PP INDEX
          KCALC=1
          C(1,1)=0.
```

```
          C(2,1)=0.
          C(1,2)=0.
          C(2,2)=0.
          DO 320 J1=1,2
          DO 320 J2=1,2
          DO 320 J3=1,H
          C(J1,J2)=C(J1,J2)+SUMK(J3,J1)*SUMK(J3,J2)/(ERR(J3)*ERR(J3))
  320     CONTINUE
          D(1)=0.
          D(2)=0.
          DO 330 J1=1,H
          ERRSQ=ERR(J1)*ERR(J1)
          D(1)=D(1)+SUMK(J1,1)*Y(J1)/ERRSQ
          D(2)=D(2)+SUMK(J1,2)*Y(J1)/ERRSQ
  330     CONTINUE
          NUM(1)=D(1)*C(2,2)-D(2)*C(1,2)
          NUM(2)=D(2)*C(1,1)-D(1)*C(2,1)
          DEN=C(1,1)*C(2,2)-C(2,1)*C(1,2)
          PP(1)=NUM(1)/DEN
          PP(2)=NUM(2)/DEN
          TEST=PP(1)*PP(2)
          IF(TEST-0.) 400,335,335
  335     IF(.0001-DEN)360,360,340
  340     GO TO (345,355),KARG
  345     WRITE(6,350) X,DEN,NUM(1),PP(1),NUM(2),PP(2)
  350     FORMAT(20HOWARNING     FOR X = ,F10.4,2H ,,7H DEN = ,E12.4,
      1   10H NUM(1) = ,E12.4,9H PP(1) = ,F12.4,10H NUM(2) = ,E12.4,
      2   9H PP(2) = ,F12.4)
          GO TO 360
  355     WRITE(6,356) ATANX,DEN,NUM(1),PP(1),NUM(2),PP(2)
  356     FORMAT(28HOWARNING     FOR ARCTAN X  = ,F10.4,2H ,,7H DEN = ,
      1   E12.4,10H NUM(1) = ,E12.4,9H PP(1) = ,F12.4/10H NUM(2) = ,E12.4,
      2   9H PP(2) = ,F12.4)
  360     SUMQSQ=0.
          DO 370 J1=1,H
          TERM=(Y(J1)-PP(1)*SUMK(J1,1)-PP(2)*SUMK(J1,2))/ERR(J1)
          SUMQSQ=SUMQSQ+TERM*TERM
  370     CONTINUE
          QSQ=SUMQSQ/RNDEG
          GO TO 380
C         THIS SECTIONS CONSTRAINS PP-S TO BE NON-NEGATIVE
  400     PP2=D(2)/C(2,2)
          IF(.0001-C(2,2))460,460,440
  440     GO TO (445,455),KARG
  445     WRITE(6,450)X,C(2,2),D(2),PP2
  450     FORMAT(20HOWARNING     FOR X = ,F10.4,2H ,,7H DEN = ,E12.4,
      1   10H NUM(1) = ,E12.4,9H PP(1) = ,F12.4)
          GO TO 460
  455     WRITE(6,456) ATANX,C(2,2),D(2),PP2
  456     FORMAT(28HOWARNING     FOR ARCTAN X  = ,F10.4,2H ,,7H DEN = ,
      1   E12.4,10H NUM(1) = ,E12.4,9H PP(1) = ,F12.4)
  460     SUMQS1=0.
          DO 470  J1=1,H
          TERM=(Y(J1)-PP2*SUMK(J1,2))/ERR(J1)
          SUMQS1=SUMQS1+TERM*TERM
  470     CONTINUE
          QS1=SUMQS1/RNDEG
          PP1=D(1)/C(1,1)
          IF(.0001-C(1,1)) 560,560,540
  540     GO TO (545,555),KARG
  545     WRITE(6,550) X,C(1,1),D(1),PP1
```

```
      550   FORMAT(20HOWARNING      FOR X = ,F10.4,2H ,,7H DEN = ,E12.4,
          1 10H NUM(1) = ,E12.4,9H PP(1) = ,F12.4)
            GO TO 560
      555   WRITE(6,556) ATANX,C(1,1),D(1),PP1
      556   FORMAT(28HOWARNING      FOR ARCTAN X  = ,F10.4,2H ,,7H DEN = ,
          1 E12.4,10H NUM(1) = ,E12.4,9H PP(1) = ,F12.4)
      560   SUMQS2=0.
            DO 570 J1=1,H
            TERM=(Y(J1)-PP1*SUMK(J1,1))/ERR(J1)
            SUMQS2=SUMQS2+TERM*TERM
      570   CONTINUE
            QS2=SUMQS2/RNDEG
            IF(QS1-QS2) 600,600,610
      600   QSQ=QS1
            PP(1)=0.
            PP(2)=PP2
            GO TO 380
      610   QSQ=QS2
            PP(1)=PP1
            PP(2)=0.
      380   RETURN
            END
$IBFTC FAK       DECK
C
C         A FUNCTION FOR F SUB K OF A,B, AND X OR ATANX
C              NEW 1/16/67
C
            FUNCTION F(AK,A,B,SIGMA,X,ATANX,KARG,KCALC)
C
C           REAL AK,A,B,ATANX
C           INTEGER SIGMA,KARG,KCALC
C
C           ATANX IN DEGREES
C
C           IF KARG=1, X IS USED
C           IF KARG=2,ATANX IS USED
C
C           IF KCALC=0, FK-S ARE CALCULATED
C           IF KCALC=1, STORED FK-S ARE USED
C
C
            DIMENSION FKR(5,3)
            INTEGER SIGMA
            ABST=0.
            GO TO (10,20),KARG
      10    XSQ=X*X
            GO TO 40
      20    ABST=ABS(ATANX)
            IF(ABST-90.) 30,40,30
      30    X=TAN(ATANX/57.295779)
            XSQ=X*X
      40    K=AK/2.+1.
            IF(KCALC-0) 100,50,100
      50    EMAX=A+B
            IF(EMAX-1.) 60,70,70
      60    ICASE=1
            GO TO 100
      70    EL=ABS(B-A)
            IF(EL.EQ.0.) EL=1.
            ELP=EL+1.
            IF(ELP-EMAX)90,90,80
```

```
      80   FKR(K,1)=FK(AK,EL,EL,B,A)
           ICASE=2
           GO TO 100
      90   PHZ=(-1.)**SIGMA
           FKR(K,1)=FK(AK,EL,EL,B,A)
           FKR(K,2)=FK(AK,EL,ELP,B,A)
           FKR(K,3)=FK(AK,ELP,ELP,B,A)
           ICASE=3
     100   GO TO (110,120,130),ICASE
     110   F=0.
           GO TO 160
     120   F=FKR(K,1)
           GO TO 160
     130   IF(ABST-90.) 150,140,150
     140   F=FKR(K,3)
           GO TO 160
     150   F=(FKR(K,1)-PHZ*2.*X*FKR(K,2)+XSQ*FKR(K,3))/(1.+XSQ)
     160   RETURN
           END
$IBFTC ADC      DECK
C
C        A FUNCTION FOR F-K(L,L',B,A), ANG. DISTRIB. COEFF.
C        REF., EQUATION (6), LOW LYING LEVELS OF F18, POLETTI AND
C        WARBURTON, PHYS REV 137, B599 (1965)
C        ALL ARGUMENTS IN FLOATING POINT
C
           FUNCTION FK(K,L,LP,B,A)
C
           REAL K,L,LP
           N = B-A-1.
           PHZF =(-1.)**N
           RF = SQRT((2.*L+1.)*(2.*LP+1.)*(2.*A+1.))
           N = LP-L
           PHZ = (-1.)**N
           ROOT = SQRT(2.*K+1.)
           CG =PHZ*ROOT*THREEJ(L,1.,LP,-1.,K,-0.)
           N = -A-A-L-LP
           PHZ = (-1.)**N
           W = PHZ*SIXJ(A,A,L,LP,K,B)
           FK = PHZF*RF*CG*W
           RETURN
           END
$IBFTC RK       DECK
C
C        A FUNCTION FOR RHO(K,A,ALPHA), STAT. TENSOR COEFFICIENTS
C        REF. EQUATION(3) OF LOW LYING LEVELS OF F18, POLETTI AND
C        WARBURTON, PHYS REV 137, B599 (1965)
C        ARGUMENTS FOR THIS FUNCTION MUST BE IN FLOATING POINT
C
           FUNCTION RHOK(K,A,ALPHA)
           REAL K
           ROOT = SQRT(2.*K + 1.)
           CG1 = ROOT*THREEJ(A,ALPHA,A,-ALPHA,K,-0.)
           ROOT = 1.
           CG2 = ROOT*THREEJ(A,ALPHA,A,-ALPHA,0.,-0.)
C
C         NOTE, BECAUSE J1=J2 AND M3=0 THE PHASE IS TAKEN AS +1.
C
           RHOK = (2. - DAB(ALPHA,0.))*CG1/CG2
           RETURN
           END
```

```
$IBFTC PLC      DECK
C
C         LEGENDRE POLYNOMIALS
C
          FUNCTION PL(L,CT)
          IF(L)1,1,2
     1    PL = 1.
          RETURN
     2    IF(L-1)3,3,4
     3    PL = CT
          RETURN
     4    N = 2
          PO = 1.0
          P1 = CT
     7    AN = N
          P2 = ((2.0*AN-1.0)*CT*P1-(AN-1.0)*PO)/AN
          N = N + 1
          IF(L-N)5,6,6
     6    PO = P1
          P1 = P2
          GO TO 7
     5    PL = P2
          RETURN
          END
$IBFTC KD       DECK
       FUNCTION DAB(A,B)                                                DAB
       IF(A-B)1,2,1                                                     DAB
     2    DAB = 1.0                                                     DAB
     3    RETURN                                                        DAB
     1    DAB = 0.0                                                     DAB
          GO TO 3                                                       DAB
          END                                                          DAB
$IBFTC DEL       NOLIST,DECK
C         FUNCTION DELTA(A,B,C)
C
C         ROTENBERG ET. AL. PAGE 13 (2.4)
C
          FUNCTION DELTA(A,B,C)
          S1 = A + B - C
          M = S1
          FS1 = FACT(M)
          S2 = A + C - B
          M = S2
          FS2 = FACT(M)
          S3 = B + C - A
          M = S3
          FS3 = FACT(M)
          DENOM = A+B+C+1.0
          M = DENOM
          FD = FACT(M)
          DELTA =   SQRT((FS1*FS2*FS3)/FD)
          RETURN
          END
$IBFTC TOR       NOLIST,DECK
C         CONTAINS FACTORIALS OF NUMBERS UP TO 33
          FUNCTION FACT(L)
          IF(L)55,1,50
     1    FACT = 1.0
          RETURN
    50    GO TO(1,2,3,4,5,6,7,8,9,10,11,12,13,14,15,16,17,18,19,20,21,22,
     1 23,24,25,26,27,28,29,30,31,32,33        ),L
```

```
 2   FACT = 2.0
     RETURN
 3   FACT = 6.0
     RETURN
 4   FACT = 24.0
     RETURN
 5   FACT = 120.0
     RETURN
 6   FACT = 720.0
     RETURN
 7   FACT = 5.04E+3
     RETURN
 8   FACT = 4.032E+4
     RETURN
 9   FACT = 3.6288E+5
     RETURN
10   FACT = 3.6288E+6
     RETURN
11   FACT = 3.9917E+7
     RETURN
12   FACT = 4.7900E+8
     RETURN
13   FACT = 6.227E+9
     RETURN
14   FACT = 8.7178E+10
     RETURN
15   FACT = 1.3077E+12
     RETURN
16   FACT = 2.0923E+13
     RETURN
17   FACT = 3.5569E+14
     RETURN
18   FACT = 6.4024E+15
     RETURN
19   FACT = 1.2165E+17
     RETURN
20   FACT = 2.4329E+18
     RETURN
21   FACT = 5.1091E+19
     RETURN
22   FACT = 1.1240E+21
     RETURN
23   FACT = 2.5852E+22
     RETURN
24   FACT = 6.2045E+23
     RETURN
25   FACT = 1.5511E+25
     RETURN
26   FACT = 4.0329E+26
     RETURN
27   FACT = 1.0889E+28
     RETURN
28   FACT = 3.0489E+29
     RETURN
29   FACT = 8.8418E+30
     RETURN
30   FACT = 2.6525E+32
     RETURN
31   FACT = 8.2228E+33
     RETURN
32   FACT = 2.6313E+35
```

```
         RETURN
     33  FACT = 8.6833E+36
         RETURN
     55  WRITE(6,200)
    200  FORMAT(29H0FACTORIAL OF NEGATIVE NUMBER /)
         STOP
         END
$IBFTC 3JS       DECK
C     A FUNCTION FOR THREE J SYMBOLS
C
C         ROTENBERG ET. AL. (1.5) PAGE 2 WITH (2.4) FROM PAGE 13
C         INPUT IS THREEJ(J1,M1,J2,M2,J3,M3) FLOATING POINT
C             ROUTINE REQUIRES FACTORIAL AND DELTA ROUTINES
C
         FUNCTION THREEJ(A1, B1, A2, B2, A3, B3)
         DIMENSION A(3), B(3)
         A(1) = A1
         A(2) = A2
         A(3) = A3
         B(1) = B1
         B(2) = B2
         B(3) = B3
         DO 35 I = 1,3
         IF(A(I).NE.0.)GO TO 36
         IF(B(I).NE.0.)GO TO 36
     35  CONTINUE
         THREEJ = 1.
         RETURN
     36  CONTINUE
         TEST = B1+B2+B3
         IF(TEST)1,2,1
      1  THREEJ = 0.0
         RETURN
      2  S1 = A1 + A2 - A3
         IF(S1)1,12,12
     12  S2 = A1 -A2 + A3
         IF(S2)1,14,14
     14  S3 = A2 + A3 - A1
         IF(S3)1,15,15
     15  N = A1 -A2 - B3
         TBA = ABS(B1)-A1
         IF(TBA)50,50,1
     50  TBA = ABS(B2)-A2
         IF(TBA)51,51,1
     51  TBA = ABS(B3)-A3
         IF(TBA)52,52,1
     52  CONTINUE
         PHZ = (-1.0)**N
         DEL = DELTA(A1, A2, A3)
         X = 1.0
         DO 3 J = 1,3
         S = A(J) + B(J)
         M = S
         FS = FACT(M)
         X = X * FS
         SM = A(J) - B(J)
         M = SM
         FSM = FACT(M)
      3  X = X*FSM
         ROOT = SQRT(X)
         SUM = 0.0
```

```
      AK = 0.0
   11 DS1 = AK+A3-A1-B2
      IF(DS1)5,4,4
    4 M = DS1
      FDS1 = FACT(M)
      DS2 = AK + B1 + A3 - A2
      IF(DS2)5,6,6
    6 M = DS2
      FDS2 = FACT(M)
      DS3 = A1 - B1 - AK
      IF(DS3)8,7,7
    7 M = DS3
      FDS3 = FACT(M)
      DS4 = A1 + A2 - A3 - AK
      IF(DS4)8,9,9
    9 M = DS4
      FDS4 = FACT(M)
      DS5 = A2 + B2 - AK
      IF(DS5)8,10,10
   10 M = DS5
      FDS5 = FACT(M)
      M = AK
      FAK = FACT(M)
      N = AK
      TOP = (-1.0)**N
      DENOM = FAK*FDS1* FDS2* FDS3* FDS4* FDS5
      SUM = SUM + (TOP/DENOM)
    5 AK = AK + 1.0
      GO TO 11
    8 THREEJ = PHZ*DEL*ROOT*SUM
      RETURN
      END
$IBFTC 6JS      DECK
C            A FUNCTION FOR SIX J SYMBOLS          2/25/64
C      ROTENBERG ET. AL. PAGE 13 EQUATION (2.3)
C          INPUT SIXJ(J1,J2,L2,L1,J3,L3) IN FLOATING POINT
C      REQUIRES DELTA AND FACTORIAL ROUTINES
      FUNCTION SIXJ(A,B,C,D,E,F)
      TRI1 = A+B-E
      IF(TRI1)2,1,1
    2 SIXJ = 0.0
      RETURN
    1 TRI1 = A-B+E
      IF(TRI1)2,3,3
    3 TRI1 = -A+B+E
      IF(TRI1)2,4,4
C      FIRST TRIANGULAR TEST COMPLETED
    4 TRI2 = D+C-E
      IF(TRI2)2,5,5
    5 TRI2 = D-C+E
      IF(TRI2)2,6,6
    6 TRI2 = -D+C+E
      IF(TRI2)2,7,7
C      SECOND TRIANGULAR TEST COMPLETED
    7 TRI3 = A+C-F
      IF(TRI3)2,8,8
    8 TRI3=A-C+F
      IF(TRI3)2,9,9
    9 TRI3 = -A+C+F
      IF(TRI3)2,10,10
C      THIRD TRIANGULAR TEST COMPLETED
```

```
   10   TRI4 = D+B-F
         IF(TRI4)2,11,11
   11   TRI4 = D-B+F
         IF(TRI4)2,12,12
   12   TRI4=-D+B+F
         IF(TRI4)2,13,13
C        FOURTH TRIANGULAR TEST COMPLETED
   13   DFL1 = DELTA(A,B,E)
        DFL2 = DELTA(D,C,E)
        DFL3 = DELTA(D,B,F)
        DFL4 = DELTA(A,C,F)
        DELX = DFL1*DEL2*DEL3*DEL4
        N = A+B+C+D
        PHZ = (-1.0)**N
        SUM = 0.0
        AK = 0.0
   24   S1 = A+B-E-AK
         IF(S1)22,16,16
   16   M = S1
        FS1 = FACT(M)
        S2 = C+D-E-AK
         IF(S2)22,18,18
   18   M = S2
        FS2 = FACT(M)
        S3 = A+C-F-AK
         IF(S3)22,19,19
   19   M = S3
        FS3 = FACT(M)
        S4 = D+B-F-AK
         IF(S4)22,20,20
   20   M = S4
        FS4 = FACT(M)
        S5 = -A-D+E+F+AK
        .IF(S5)17,21,21
   21   M = S5
        FS5 = FACT(M)
        S6 = -B-C+E+F+AK
         IF(S6)17,23,23
   23   M = S6
        FS6 = FACT(M)
        N = AK
        SPHZ = (-1.0)**N
        TOP = A+B+C+D+1.0-AK
        M = TOP
        FTOP = FACT(M)
        TOP = SPHZ*FTOP
        M = AK
        FAK = FACT(M)
        DENOM = FAK*FS1*FS2*FS3*FS4*FS5*FS6
        SUM = SUM + (TOP/DENOM)
   17   AK = AK + 1.0
        GO TO 24
   22   SIXJ = PHZ*DELX*SUM
        RETURN
        END
```

APPENDIX E. PROGRAM FOR THE ANGULAR DISTRIBUTIONS OF GAMMA RAYS FROM ALIGNED STATES
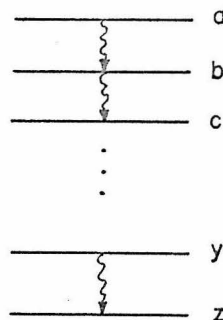
Let a be the spin of an aligned state and let b, c, ... y, z be the spins of succeeding levels populated in a cascade. Then the angular distribution of the N-th gamma ray in a cascade is given by (Poletti and Warburton, 1965)

$$W(\theta_n) = \sum_{\substack{k \\ \text{even}}} \rho_k(a) U_k(ab) U_k(bc) \ldots U_k(xy) F_k(yz) Q_k P_k(\cos \theta_n) \qquad \text{(E. 1.)}$$

where the sum in Formula E. 1 contains the product of n-1 U_k coefficients. The various factors are given by

$$\rho_k(a) = \sum_{\alpha \geq 0} \rho_k(a, \alpha) P(\alpha)$$

$$\rho_k(a, \alpha) = (2 - \delta_{\alpha 0}) \frac{(a\, \alpha\, a - \alpha \mid k\, 0)}{(a\, \alpha\, a - \alpha \mid 0\, 0)}$$

$$U_k(ab) = \frac{U_k(Lab) + x^2\, U_k(L'ab)}{1 + x^2}$$

$$U_k(Lab) = \frac{W(a\ b\ a\ b;\ L\ k)}{W(a\ b\ a\ b;\ L\ 0)}$$

$$F_k(ab) = \frac{F_k(LLba) - (-)^{\sigma} 2xF_k(LL'ba) + x^2 F_k(L'L'ba)}{1 + x^2} \qquad (E.2.)$$

$$F_k(LL'ba) = (-)^{b-a-1}[(2L+1)(2L'+1)(2a+1)]^{1/2}$$

$$\times\ (L\ 1\ L'\ -\ 1|k\ 0)W)aaLL',\ kb)$$

$$L = \max (1, |b - a|)$$

$$L' = L + 1$$

where

$P(\alpha)$ is the population parameter for magnetic substate α,

W is a Racah coefficient,

Q_k is the N-th attenuation coefficient and

$P_k(\cos \theta_n)$ is the k-th Legendre polynomial.

The program WOT calculates $W(\theta_n)$ for $n \le 3$. The required coefficients are calculated in subprograms. The input consists of the following cards:

Card 1   H, P, SIGMA, RQ, NPC, NG, NA, NB, NX(1), NC, NX(2), ND, NX(3), CTOA, ALLOUT

Card(s) 2   Q(H, 5)

Card(s) 3   PC(NPC, P)

Card 4   A(NA)

Card 5   B(NB)

Card 6   X(NX1)

Card 7   C(NC)

Card 8   X(NX2)

Card 9   D(ND)

Card 10   X(NX3)

Card 11   THETA(H) or (COS(THETA(H)))**2

where

H   =   number of angles, ≤ 8 .

P   =   number of magnetic substates $(P \leq 3)$ with
              $m_z = \alpha \geq 0$.

SIGMA   = σ in Formula (E. 2) .

RQ   =   0 if the set of attenuation coefficients Q_k is
              the same at all angles. $\neq 0$ if the set of
              attenuation coefficients Q_k is not the same
              at all angles. In this case a set must be read
              in for each of the H angles, and Card 2 is
              replaced by H cards.

NPC   =   number of sets of the population parameters
              $P(\alpha)$ to be read in. If NPC > 1, card 3 is
              replaced by NPC cards.

NG   =   n, the number of the gamma ray in the
              cascade.

NA   =   number of values for spin a .

NB   =   number of values for spin b .

NX(1)	=	number of values for the mixing ratio x in the transitions a → b.
		If NX(1) = 0 then the first entry on Card 6 will be read as DPHI. The mixing ratio x will be set equal to tan PHI and PHI will be stepped from -90° to 90° in steps of DPHI.
NC	=	number of values for spin c.
NX(2)	=	number of values for the mixing ratio x in the transition b → c.
		If NX(2) = 0, then the first entry on Card 8 will be read as DPHI.
ND	=	number of values for spin d.
NX(3)	=	number of values for the mixing ratio x in the transition c → d. If NX(3) = 0, then the first entry on Card 10 will be read as DPHI.
CTOA	=	0, entries on Card 11 will be read as THETA. ≠ 0, entries on Card 11 will be read as (COS(THETA))**2.
ALLOUT	=	a print out option. If ALLOUT ≠ 0, all components of W(N) will be printed out.
Q(H, 5)	=	array of attenuation coefficients. If RQ = 0, then Q(1, 5) = Q(2, 5) = Q(3, 5) = ... Q(H, 5).
PC(NPC, P)	=	array of population parameters.
A(NA)	=	spins for state a.
B(NB)	=	spins for state b.
X(NXI)	=	mixing parameters for the transition a → b if NX(1) ≠ 0. DPHI if NX(1) = 0.
C(NC)	=	spins for state c.

X(NX2)   =   mixing parameter for the transition b → c,
if $NX(2) \neq 0$. DPHI if $NX(2) = 0$.

D(NX3)   =   spins for state d.

X(NX3)   =   mixing parameter for the transition c → d if
$NX(3) \neq 0$. DPHI if $NX(3) = 0$.

THETA(H)   =   angles at which the distribution is calculated.

A listing of the program is given below.

```
$IBFTC WOT
C
C          TO TABULATE W(THETA) FROM POLETTI AND WARBURTON, LOW LYING
C          LEVELS OF F18, PHYS REV 137,B600 (1965), EQUATION (10)
C     TO BE READ IN
C          THE FIRST DATA CARD IS TO CONTAIN THE FOLLOWING 15 INTEGERS
C          FORMAT(15I2)
C          H,P,SIGMA
C          RQ           IF RQ.NE.0 THE ENTIRE Q ARRAY WILL BE READ IN BY ROWS
C          NPC          THE NUMBER OF ROWS OF THE PC MATRIX TO BE READ IN
C          NG      THE NUMBER OF GAMMA TRANSITIONS    1, 2, OR 3
C          NA      NUMBER OF VALUES FOR SPIN A     (F5.0 LIMIT 16 PER CARD )
C                  IF NA=0 AMIN,AMAX WILL BE READ IN (2F5.0)
C          NB      NUMBER OF VALUES FOR SPIN B   (F5.0 LIMIT 16 PER CARD )
C                  IF NB=0 BMIN,BMAX WILL BE READ IN (2F5.0)
C          NX(1)       THE NUMBER OF X VALUES FOR A-B
C                      IF NX(1)=0 DPHI WILL BE READ    (F10.0)
C          NC      NUMBER OF VALUES FOR SPIN C     (F5.0 LIMIT 16 PER CARD )
C                  IF NC=0 CMIN,CMAX WILL BE READ IN (2F5.0)
C          NX(2)      X VALUES FOR B-C
C                  IF NX(2)=0 DPHI WILL BE READ IN (F10.0)
C          ND      NUMBER OF VALUES FOR SPIN D      (F5.0 LIMIT 16 PER CARD )
C                  IF ND=0 DMIN,DMAX WILL BE READ IN (2F5.0)
C          NX(3)       THE NUMBER OF X VALUES FOR C-D
C                  IF NX(3)=0 DPHI WILL BE READ IN (F10.0)
C          CTOA     IF  = 0   PROGRAM EXPECTS ANGLES IN DEG. TO BE READ IN
C                   IF .NE.0 PROGRAM EXPECTS COS(THETA(H))**2
C          ALLOUT    A PRINT OUT OPTION, IF .NE. 0 ALL COMPONENTS OF W(N)
C                    WILL BE PRINTED OUT
C          THE PROGRAM THEN EXPECTS THE FOLLOWING CARDS IF NG = 3
C          ATTENUATION COEFFICIENTS Q(H,5)         5 PER CARD F10.0
C          POPULATION PARAMETERS PC(NPC,P)         3F10.0  NPC CARDS
C          SPINS OF INITIAL STATE A(NA)            F5.0 ONE OR MORE ON A CARD
C          SPINS OF INITIAL STATE B(NB)            F5.0 ONE OR MORE ON A CARD
C          MIXING PARAMETERS FOR A-B X(NX1)        F10.0  ONE OR MORE ON A CARD
C          SPINS OF INITIAL STATE C(NC)            F5.0 ONE OR MORE ON A CARD
C          MIXING PARAMETERS FOR B-C X(NX2)        F10.0  ONE OR MORE ON A CARD
C          SPINS OF INITIAL STATE D(ND)            F5.0 ONE OR MORE ON A CARD
C          MIXING PARAMETERS FOR C-D X(NX3)        F10.0  ONE OR MORE ON A CARD
C          THETA(H) OR COS(THETA(H))**2            F5.0 ONE OR MORE PER CARD
C                                                  11 VALUES MAXIMUM
C          IF NG = 2 OMIT SPIN D CARD AND X(NX3) CARD
C          IF NG=1 OMIT SPIN C, SPIN D, X(NX2), AND X(NX3) CARDS
C     IF ALLOUT.NE.0 AND NG.EQ.3 OUTPUT WILL BE
C          K
C          F(X3)      U(X2)       U(X1)
C                                 RHO(K,A)
C                                 Q(THETA,K)
C                                 P(K,COS(THETA))
C                                 F(X3)*U(X2)*U(X1)*RHO(K,A)
C                                 F(X3)*U(X2)*U(X1)*RHO(K,A)*Q(N,K)
C          X3         X2          X1       W(1)      W(2) . . .        W(H)
C
C
C
C
C
      INTEGER SIGMA,P,H,ABCD,RQ,CTOA,ALLOUT
      DIMENSION Q(11,5),XAR(50,3), A(16), B(16),C(16), D(16), CSQT(11) ,
     1      IN1(3), IN2(3), W(11), NX(3), PC(20,3)
      DIMENSION ISO(3),IWO(4), IW2(5), IW1(5),ITHO(6)
```

```
      DIMENSION KWO(4)
      DATA IN2/1H(, 6H        , 6HF5.0) /
      DATA IN1/1H(,6H        ,6HF10.0)  /
        DATA ISO / 4H(1H , 6H        , 6HF5.1) /
        DATA IWO / 4H(1H , 6H3F7.4,, 6H       , 6HF10.4) /
        DATA IW1 / 4H(1H , 3H14X, 5HF7.4,, 6H      , 6HF10.4) /
      DATA IW2 / 4H(1H , 2H7X, 6H2F7.4,, 6H      , 6HF10.4) /
        DATA KWO/4H(1H , 3H21X, 6H        , 6HF10.4) /
      DATA ITHO /6H(1H05X, 6H2HX35X, 6H2HX25X, 6H2HX1  , 6H        ,
     1 6HF10.2) /
        COMMON/WTHT/ALMIN,KMAX
C
C
   91 READ(5, 99) H, P, SIGMA, RQ, NPC, NG, NA, NB,NX(1),NC,NX(2),ND,
     1NX(3),CTOA,ALLOUT
   99 FORMAT(15I2)
        KWO(3) = ABCD(H)
      ITHO(5) = ABCD(H)
        NX1 = NX(1)
        NX2 = NX(2)
      NX3 = NX(3)
        WRITE(6,6523)NX1,NX2,NX3
 6523  FORMAT(1H02X3HNX1 2X3HNX2 2X3HNX3 / 1H 3I5)
      IF(RQ.EQ.0) GO TO 1
      DO 2 I=1,H
    2 READ(5,100) (Q(I,J),J=1,5)
  100 FORMAT(5F10.0)
      GO TO 3
    1 READ(5,100) (Q(1,J), J=1,5)
      DO 4 I=2,H
      DO 4 J=1,5
    4 Q(I,J) = Q(1,J)
    3 CONTINUE
        DO 5 I = 1,NPC
    5  READ(5,150)(PC(I,J),J=1,3)
  150   FORMAT(3F10.0)
    6 CONTINUE
      IF(NA.EQ.0) GO TO 8
      IN2(2) = ABCD(NA)
      READ(5,IN2) (A(I), I=1,NA)
      GO TO 9
    8 READ(5,105) AMIN, AMAX
  105   FORMAT(2F5.0)
      NA = (AMAX-AMIN)+1.
      DO 10 I=1,NA
   10 A(I) = AMIN + FLOAT(I-1)
    9 CONTINUE
      IF(NB.EQ.0 ) GO TO 11
      IN2 = ABCD(NB)
      READ(5,IN2) (B(I) , I= 1,NB)
      GO TO 12
   11  READ(5,105)BMIN,BMAX
      NB = (BMAX -BMIN) + 1.
      DO 13 I=1,NB
   13 B(I) = FLOAT(I-1) + BMIN
   12 CONTINUE
        NX1 = NX(1)
      IF(NX1.EQ.0)GO TO 21
      IN1 = ABCD(NX1)
      READ(5,IN1) (XAR(I,1), I=1,NX1)
C
```

```
C          PROGRAM FXPECTS TANGENTS OF PHI TO BE READ IN
C
           I901 = 0
        GO TO 22
   21   READ(5,106)DPHI
  106   FORMAT(F10.0)
           NX1 = 180./DPHI + 1.
           NX(1) = NX1
           I901 = 2
        DO 23 I= 1,NX1
   23   XAR(I,1) = -90. + FLOAT(I-1)*DPHI
        DO 40 I = 1,NX1
           IF(I.EQ.1.OR.I.EQ.NX1.AND.I901.NE.0)GO TO 40
           XAR(I,1) = TAN(XAR(I,1)/57.295779)
   40   CONTINUE
   22   CONTINUE
        IF(NG.LE. 1) GO TO 14
        IF(NC.EQ.0) GO TO 15
        IN2(2) = ABCD(NC)
        READ(5,IN2) (C(I) , I= 1,NC)
        GO TO 16
   15   READ(5,105)CMIN,CMAX
        NC = (CMAX-CMIN) + 1.
        DO 17 I= 1, NC
   17   C(I) = FLOAT(I-1) +CMIN
   16   CONTINUE
           NX2 = NX(2)
        IF(NX2.EQ.0)GO TO 24
        IN1 = ABCD(NX1)
        READ(5,IN1) (XAR(I,2), I=1,NX2)
           I902 = 0
        GO TO 25
   24   READ(5,106)DPHI
           NX2 = 180./DPHI + 1.
        NX(2) = NX2
           I902 = 2
        DO 26 I= 1,NX2
   26   XAR(I,2) = -90. + FLOAT(I-1)*DPHI
        DO 41 I = 1,NX2
           IF(I.EQ.1.OR.I.EQ.NX2.AND.I902.NE.0)GO TO 41
           XAR(I,2) = TAN(XAR(I,2)/57.295779)
   41   CONTINUE
   25   CONTINUE
        IF(NG.LE. 2) GO TO 14
        IF(ND.EQ.0) GO TO 18
        IN2(2) = ND
        READ(5,IN2) (D(I), I=1,ND)
        GO TO 140
   18   READ(5,105)DMIN,DMAX
        ND = DMAX- DMIN + 1.
        DO 20 I= 1,ND
   20   D(I) = FLOAT(I-1) + DMIN
  140   CONTINUE
           NX3 = NX(3)
        IF(NX3.EQ.0)GO TO 27
        IN1 = ABCD(NX1)
        READ(5,IN1) (XAR(I,3), I=1,NX3)
           I903 = 0
        GO TO 28
   27   READ(5,106)DPHI
           NX3 = 180./DPHI + 1.
```

```
          NX(3) = NX3
      DO 29 I= 1,NX3
        I903 = 2
 29   XAR(I,3) = -90. + FLOAT(I-1)*DPHI
      DO 42 I = 1,NX3
      IF(I.EQ.1.OR.I.EQ.NX3.AND.I903.NE.0)GO TO 42
      XAR(I,3) = TAN(XAR(I,3)/57.295779)
 42   CONTINUE
 28 CONTINUE
 14 CONTINUE
      IF(CTOA.EQ.0)GO TO 30
      READ (5,103) (CSQT(I), I= 1,H)
103 FORMAT(11F5.0)
      GO TO 31
 30 IN2 = ABCD(H)
      READ(5,IN2) (CSQT(I) , I= 1,H)
      DO 32 I= 1,H
 32 CSQT(I) =(COS(CSQT(I)/57.295779)**2)
 31 CONTINUE
      WRITE(6,200)
200 FORMAT(21H1OUTPUT OF INPUT DATA /  7H0SPIN A )
      ISO(2) = ABCD(NA)
      WRITE(6,ISO)(A(I),I=1,NA)
      WRITE(6,201)
201 FORMAT(7H0SPIN B )
      ISO(2) = ABCD(NB)
      WRITE(6,ISO)(B(I),I=1,NB)
      IF(NG.LE.1)GO TO 51
      WRITE(6,203)
203 FORMAT(7H0SPIN C )
      ISO(2) = ABCD(NC)
      WRITE(6,ISO)(C(I),I=1,NC)
      IF(NG.LE.2)GO TO 51
      WRITE(6,204)
204 FORMAT(7H0SPIN D )
      ISO(2) = ABCD(ND)
      WRITE(6,ISO)(D(I),I=1,ND)
 51 CONTINUE
      WRITE(6,202)
202 FORMAT(13H0 THE X ARRAY )
      NMAX = NX(1)
      DO 50 I = 1,NG
      IF(NX(I).GT.NMAX)NMAX=NX(I)
 50 CONTINUE
      IWO(2) = ABCD(NG)
      WRITE(6,IWO)((XAR(I,J),J=1,NG),I=1,NMAX)
      WRITE(6,205)
205 FORMAT(21H1OUTPUT OF INPUT DATA / /12H0THE Q ARRAY )
      WRITE(6,206)((Q(I,J),J=1,5),I=1,H)
206 FORMAT(1H 5F10.4)
      WRITE(6,207)
207 FORMAT(18H0THE VALUES FOR PC )
      WRITE(6,273)((PC(I,J),J=1,3),I=1,NPC)
273 FORMAT(1H 3F10.4)
C
C
C      COMPLETES OUTPUT OF INPUT PARAMETERS
C
      IA = 1
 61 CONTINUE
      AP = A(IA)
      WRITE(6,210) AP
```

```
210 FORMAT(10H1SPIN A = F4.1)
    IAP = AP
    IF(FLOAT(IAP).EQ.AP)ALMIN = 0
    IF(FLOAT(IAP).NE.AP)ALMIN = 0.5
    TWOA = 2.*AP
    IAP = TWOA/2.
    IF(FLOAT(2*IAP).EQ.TWOA)KMAX = TWOA
    IF(FLOAT(2*IAP).NE.TWOA)KMAX = TWOA-1.
    IB = 1
 62 CONTINUE
    BP = B(IB)
    WRITE(6,211) BP
211 FORMAT(10H SPIN B = F4.1)
    GO TO (63,64,64) , NG
 64 IC = 1
 66 CONTINUE
    CP = C(IC)
    WRITE(6,212) CP
212 FORMAT(10H SPIN C = F4.1)
    GO TO (63,63,86),NG
 86 CONTINUE
    ID = 1
 65 CONTINUE
    DP = D(ID)
    WRITE(6,213) DP
213 FORMAT(10H SPIN D = F4.1)
 63 CONTINUE
    IPC = 1
  7 CONTINUE
    WRITE(6,ITHO) (CSQT(I),I=1,H)
    GO TO (83,67,68) , NG
 68 IX3 = 1
 69 CONTINUE
    WRITE(6,6526)NX3
6526 FORMAT(1H0 5X3HNX3 1X I5)
    X3 = XAR(IX3, 3)
    EL = ABS(D-C)
    IF(EL.EQ.0.)EL = 1.
    ELP = EL + 1.
    EMAX = CP+DP
    K903 = 1
    IF(I903.EQ.0)GO TO 87
    IF                (IX3.EQ.1.OR.IX3.EQ.NX3) X3 = 1.
    IF(             IX3.NE.1.OR.IX3.NE.NX3 .AND.ELP.LE.EMAX)K903=1
    IF(             IX3.EQ.1.OR.IX3.EQ.NX3 .AND.ELP.LE.EMAX)K903=2
 87 IF(ELP.GT.EMAX)K903=3
 67 IX2 = 1
 70 CONTINUE
    WRITE(6,6525)NX2
6525 FORMAT(1H0 5X3HNX2 1X I5)
    X2 = XAR(IX2,2)
    EMAX = BP+CP
    EL = ABS(C-B)
    IF(EL.EQ.0.)EL = 1.
    ELP = EL + 1.
    K902 = 1
    IF(I902.EQ.0)GO TO 88
    IF(             IX2.EQ.1.OR.IX2.EQ.NX2)X1=1.
    IF(             IX2.NE.1.OR.IX2.NE.NX2 .AND.ELP.LE.EMAX)K902=1
    IF(             IX2.EQ.1.OR.IX2.EQ.NX2 .AND.ELP.LE.EMAX)K902=2
 88 IF(ELP.GT.EMAX)K902=3
```

```
   83  IX1 = 1
       WRITE(6,6523)NX1,NX2,NX3
   71 CONTINUE
       X1 = XAR(IX1,1)
       EMAX = AP+BP
       EL = ABS(B-A)
       IF(EL.EQ.0.)EL = 1.
       ELP = EL + 1.
       K901 = 1
       IF(I901.EQ.0)GO TO 89
       IF(              IX1.EQ.1.OR.IX1.EQ.NX1)X1 = 1.
   IF(                  IX1.NE.1.OR.IX1.NE.NX1 .AND.ELP.LE.EMAX)K901=1
   IF(                  IX1.EQ.1.OR.IX1.EQ.NX1 .AND.ELP.LE.EMAX)K901=2
   89  IF(ELP.GT.EMAX)K901=3
       DO 90 KN = 1,H
   90  W(KN) = 0.
       DO 72 N=1,H
       W(N) = 0.0
       CT = SQRT(CSQT(N))
       K = 0
       NK = 1
       T1 = 1.
       T2 = 1.
       T3 = 1.
       T4 = 1.
       T5 = 1.
   73 PK        = PL(K,CT)
       AK = K
       TR = RHO(AK,AP,P,IPC,PC)
       TERM = TR*PK    *Q(N,NK)
       GO TO (74,75,76 ),NG
   74 T1 = F(AK,AP,BP,SIGMA,X1,K901)
       T4 = T1*TR
       T5 = T1*TR*Q(N,NK)
       W(N) = W(N) +T1*TERM
       GO TO 77
   75 T2 = F(AK,BP,CP,SIGMA,X2,K902)
       T1 = U(AK,AP,BP,X1,K901)
       T4 = T1*T2*TR
       T5 = T1*T2*TR*Q(N,NK)
       W(N) = W(N)+TERM*T1*T2
       GO TO 77
   76 T1 = U(AK,AP,BP,X1,K901)
       T2 = U(AK,BP,CP,X2,K902)
       T3 = F(AK,CP,DP,SIGMA,X3,K903)
       T4 = T1*T2*T3*TR
       T5 = T1*T2*T3*TR*Q(N,NK)
       W(N) = W(N)+TERM*T1*T2*T3
   77 IF(ALLOUT.EQ.0)  GO TO 78
       WRITE(6,214 )   K, T3, T2, T1, TR, Q(N,NK), PK,T4, T5
  214   FORMAT(1H 14X 4HK = I1,2X/ 1H 3F7.4,/1H 14X F7.4, / 1H 14XF7.4,/
      1 1H 14X F7.4,/1H 14X F7.4, / 1H 14X F7.4 )
       WRITE(6,KWO)(W(KN),KN=1,H)
   78  CONTINUE
       K = K + 2
       NK = NK + 1
       IF(K.LE.KMAX) GO TO 73
  C
  C    W(N) FOR ONE SET FINISHED
  C
   72 CONTINUE
```

```
      GO TO (79,80,81) , NG
  79    IW1(4) = ABCD(H)
       WRITE(6,IW1) X1, (W(NW),NW=1,H)
       GO TO 82
  80  IW2(4) = ABCD(H)
       WRITE(6,IW2) X2, X1, (W(NW),NW=1,H)
       GO TO 82
  81  IWO(3) = ABCD(H)
       WRITE(6,IWO) X3, X2, X1, (W(NW),NW=1,H)
  82  CONTINUE
       WRITE(6,6524)NX1,NX2,NX3,IX1,IX2,IX3
6524  FORMAT(1H02X3HNX1 2X3HNX2 2X3HNX3 2X3HIX1 2X3HIX2 2X3HIX3 /1H 6I5
     1 )
       IX1 = IX1 + 1
       IF(IX1.LE.NX1)GO TO 71
       IX2 = IX2 + 1
       IF(IX2.LE.NX2)GO TO 70
       IX3 = IX3 + 1
       IF(IX3.LE.NX3)GO TO 69
       IPC = IPC + 1
       IF(IPC.LE.NPC)GO TO 7
       ID = ID + 1
       IF(ID.LE.ND)GO TO 65
       IC = IC + 1
       IF(IC.LE.NC)GO TO 66
       IB = IB + 1
       IF(IB.LE.NB)GO TO 62
       IA = IA + 1
       IF(IA.LE.NA)GO TO 61
       GO TO 91
       END
$IBFTC UAK      DECK
C
C       A FUNCTION FOR U SUB K OF A, B, AND X
C
       FUNCTION U(AK,A,B,X,K90)
       XSQ=X*X
       EL=ABS(B-A)
       IF(FI .EQ.0.) EL=1.
       ELP=EL+1.
       GO TO (10,11,12),K90
  10  U=(UK(AK,EL,A,B)+XSQ*UK(AK,ELP,A,B))/(1.+XSQ)
       RETURN
  11  U=UK(AK,ELP,A,B)
       RETURN
  12  U=UK(AK,EL,A,B)
       RETURN
       END
$IBFTC UKL      DECK
C
C       THE ANGULAR DISTRIBUTION COEFFICIENT UK(LAB)
C
       FUNCTION UK(AK,EL,A,B)
       N = -A-B-A-B
       PHZ = (-1.)**N
       W1 = PHZ*SIXJ(A,B,A,B,EL,AK)
       W2 = PHZ*SIXJ(A,B,A,B,EL,0.)
       IF(W2.EQ.0.)GO TO 1
       UK = W1/W2
   2  RETURN
   1  WRITE(6,200)
```

```
  200   FORMAT(37H0THE FUNCTION UK(K,L,A,B) IS INFINITE )
        GO TO 2
        END
$IBFTC ADC     DECK
C
C          A FUNCTION FOR F-K(L,L',B,A) , ANG.DISTRIB. COEFF.
C          REF., EQUATION (6),LOW LYING LEVELS OF F18, POLETTI AND
C          WARBURTON, PHYS REV 137, B599 (1965)
C          ALL ARGUMENTS IN FLOATING POINT
C
        FUNCTION FK(K,L,LP,B,A)
        REAL K,L,LP
        N = B-A-1.
        PHZF =(-1.)**N
        RF = SQRT((2.*L+1.)*(2.*LP+1.)*(2.*A+1.))
        N = LP-L
        PHZ = (-1.)**N
        ROOT = SQRT(2.*K+1.)
        CG =PHZ*ROOT*THREEJ(L,1.,LP,-1.,K,-0.)
        N = -A-A-L-LP
        PHZ = (-1.)**N
        W = PHZ*SIXJ(A,A,L,LP,K,B)
        FK = PHZF*RF*CG*W
        RETURN
        END
$IBFTC FAK  ·  DECK
C
C              A FUNCTION FOR F SUB K OF A, B, AND X
C
        FUNCTION F(AK,A,B,SIGMA,X,K90)
        INTEGER SIGMA
        XSQ = X*X
        EL = ABS(B-A)
        IF(EL.EQ.0.)EL=1.
        ELP = EL + 1.
        PHZ = (-1.)**SIGMA
        GO TO (10,11,12),K90
   10   F =(FK(AK,EL,EL, B,A)-PHZ*2.*X*FK(AK,EL,ELP,B,A) + XSQ*
      1 FK(AK,ELP,ELP,B,A))/(1.+XSQ)
        RETURN
   11   F=FK(AK,ELP,ELP,B,A)
        RFTURN
   12   F=FK(AK,EL,EL,B,A)
        RETURN
        END
$IBFTC STR     DECK
C
C        STATISTICAL TENSOR RHO-K(A)
C
        FUNCTION RHO(AK,A,P,IPC,PC)
        INTFGER P
        DIMENSION PC(20,3)
         COMMON/WTHT/ALMIN,KMAX
        SUM = 0.
        AL = ALMIN
        DO 1 I = 1,P
      SUM = SUM + RHOK(AK,A,AL)*PC(IPC,I)
    1   AL = AL + 1.
        RHO = SUM
        RETURN
        END
```

```
$IBFTC RK        DECK
C
C           A FUNCTION FOR RHO(K,A,ALPHA), STAT. TENSOR COEFFICIENTS
C           REF. EQUATION(3) OF LOW LYING LEVELS OF F18, POLETTI AND
C           WARBURTON, PHYS REV 137, B599 (1965)
C           ARGUMENTS FOR THIS FUNCTION MUST BE IN FLOATING POINT
C
            FUNCTION RHOK(K,A,ALPHA)
            REAL K
            ROOT = SQRT(2.*K + 1.)
            CG1 = ROOT*THREEJ(A,ALPHA,A,-ALPHA,K,-0.)
            ROOT = 1.
            CG2 = ROOT*THREEJ(A,ALPHA,A,-ALPHA,0.,-0.)
C
C          NOTE, BECAUSE J1=J2 AND M3=0 THE PHASE IS TAKEN AS +1.
C
            RHOK = (2. - DAB(ALPHA,0.))*CG1/CG2
            RETURN
            END
$IBFTC PLC        DECK
C
C          LEGENDRE POLYNOMIALS
C
            FUNCTION PL(L,CT)
            IF(L)1,1,2
      1     PL = 1.
            RETURN
      2     IF(L-1)3,3,4
      3     PL = CT
            RETURN
      4     N = 2
            PO = 1.0
            P1 = CT
      7     AN = N
            P2 = ((2.0*AN-1.0)*CT*P1-(AN-1.0)*PO)/AN
            N = N + 1
            IF(L-N)5,6,6
      6     PO = P1
            P1 = P2
            GO TO 7
      5     PL = P2
            RETURN
            END
$IBFTC KD         DECK
            FUNCTION DAB(A,B)                                                    DAB
            IF(A-B)1,2,1                                                         DAB
      2     DAB = 1.0                                                            DAB
      3     RETURN                                                              DAB
      1     DAB = 0.0                                                            DAB
            GO TO 3                                                              DAB
            END                                                                 DAB
$IBFTC DEL        NOLIST,DECK
C          FUNCTION DELTA(A,B,C)
C
C          ROTENBERG ET. AL. PAGE 13 (2.4)
C
            FUNCTION DELTA(A,B,C)
            S1 = A + B - C
            M = S1
            FS1 = FACT(M)
            S2 = A + C - B
```

```
      M = S2
      FS2 = FACT(M)
      S3 = B + C - A
      M = S3
      FS3 = FACT(M)
      DENOM = A+B+C+1.0
      M = DENOM
      FD = FACT(M)
      DELTA =  SQRT((FS1*FS2*FS3)/FD)
      RETURN
      END
$IBFTC TOR      NOLIST,DECK
C      CONTAINS FACTORIALS OF NUMBERS UP TO 33
      FUNCTION FACT(L)
       IF(L)55,1,50
   1   FACT = 1.0
       RETURN
  50   GO TO(1,2,3,4,5,6,7,8,9,10,11,12,13,14,15,16,17,18,19,20,21,22,
     1 23,24,25,26,27,28,29,30,31,32,33         ),L
   2   FACT = 2.0
       RETURN
   3   FACT = 6.0
       RETURN
   4   FACT = 24.0
       RETURN
   5   FACT = 120.0
       RETURN
   6   FACT = 720.0
       RETURN
   7   FACT = 5.04E+3
       RETURN
   8   FACT = 4.032E+4
       RETURN
   9   FACT = 3.6288E+5
       RETURN
  10   FACT = 3.6288E+6
       RETURN
  11   FACT = 3.9917E+7
       RETURN
  12   FACT = 4.7900E+8
       RETURN
  13   FACT = 6.227E+9
       RETURN
  14   FACT = 8.7178E+10
       RETURN
  15   FACT = 1.3077E+12
       RETURN
  16   FACT = 2.0923E+13
       RETURN
  17   FACT = 3.5569E+14
       RETURN
  18   FACT = 6.4024E+15
       RETURN
  19   FACT = 1.2165E+17
       RETURN
  20   FACT = 2.4329E+18
       RETURN
  21   FACT = 5.1091E+19
       RETURN
  22   FACT = 1.1240E+21
       RETURN
```

```
   23   FACT = 2.5852E+22
        RETURN
   24   FACT = 6.2045E+23
        RETURN
   25   FACT = 1.5511E+25
        RETURN
   26   FACT = 4.0329E+26
        RETURN
   27   FACT = 1.0889E+28
        RETURN
   28   FACT = 3.0489E+29
        RETURN
   29   FACT = 8.8418E+30
        RETURN
   30   FACT = 2.6525E+32
        RETURN
   31   FACT = 8.2228E+33
        RETURN
   32   FACT = 2.6313E+35
        RETURN
   33   FACT = 8.6833E+36
        RETURN
   55   WRITE(6,200)
  200   FORMAT(29H0FACTORIAL OF NEGATIVE NUMBER /)
        STOP
        END
$IBFTC 3JS        DECK
C     A FUNCTION FOR THREE J SYMBOLS
C
C         ROTENBERG ET. AL. (1.5) PAGE 2 WITH (2.4) FROM PAGE 13
C         INPUT IS THREEJ(J1,M1,J2,M2,J3,M3) FLOATING POINT
C             ROUTINE REQUIRES FACTORIAL AND DELTA ROUTINES
C
        FUNCTION THREEJ(A1, B1, A2, B2, A3, B3)
        DIMENSION A(3), B(3)
        A(1) = A1
        A(2) = A2
        A(3) = A3
        B(1) = B1
        B(2) = B2
        B(3) = B3
        DO 35 I = 1,3
        IF(A(I).NE.0.)GO TO 36
        IF(B(I).NE.0.)GO TO 36
   35   CONTINUE
        THREEJ = 1.
        RETURN
   36   CONTINUE
        TEST = B1+B2+B3
        IF(TEST)1,2,1
    1   THREEJ = 0.0
        RETURN
    2   S1 = A1 + A2 - A3
        IF(S1)1,12,12
   12   S2 = A1 -A2 + A3
        IF(S2)1,14,14
   14   S3 = A2 + A3 - A1
        IF(S3)1,15,15
   15   N = A1 -A2 - B3
        TBA = ABS(B1)-A1
        IF(TBA)50,50,1
```

```
   50  TBA = ABS(B2)-A2
       IF(TBA)51,51,1
   51  TBA = ABS(B3)-A3
       IF(TBA)52,52,1
   52  CONTINUE
       PHZ = (-1.0)**N
       DEL = DELTA(A1, A2, A3)
       X = 1.0
       DO 3 J = 1,3
       S = A(J) + B(J)
       M = S
       FS = FACT(M)
       X = X * FS
       SM = A(J) - B(J)
       M = SM
       FSM = FACT(M)
   3   X = X*FSM
       ROOT = SQRT(X)
       SUM = 0.0
       AK = 0.0
   11  DS1 = AK+A3-A1-B2
       IF(DS1)5,4,4
   4   M = DS1
       FDS1 = FACT(M)
       DS2 = AK + B1 + A3 - A2
       IF(DS2)5,6,6
   6   M = DS2
       FDS2 = FACT(M)
       DS3 = A1 - B1 - AK
       IF(DS3)8,7,7
   7   M = DS3
       FDS3 = FACT(M)
       DS4 = A1 + A2 - A3 - AK
       IF(DS4)8,9,9
   9   M = DS4
       FDS4 = FACT(M)
       DS5 = A2 + B2 - AK
       IF(DS5)8,10,10
   10  M = DS5
       FDS5 = FACT(M)
       M = AK
       FAK = FACT(M)
       N = AK
       TOP = (-1.0)**N
       DENOM = FAK*FDS1* FDS2* FDS3* FDS4* FDS5
       SUM = SUM + (TOP/DENOM)
   5   AK = AK + 1.0
       GO TO 11
   8   THREEJ = PHZ*DEL*ROOT*SUM
       RETURN
       END
$IBFTC 6JS      DECK
C          A FUNCTION FOR SIX J SYMBOLS          2/25/64
C      ROTENBERG ET. AL. PAGE 13 EQUATION (2.3)
C          INPUT SIXJ(J1,J2,L2,L1,J3,L3) IN FLOATING POINT
C      REQUIRES DELTA AND FACTORIAL ROUTINES
       FUNCTION SIXJ(A,B,C,D,E,F)
       TRI1 = A+B-E
       IF(TRI1)2,1,1
   2   SIXJ = 0.0
       RETURN
```

```
      1   TRI1 = A-B+F
          IF(TRI1)2,3,3
      3   TRI1 = -A+B+E
             IF(TRI1)2,4,4
C         FIRST TRIANGULAR TEST COMPLETED
      4   TRI2 = D+C-E
          IF(TRI2)2,5,5
      5   TRI2 = D-C+E
          IF(TRI2)2,6,6
      6   TRI2 = -D+C+E
          IF(TRI2)2,7,7
C         SECOND TRIANGULAR TEST COMPLETED
      7   TRI3 = A+C-F
          IF(TRI3)2,8,8
      8   TRI3=A-C+F
          IF(TRI3)2,9,9
      9   TRI3 = -A+C+F
          IF(TRI3)2,10,10
C         THIRD TRIANGULAR TEST COMPLETED
     10   TRI4 = D+B-F
          IF(TRI4)2,11,11
     11   TRI4 = D-B+F
          IF(TRI4)2,12,12
     12   TRI4=-D+B+F
             IF(TRI4)2,13,13
C         FOURTH TRIANGULAR TEST COMPLETED
     13   DEL1 = DELTA(A,B,E)
          DEL2 = DELTA(D,C,E)
          DEL3 = DELTA(D,B,F)
          DEL4 = DELTA(A,C,F)
          DELX = DEL1*DEL2*DEL3*DEL4
          N = A+B+C+D
          PHZ = (-1.0)**N
          SUM = 0.0
          AK = 0.0
     24   S1 = A+B-E-AK
          IF(S1)22,16,16
     16   M = S1
          FS1 = FACT(M)
          S2 = C+D-E-AK
          IF(S2)22,18,18
     18   M = S2
          FS2 = FACT(M)
          S3 = A+C-F-AK
          IF(S3)22,19,19
     19   M = S3
          FS3 = FACT(M)
          S4 = D+B-F-AK
          IF(S4)22,20,20
     20   M = S4
          FS4 = FACT(M)
          S5 = -A-D+E+F+AK
          IF(S5)17,21,21
     21   M = S5
          FS5 = FACT(M)
          S6 = -B-C+E+F+AK
          IF(S6)17,23,23
     23   M = S6
          FS6 = FACT(M)
          N = AK
          SPHZ = (-1.0)**N
```

```
      TOP  = A+B+C+D+1.0-AK
      M  = TOP
      FTOP  = FACT(M)
      TOP  = SPHZ*FTOP
      M  = AK
      FAK  = FACT(M)
      DENOM = FAK*FS1*FS2*FS3*FS4*FS5*FS6
      SUM = SUM + (TOP/DENOM)
   17 AK = AK + 1.0
      GO TO 24
   22 SIXJ = PHZ*DELX*SUM
      RETURN
      END
```

APPENDIX F. ARRAY ELECTRONICS

Because the array electronics as built and maintained by Mr. L. J. Graham have been modified since McNally (1966) described them and because a subtlety in the operation of the electronics has become apparent in the course of this experiment, a new discussion of the electronics is desirable. For completeness. some of the things discussed by McNally will be repeated.

Figure 65 shows a block diagram of the present (May, 1967) system. Each of the sixteen detectors has its own charge sensitive preamplifier and linear amplifier. The outputs of the sixteen amplifiers are fed into a summing amplifier which, in turn, is fed into the F input of the Nuclear Data 160 pulse-height analyzer. The outputs of the sixteen linear amplifiers are also fed into a logic section which routes the pulses to the appropriate channels in the Nuclear Data analyzer. The analyzer is operated in a 16 x 64 mode so that the pulses from each detector are analyzed into 64 channels.

The charge-sensitive preamplifiers, designed by R. Y. Cusson, have a conversion gain of 7 mv/MeV. They are contained in a box mounted on the brass plate on which the array is mounted. Inside this box the preamplifiers are shielded from each other. Originally the preamplifiers were contained in the box containing the other array electronics and mounted in the spectrometer electronics rack. The detectors were connected to the detectors by one meter coaxial cables. However, a severe noise problem caused the adoption of the present system.

The pulse shaping amplifier is an adaptation of the RIDL 31-17 amplifier with a nominal gain of x 10. A toggle switch

provides two gain settings. In the LO position with the potentio-
meter between the pulse shaping amplifier and the linear amplifier
at maximum, the linear amplifier saturates at 15 MeV. In the
HI position it saturates at 45 MeV.

The linear amplifier is an adaptation from the RIDL 31-12
with a nominal gain of $\times$ 10. A helipot at the input controls the
size of the output of the amplifier which saturates at 10 volts.

The routing trigger pair designed by Mr. L. J. Graham
is set so that with the switches on LO and helipots at maximum,
it triggers at approximately 750 keV. The 5 μsec pulse produced
goes to a binary encoder. In the four bit code used, detector 1 is
0000, detector 2 is 0001, detector 3 is 0010, and so on. These
four pulses are fed directly into the address scalers of the
Nuclear Data analyzer to route the linear pulses to the proper
group of 64 channels. The analyzer generates a pulse (called
Linear Gate Open) 4 μsec after the arrival of a pulse at the F
ADC input. The LGO pulse is fed back to the binary encoder
to suppress further routing pulses during the time the analyzer
is processing a pulse.

A common bias is applied to all of the detectors by means
of a control located on the Nuclear Data analyzer rack.

The overall conversion gain of the array in 700 mv/MeV
with the switches on LO and all of the helipots at maximum. The
noise is less than 50 keV, and the system is limited by the noise
of the silicon surface barrier detectors.

The subtlety that has caused difficulty is the fact that the
address scalers are not reset unless the ADC receives a pulse.
This situation can arise if the Nuclear Data analyzer threshold
is set too high. Even if the threshold control reads zero there

is still a threshold of approximately 400 mv at the 0-10 volts input. The effect is to misroute some of the data.

In the present work this difficulty was always avoided by setting the routing threshold above the linear pulse threshold for every detector. The threshold control on the analyzer was always set as low as possible (usually 000) without significant dead time (< 2%). The routing threshold is controlled by the 16 switches and helipots. The linear threshold is controlled by the 16 switches and helipots, the helipot at the F ADC input, and the analyzer threshold. When the routing threshold lies higher, a pulse fed into the array will route into the correct group of 64 channels, and then as the pulse height is decreased it will suddenly route into the first group of 64 channels corresponding to no routing pulse. Storage will stop when the linear threshold is reached. When the linear threshold lies higher, storage will stop before the transition to the first group of 64 channels occurs. Obviously, this should be checked for all 16 detectors.

APPENDIX G

NON-EXISTENCE OF A LEVEL AT 1.35 MeV IN ^{33}S

C. E. MOSS

California Institute of Technology, Pasadena, California [†]

Abstract: A natural sulphur target has been bombarded with 2.541 MeV deuterons and the emitted protons have been observed with a magnetic spectrometer. The peak tentatively attributed earlier to a level at an excitation energy of 1.35 in ^{33}S is shown to be due to levels in ^{34}S at excitation energies of 4.08 and 4.12 MeV.

E

> NUCLEAR REACTIONS ^{32}S(d, p), $E = 2.541$ MeV; measured $\sigma(E_p, \theta)$. ^{33}S deduced levels. Natural target.

1. Introduction

A shell-model calculation by Glaudemans *et al.* [1]) predicted a $\frac{5}{2}^+$ level in ^{33}S at an excitation energy of 1.38 MeV. If this level consists of an inert ^{28}Si core and two protons and three neutrons in the $(2s_{\frac{1}{2}} d_{\frac{3}{2}})$ shell coupled to give a total spin of $\frac{5}{2}^+$, then it should not be populated in the stripping reaction ^{32}S(d, p)^{33}S. A recent study of this reaction by O'Dell *et al.* [2]) produced evidence which was tentatively interpreted as a weakly populated level in ^{33}S at an excitation energy of 1.35 MeV. The peak attributed to the "1.35" MeV level is shown in the present experiment to be due to levels in ^{34}S at 4.08 and 4.12 MeV which can be formed by the reaction ^{33}S(d, p)^{34}S on the 0.76 % abundance of ^{33}S in natural S.

2. Experimental procedure

Deuterons were accelerated by the ONR-CIT tandem accelerator. The target was prepared by evaporating $BaCl_2$, Au($\approx$ 290 μg/cm^2), and CdS ($\approx$ 90 μg/cm^2) containing natural S, onto a glass slide and then floating off the Au and CdS in distilled water. The protons were detected in an array of 16 Au-Si surface barrier detectors [3]) in the focal plane of a 61 cm double-focussing magnetic spectrometer [4]). Since the (He$_4$)$^{++}$ and protons which are focussed by the spectrometer at a given magnetic field have the same energy, an aluminium foil of thickness 1.7 mg/cm^2 was placed in front of the counters to degrade the energy of the (He^4)$^{++}$ relative to the energy of the protons. Slits in front of each counter defined a momentum window $\Delta P = P/720$. The total instrumental resolution (FWHM) was $\approx$ 30 keV.

2   C. E. MOSS
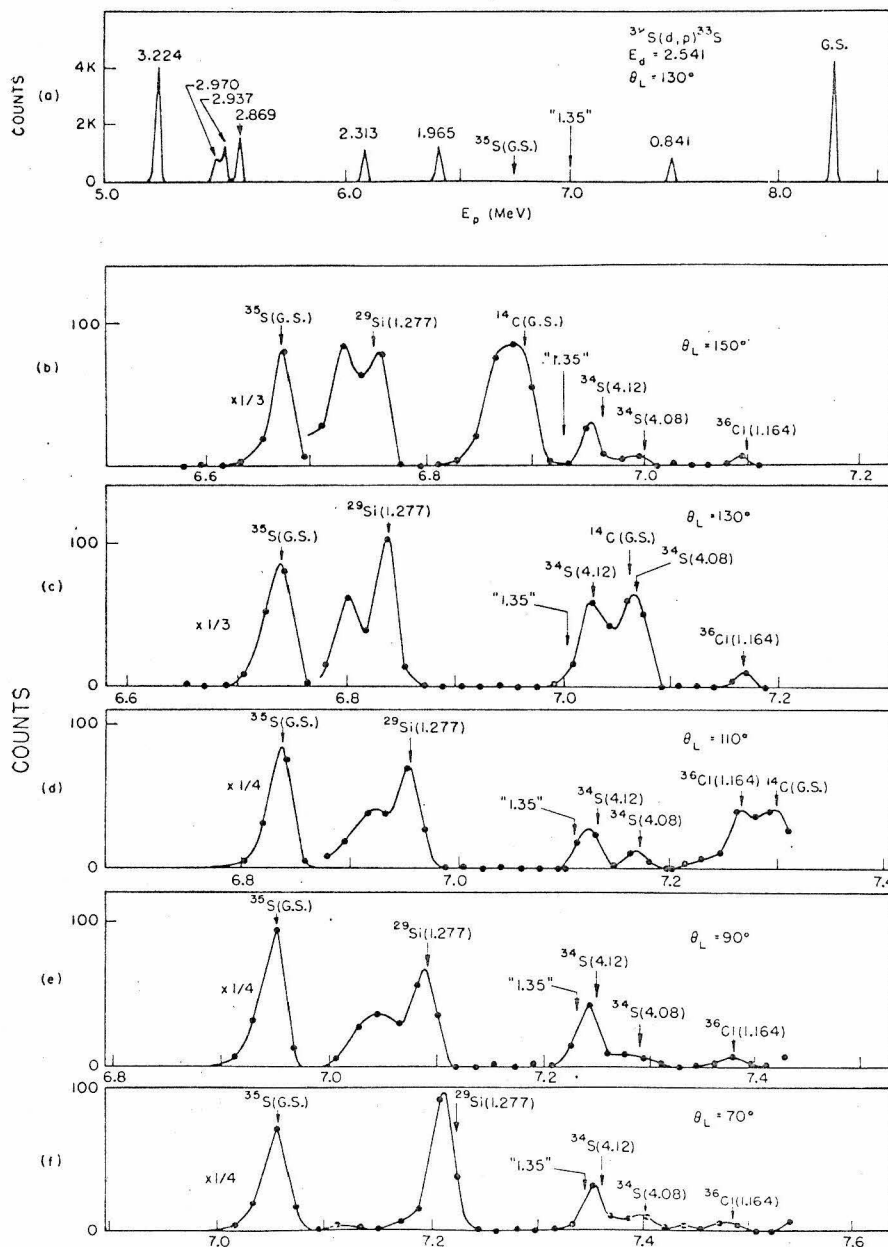
Fig. 1. Proton spectra from bombardment of a natural sulphur target with 2.541 MeV deuterons.
(a) a spectrum at $\theta_L = 130°$ with each point corresponding to 150 μC of incident deuterons. (b)-
(i) expanded plots of the spectra in the region of the "1.35" level at various angles with each point
corresponding to 750 μC of incident deuterons. The peaks are labelled by the corresponding residual
nucleus and its excitation energy. The scale factor applies only to the ^{35}S(G.S.) peak.
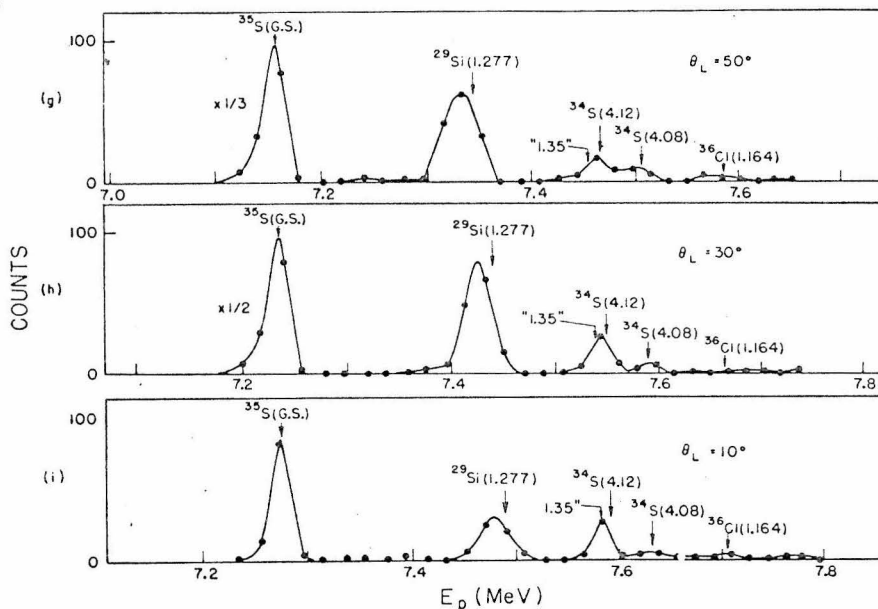
Fig. 1. (continued).

3. Results

Fig. 1 shows the proton spectra. The number of counts in a momentum window $\Delta P = P/720$ is plotted against the proton energy. Fig. 1(a) shows the proton spectrum obtained at a lab angle of 130° with a bombarding energy of 2.541 MeV. Each point corresponds to 150 μC of incident deuterons. The spectrum is to be compared with the one shown in fig. 1 of ref. [2]) which was taken at the same angle and bombarding energy. The peaks attributed to levels in ^{33}S are labelled by their corresponding excitation energies. The position of the proton peak from the ^{35}S ground state which can be formed by the reaction ^{34}S(d, p)^{35}S and the position of the peak from a "1.35" level in ^{33}S are shown.

Fig. 1(c) shows a proton spectrum in the region of the "1.35" level at 130°, and figs. 1(b)-(i) give the kinematic shift of the levels in this region with angle at 20° intervals. In these spectra each point corresponds to 750 μC of incident deuterons. The ^{35}S(G.S.) peak is scaled down as indicated; all other peaks are full size.

The identification of the peaks was made with a non-relativistic kinematics program which calculated the mass of the target nucleus and the Q-value of the reaction from the energies of the protons at two or more angles and the incident beam energy. A relativistic kinematics program was then used to calculate the positions of the peaks. Masses in the program from the 1961 mass table[5]) were used. The excitation energies for the ^{29}Si(1.277) level and the ^{36}Cl(1.164) level were taken from Endt and van

der Leun [6]). For the ^{34}S(4.12) level, the excitation energy of 4.120 ± 0.008 MeV reported by Brenner [7]) in the reaction ^{33}S(d, p)^{34}S was used. Brenner's value differed by 6 keV from the value of 4.114 ± 0.008 MeV reported by Endt *et al.* [8]) in the reaction ^{37}Cl(p, α)^{34}S. Since Brenner did not see the ^{34}S(4.08) and Endt *et al.* did, the latter's excitation energy of 4.073 ± 0.008 MeV for this level was raised by 6 keV to yield an excitation of 4.079 MeV. Finally, to correct for energy loss in the target, errors in the calibration of the 90° beam analysing magnet, and errors in the calibration of the spectrometer, the peak positions predicted by the relativistic kinematics program were shifted down in energy at each angle by a constant amount equal to the energy difference between the peak position predicted by the relativistic kinematics program for ^{35}S(G.S.) and its observed position. The shift was never more than 13 keV. In effect, the proton energies are measured relative to the energy of protons in the ^{35}S(G.S.) peak. The resulting final predictions for the peak positions are shown by arrows in figs. 1(b)-(i).

The fact that the predictions for the position of the ^{29}Si(1.277) peaks at $\theta_L \leq 70°$ are higher than the observed ones can be explained by assuming that the ^{28}Si contaminant was on the front and back of the target. At $\theta_L \geq 90°$, the beam was incident on the CdS side of the target and the protons were detected on the same side. The peak nearest the ^{29}Si(1.277) arrow was produced by ^{28}Si on the incident side of the target, and the peak at slightly lower energy was produced by ^{28}Si on the back side of the target. The latter was shifted down in energy relative to the other ^{29}Si peak by an amount equal to the sum of the energy lost by deuterons and protons in passing through the target. This peak is larger at $\theta_L = 150°$ because the spectrum at this angle was taken after the spectra at $\theta_L = 130°$ through 10° had been taken and more ^{28}Si had been deposited on the gold side. At $\theta_L \leq 70°$, the beam was incident on the CdS side and the protons were detected on the opposite side. The ^{29}Si(1.277) protons from the ^{28}Si on the CdS side were shifted down by approximately one-half of the energy loss in passing through the CdS. The ^{29}Si(1.277) protons from the ^{28}Si on the gold side were shifted down by approximately an amount equal to the difference in energy lost of the deuterons and protons in passing through one-half of the CdS and the full thickness of gold. The result was an unresolved doublet shifted down in energy relative to its predicted position.

Similarly, ^{13}C was also probably present on both sides of the target. The peak at 110° labelled ^{36}Cl(1.164) and the peak at 130° labelled ^{34}S(4.12) may be partly due to ^{14}C(G.S.).

From a comparison of the spectra at $\theta_L = 150°$ and $\theta_L = 10°$ it is apparent that the peak near the arrow labelled "1.35" is due mainly to the level in ^{34}S at an excitation energy of 4.12 MeV. The small discrepancy between the predicted position and the observed position is within the error and is essentially independent of angle. The level in ^{34}S at an excitation energy of 4.08 MeV is also seen.

4. Conclusions

No evidence was seen in this experiment for a level in ^{33}S at an excitation energy of 1.35 MeV. The peak observed by O'Dell *et al.* [2] was probably due to the levels in ^{34}S at excitation energies of 4.12 and 4.08 MeV. Some of the gamma rays they observed in coincidence with the protons in this peak were probably from the gamma decays of the 4.12 and the 4.08 MeV levels (see ref. [6]).

References

1) P. W. M. Glaudemans, G. Wiechers and P. J. Brussaard, Nuclear Physics 56 (1964) 548
2) J. M. O'Dell, R. W. Krone and F. W. Prosser, Jr., Nuclear Physics 82 (1966) 574
3) J. H. McNally, thesis, California Institute of Technology (1966)
4) D. E. Groce, thesis, California Institute of Technology (1963)
5) L. A. König, J. H. E. Mattauch and A. H. Wapstra, Nuclear Physics 31 (1962) 18
6) P. M. Endt and C. van der Leun, Nuclear Physics 34 (1962) 1
7) M. W. Brenner, Phys. Rev. 129 (1963) 765
8) P. M. Endt, C. H. Paris, A. Sperduto and W. W. Buechner, Phys. Rev. 103 (1956) 961

REFERENCES

Ajzenberg-Selove, F., and Lauritsen, T., 1959, Nuclear Physics 11, 1.

Ajzenberg-Selove, F., and Wiza, J. L., 1966, Phys. Rev. 143, 853.

Bardin, R. K., 1961, Ph.D. Thesis, California Institute of Technology.

Bassel, R. H., Drisko, D. H., and Satchler, G. R., 1962, Oak Ridge National Laboratory Report ORNL-3240, unpublished.

Bassel, R. H., Satchler, G. R., Drisko, R. M., and Rost, E., 1962, Phys. Rev. 128, 2693.

Becker, J. A., Chase, L. F., Jr., Fossan, D. B., and McDonald, R. E., 1966, Phys. Rev. 146, 761.

Bishop, 1959, Nucl. Phys. 14, 376.

Bishop, G. R., Bottino, A., and Lombard, R. M., 1965, Physics Letters 15, 323.

Blau, L. M., Alford, W. P., Cline, D., and Gove, H. E., 1965, Nucl. Phys. 76, 45.

Booth, E. C., and Wright, K. A., 1962, Nucl. Phys. 35, 472.

Brink, D. M., and Kerman, A. K., 1959, Nucl. Phys. 12, 314.

Broude, C., Green, L. L., and Willmott, J. C., 1958, Proc. Phys. Soc. 72, 1122.

Chi, B. E., and Davidson, J. P., 1963, Phys. Rev. 131, 366.

Clegg, A. B., and Foley, K. J., 1961, Phil. Mag. (8), 7, 247.

Crawley, G. M., 1965, Ph. D. Thesis, Princeton University.

Cujec, B., Davies, W. G., Dawson, W. K., Grandy, T. B., Neilson, G. C., and Ramavataram, K., 1965, Phys. Lett. 15, 266.

Davies, W. G., Dawson, W. K., and Neilson, G. C., 1965, Phys. Lett. 19, 576.

Demirlioglu, D., and Whaling, W., 1962, unpublished.

Endt, P. M., and Paris, C. H., 1958, Phys. Rev. 110, 89.

Endt, P. M., and van der Leun, C., 1962, Nucl. Phys. 34, 1.

Erné, F. C., 1966, Nucl. Phys. 84, 91.

Ferguson, A. J., 1965, "Angular Correlation Methods in Gamma-ray Spectroscopy", North-Holland, Amsterdam.

Fisher, T. R., and Whaling, W., 1964, Phys. Rev. 133, B1502.

Fou, C. M., and Zurmuhle, R. W., 1966, Phys. Rev. 151, 927.

Glashausser, C., and Rickey, M. E., 1967, Phys. Rev. 154, No. 4, 1033.

Glaudemans, P. W. M., Wiechers, G., Brussaard, P. J., 1964, Nucl. Phys. 56, 548.

Goosman, D. R., 1967, Ph. D. Thesis, California Institute of Technology.

Groce, D. E., 1963, Ph. D. Thesis, California Institute of Technology.

Grodstein, G. W., 1957, N. B. S. Circular 583.

Harris, G. I., and Breitenbecher, D. V., 1966, Phys. Rev. <u>145</u>, 866.

Harris, G. I., Hennecke, H. J., and Prosser, F. W., Jr., 1964, Phys. Lett. <u>9</u>, 324.

Harris, G. I., and Seagondollar, L. W., 1962, Phys. Rev. <u>128</u>, 338.

Harris, G. I., and Seagondollar, L. W., 1963, Phys. Rev. <u>131</u>, 787.

Hazewindus, N., Lourens, W., Scheepmaker, A., and Wapstra, A. H., 1963, Physica <u>29</u>, 681.

Hodgson, P. E., 1963a, in "Proceedings of the Conference on Direct Interactions and Nuclear Reaction Mechanisms", Clemental, E., and Villi, C., Gordon and Breach, New York, 103.

Hodgson, P. E., 1963b, "The Optical Model of Elastic Scattering", Oxford, London.

Kamavataram, K., 1966, Phys. Lett. <u>21</u>, 690.

Kavaloski, C. D., Bassani, G., and Hintz, N. M., 1963, Phys. Rev. <u>132</u>, 813.

Kossanyi-Demay, P., Lombard, R. M., and Bishop, G. R., 1965, Nucl. Phys. <u>62</u>, 615.

Kozub, R. L., 1967, Bull. Am. Phys. Soc. <u>12</u>, 72.

Lauritsen, T., and Ajzenberg-Selove, F., 1962, "Nuclear Data Sheets", Printing and Publishing Office, National Academy of Sciences - National Research Council, Washington 25, D. C.

Levesque, R. J. A., Swann, C. P., Rasmussen, V. K., 1962, Bull. Am. Phys. Soc. 7, 301.

Litherland, A. E., and Ferguson, A. J., 1961, Can. J. Phys. 39, 788.

Litherland, A. E., McManus, H., Paul, E. B., Bromley, D. A., and Gove, H. E., 1958, Can. J. Phys. 36, 378.

Lonsjo, O., 1962, Physica Norvegica 1, 47.

Maples, C., Goth, G. W., and Cerny, J., 1966, "Nuclear Reaction Q-values", Lawrence Radiation Laboratory Report No. UCRL-16964.

Mattauch, J. H. E., Thiele, W., and Wapstra, A. H., 1965, Nucl. Phys. 67, 1.

McMurray, W. R., van der Merwe, P., and van Heerden, I. J., 1967, Nucl. Phys. A92, 401.

McNally, J. H., 1966, Ph. D. Thesis, California Institute of Technology.

Miller, R. G., 1966, Ph. D. Thesis, California Institute of Technology.

Misch, R. D., and Ruther, W. E., 1953, J. Electrochem. Soc. 100, 531.

Moss, C. E., 1967, Nucl. Phys. A96, 1.

Mubarakmand, and Macefield, B. E. F., 1967, Nucl. Phys. A98, 82.

Newton, J. O., 1952, Ph. D. Thesis, University of Cambridge.

Nijgh, G. J., Wapstra, A. H., and van Lieshout, R., 1959,
      "Nuclear Spectroscopy Tables", North-Holland,
      Amsterdam.

O'Dell, J. M., Krons, R. W., and Prosser, F. W., Jr., 1966,
      Nucl. Phys. 82, 574.

Pearson, J. D., 1963, Ph.D. Thesis, California Institute of
      Technology.

Perey, C. M., and Perey, F. G., 1963, Phys. Rev. 132, 755.

Poletti, A. R., and Warburton, E. K, 1965, Phys. Rev. 137,
      B595.

Preston, M. A., 1962, "Physics of the Nucleus", Addison-Wesley,
      Reading, Mass., 259.

Prosser, F. W., Jr., and Gordon, J. W., 1967, Bull. Am.
      Phys. Soc. 12, 572.

Ramavataram, K., 1966, Physics Letters 21, 690.

Rose, M. E., 1953, Phys. Rev. 91, 610.

Seidlitz, L., Blueler, E., Tendam, D. J., 1958, Phys. Rev.
      110, 682.

Skorka, S. J., Hertel, J., and Retz-Schmidt, T. W., 1966,
      Nuclear Data A 2, No. 4, 347.

Smith, P. B., 1964, Can. J. Phys. 42, 1101.

Thankappan, V. K., 1962, Physics Letters 2, 122.

van Rinsvelt, H. A., and Endt, P. M., 1964, Physics Letters
      9, 266.

156

van Rinsvelt, H. A., and Endt, P. M., 1966, Physica 32, 529.

van Rinsvelt, H., and Smith, P. B., 1964, Physica 30, 59.

Wapstra, A. H., 1964, Nucl. Phys. 57, 48.

Weitkamp, C., 1963, Nucl. Inst. and Meth. 23, 13.

Wiechers, G., and Brussaard, P. J., 1965, Nucl. Phys. 73, 604.

Willmes, H., and Harris, G. I., 1967, Bull. Am. Phys. Soc. 12, 91.

Wilkinson, D. H., 1960, in "Nuclear Spectroscopy Part B",
     Ajzenberg-Selove, F., Academic Press, New York, 859.

TABLE I

Slit Settings and Detector Foil Thickness

Notation

$\delta r_{s,a}$ = FW of the object slit of the beam analyzing magnet

$\delta r_{c,a}$ = FW of the image slit of the beam analyzing magnet

$\delta z_{s,sp}$ = FW of the slit 42 cm in front of the target which defines the horizontal dimension of the beam spot

$\delta r_{s,sp}$ = FW of the slit 46 cm in front of the target which defines the vertical dimension of the beam spot

$\delta \theta$ = FW of the angular acceptance slit in the θ direction

$\delta \phi$ = FW of the angular acceptance slit in the ϕ direction

$\delta r_{c,sp}$ = FW measured perpendicular to the mean orbit of the slit in front of the detector(s)

t = Thickness of the foil in front of the detector(s) measured normal to the foil surface

	a	b	c	d	e	f	g	h	i	j
$\delta r_{s,a}$	3.81 mm	1.916 mm	0.381 mm	2.03 mm	3.81 mm	2.54 mm	3.81 mm	3.81 mm	2.54 mm	2.54 mm
$\delta r_{c,a}$	3.81 mm	1.916 mm	0.381 mm	2.03 mm	3.81 mm	2.54 mm	3.81 mm	3.81 mm	2.54 mm	2.54 mm
$\delta z_{s,sp}$	2.03 mm	1.016 mm	1.016 mm	1.016 mm	1.016 mm	1.016 mm	1.016 mm	1.016 mm	1.016 mm	1.016 mm
$\delta r_{s,sp}$	2.03 mm	0.508 mm	0.761 mm	.761 mm	1.016 mm	.761 mm	1.016 mm	1.016 mm	1.016 mm	1.016 mm
$\delta \theta$	1.5°	2.0°	2.0°	0.64°	4.2°	0.64°	1.5°	2.0°	4.2°	2.0°
$\delta \phi$	11.6°	9.0°	9.0°	7.4°	5.2°	7.4°	11.6°	9.0°	11.6°	6.6°
$\delta r_{c,sp}$	3.18 mm	0.794 mm	0.794 mm	1.84 mm	3.18 mm	1.84 mm	3.18 mm	12.7 mm	3.18 mm	3.18 mm
$t(Al)$	0	0	0	1.7 mg/cm²	1.7 mg/cm²	1.7 mg/cm²	1.7 mg/cm²	0	0	1.7 mg/cm²

a   Used for the thin target spectrum shown in Figure 5(a) (see page 4).

b   Used for the thick target spectrum shown in Figure 5(b) (see page 4).

c   Used for the calibration spectrum shown in Figure 7(b) (see page 10).

d   Used for the spectra shown in Figure 11 (see page 18) and Figure 55 (see page 70).

e   Used for the excitation functions shown in Figure 27 (see page 37).

f   Used for all of the angular distributions except those for levels 3, 4, and 6 in ^{31}S (see page 24).

g   Used for the angular distributions for levels 3, 4, and 6 in ^{31}S (see page 24).

h   Used for the single detector deuteron spectra shown in Figure 56 (see page 75).

i   Used for the four detector deuteron spectra (see page 77).

j   Used for the spectra shown in Figure 61 (see page 84).

TABLE II

Frequency Factors and Yield Factors

Detector Number	Frequency Factor	Yield Factor		
		a	b	c
1	.98149	.879	.969	.883
2	.98416	1.018	1.056	1.068
3	.98689	.950	.976	.924
4	.98961	.954	.954	.918
5	.99230	.949	.986	.934
6	.99494	.995	1.010	.968
7	.99749	1.033	1.054	.982
8	1.00000	1.000	1.000	1.000
9	1.00257	1.124	1.171	1.017
10	1.00502	1.005	1.052	1.030
11	1.00749	1.109	1.179	1.063
12	1.00984	1.160	1.225	1.056
13	1.01222	1.171	1.298	1.078
14	1.01453	1.232	1.448	1.121
15	1.01692	1.254	1.473	1.119
16	1.01912	1.279	1.479	1.135

a Used for the spectra shown in Figure 11 (see page 18) and Figure 55 (see page 70) and for all of the angular distributions except those for levels 3, 4, and 6 in ^{31}S (see page 24).

b Used for the angular distributions for levels 3, 4, and 6 in ^{31}S (see page 24).

c Used for the spectra shown in Figure 61 (see page 84).

TABLE III

Input for the Calculation of the Ground State Q-value of the Reaction $^{32}S(^3He, \alpha)^{31}S$

The notation is given in Appendix A.

K_1 = $.0199062 \pm .0000033$ MeV/(Mc/sec)^2

F_{1GS} = $17.897 \pm .001$ Mc/sec

X_{GS90} = 0 ± 20 mils (position of the beam in the beam analyzing magnet slits)

K_{3GS} = $.0113934 \pm .0000013$ MeV/(Mc/sec)^2

F_{3GS} = $29.694 \pm .004$ Mc/sec

Y_{GSTGT} = 0 ± 10 mils (vertical position of the beam spot)

θ_3 = $149.898 \pm .05^{\circ}$

Result

Q = $5.538 \pm .006$ MeV

TABLE IV

Target Thickness

Target[a]			$Au(\mu g/cm^2)$	$CdS(\mu g/cm^2)$
CdS	1	(natural)	282 ± 60	78.4 ± 16
CdS	2	(natural)	282 ± 30	78.4 ± 8
CdS	7	(enriched)	323 ± 30	141 ± 10

a Targets used for spectra shown in Figures 11 and 55.

TABLE V

Contributions to the Resolution of Peak (9) in Figure 11(b).
All FWHM

1) Variation of the beam intensity across the beam
   analyzer slits   0

2) Variation of the beam magnet analyzer current   0

3) Vertical dimension of the beam spot, $\delta r_{s,sp} =$
   0.762 mm   7.1 keV

4) Energy dependence of the reaction cross section   0

5) Homogeneity of the target material and the backing
   foil   0

6) Target thickness   3.0 keV

7) Energy straggle in the target material $\leq$ 13.0 keV

8) Energy straggle in the supporting gold foil   25.2 keV

9) Energy dependence of the stopping cross section
   in the target and supporting foil   0

10) Aberrations in the spectrometer   < 3   keV

11) The θ angular acceptance of the spectrometer and
    the variation of $d\sigma/d\Omega$ over this angular range 22.5 keV

12) The variation of the spectrometer current $\leq$ 2   keV

13) The width of the slit in front of the detector in the
    focal plane of the spectrometer, $\delta r_{c,sp} = 1.84$ mm   19.7 keV

TABLE VI

Excitation Energies of Levels in ^{31}S. Units: MeV ± keV

Level Number	10° natural	20° natural	45° natural	20° enriched	45° enriched	45° natural	45° enriched	Average	Aizenberg-Selove and Wiza 1966
0	0	0	0	0	0	0	0	0	0
1	1.248 ± 21	1.254 ± 23	1.245 ± 22	1.248 ± 21	1.237 ± 21			1.246 ± 10	1.242 ± 20
2	2.237 ± 21	2.237 ± 22	2.235 ± 22	2.234 ± 21	2.229 ± 21			2.234 ± 10	2.232 ± 15
3	3.070 ± 22	3.084 ± 22	3.071 ± 22	3.079 ± 21	3.069 ± 21			3.075 ± 10	-
4	3.284 ± 21	3.292 ± 22	3.289 ± 22	3.285 ± 21	3.278 ± 20			3.286 ± 10	3.287 ± 15
5	3.357 ± 22	3.350 ± 22	3.343 ± 22	3.343 ± 22	3.342 ± 21			3.347 ± 10	3.359 ± 15
6	3.436 ± 21	3.439 ± 22	3.447 ± 22	3.442 ± 22	3.420 ± 21			3.437 ± 10	3.435 ± 15
7	4.084 ± 21		4.089 ± 22		4.075 ± 21			4.083 ± 12	4.085 ± 20
8	4.206 ± 21	4.210 ± 22	4.228 ± 22	4.199 ± 22	4.201 ± 21		4.202 ± 21	4.209 ± 11	4.208 ± 25
9	4.450 ± 21	4.462 ± 22	4.460 ± 23	4.453 ± 21	4.444 ± 21		4.440 ± 20	4.452 ± 9	4.451 ± 15
10	4.521 ± 21	4.526 ± 22		4.520 ± 21	4.506 ± 21		4.506 ± 21	4.522 ± 12	4.526 ± 15
11	4.579 ± 21	4.588 ± 22	4.585 ± 22	4.583 ± 21	4.579 ± 20		4.574 ± 21	4.581 ± 9	4.582 ± 15
12	4.720 ± 21	4.722 ± 21	4.727 ± 22	4.718 ± 21	4.712 ± 20		4.704 ± 21	4.717 ± 9	4.718 ± 15
13	4.866 ± 21	4.877 ± 22	4.872 ± 22	4.868 ± 21	4.863 ± 21		4.856 ± 21	4.866 ± 9	4.85 ± 30
14	4.972 ± 21	4.972 ± 23	4.973 ± 22	4.970 ± 21	4.966 ± 21		4.962 ± 21	4.968 ± 10	4.976 ± 15
15		5.024 ± 23		5.027 ± 21			5.006 ± 22	(5.026 ± 16)	(5.17 ± 30)
16	5.155 ± 21	5.156 ± 22		5.152 ± 21	5.141 ± 23		5.138 ± 22	5.154 ± 12	5.315 ± 15
17	5.300 ± 21	5.307 ± 22	5.305 ± 22	5.298 ± 21		5.309 ± 22	5.300 ± 21	5.301 ± 11	
18		5.414 ± 22	5.407 ± 22	5.408 ± 21		5.411 ± 22	5.393 ± 21	5.407 ± 10	5.42 ± 30
19		5.451 ± 22	5.456 ± 22	5.494 ± 21		5.449 ± 22	5.425 ± 20	5.440 ± 11	
20		5.519 ± 22	5.515 ± 22	5.514 ± 21		5.535 ± 22	5.508 ± 21	5.517 ± 15	(5.52 ± 30)
21		5.685 ± 22	5.681 ± 22	5.676 ± 21		5.685 ± 22	5.673 ± 21	(5.680 ± 10)	5.697 ± 15
22		5.772 ± 22	5.774 ± 22	5.773 ± 21		5.788 ± 22	5.773 ± 22	5.777 ± 11	5.792 ± 15
23		5.842 ± 22	5.819 ± 22			5.829 ± 22	5.824 ± 21	5.824 ± 13	5.84 ± 30
24		5.887 ± 22	5.890 ± 22	5.889 ± 21		5.904 ± 22	5.897 ± 21	5.893 ± 10	5.91 ± 30
25		5.991 ± 22	5.978 ± 22	5.977 ± 21		5.994 ± 22	5.978 ± 21	5.983 ± 13	5.994 ± 20
26		6.160 ± 22		6.152 ± 21		6.161 ± 22	6.150 ± 20	6.154 ± 12	6.165 ± 25
27		6.269 ± 22		6.267 ± 22		6.269 ± 22	6.268 ± 21	6.268 ± 13	6.273 ± 20
28		6.353 ± 12		6.346 ± 21		6.344 ± 23	6.353 ± 21	6.348 ± 13	6.34 ± 30
29		6.409 ± 22		6.389 ± 21		6.397 ± 22	6.386 ± 21	6.395 ± 11	6.40 ± 30
30		6.539 ± 22		6.541 ± 21		6.570 ± 22	6.540 ± 21	6.540 ± 12	6.56 ± 30
31		6.590 ± 22		6.595 ± 21		6.581 ± 22	6.572 ± 20	(6.593 ± 15)	
32		6.628 ± 22		6.628 ± 21		6.635 ± 22	6.636 ± 21	(6.628 ± 15)	6.63 ± 30
33		6.718 ± 22		6.704 ± 21		6.711 ± 22	6.724 ± 21	(6.711 ± 13)	
34		6.750 ± 22		6.736 ± 21		6.742 ± 22		6.743 ± 13	6.763 ± 20
35		6.837 ± 22		6.836 ± 21		6.839 ± 22	6.823 ± 21	6.834 ± 11	(6.84 ± 30)
36		6.868 ± 22		6.861 ± 21		6.878 ± 23	6.857 ± 21	6.862 ± 12	6.896 ± 25
									6.99 ± 30
37		7.039 ± 22		7.031 ± 21		7.035 ± 22	7.037 ± 20	7.036 ± 11	7.048 ± 20
38		7.167 ± 22		7.154 ± 21		7.165 ± 22	7.157 ± 21	7.161 ± 11	7.181 ± 20
39		7.196 ± 22		7.196 ± 21		7.204 ± 22	7.183 ± 21	7.199 ± 13	
40		7.312 ± 22		7.293 ± 21		7.325 ± 22	7.310 ± 21	7.310 ± 11	
									7.522 ± 20
									7.60 ± 30
									7.66 ± 30
41		7.731 ± 22		7.720 ± 21		7.737 ± 23		(7.726 ± 15)	7.738 ± 20

TABLE VII

^{34}S(^{3}He,α)^{33}S

Units: MeV ± keV

10°(natural)		20°(natural)		45°(natural)		Average		Endt & Paris (1958)
Q	E_x in ^{33}S [a]	Q	E_x in ^{33}S [a]	Q	E_x in ^{33}S [a]	Q	E_x in ^{33}S [a]	E_x in ^{33}S
5.328 ± 18	3.828 ± 18	5.330 ± 18	3.826 ± 18			5.329 ± 13	3.827 ± 13	3.834 ± 5
		3.692 ± 17	5.464 ± 17	3.677 ± 17	5.479 ± 17	3.685 ± 12	5.472 ± 12	5.479 ± 6
								7.330 ± 6
1.815 ± 18	7.341 ± 18					1.815 ± 18	7.341 ± 18	(7.335 ± 6)
								7.353 ± 6

a   Assumed Q_{GS} = 9.156 ± 4 (Endt and van der Leun, 1962).

TABLE VIII

Input and Results for Typical Calculations with the Q-value and Excitation Program
Described in Appendix A

Arguments	Units	Level (1), 20° (natural) in Figure 11				Level (25), 20° (natural) in Figure 11			
		Input	Error introduced in QGS (MeV)	Error introduced in QN (MeV)	Error introduced in EX (MeV)	Input	Error introduced in QGS (MeV)	Error introduced in QN (MeV)	Error introduced in EX (MeV)
K1	MeV/(Mc/sec)^2	.0199048 ± .0000042	-.0026	-.0026	-.0000	.0199048 ± .0000042	-.0026	-.0025	-.0001
FIGS	Mc/sec	21.272 ± .001	-.0012		-.0012	21.272 ± .001	-.0012		-.0012
XGS90	mils	0. ± 40.[a]	-.0145		-.0145	0. ± 40.[a]	-.0145		-.0145
TTGT	μg/cm^2	78.4 ± 8.0	.0015	.0015	-.0000	78.4 ± 8.0	.0015	.0016	-.0002
CDSHE3		0. ± .06	.0004	.0004	.0000	0. ± .06	.0004	.0004	.0000
CDSHE4		0. ± .06	.0004	.0004	.0000	0. ± .06	.0004	.0005	-.0001
AUHE4		0. ± .04	.0015	.0015	.0000	0. ± .04	.0015	.0018	-.0003
THIN	degrees	10.0 ± 0.0[b]				10. ± 0.0[b]			
THOUT	degrees	10.0 ± 0.0[b]				10. ± 0.0[b]			
FIN	Mc/sec	21.272 ± .001		-.0012	.0012	21.272 ± .001		-.0011	.0011
XN90	mils	0. ± 40.[a]		-.0145	.0145	0. ± 40.[a]		-.0142	.0142
K30	MeV/(Mc/sec)^2	.0113819 ± .0000012	.0019	.0017	.0001	.0113819 ± .0000012	.0019	.0012	.0007
EK3GS		0. ± .00005	.0009		.0009	0. ± .00005	.0009		.0009
EK3N		0. ± .00005		.0008	-.0008	0. ± .00005		.0006	-.0006
F3GS	Mc/sec	38.635 ± .005	.0046	.0046	.0046	38.635 ± .005	.0046		.0046
YGSTGT	mils	0. ± 15.[a]	.0025	.0025	.0025	0. ± 15.[a]	.0025		.0025
TBACK	μg/cm^2	282. ± 30.	.0039	.0040	-.0001	282. ± 30.	.0039	.0047	-.0009
YNTGT	mils	0. ± 15.[a]		.0023	-.0023	0. ± 15.[a]		.0016	-.0016
TH3	degrees	20.109 ± .050	.0010	.0009	-.0000	20.109 ± .050	.0010	.0008	.0002
F3N	Mc/sec	37.257 ± .010		.0089	-.0089	31.438 ± .010		.0074	-.0074

Results: QGS = 5.539 ± .016   QN = 4.285 ± .018   EX = 1.254 ± .023   QGS = 5.539 ± .016   QN = -.452 ± .017   EX = 5.991 ± .022

a   Slit half width. The error calculated equals one half of the maximum geometrically allowed error.

b   The error in setting the target angle is ignored.

TABLE IX

Q_{GS} for $^{32}S(^{3}He, \alpha)^{31}S$

Units: MeV ± keV

Angle	10°	20°	45°	20°	45°
Target	natural	natural	natural	enriched	enriched
Q-value	5.531 ± 18	5.539 ± 16	5.537 ± 17	5.528 ± 16	5.524 ± 16

TABLE X

Optical Parameters for $^{32}S(^3He, \alpha)^{31}S$

^{3}He Parameters

	V	W	r_o	a	r_o'	a'
Set I	181.0	16.12	1.07	.854	1.81	.592
Set II	30	32	1.60	.85	1.60	.85
Set III	33	9.5	1.66	.62	1.67	.81

^{4}He Parameters

	V	W	r_o	a	r_o'	a'
Set I	40.0	10.0	1.75	.520	1.75	.520
Set II	30	12	2.00	.5	2.00	.5
Set III	95	15.0	1.57	.60	1.57	.60

TABLE XI

ℓ_n-values and Spins for ^{31}S

from Angular Distribution Measurements

Level Number in ^{31}S	E_x in ^{31}S	a		b		c		d		e	
		ℓ-value	J^π	ℓ-value	J^π	ℓ-value	J^π	ℓ-value	J^π	ℓ-value	J^π
0	0	0	$1/2^+$	0	$1/2^+$	0			$1/2^+$		
1	1.246			2	$(3/2)^+$	2			$3/2^+$	2	$(3/2)^+$
2	2.234	0		2	$(5/2)^+$	2			$5/2^+$	2	$(5/2)^+$
3	3.075	0	$1/2^+$								
4	3.286	2	$(5/2)^+$	2	$(5/2)^+$	1		2			
5	3.347										
6	3.437	(2)	$(3/2^+)$								
7	4.083	(2)	$(5/2^+)$	2	$(5/2^+)$			2			
8	4.209										
9	4.452	3		2	$(5/2)^+$						
10	4.522	2									
11	4.581										
12	4.717	2, (3)	$(5/2^+)$								
13	4.866	(1)									
14	4.968	1									
15	(5.026)										
16	5.154	0	$1/2^+$								
17	5.301										
18	5.407										
19	5.440										
20	5.517										
37	7.036									2	

a   Present experiment on ^{32}S(^{3}He,α)^{31}S

b   Fou and Zurmuhle (1966), ^{32}S(^{3}He,α)^{31}S

c   Kavaloski et al.(1963), ^{32}S(p,d)^{31}S

d   Kozub (1967), ^{32}S(p,d)^{31}S

e   Glashauser and Rickey (1967), ^{32}S(p,d)^{31}S

TABLE XII

Correlation and Branching Ratio Measurements in ^{31}S

Level	J^π	Transition	E_γ (MeV)	H(cm)	Q_2	Q_4	Q_6	Q_8	Multipolarity Mixture	x	Branching Ratio	a_2	a_4	a_6
						For Correlation								
^{31}S(1)	$3/2^+$	^{31}S(1) → ^{31}S(0)	1.25	13.73	.8976	.6870	.4257	.1792	E2/M1	$-.349 \pm .015$ or $5.272 \pm .393$	100%	$.1480 \pm .0267$		
^{31}S(2)	$5/2^+$	^{31}S(2) → ^{31}S(0)	2.23	14.41	.9075	.7149	.4698	.2288	M3/E2	$-.053 \pm .036$ or $-2.411 \pm .243$	≥ 97%	$.5311 \pm .0044$	$-.6772 \pm .0067$	
		^{31}S(2) → ^{31}S(1)	0.99								≤ 3%			
^{31}S(3)	$1/2^+$	^{31}S(3) → ^{31}S(0)	3.08	14.41	.9082	.7170	.4733	.2328			≥ 85%			
		^{31}S(3) → ^{31}S(1)	1.83								≤ 13%			
		^{31}S(3) → ^{31}S(2)	0.84								≤ 8%			
^{31}S(4)	$5/2^+, (3/2)^+$	^{31}S(4) → ^{31}S(0)	3.29	13.73							≤ 12%			
		^{31}S(4) → ^{31}S(1)	2.04	13.73	.8999	.6936	.4364	.1916	E2/M1 / E2/M1	$.213 \pm .107$ or $1.882 \pm .521$ for J=5/2; $1.291 \pm .585$ for J = (3/2)	75^{+3}_{-17}%	$-.8352 \pm .2088$	$-.2444 \pm .4067$	
		^{31}S(4) → ^{31}S(2)	1.05							undetermined	25^{+3}_{-6}%			
		^{31}S(4) → ^{31}S(3)	0.21								≤ 15%			
^{31}S(5)	$(7/2^+, 3/2)$	^{31}S(5) → ^{31}S(0)	3.35								≤ 6%			
		^{31}S(5) → ^{31}S(1)	2.10	13.73	.9000	.6938	.4367	.1920	M3/E2 / E2/M1	$-.467 \pm .521$ or -2.204 ± 2.920 for J=(7/2); $-.775 \pm .616$ for J = (3/2)	≥ 78%	$.4022 \pm .550$	-1.9735 ± 1.273	$-.4197 \pm 1.9938$
		^{31}S(5) → ^{31}S(2)	1.11								≤ 21%			
		^{31}S(5) → ^{31}S(3)	0.27								≤ 6%			
^{31}S(6)	$3/2^{(+)}$	^{31}S(6) → ^{31}S(0)	3.44	13.73	.9010	.6967	.4414	.1974	E2/M1	$.577 \pm .220$	46^{+3}_{-4}%	$-1.105 \pm .018$		
		^{31}S(6) → ^{31}S(1)	2.19							undetermined	54^{+3}_{-4}%			
		^{31}S(6) → ^{31}S(2)	1.20							undetermined				
		^{31}S(6) → ^{31}S(3)	0.36								≤ 2%			

TABLE XIII

Mixing Ratios

^{31}P

Transition	x
1.27 → 0	-0.28 ± 0.02 [b]
2.23 → 0	0.028 ± 0.018 or -5.23 ± 0.06 [c]
3.29 → 1.27	-0.44 ± 0.02 [a]
3.41 → 1.27	0.13 ± 0.02 [b]
3.51 → 0	-0.41 ± 0.03 or 7.1 ± 1.0 [a]

^{31}S

Transition	x
1.25 → 0	-0.349 ± .015 or 5.272 ± 0.393
2.23 → 0	0.053 ± 0.036 or 2.411 ± 0.243
3.29 → 1.25	0.213 ± 0.107 or 1.882 ± 0.521 for J = 5/2 1.291 ± 0.585 for J = (3/2)
3.35 → 1.25	0.467 ± 0.521 or 2.204 ± 2.920 for J = (7/2) -0.775 ± 0.616 for J = (3/2)
3.44 → 0	0.577 ± 0.220

a   Harris and Breitenbecker (1966)

b   Harris and Seagondollar (1963)

c   Broude et al.(1958)

TABLE XIV

Contributions to the Resolution in Figure 55. All FWHM

1)	Variation of the beam intensity across the beam analyzer slits	0
2)	The variation of the beam analyzer current	0
3)	The vertical dimension of the beam spot, = 0.762 mm	4.3 keV
4)	The energy dependence of the reaction cross section	0
5)	The homogeneity of the target material and the backing foil	0
6)	The target thickness	$\leq$ 15.0 keV
7)	The energy straggle in the target material	< 13.0 keV
8)	The energy straggle in the supporting gold foil	6.5 keV
9)	Energy dependence of the stopping power in the target	0
10)	Energy dependence of the stopping power in the supporting foil	0
11)	Aberrations in the spectrometer	< 1.5 keV
12)	The angular acceptance of the spectrometer $\delta\theta$ and the variation of $d\sigma/d\Omega$ over this angular range ($\delta\theta = 0.64^{\circ}$)	5.7 keV
13)	The variation of the spectrometer current	< 1 keV
14)	The width of the slit in front of the counter in the focal plane of the spectrometer	12.4 keV

TABLE XV

Excitation Energies of Levels in ^{33}Cl

Units: MeV ± keV

Level Number	16 Detector Array							4 Detector Array					b	c
	10° natural	20° natural	45° natural	20° enriched	45° enriched	45° natural	45° enriched	Single Detector	45° enriched	110° enriched	150° enriched	Average		
0	0	0	0	0	0							0	0	0
1	.810 ± 20	.811 ± 20	.810 ± 19	.811 ± 20	.809 ± 19							.810 ± 9	.806 ± 4	.813 ± 4
2	1.981 ± 20		1.965 ± 20		1.975 ± 19							1.978 ± 14	2.11 ± 60	1.990 ± 4
3	2.354 ± 20	2.357 ± 20	2.354 ± 19	2.351 ± 20	2.348 ± 19		2.345 ± 19					2.351 ± 9	2.53 ± 60	2.315 ± 15
4	2.684 ± 19	2.687 ± 19	2.681 ± 19	2.683 ± 19		2.693 ± 19	2.687 ± 19		2.693 ± 19	2.688 ± 18	2.698 ± 17	2.686 ± 8[a]		
5	2.845 ± 19	2.847 ± 19				2.854 ± 19	2.851 ± 19	2.850 ± 26	2.850 ± 19	2.846 ± 18	2.845 ± 17	2.848 ± 9[a]	2.848 ± 12	2.847
6				2.843 ± 19									2.856 ± 12	2.855
7	2.981 ± 20	2.980 ± 20		2.976 ± 20		2.986 ± 19	2.977 ± 19					2.980 ± 9		2.979 ± 4
8													3.986 ± 12	3.986
9								4.120 ± 27	4.133 ± 19	4.114 ± 19	4.111 ± 18	4.119 ± 10	4.127 ± 12	4.127

a Average of 16 detector array results only.

b From the compilation by Endt and van der Leun (1962).

c From a study of the reaction ^{32}S(p,γ)^{33}Cl by Prosser and Gordon (1967).

TABLE XVI

Q_{GS} for $^{32}S(^{3}He, d)^{33}Cl$

Angle	10^{0}	20^{0}	45^{0}	20^{0}	45^{0}	45^{0}	45^{0}	Average
Target	natural	natural	natural	enriched	enriched	natural	enriched	
Q-value	-3.217±14	-3.212±14	-3.214±14	-3.217±14	-3.221±14	-3.214±14	-3.221±14	-3.217±5

TABLE XVII
^{34}S(^{3}He, d)^{35}Cl
Units: MeV ± keV

16 Detector Array

	10° natural	20° natural	45° natural	20° enriched	45° enriched	Average	Present[a]	b	c
	Q	Q	Q	Q	Q	Q	E_x	E_x	E_x
								0	
								1.220 ± 3	
								1.762 ± 3	
								2.645 ± 5	
								2.695 ± 5	
								3.006 ± 5	
								3.163 ± 5	
	-3.182 ± 14	-3.178 ± 15	-3.180 ± 14	-3.182 ± 14	-3.176 ± 14	-3.180 ± 6	4.056 ± 7	4.058 ± 5	
								4.113 ± 5	
	-3.301 ± 14	-3.296 ± 14	-3.300 ± 14	-3.304 ± 15	-3.310 ± 15	-3.302 ± 6	4.178 ± 7	4.174 ± 5	
	-4.131 ± 15	-4.120 ± 15		-4.135 ± 15		-4.129 ± 9	5.005 ± 10		5.03 ± 50
	-4.516 ± 14	-4.520 ± 15	-4.552 ± 14	-4.531 ± 15	-4.550 ± 15	-4.530 ± 7	5.406 ± 8		5.22 ± 40
	-4.774 ± 15	-4.771 ± 15	-4.778 ± 14		-4.780 ± 14	-4.775 ± 7	5.651 ± 8		
	-4.799 ± 15	-4.801 ± 15	-4.808 ± 14		-4.800 ± 14	-4.802 ± 8	5.678 ± 9		
	-4.877 ± 15	-4.873 ± 15	-4.880 ± 14	-4.873 ± 15		-4.876 ± 7	5.752 ± 8		

Single Detector

	20° natural	45° natural	Average	Present[a]	b
	-6.680 ± 37	-6.685 ± 38	-6.683 ± 27	7.559 ± 27	7.545
					7.597
					7.597

4 Detector Array

	45° enriched	Average	Present[a]	b
	-6.688 ± 18	-6.688 ± 18	7.564 ± 18	7.545
				7.559
				7.597

a Q_{GS} = .8764 ± .0030 MeV was assumed (Maples et al., 1966).

b   From the compilation by Endt and van der Leun (1962).

c   From a study of ^{34}S(p, γ)^{35}Cl by Hazewindus et al (1963).

TABLE XVIII

Optical Parameters for $^{32}S(^{3}He, d)^{33}Cl$

^{3}He Parameters

	V	W	r_o	a	r_o'	a'
Set I	181.0	16.12	1.07	.854	1.81	.592
Set II	30	32	1.60	.85	1.60	.85
Set III	33	9.5	1.66	.62	1.67	.81

Deuteron Parameters

	V	W'	r_o	a	r_o'	a'
Set IV	57.8	203.2	1.563	.650	1.558	.374

TABLE XIX

ℓ_p-values for ^{33}Cl

Number	Excitation (MeV)	a	b	c	J^{π} d
0	0	(2)	2	2	$3/2^+$
1	.810		0	0	$1/2^+$
2	1.978			2	$3/2^+, 5/2^+$
3	2.351	(2)			$(3/2^+, 5/2^+)$
4	2.686				
5	2.848		1		$5/2^+$
6					$3/2^-$
7	2.980				
8	3.986				
9	4.119		1		$3/2^-$

a   Present experiment.

b   Endt and van der Leun (1962) from $^{32}S(d, n)^{33}Cl.$

c   Mubarakmand and Macefield (1967) from $^{32}S(d, n)^{33}Cl.$

d   Known values of J^{π} or the values of J^{π} implied by these ℓ_p-values.

TABLE XX

Energy Losses for a Typical Peak in Figure 61
(.810 MeV level in ^{33}Cl at $\theta_{Lab} = 40^{O}$)

Beam energy, protons	12.011 MeV
Energy loss of protons in nickel entrance foil	.011
Energy loss of protons in 1.1 cm of ^{36}Ar at 14 cm of Hg pressure and 340° K	.007
Resulting incident energy	11.993
Energy loss of alphas in 1.1 cm of ^{36}Ar at 14 cm of Hg pressure and 340° K	.130
Energy loss of alphas in 10^{4} $\overset{O}{A}$ nickel foil	.402
Energy of alphas entering the spectrometer	5.964

TABLE XXI

Comparison of Yields

	$^{32}S(d,p)^{33}S$		$^{32}S(^3He,d)^{33}Cl$	
Number	Excitation Energy in ^{33}S (MeV)	$(2J+1)\theta_n^2$ (relative)[a]	Excitation Energy in ^{33}Cl (MeV)	Intensity at 45° (relative)[b]
0	0	4.0	0	4.0
1	0.839	1.1	.810	1.6
2	1.965	(0.4)	1.978	0.05
3	2.314	0.8	2.351	.2
4	2.869	1.2	2.686	4.2
5	2.936	9.1	2.848	3.8
6	2.971	weak		
7	3.222	8.1	2.980	0.06

a   Quoted by Endt and van der Leun (1962).

b   Taken from the spectra shown in Figure 55.

Figure 1

Initial Experimental Information for ^{31}P and ^{31}S

     A summary of the experimental information on ^{31}P and ^{31}S that was available at the start of the present investigation is shown. This summary is essentially the same as that given by Endt and van der Leun (1962). (See page 1.)

7.768 — 7.886 — 7.934 1/2+ 3/2+
                              3/2+

7.286
^{30}Si+p

6.43 — 6.55
      (6.25)
(6.05)

6.4

5.9

6.08
^{30}P+p

5.48
^{32}S+^{3}He+α

5.012   (1/2,3/2+)
4.784
      4.633 4.590   (5/2)
4.430
4.188 — 4.257 — 5/2+

4.5

3.414 — 3.505   3/2+
      3.292   5/2+
3.133   3/2+

3.3

2.232   5/2+

2.3

1.265   3/2+

1.1

                         1/2+

                         1/2+

^{31}P

^{31}S

Figure 2

Models for A = 31

Two models which were available at the start of
the present investigation are shown.   Both the shell model
calculation by Glaudemans et al.(1964) and the Nilsson
model calculation by Broude et al.(1958) predicted a low-
lying $1/2^+$ level and a $7/2^+$ level, neither of which had been
identified.   Both of these levels were located in ^{31}S in the
present experiment.   (See page 1.)

A = 31

GLAUDEMANS ET AL
(1964)

BROUDE ET AL
(1958)
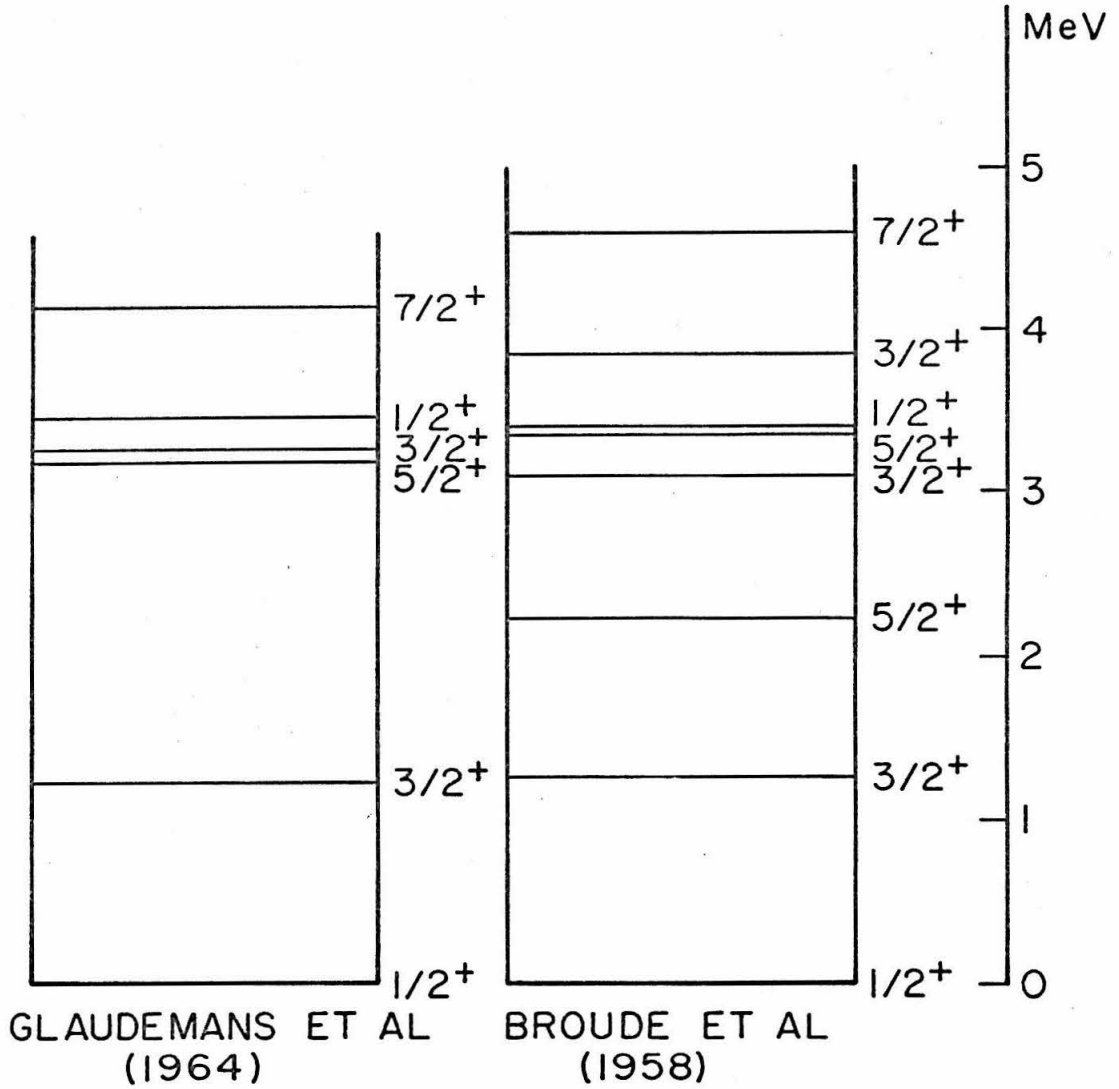
Figure 3

Initial Experimental Information for ^{33}S and ^{33}Cl

A summary of the experimental information on ^{33}S
and ^{33}Cl that was available at the start of the present
investigation is shown. This summary is essentially the
same as that given by Endt and van der Leun (1962). (See
page 2.)
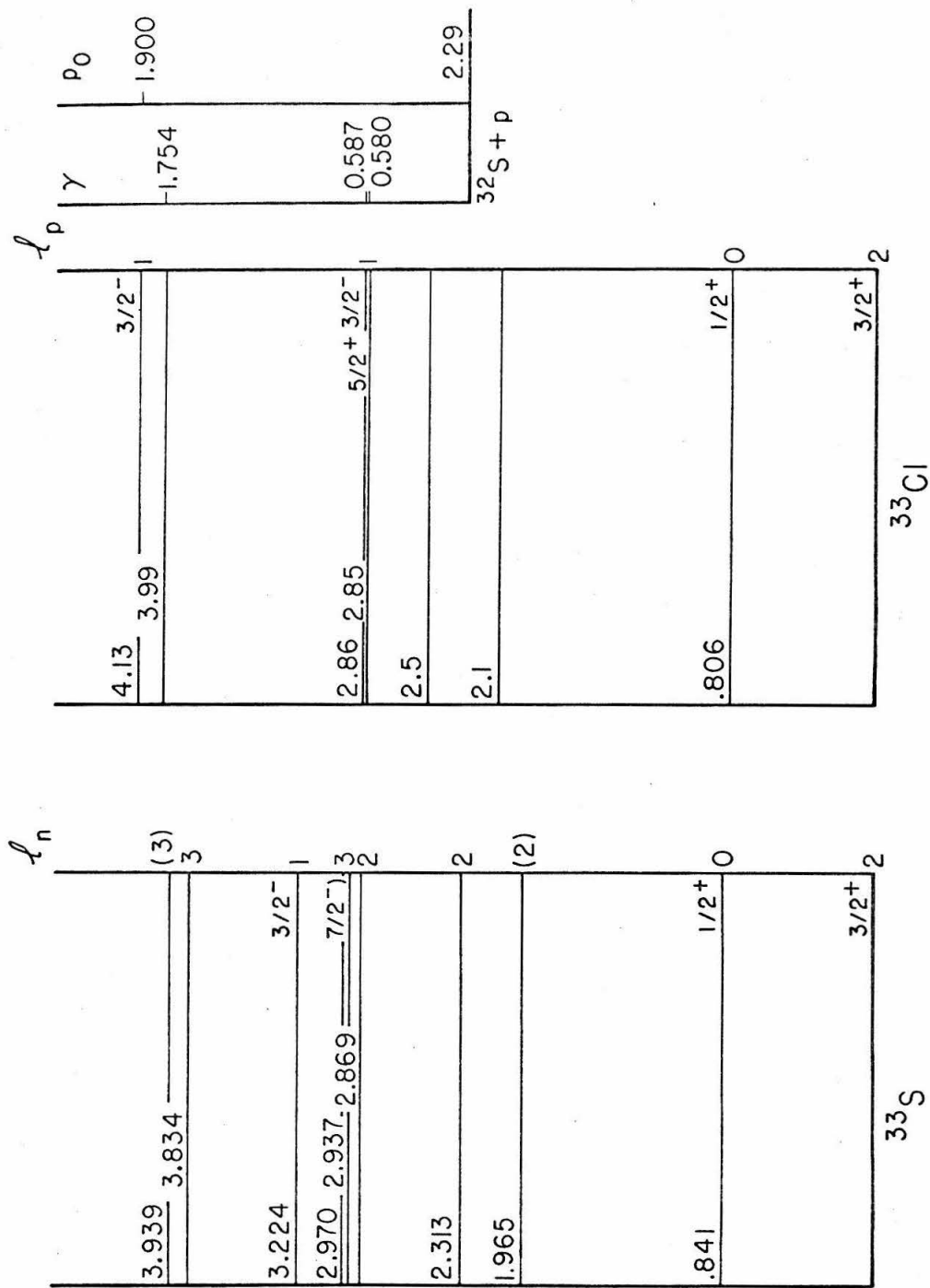
Figure 4

Model for A = 33

The result of a shell model calculation by
Glaudemans et al.(1964) which was available at the
beginning of this investigation is shown.   (See page 2.)

A = 33

	MeV
	— 5
7/2⁺	
1/2⁺	— 4
5/2⁺	
3/2⁺	
3/2⁺	— 3
7/2⁺	
	— 2
5/2⁺	
1/2⁺	— 1
3/2⁺	— 0
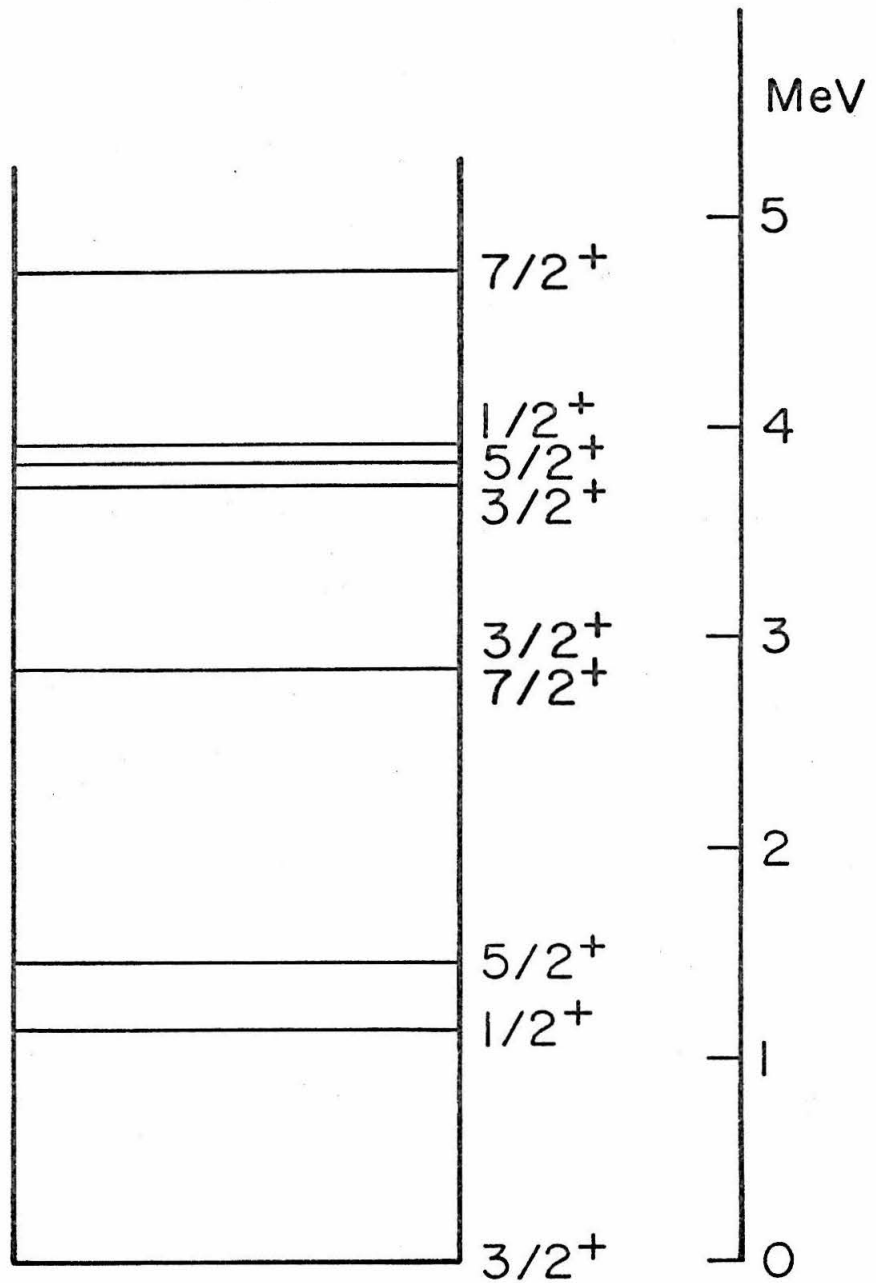
GLAUDEMANS ET AL
(1964)

Figure 5

(a) Thin Target Spectrum of the ^{31}S Ground State Group

A spectrum of alpha particles from the bombardment of a thin ZnS target with 8. 5 MeV ^{3}He^{++} particles is shown. The spectrum was taken to check for the presence of other groups near the ^{31}S (G. S.) group. None were observed.

(b) Thick Target Spectrum of the ^{31}S Ground State Group

A spectrum of alpha particles from the bombardment of a thick ZnS target with 8. 5 MeV ^{3}He^{++} particles is shown. The contribution to the step width from $\delta r_{s, sp}$, $\delta \theta$, and $\delta r_{c, sp}$ are shown. The midpoint shown was used to calculate the ground state Q-value. (See page 4.)

(a) ^{31}S(g.s.)

(b) $\delta r_{s,sp}$ $\delta\theta$ $\delta r_{c,sp}$ MIDPOINT

COUNTS/150 μC

COUNTS/250 μC

FREQUENCY (Kc/sec)
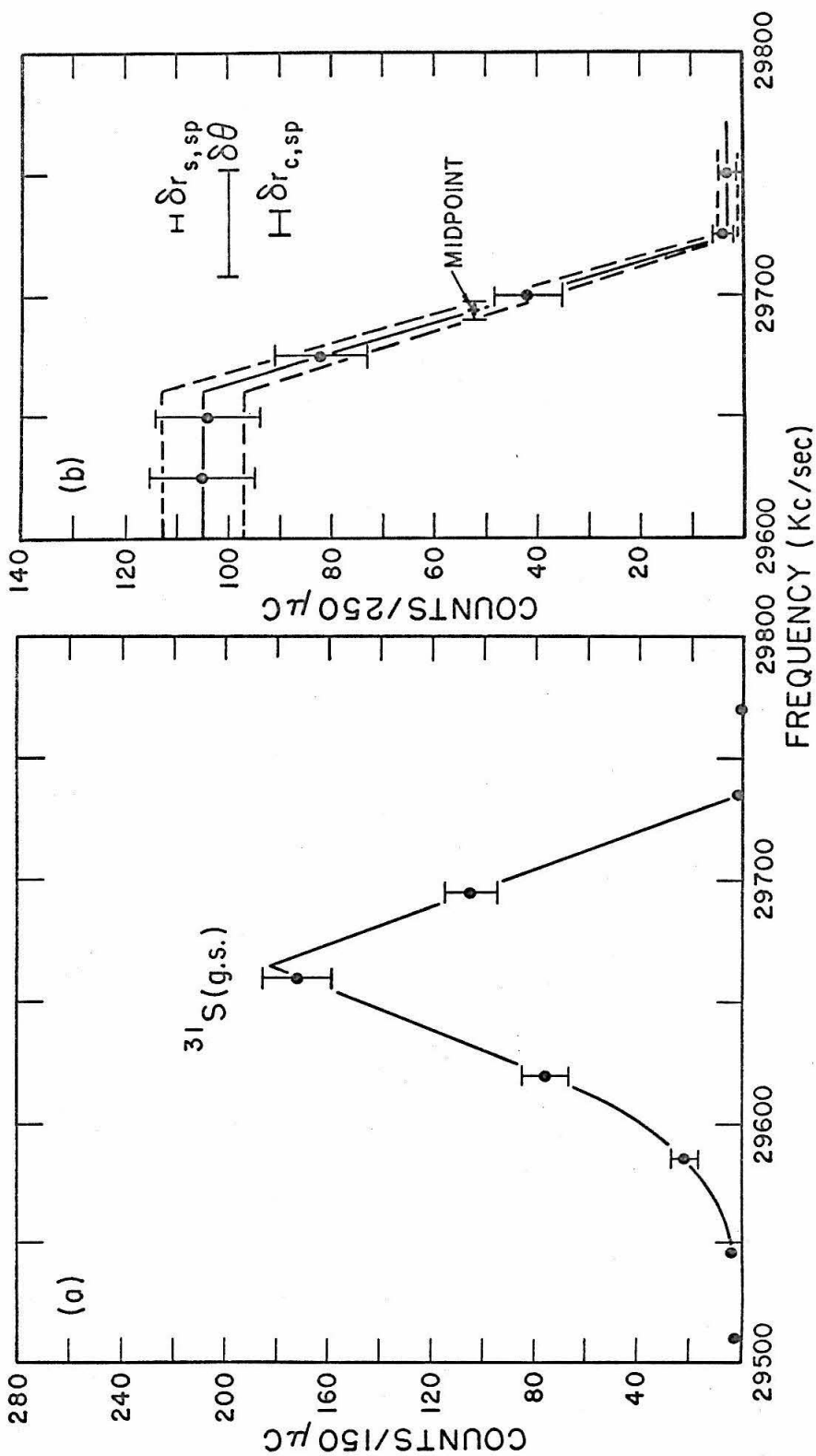
Figure 6

Electronics for Single Detector

The electronics used with the single detector in
the focal plane of the magnetic spectrometer are shown.
The RIDL 400-channel analyzer was used as a monitor,
and the single channel analyzer window was set so that
only the particles of interest were counted by the scaler.
(See pages 6, 10, 17, and 83.)

SILICON SURFACE BARRIER
DETECTOR

PREAMPLIFIER
AND
BIAS SUPPLY

PREAMP: TENNELEC
MODEL 100 A
POWER SUPPLY: TENNELEC
MODEL 901 RM

DOUBLE DELAY
LINE
AMPLIFIER

RIDL
MODEL 30-23

RIDL
400-
CHANNEL
ANALYZER

SINGLE
CHANNEL
ANALYZER

RIDL
MODEL 33-10B

SCALER

RIDL
MODEL 49-28
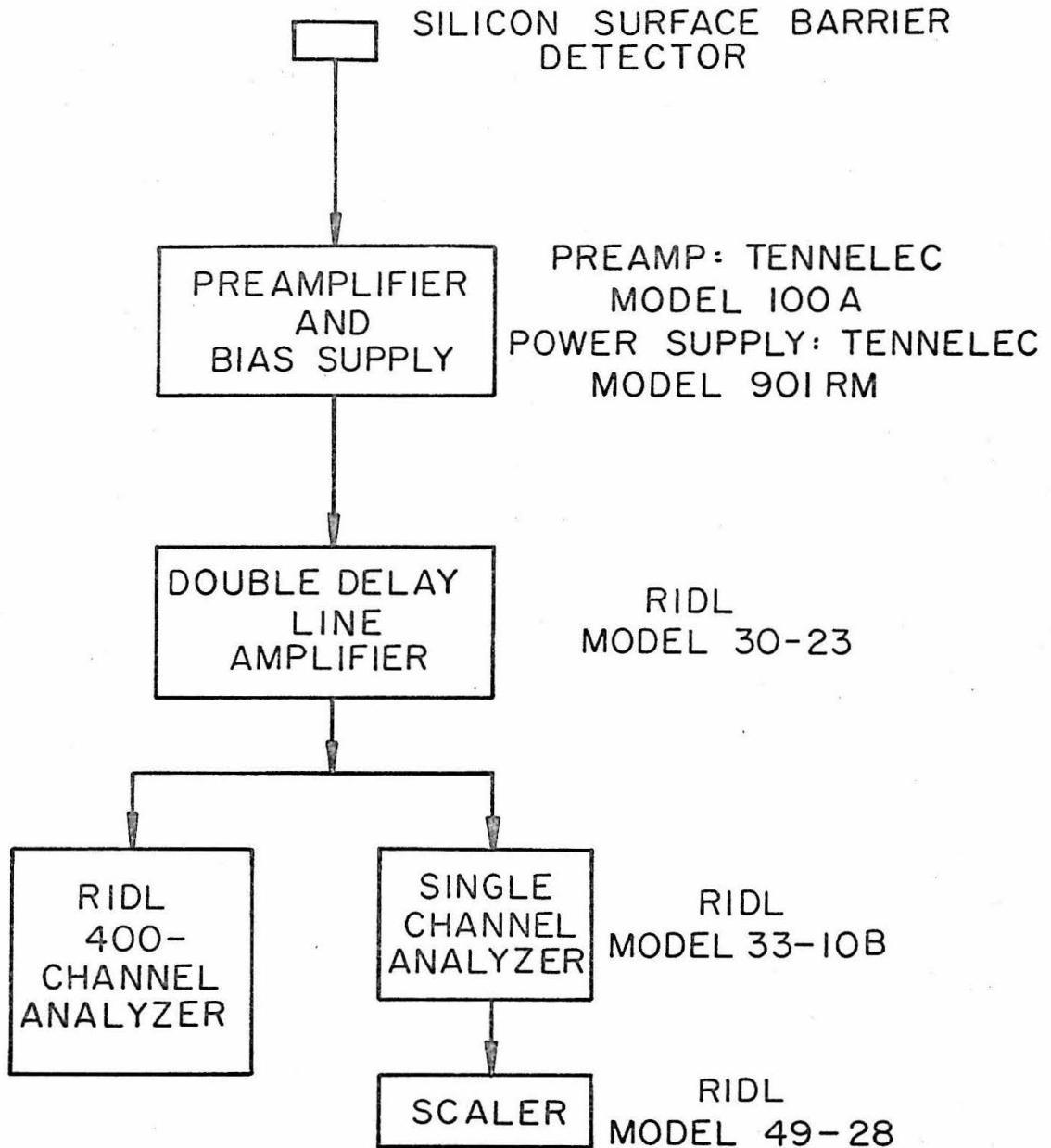
Figure 7

(a) Calibration Spectrum for the Magnetic Spectrometer with
the Single Detector

A spectrum of the 8785 keV (Wapstra, 1964) alpha
particle group from a standard ^{212}Po source (described by
Groce, 1963) obtained with a single detector in the focal
plane of the magnetic spectrometer is shown. The peak
frequency of 27689 ± 1 Kc/sec was used to calculate the
calibration constant for the spectrometer, $k_{s\alpha}$. (See page 10.)

(b) Calibration Spectrum for the Beam Analyzing Magnet

A spectrum of a beam of ^{4}He^{++} particles from the
tandem accelerator passing through a 0.203 mm diameter
hole in 0.127 mm thick sheet of tantalum placed at the target
position is shown. The spectrum was obtained with a single
detector in the focal plane. The spectrometer was placed at
0°, and the beam analyzing magnet NMR magnetometer
frequency was 20935 Kc/sec. The peak frequency of 27672 ± 1
Kc/sec was used to calculate the calibration constant for the
beam analyzing magnet k_{a}. (See page 10.)
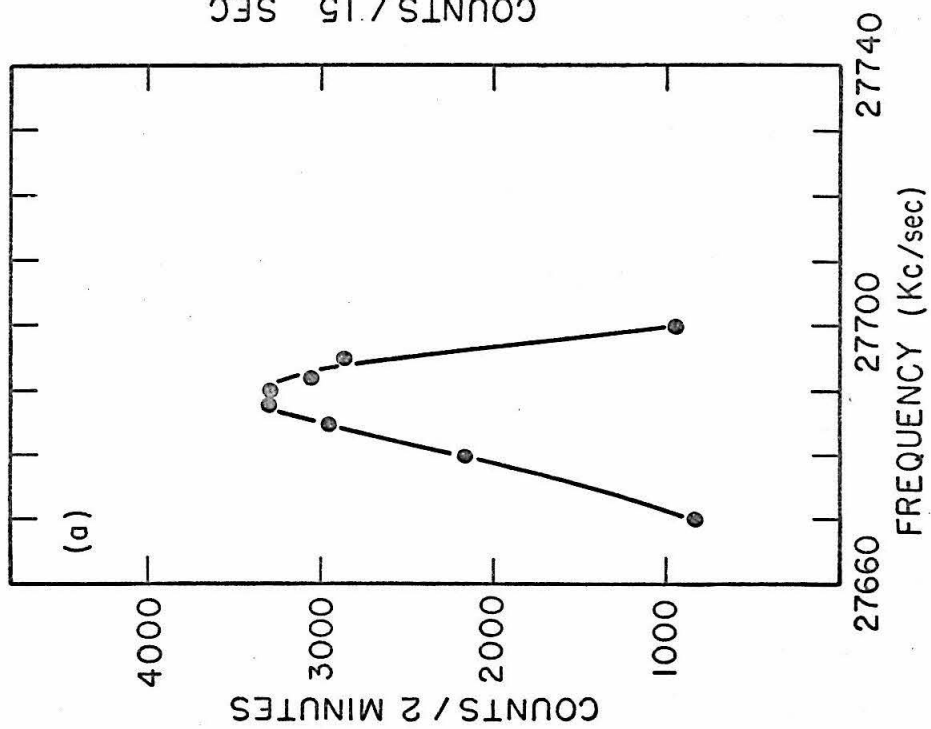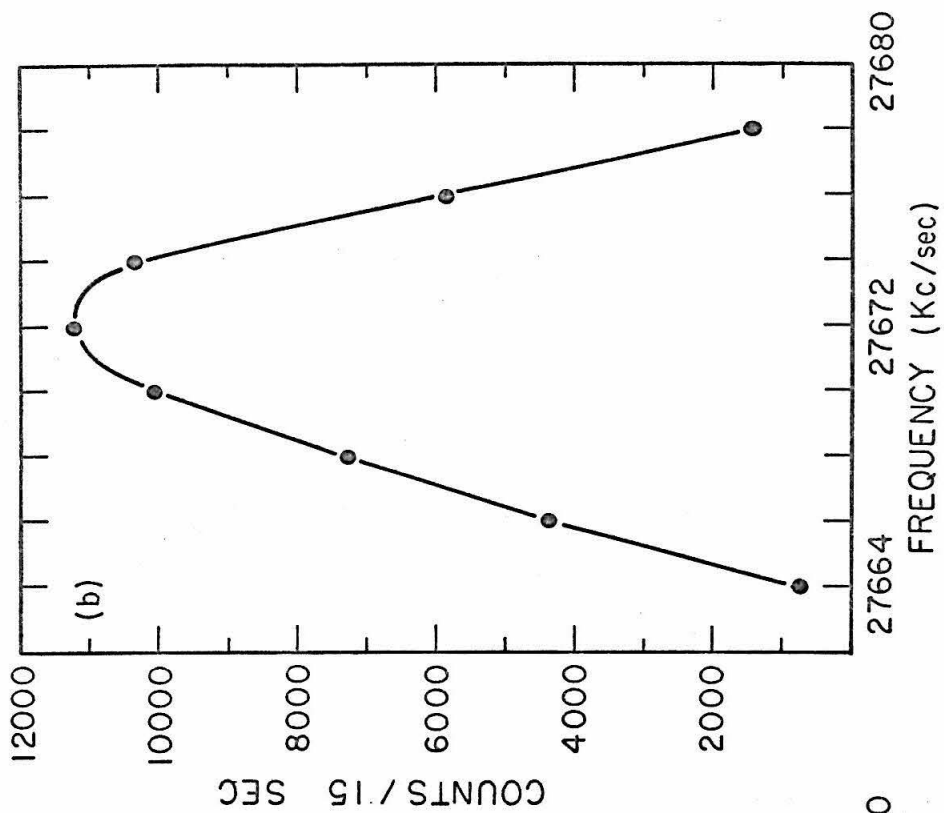
Figure 8

A spectrum of 10 MeV $^3\text{He}^{++}$ particles scattered from a target of CdS on a gold foil is shown. The spectrum was measured with the spectrometer and the 16 detector array. A similar spectrum was taken with the target rotated 180$^\text{o}$. The shifts in the midpoints of the high energy sides of the peaks from gold and cadmium were used to calculate the target thickness. (See page 17.)

INCIDENT $E_{3_{He}}$ = 10.0

θ_{LAB} = 150°
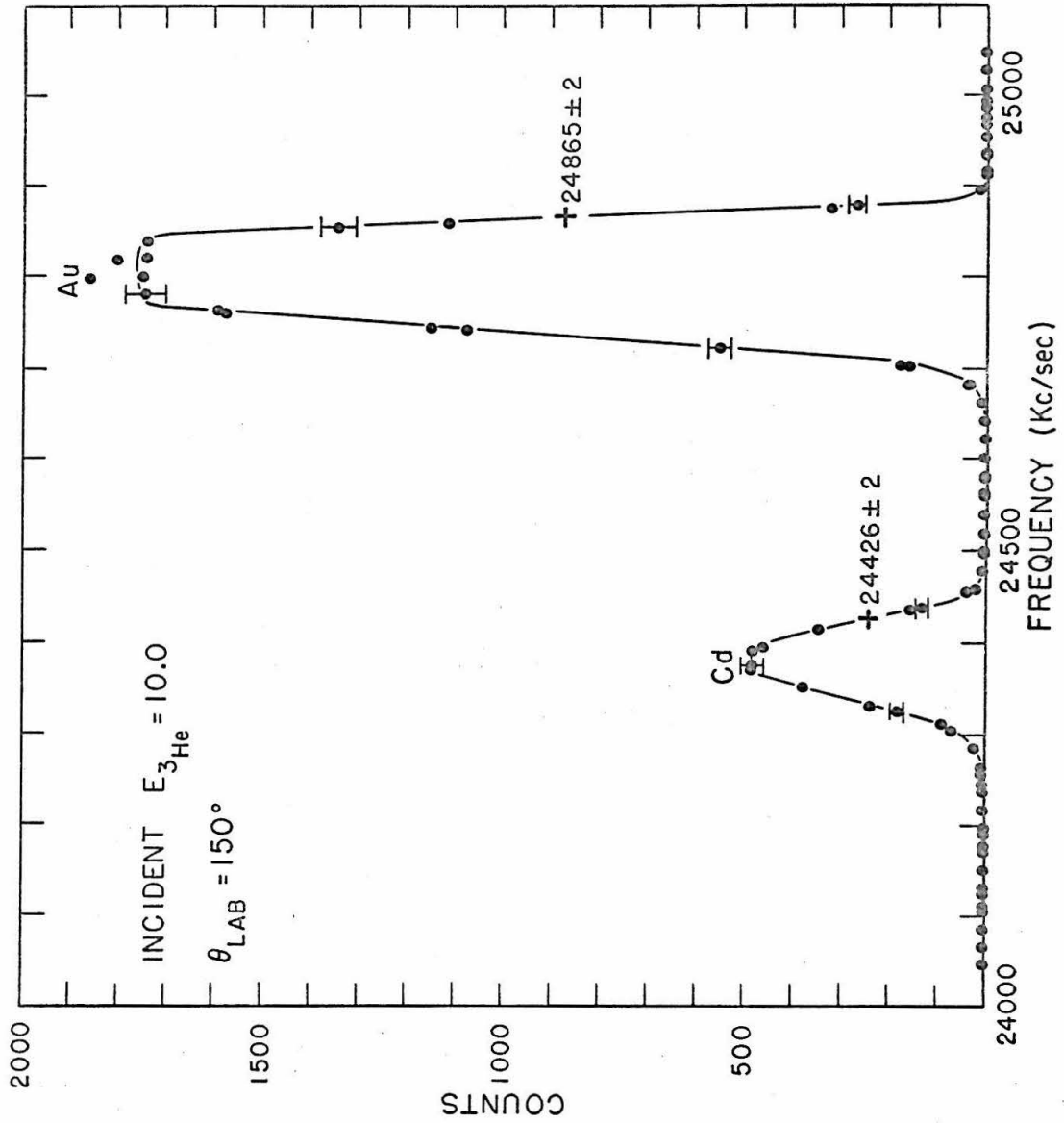
Figure 9

Calibration Spectrum for the Magnetic Spectrometer
with the 16 Detector Array

A spectrum of the 8785 keV (Wapstra, 1964) alpha
particle group from a standard ^{212}Po source (described by
Groce, 1963) obtained with detector 8 in the 16 detector
array and the 1.84 mm slits is shown. The peak frequency
of 27703 ± 1 Kc/sec was used to calculate the calibration
constant for the spectrometer $k_{s\alpha}$. (See page 17.)
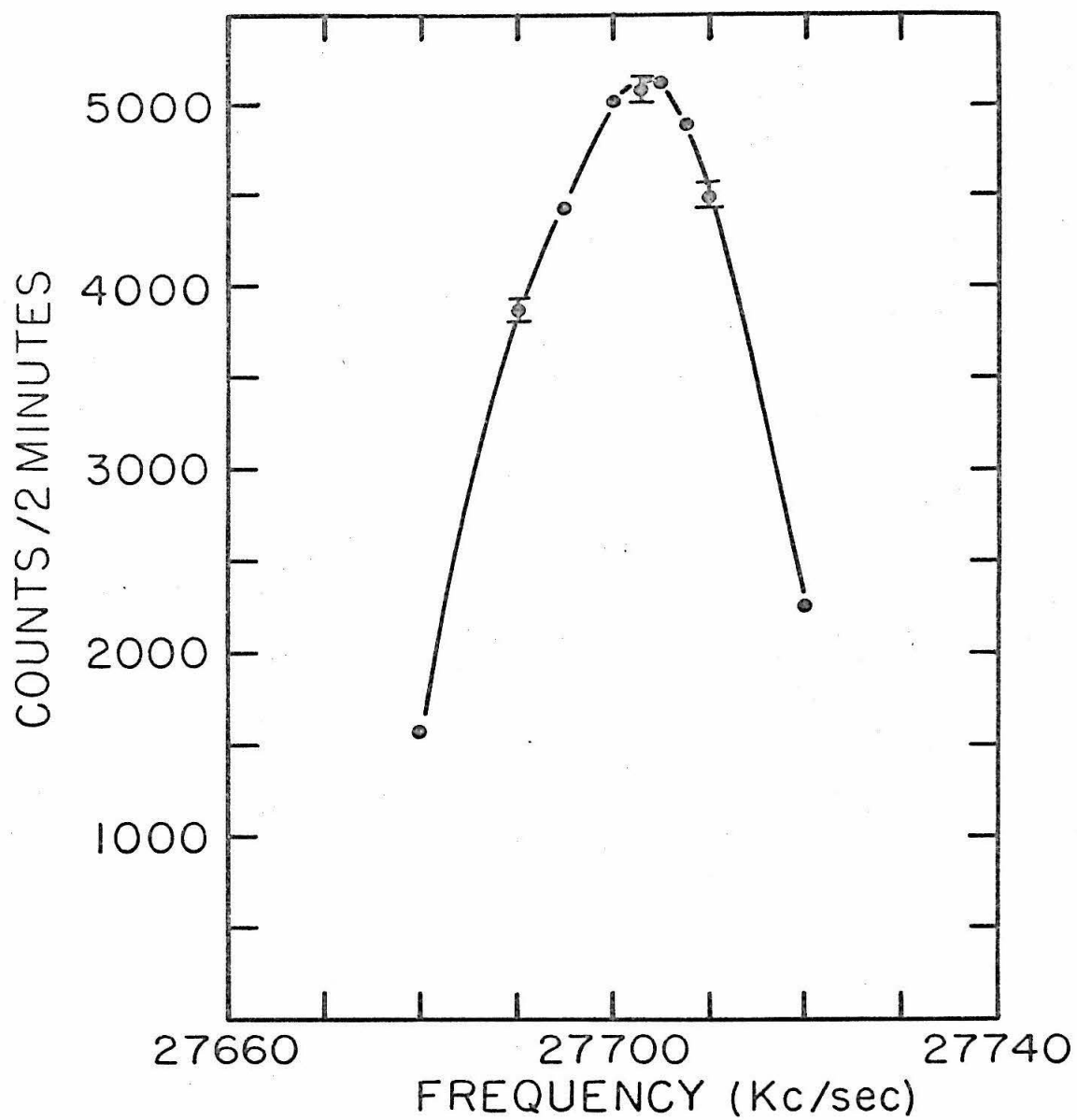
Figure 10

Yield Factors Spectrum

A region of a spectrum at 150° of the elastic scattering of 12. 0 MeV $^3He^{++}$ particles from a thick tantalum target is shown. The open circles shown the region as scanned by detector 8 of the 16 detectors, and the straight line is an approximation to this spectrum. The solid circles shown the region as observed with the array. The yield factors are shown in Table II, column a. (See page 18.)
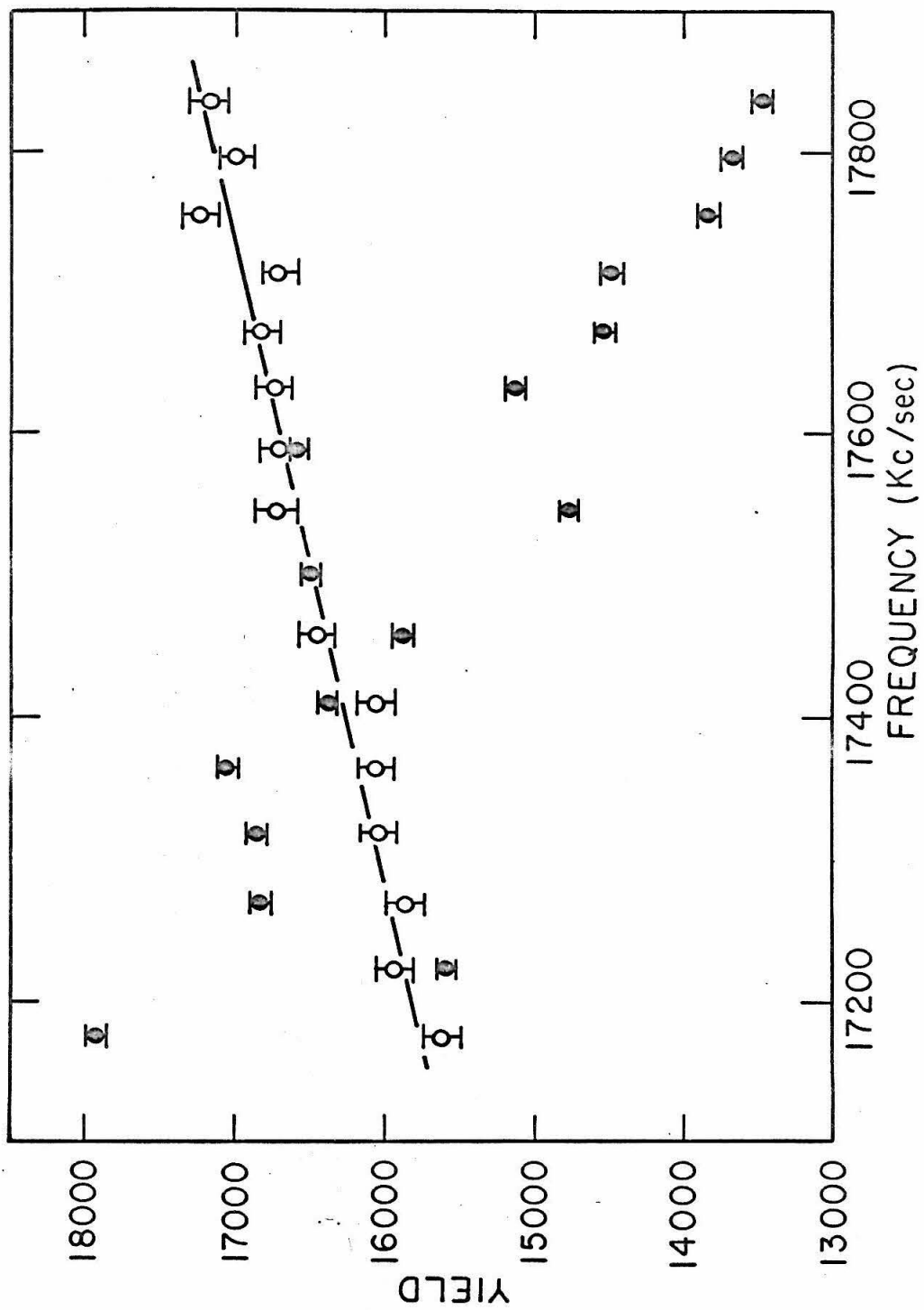
Figure 11

16 Detector Array Spectra from the Reaction $^{32}S(^3He, \alpha)^{31}S$
(This figure is in the rear pocket.)

a) An alpha particle spectrum obtained at $\theta_{Lab} = 10^O$ from the bombardment of natural sulfur with 12.0 MeV $^3He^{++}$ particles is shown. Each point represents 150 μC of incident charge. The lower scale is the NMR magnetometer frequency for the magnetic spectrometer, and the upper scale is the corresponding alpha particle energy. The scales are shifted so that corresponding levels fall on a vertical line. The levels are numbered as in Table VI.

b) An alpha particle spectrum obtained at $\theta_{Lab} = 20^O$ from the bombardment of natural sulfur is shown. Each point above FREQUENCY = 33600 represents 150 μC of incident charge, and the scale on the right is to be used. Each point below FREQUENCY = 33600 represents 300 μC of incident charge, and the scale on the left is to be used.

c) An alpha particle spectrum obtained at $\theta_{Lab} = 20^O$ from the bombardment of sulfur enriched to 98.1% ^{32}S (natural sulfur contains 95.0% ^{32}S) is shown. The scales are similar to those in b).

d) An alpha particle spectrum obtained at $\theta_{Lab} = 45^O$ from the bombardment of natural sulfur is shown. Each point represents 300 μC of incident charge.

e) An alpha particle spectrum obtained at $\theta_{Lab} = 45^O$ from the bombardment of sulfur enriched to 98.1% ^{32}S is shown. The scales are similar to those in d).

Figure 12

Comparison of the Predictions of Sets I, II, and III

Typical examples of the angular distributions predicted by DWBA calculations with the optical model parameters in Sets I, II, and III are shown. Set I was used for all of the levels in the present experiment. (See page 27.)

$^{32}S(^3He, \alpha)^{31}S(3.29)$

$E_{3_{He}} = 12.0$
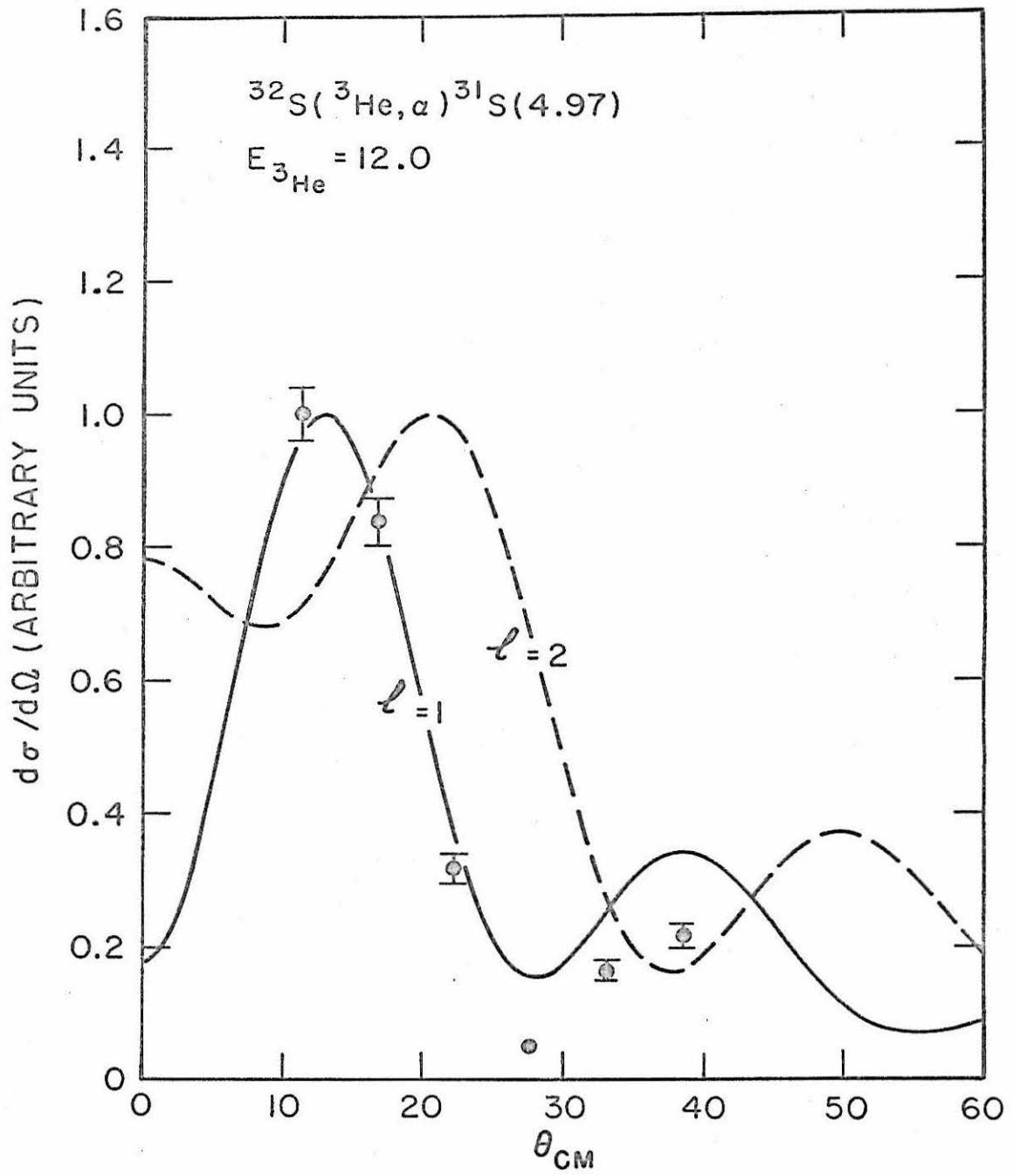
$\ell = 2$

--- SET I

——— SET II

········ SET III
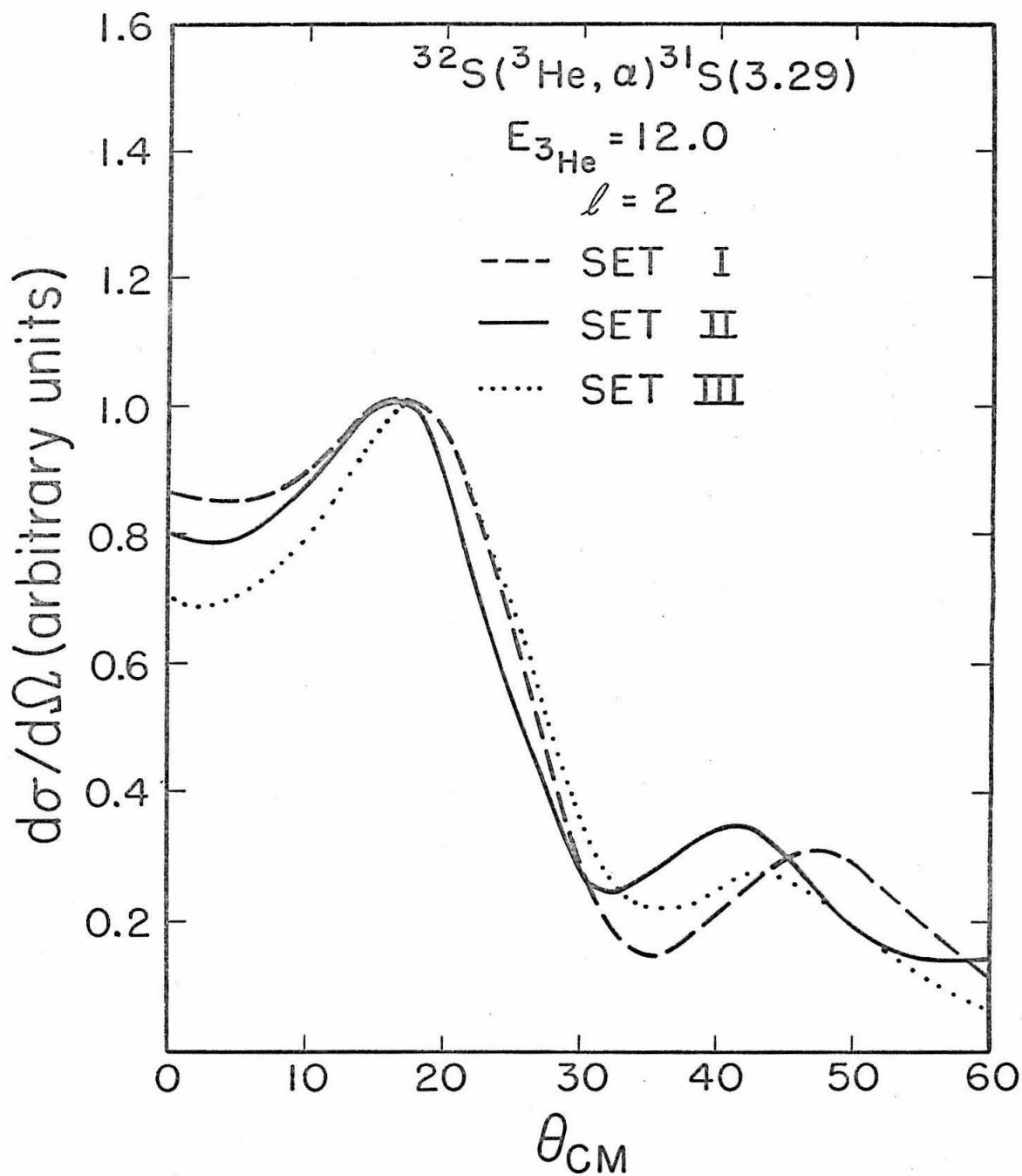
Figure 13

Angular Distribution for ^{31}S(G. S.)

The angular distribution of the alpha particles from the reaction ^{32}S(^{3}He, α)^{31}S (G. S.) is shown. The curves are DWBA predictions. Level ^{31}S (G. S.) must have $\ell_n = 0$ because $J^\pi = 1/2^+$ (Endt and van der Leun, 1962). (See page 27.)
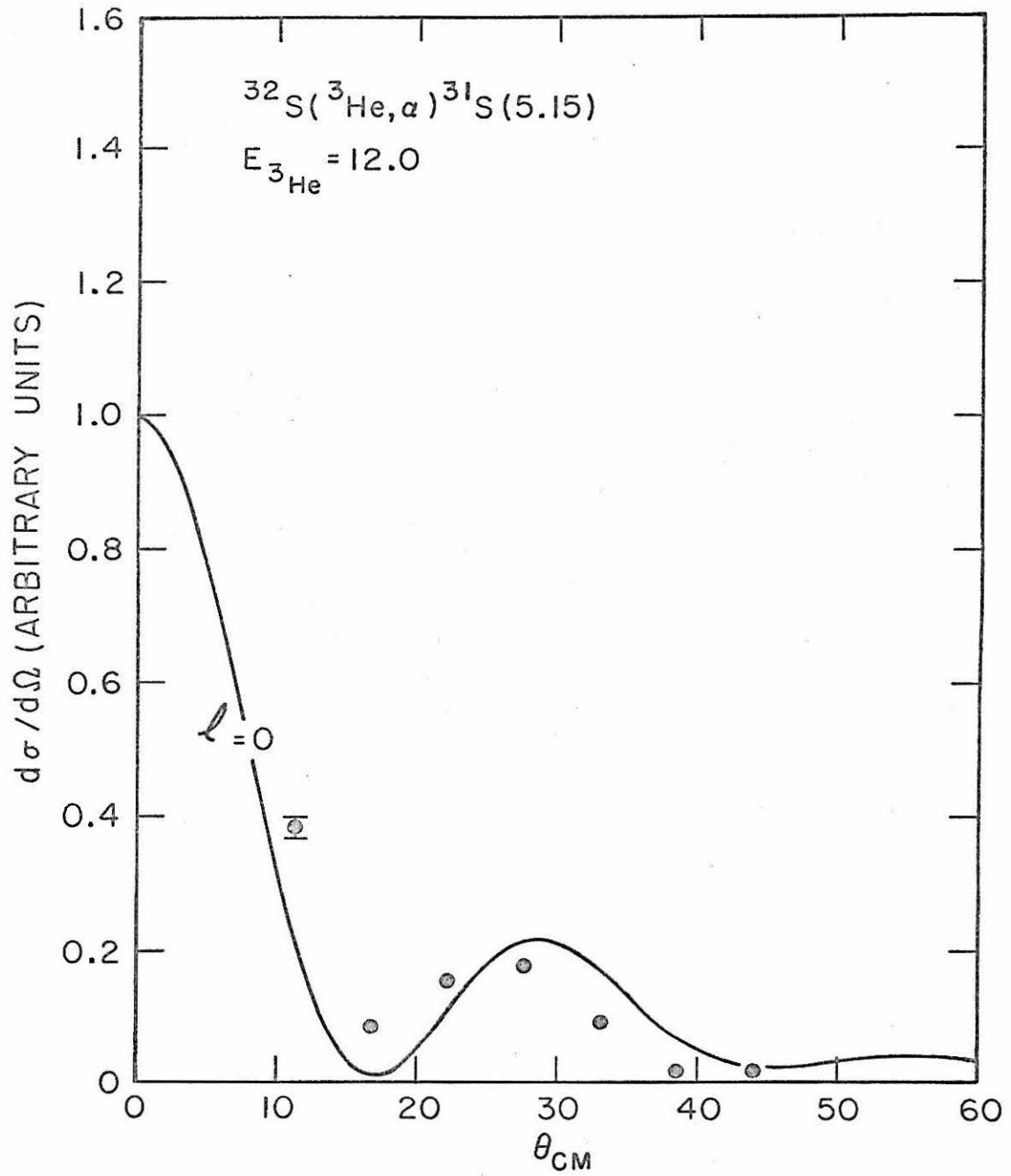
$^{32}S(^3He,\alpha)^{31}S(G.S.)$

$E_{3_{He}} = 12.0$
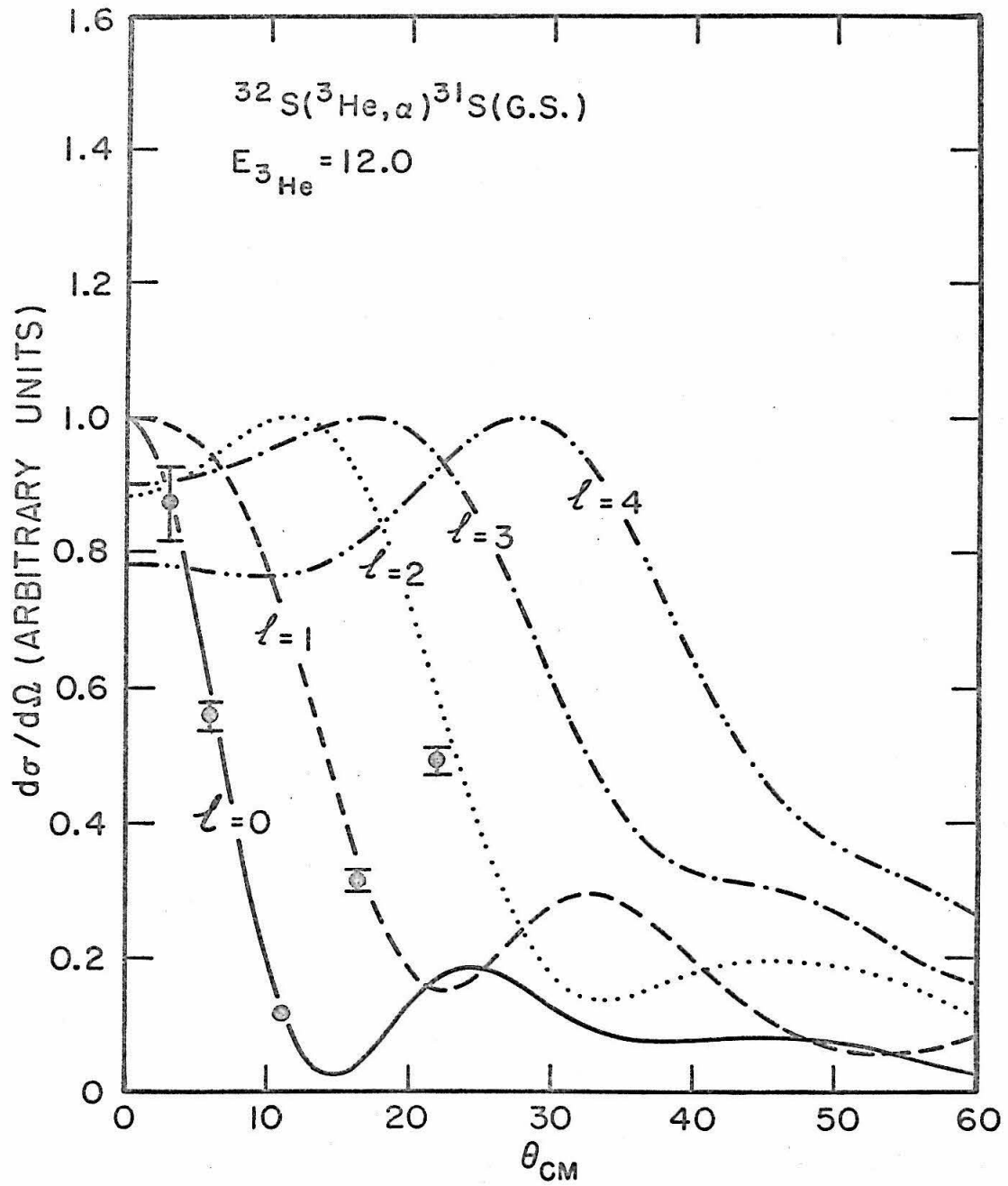
Figure 14

Angular Distribution for ^{31}S (3.08)

The angular distribution of the alpha particles from the reaction ^{32}S(^{3}He, α)^{31}S (3.08) is shown. The curve is a DWBA prediction. Level ^{31}S (3.08) is assigned $\ell_n = 0$. (See page 28.)
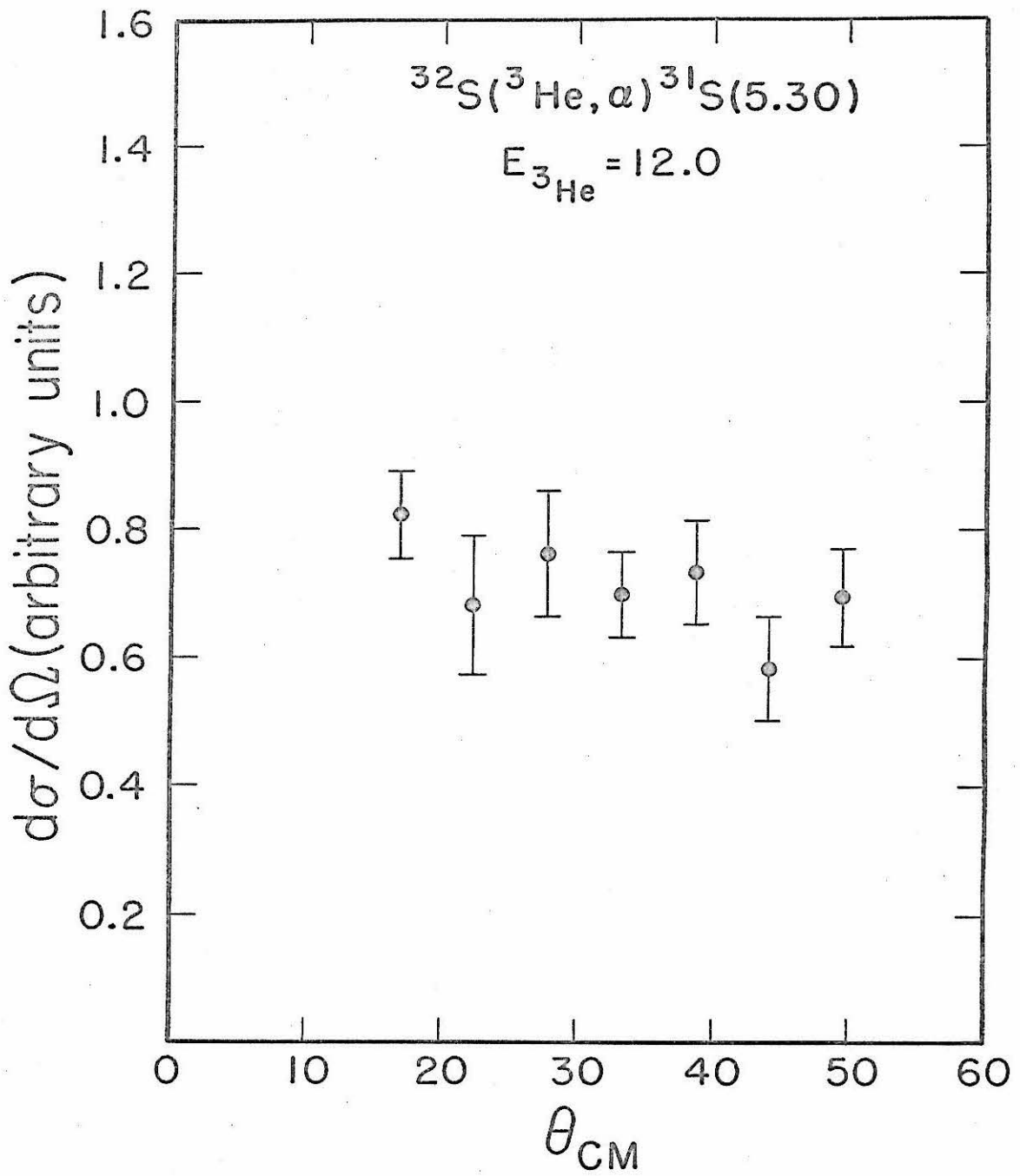
$^{32}S(^3He,\alpha)^{31}S(3.08)$

$E_{3_{He}} = 12.0$
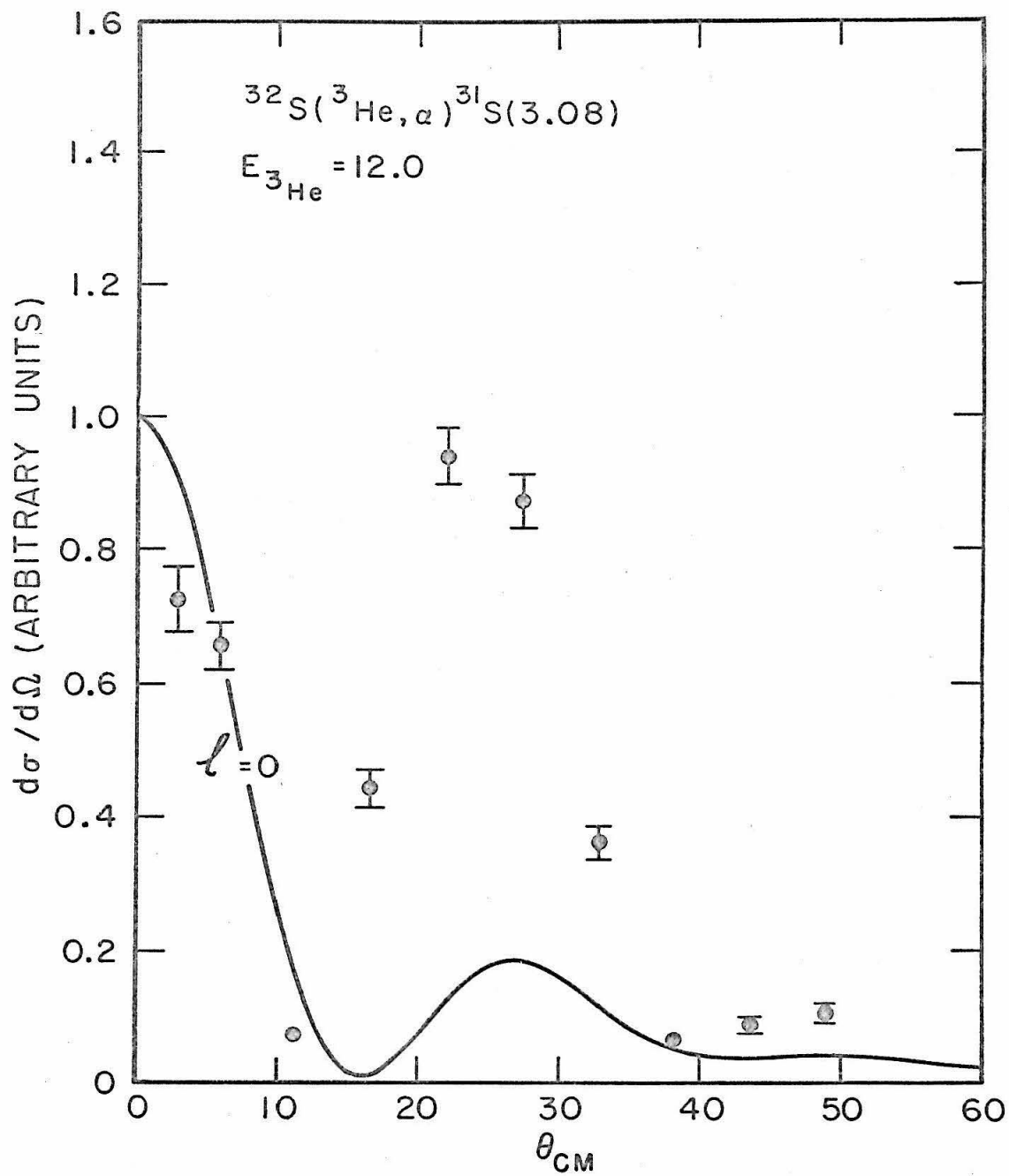
Figure 15

Angular Distribution for ^{31}S (3.29)

The angular distribution of the alpha particles from the reaction ^{32}S(^{3}He, α)^{31}Cl (3.29) is shown. The curves are DWBA predictions. Level ^{31}S (3.29) is assigned ℓ_n = 2 and on the basis of J-dependence, J = (5/2). (See page 28.)

^{32}S(^{3}He,α)^{31}S(3.29)

$E_{3He} = 12.0$
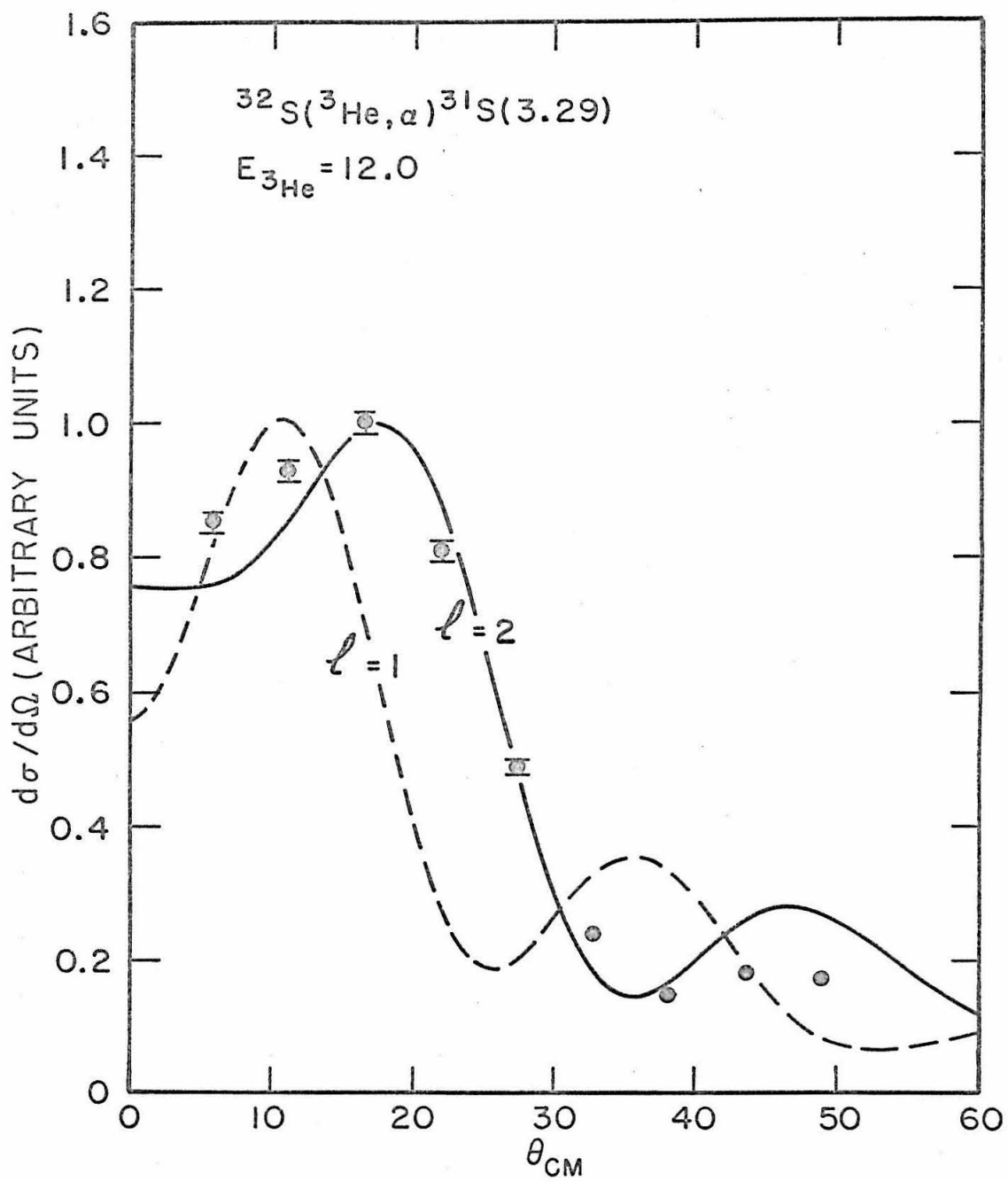
Figure 16

Angular Distribution for ^{31}S (3.44)

    The angular distribution of the alpha particles from the reaction ^{32}S(^{3}He, α)^{31}S (3.44) is shown. The curves are DWBA predictions.   Level ^{31}S (3.44) is assigned ℓ_n = (2) and on the basis of J-dependence, J = (3/2). (See page 29.)

$^{32}S(^3He,\alpha)^{31}S(3.44)$

$E_{3_{He}} = 12.0$

$\ell = 2$

$\ell = 1$

$d\sigma/d\Omega$ (ARBITRARY UNITS)

θ_{CM}
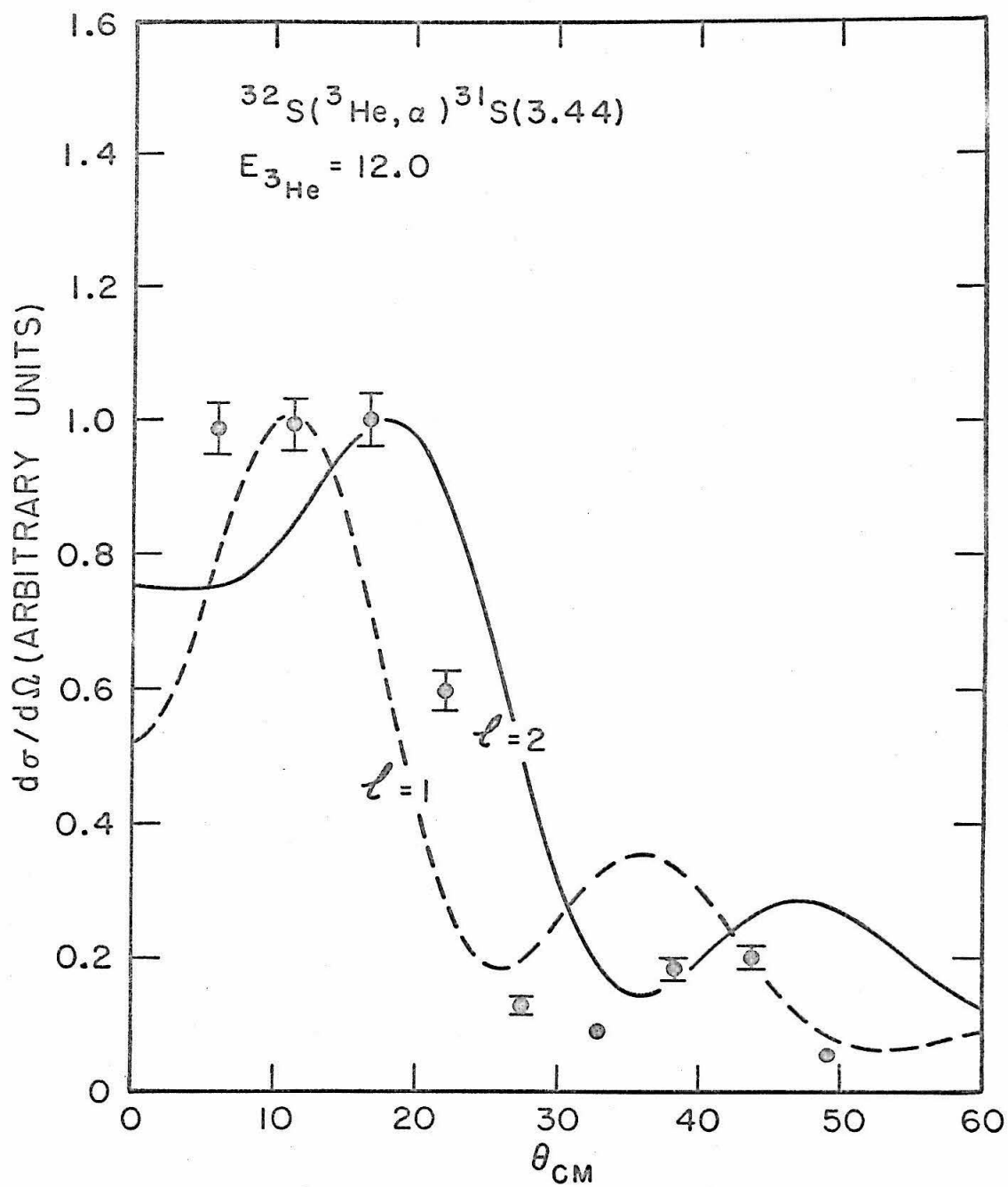
Figure 17

Angular Distribution for ^{31}S (4.08)

      The angular distribution of the alpha particles from the reaction ^{32}S(^{3}He, α)^{31}S (4.08) is shown. At forward angles the ^{31}S (4.08) group was obscured by the ^{11}C (G.S.) group. The curves are DWBA predictions. Level ^{31}S (4.08) is assigned ℓ_n = (2) and on the basis of J-dependence, J = (5/2). (See page 29.)

$^{32}S(^3He,\alpha)^{31}S(4.08)$

$E_{^3He} = 12.0$

$^{11}C(g.s.)$

$\ell = 1$

$\ell = 2$
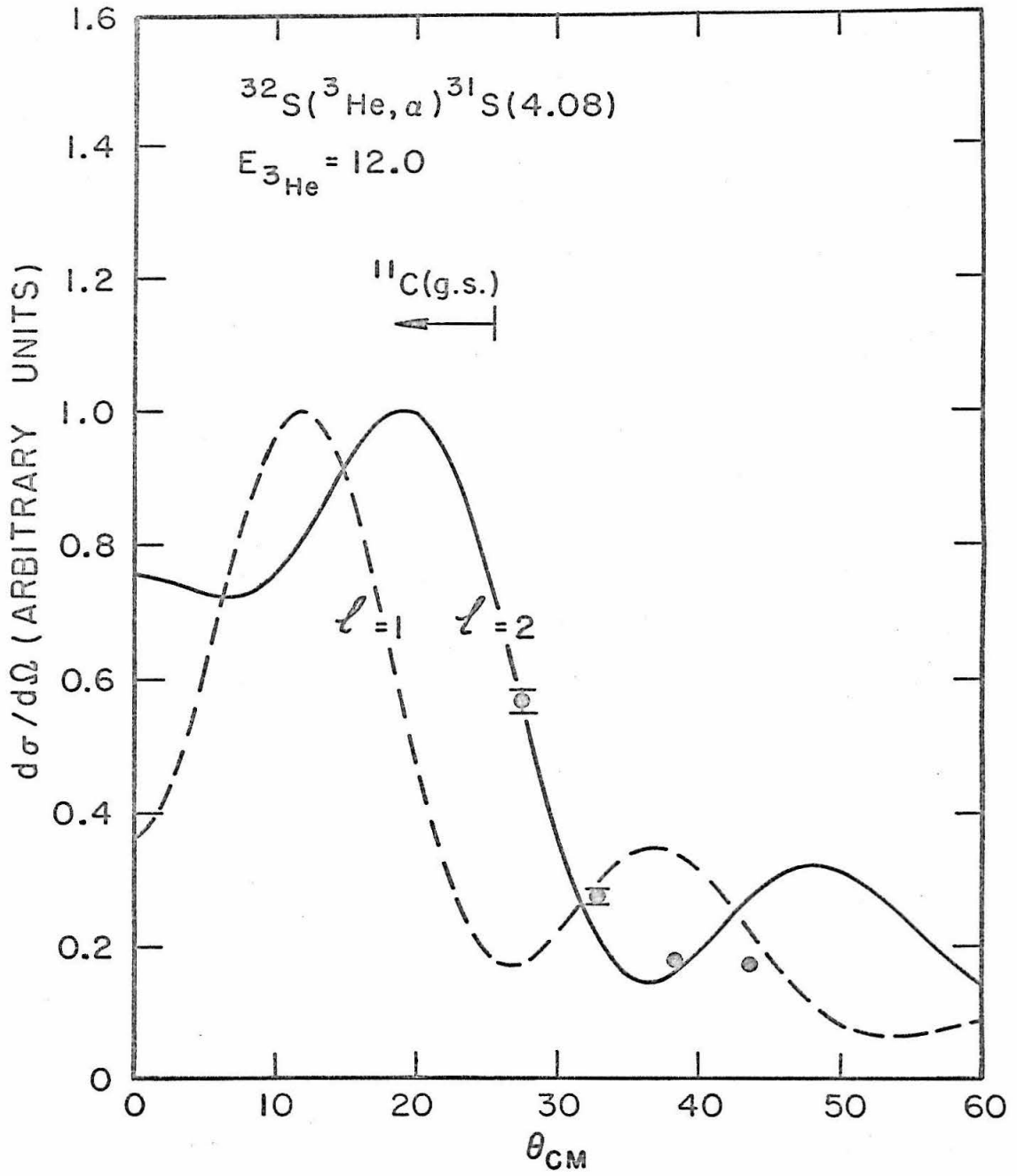
Figure 18

Angular Distribution for ^{31}S (4.45)

The angular distribution of the alpha particles from the reaction ^{32}S(^{3}He, α)^{31}S (4.45) is shown. The angular range where the ^{31}S (4.08) group was obscured by the ^{11}C (G.S.) group is indicated. The curves are DWBA predictions. Level ^{31}S (4.45) is assigned ℓ_n = 3. (See page 29.)

$^{32}S(^3He,\alpha)^{31}S(4.45)$

$E_{3_{He}} = 12.0$
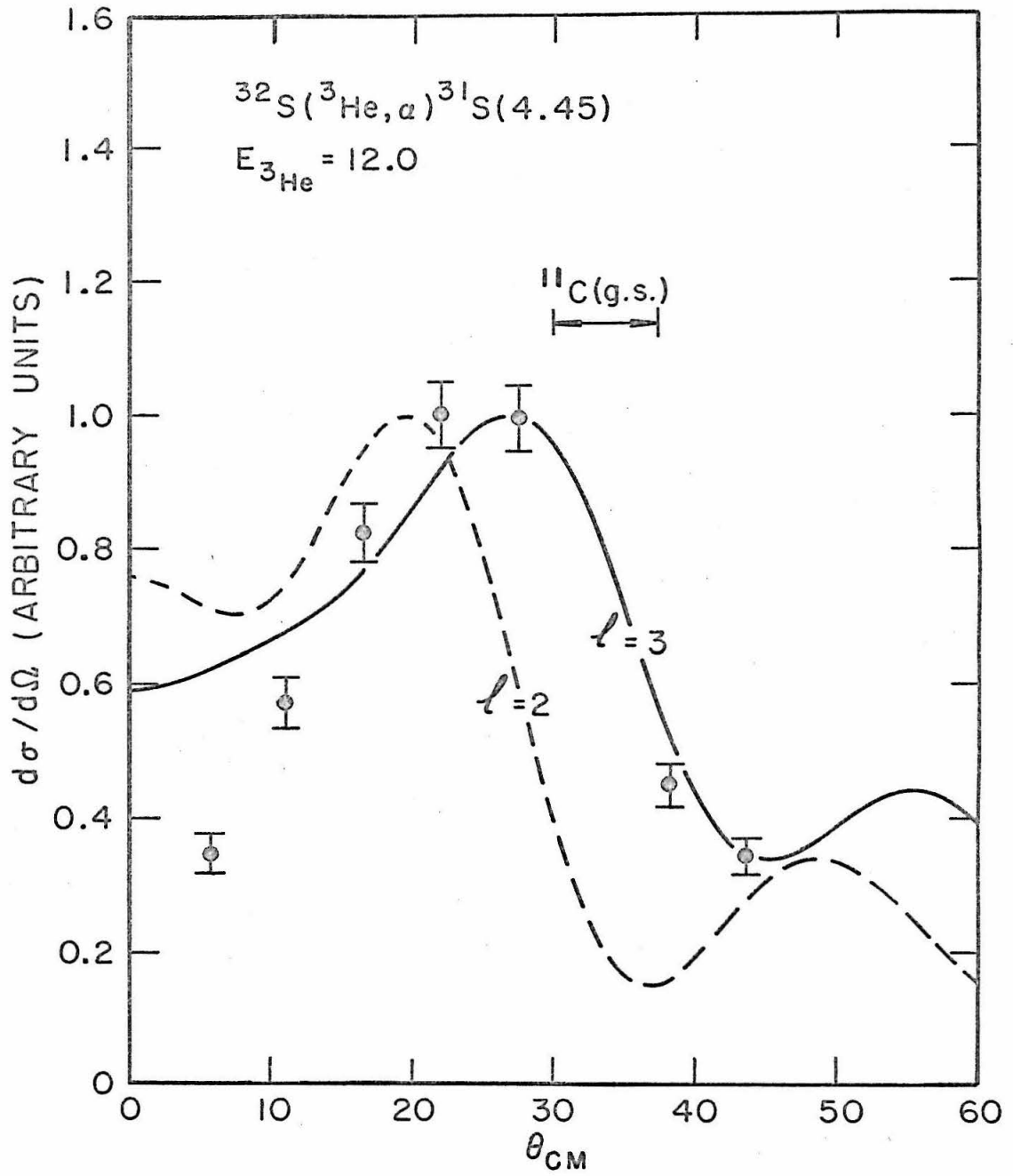
Figure 19

Angular Distribution for ^{31}S (4.52)

The angular distribution of the alpha particles from the reaction ^{32}S(^{3}He, α)^{31}S (4.52) is shown. The angular range where the ^{31}S (4.52) group was obscured by the ^{11}C (G.S.) group is indicated. The curves are DWBA predictions. Level ^{31}S (4.52) is assigned ℓ_n = 2. (See page 29.)

$^{32}S(^{3}He,\alpha)^{31}S\,(4.52)$

$E_{3_{He}} = 12.0$

$\ell = 1$

$\ell = 2$

$^{11}C(g.s.)$

$d\sigma/d\Omega$ (ARBITRARY UNITS)

θ_{CM}
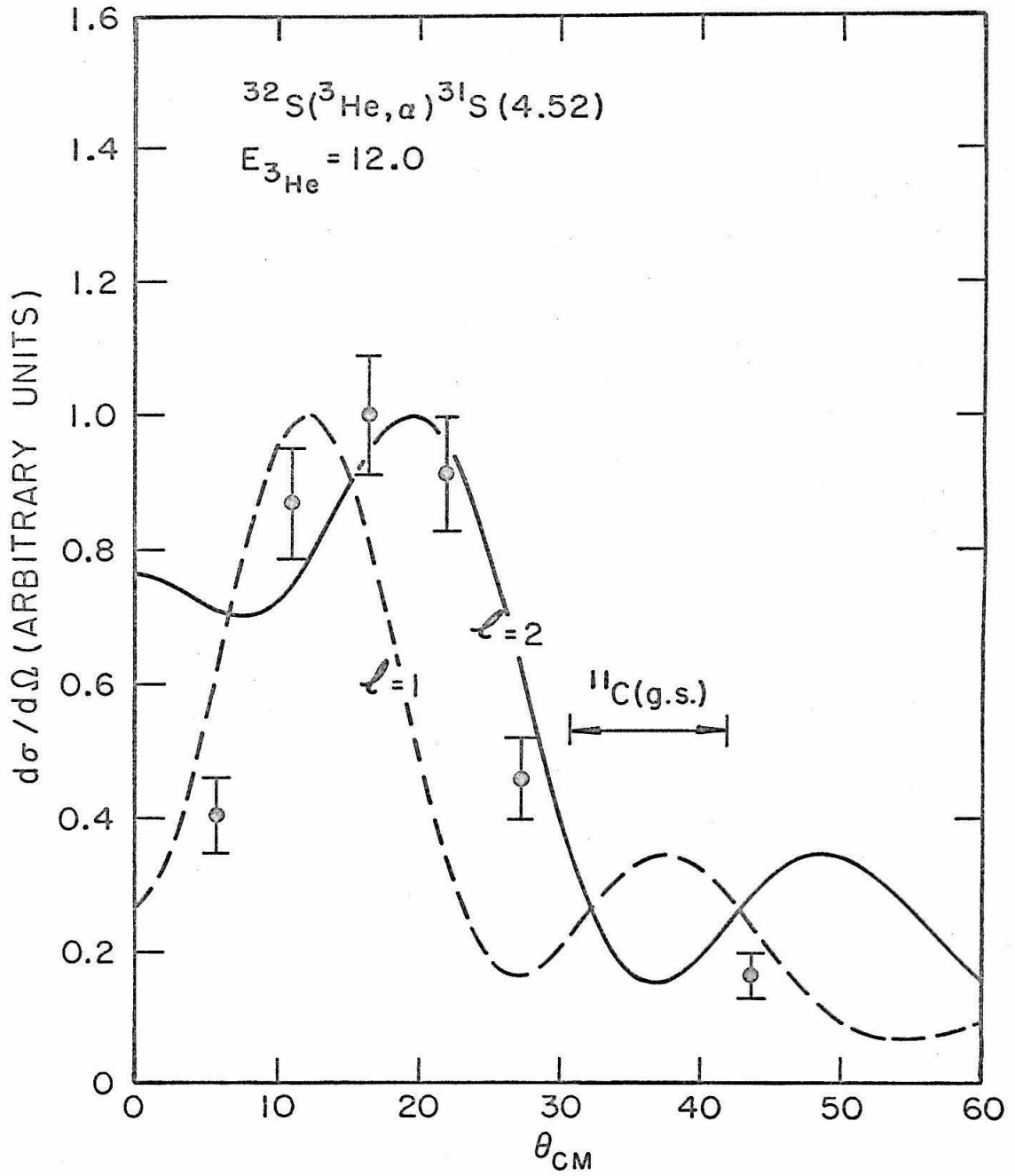
Figure 20

Angular Distribution for ^{31}S (4.58)

The angular distribution of the alpha particles from the reaction ^{32}S(^{3}He, α)^{31}S (4.58) is shown. The angular range where the ^{31}S (4.58) group was obscured by the ^{11}C (G.S.) group is indicated. The curves are DWBA predictions. No assignment is made for level ^{31}S (4.58). (See page 29.)

$^{32}S(^{3}He, \alpha)^{31}S(4.58)$

$E_{3_{He}} = 12.0$

$^{11}C(g.s.)$

$\ell = 0$

$\ell = 1$

$\ell = 3$

$\ell = 4$

$d\sigma/d\Omega$ (ARBITRARY UNITS)

θ_{CM}
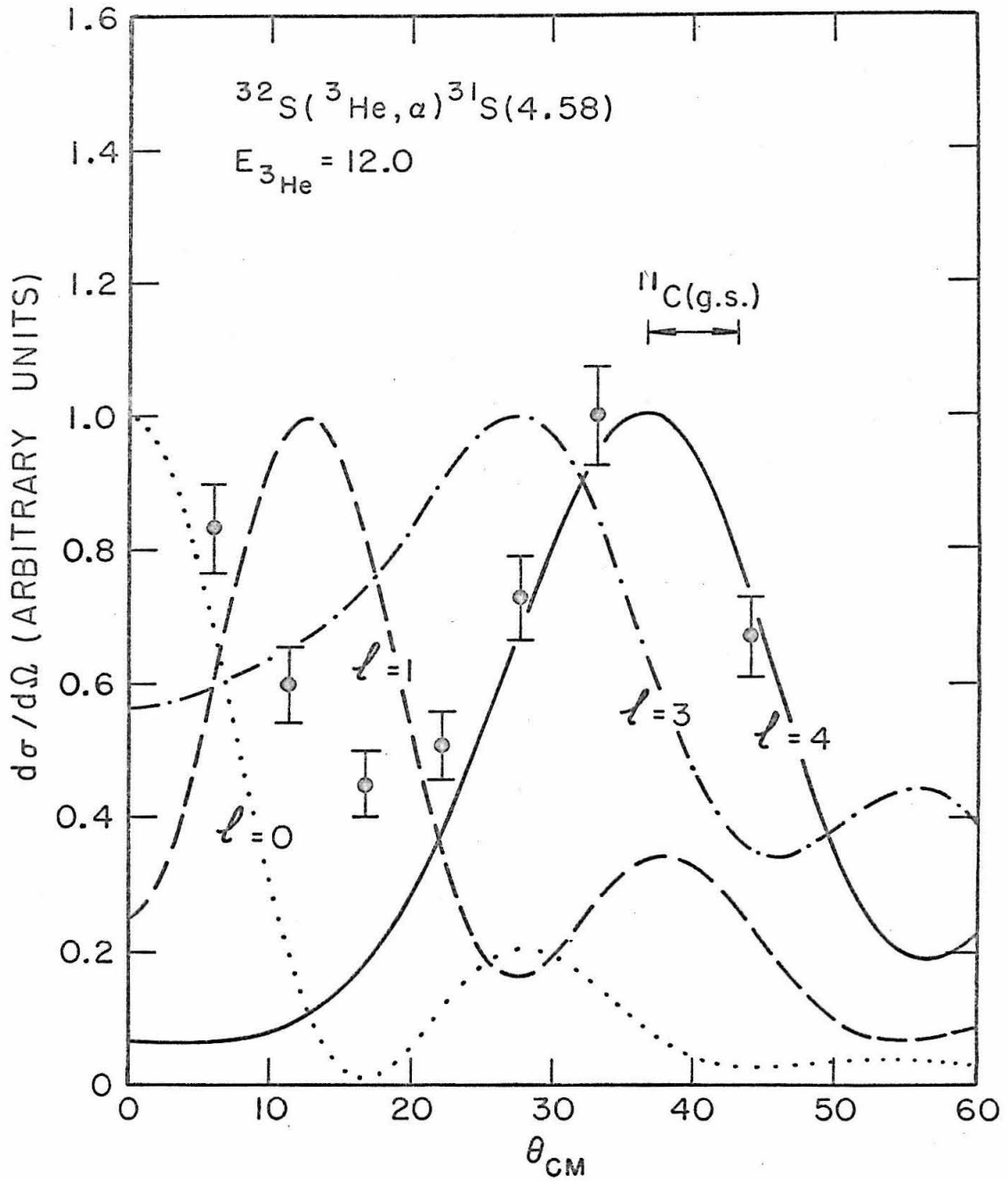
Figure 21

Angular Distribution for ^{31}S (4.72)

The angular distribution of the alpha particles from the reaction ^{32}S(^{3}He, α)^{31}S (4.72) is shown. The angular range where the ^{31}S (4.72) group was obscured by the ^{11}C (G.S.) group is indicated. The curves are DWBA predictions. Level ^{31}S (4.72) is assigned ℓ_n = 2, (3), and on the basis of J-dependence, J = (5/2). (See page 29.)

$^{32}S(^3He, \alpha)^{31}S(4.72)$

$E_{3_{He}} = 12.0$
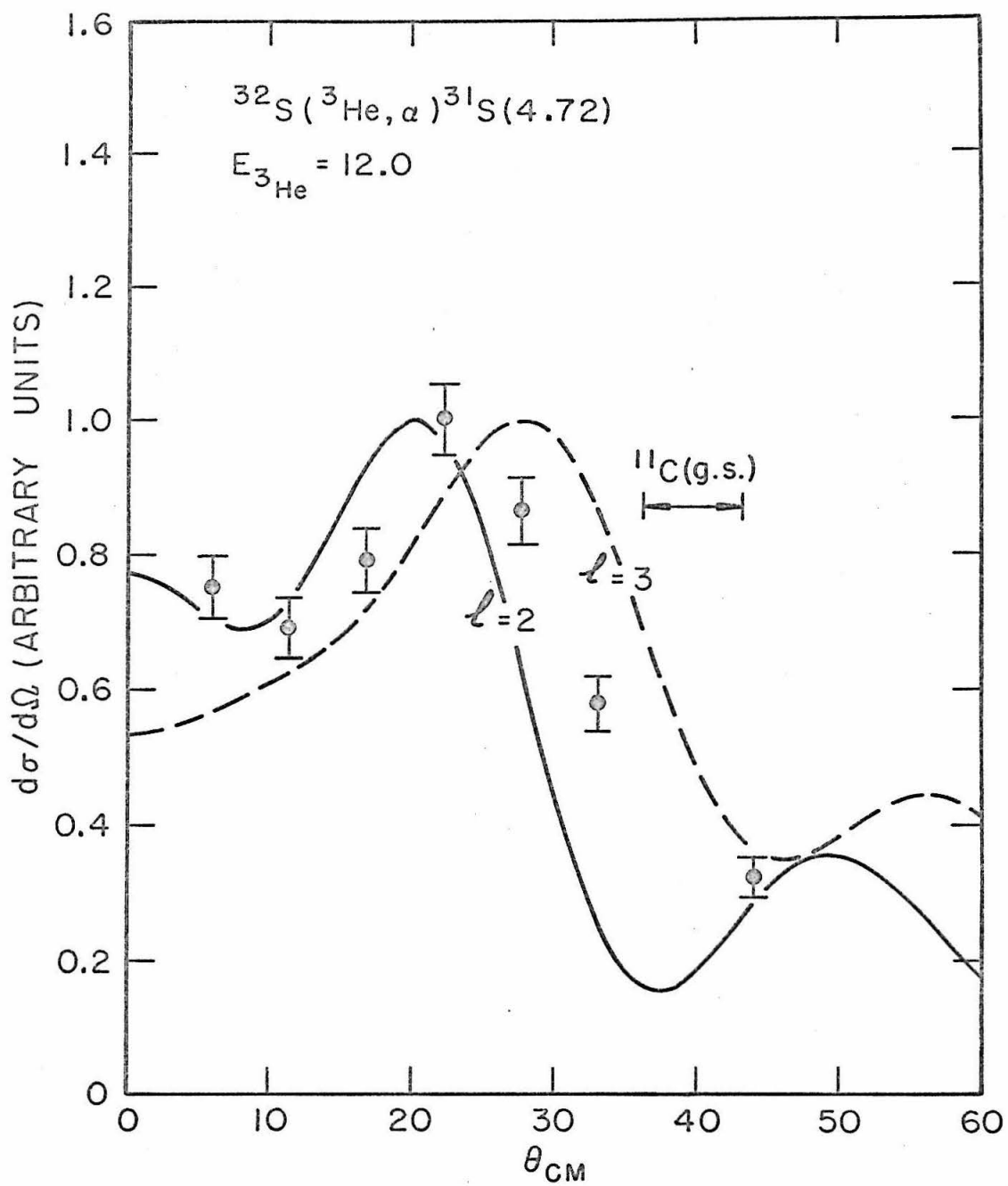
Figure 22

Angular Distribution for ^{31}S (4.87)

The angular distribution of the alpha particles from the reaction ^{32}S(^{3}He, α)^{31}S (4.87) is shown. The curves are DWBA predictions. Level ^{31}S (4.87) is assigned ℓ_n = (1). (See page 29.)

$^{32}S(^3He,\alpha)^{31}S(4.87)$

$E_{3_{He}} = 12.0$

$\ell = 1$

$\ell = 0$

$d\sigma/d\Omega$ (ARBITRARY UNITS)

θ_{CM}
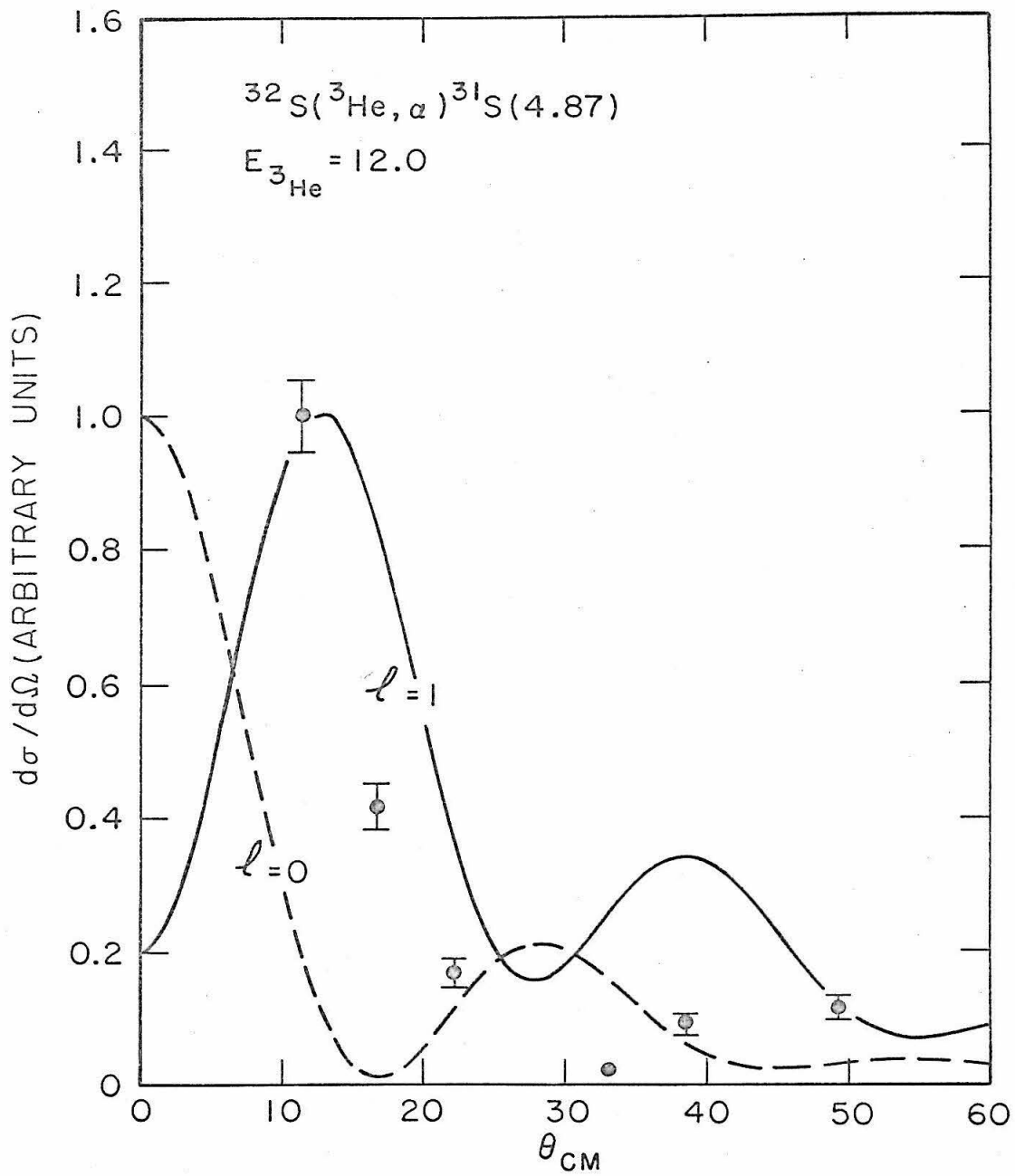
Figure 23

Angular Distribution for ^{31}S (4.97)

    The angular distribution of the alpha particles from the reaction ^{32}S(^{3}He, α)^{31}S (4.97) is shown. The curves are DWBA predictions. Level ^{31}S (4.97) is assigned $\ell_n = 1$. (See page 30.)

^{32}S(^{3}He,α)^{31}S(4.97)

$E_{3_{He}} = 12.0$

Figure 24

Angular Distribution for ^{31}S (5.15)

The angular distribution of the alpha particles from the reaction ^{32}S(^{3}He, α)^{31}S (5.15) is shown. The curve is a DWBA prediction. Level ^{31}S (5.15) is assigned $\ell_n = 0$. (See page 30.)

$^{32}S(^3He,\alpha)^{31}S(5.15)$

$E_{3_{He}} = 12.0$

$\ell = 0$

225

Figure 25

Angular Distribution for ^{31}S (5.30)

     The angular distribution of the alpha particles from the reaction ^{32}S(^{3}He, α)^{31}S (5.30) is shown. The lack of structure suggests that level ^{31}S (5.30) is not populated by a pickup reaction, and no assignment is made. (See page 30.)

$^{32}S(^{3}He,\alpha)^{31}S(5.30)$

$E_{3_{He}} = 12.0$

Figure 26

Angular Distribution for ^{31}S (5.52)

The angular distribution of the alpha particles from the reaction ^{32}S(^{3}He, α)^{31}S (5.52) is shown. The curves are DWBA predictions. No assignment is made for level ^{31}S (5.52). (See page 30.)

$^{32}S(^3He,\alpha)^{31}S(5.52)$

$E_{3_{He}} = 12.0$

$\ell = 3$

$\ell = 2$

$d\sigma/d\Omega$ (ARBITRARY UNITS)

θ_{CM}
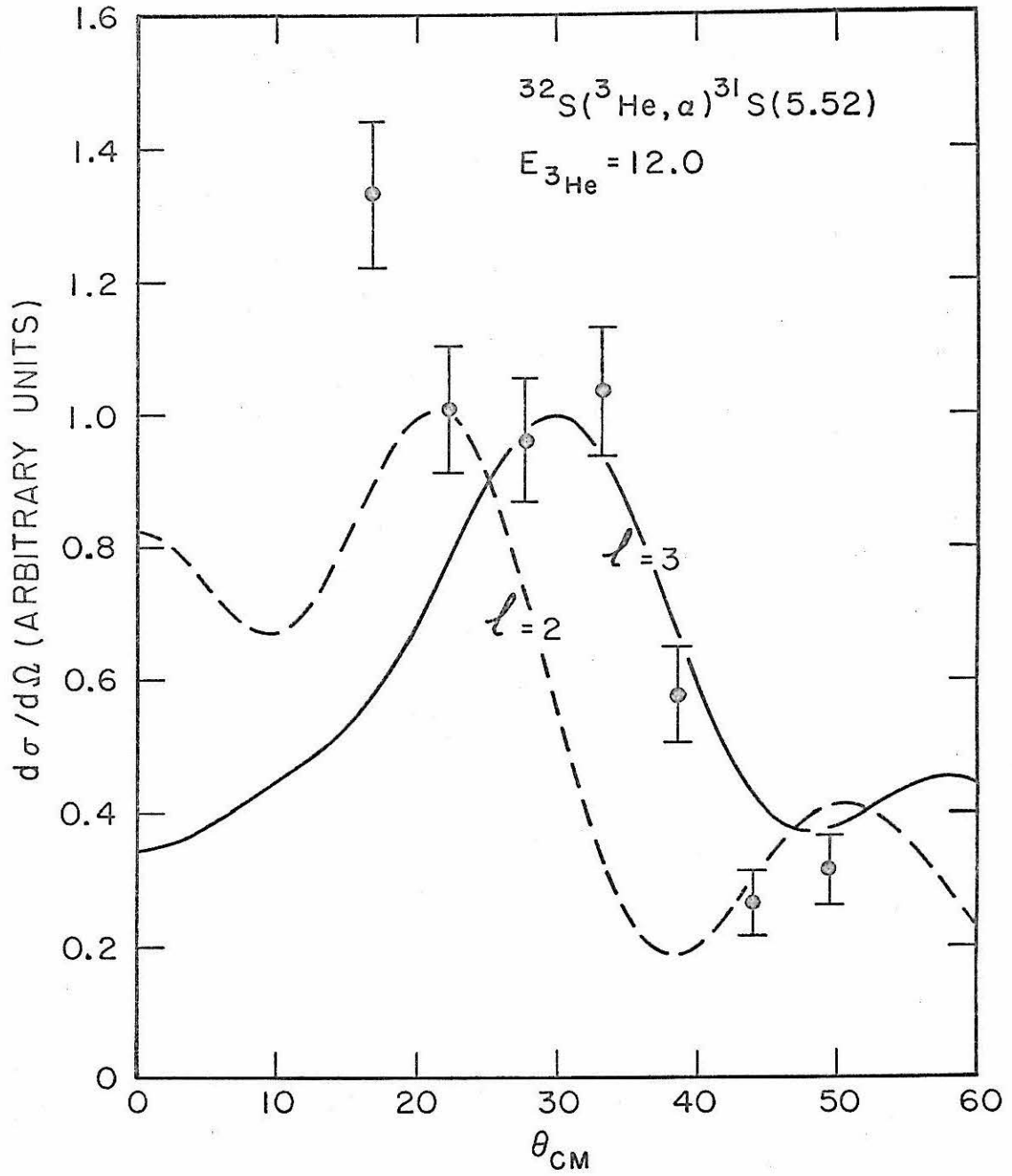
Figure 27

Excitation Functions for $^{32}S(^3He, \alpha)^{31}S$

The excitation functions measured at $\theta_{LAB} = 10^O$ for the reaction $^{32}S(^3He, \alpha)^{31}S$ to the first six excited states of ^{31}S are shown. The arrows indicate the beam energies selected for the correlation and branching ratio measurements. (See page 37.)

EXCITATION FUNCTIONS FOR $^{32}S(^{3}He, \alpha)^{31}S$

$\theta_{LAB} = 10°$

BR = BRANCHING RATIO
C = CORRELATION
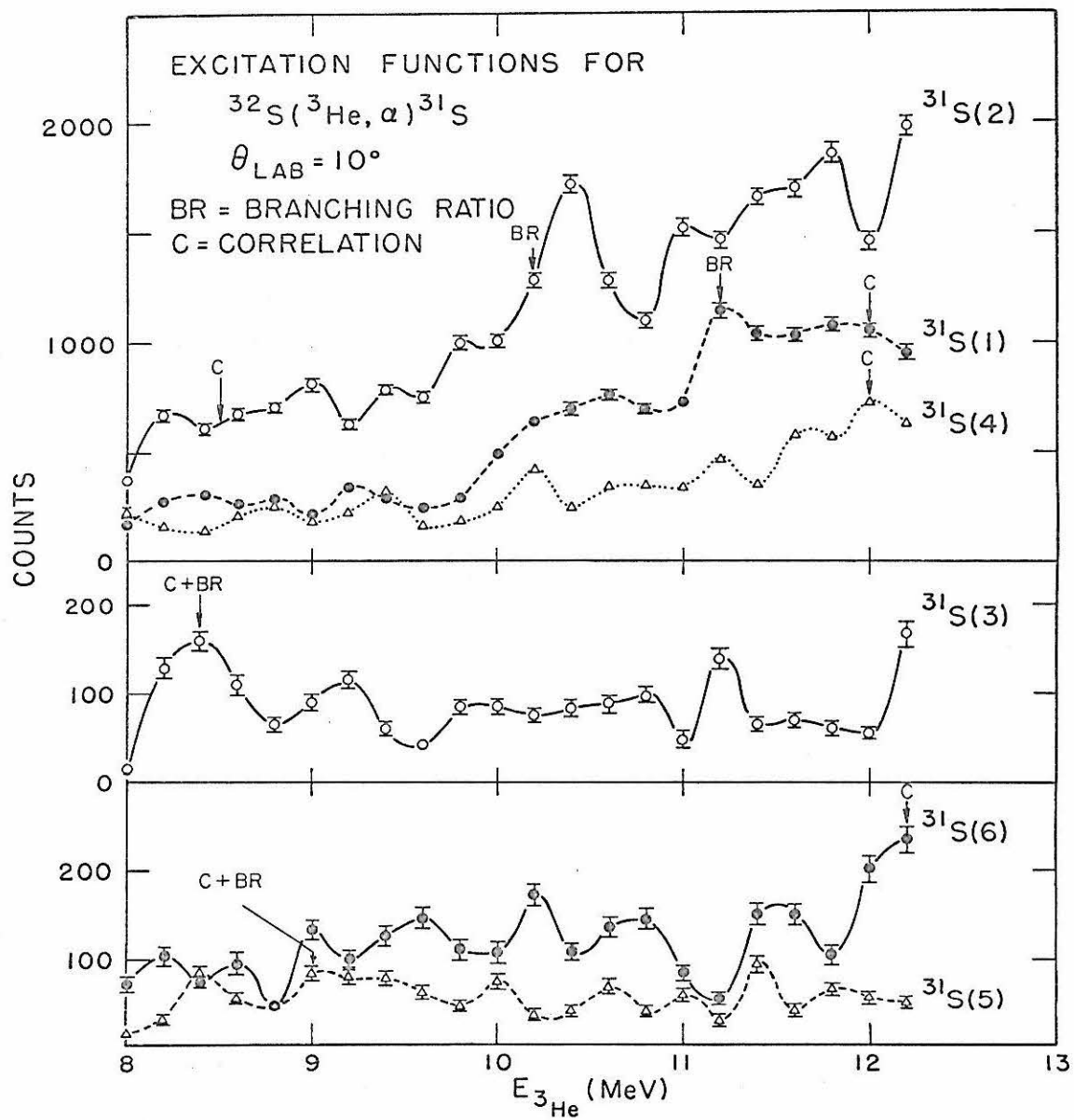
Figure 28

Schematic Diagram of the Correlation Setup

A schematic diagram of the setup used for the measurement of the correlations in the reaction ^{32}S(^{3}He, $\alpha\gamma$)^{31}S is shown. The alpha particles were detected in the magnetic spectrometer at 0° with a silicon surface barrier detector. The beam was stopped in a tantalum cup. The gamma rays were detected in 12. 70 cm (diameter) x 10. 16 cm (length) NaI(Tl) crystal which could be moved from 90° to 150°. (See page 37.)
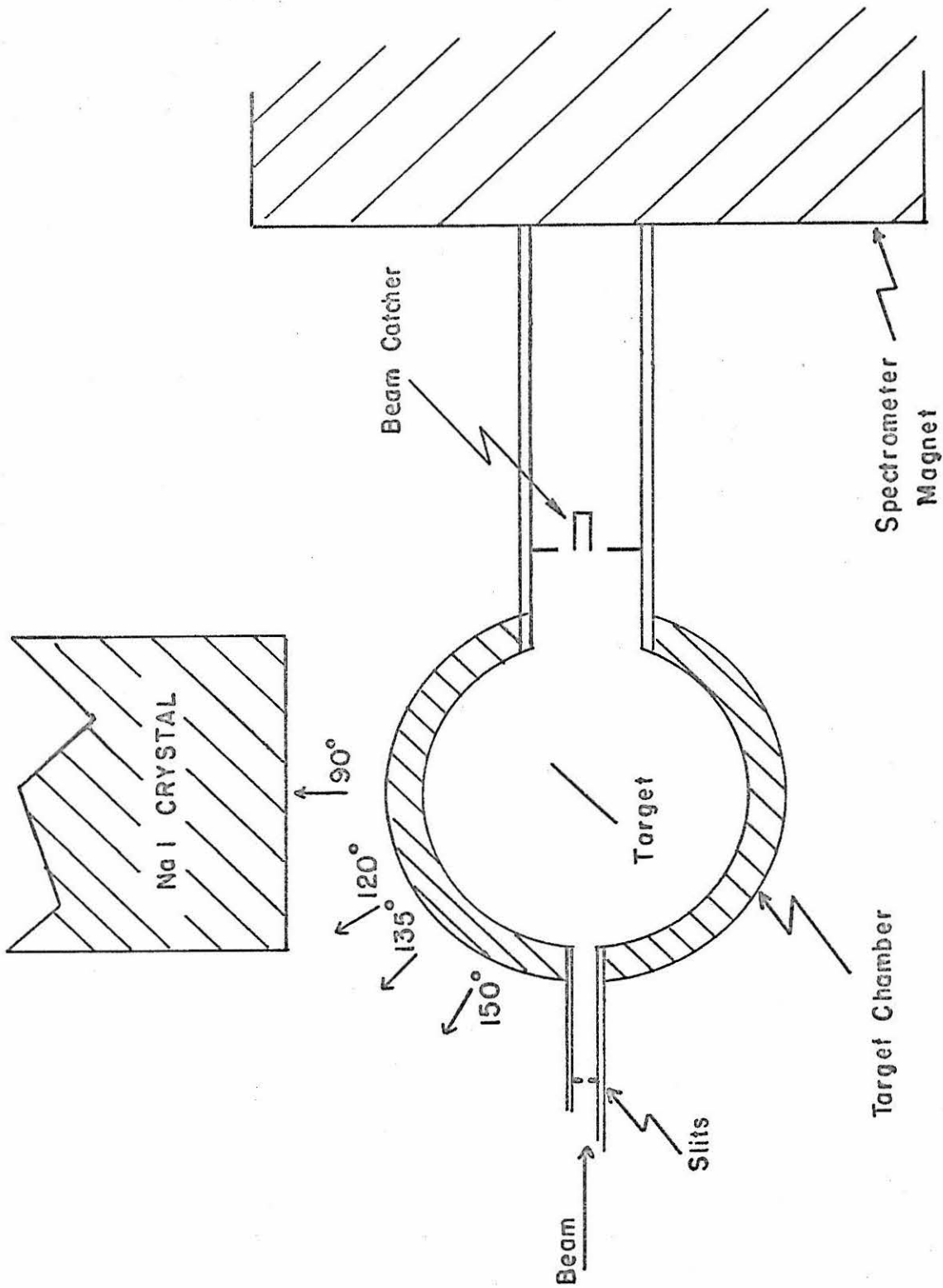
Figure 29

Electronics for the Correlation and Branching
Ratio Measurements

A diagram of the electronics for the correlation and
branching ratio measurements is shown. The lower level
discriminator gate is a modification of the RIDL 400-channel
analyzer which reduces the dead time for high count rates.
The two diodes prevented cross-talk between the two
coincidence units (RIDL 32-3). (See page 38.)
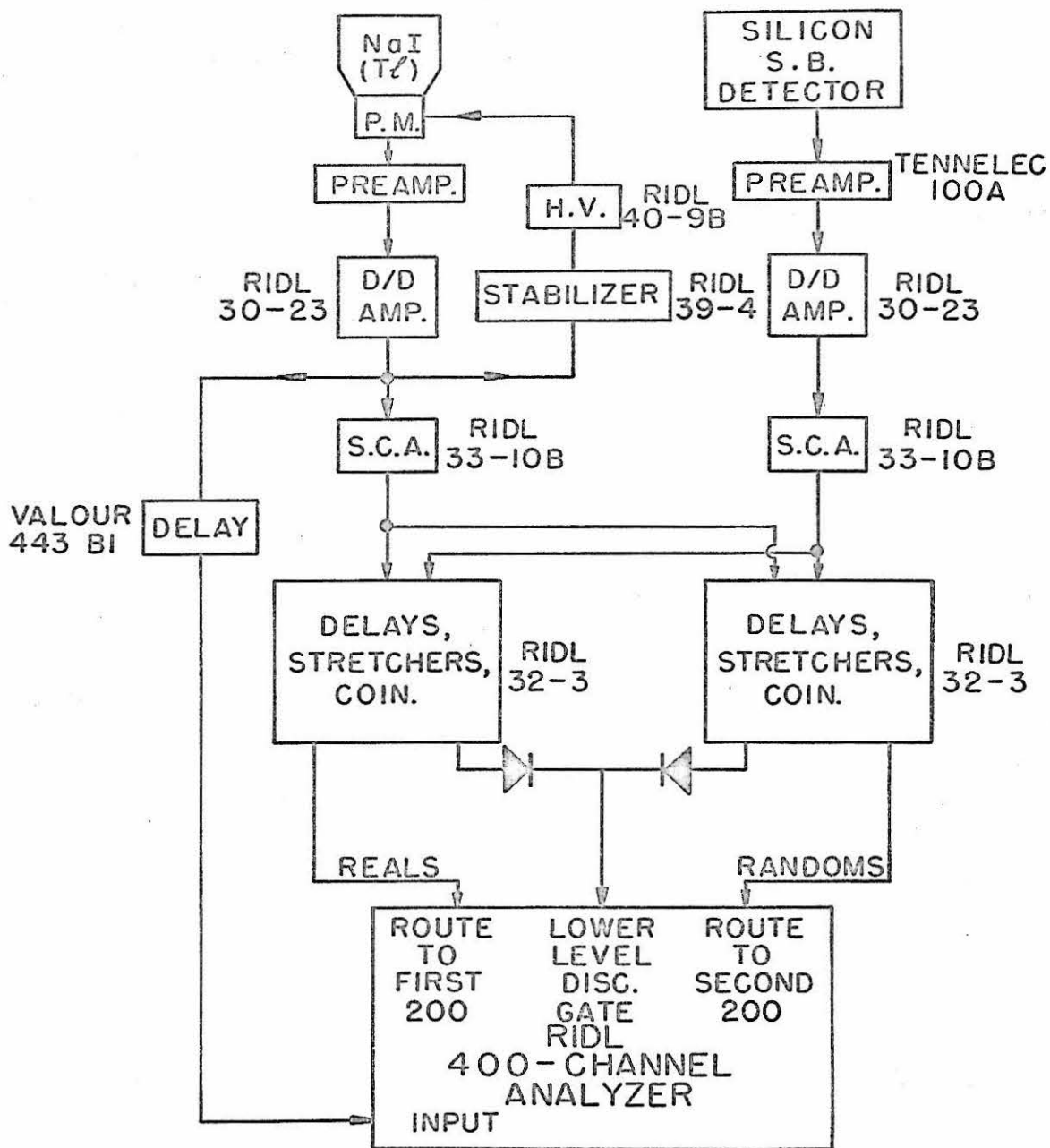
Figure 30

Gamma-Ray Spectrum from the Decay of ^{31}S (1.25)

The gamma-ray spectrum at $\theta_\gamma = 120^O$ from the decay of the level at 1.25 MeV excitation energy in ^{31}S is shown. The gamma-ray S.C.A. was set so that pulses were stored only above channel 34. The randoms spectrum multiplied by the ratio $\frac{\text{number of reals}}{\text{number of randoms}}$ has already been subtracted. (See page 40.)
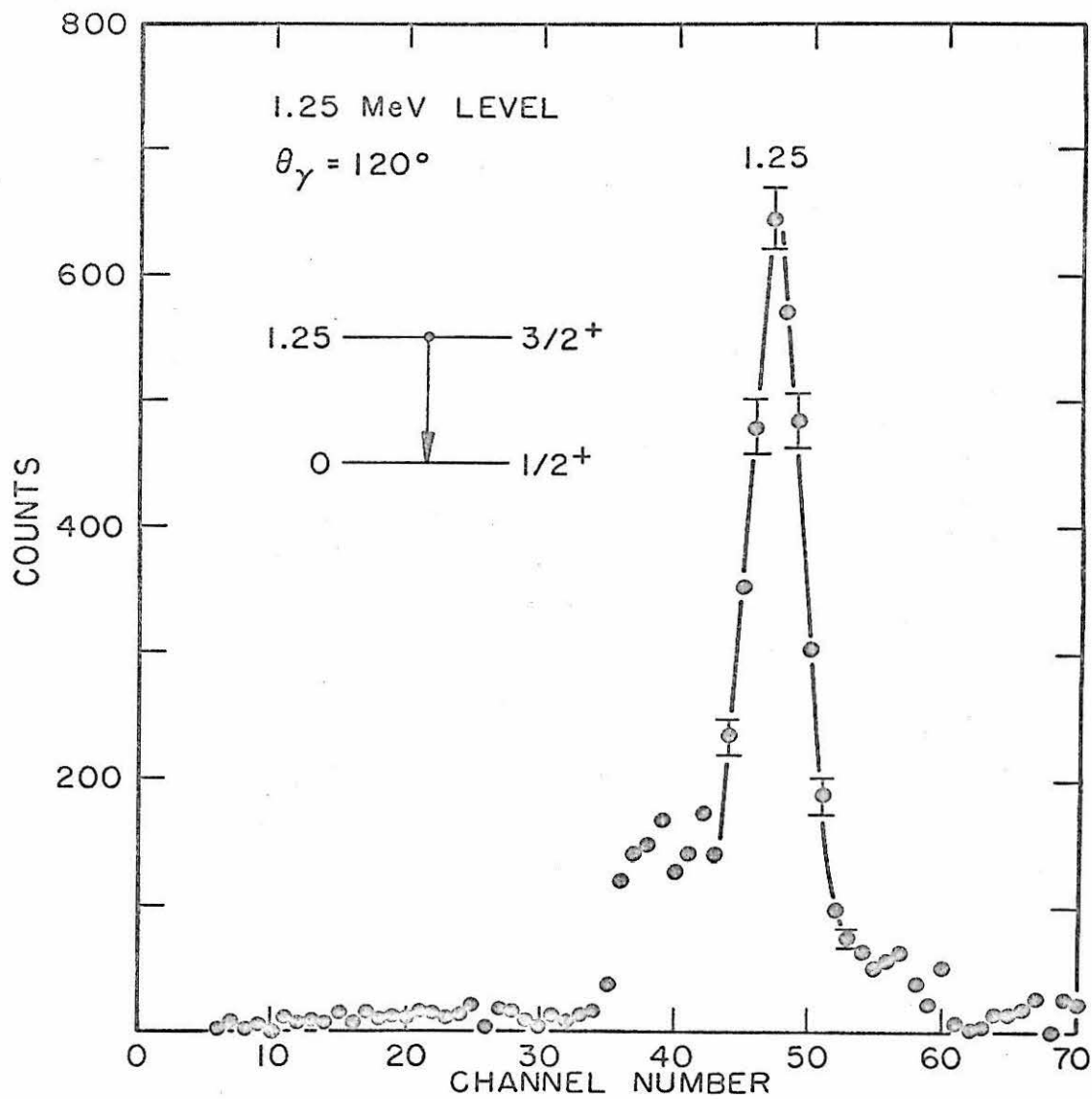
Figure 31

Angular Correlation of ^{31}S (1.25)

The angular correlation of the photopeak of the 1.25 MeV gamma rays detected in coincidence with the alpha particles at 0° corresponding to ^{31}S (1.25) is shown. The number of counts has been normalized to the number of alpha particles detected. The error bars represent the statistical uncertainties. For one of the two solutions the mixing parameter is X = -.349 ± .015, and the lines are for X = -.349, -.015 = 0.364, -.349, and -.349 + .015 = -.334. The lines for the other solution which are not shown are very similar. (See pages 41 and 48.)
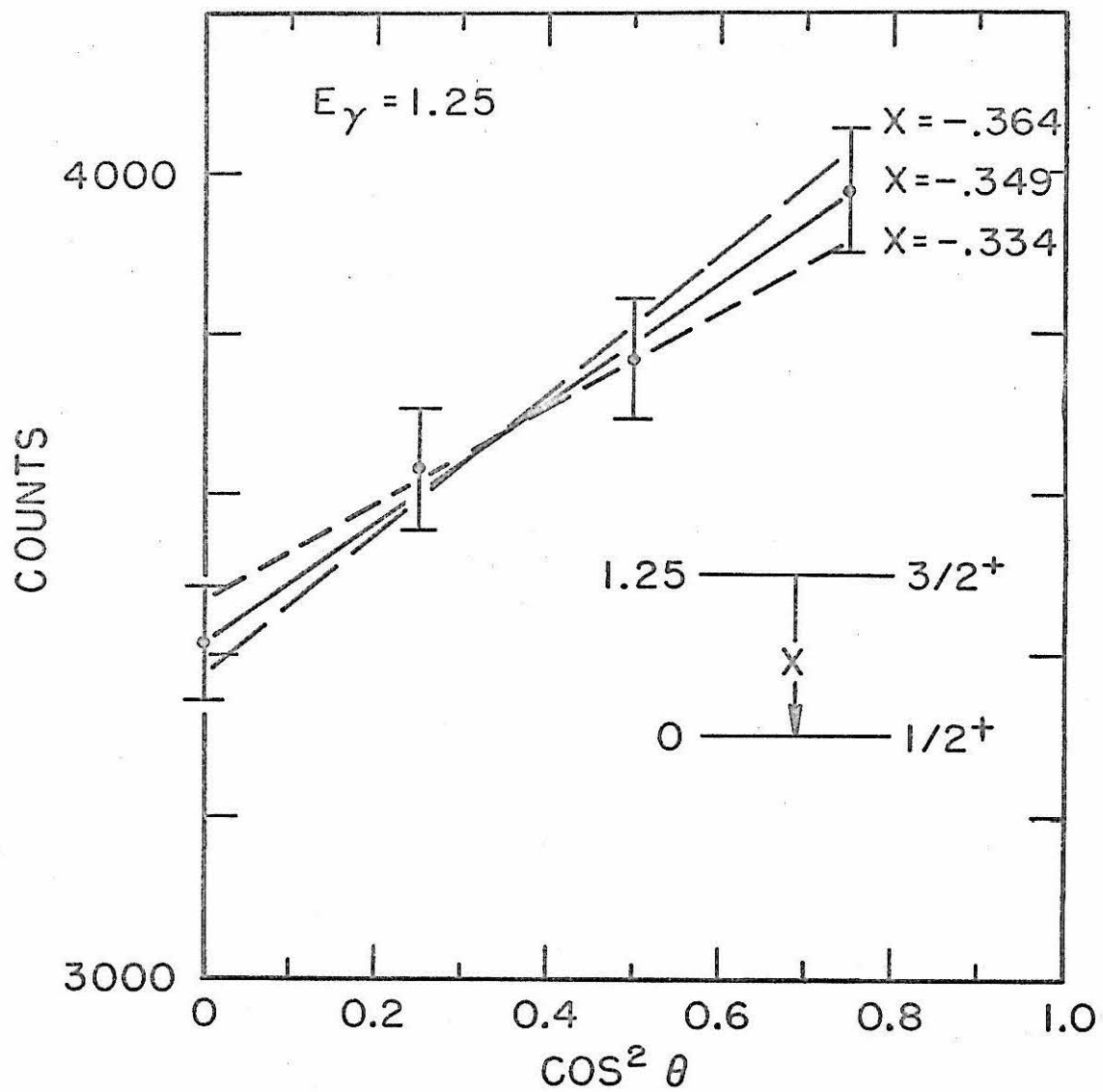
Figure 32

Gamma-Ray Spectrum from the Decay of ^{31}S (2.23)

The gamma-ray spectrum at $\theta_\gamma = 135^O$ from the decay of the level at 2.23 MeV excitation energy in ^{31}S is shown. The gamma-ray S.C.A. was set so that pulses were stored only above channel 27. The randoms spectrum multiplied by the ratio $\frac{\text{number of reals}}{\text{number of randoms}}$ has already been subtracted. The gamma-ray energy calibration was established with gamma-ray sources. (See page 41.)
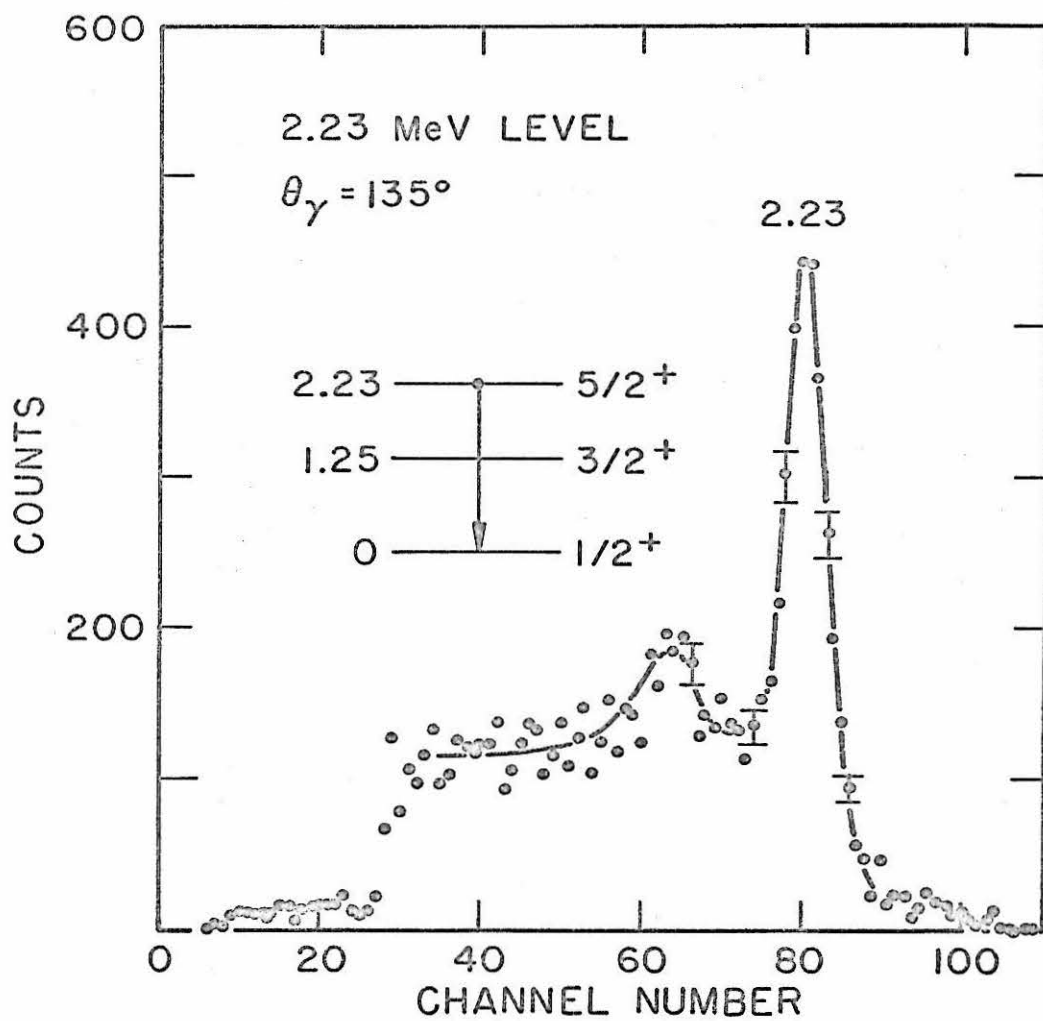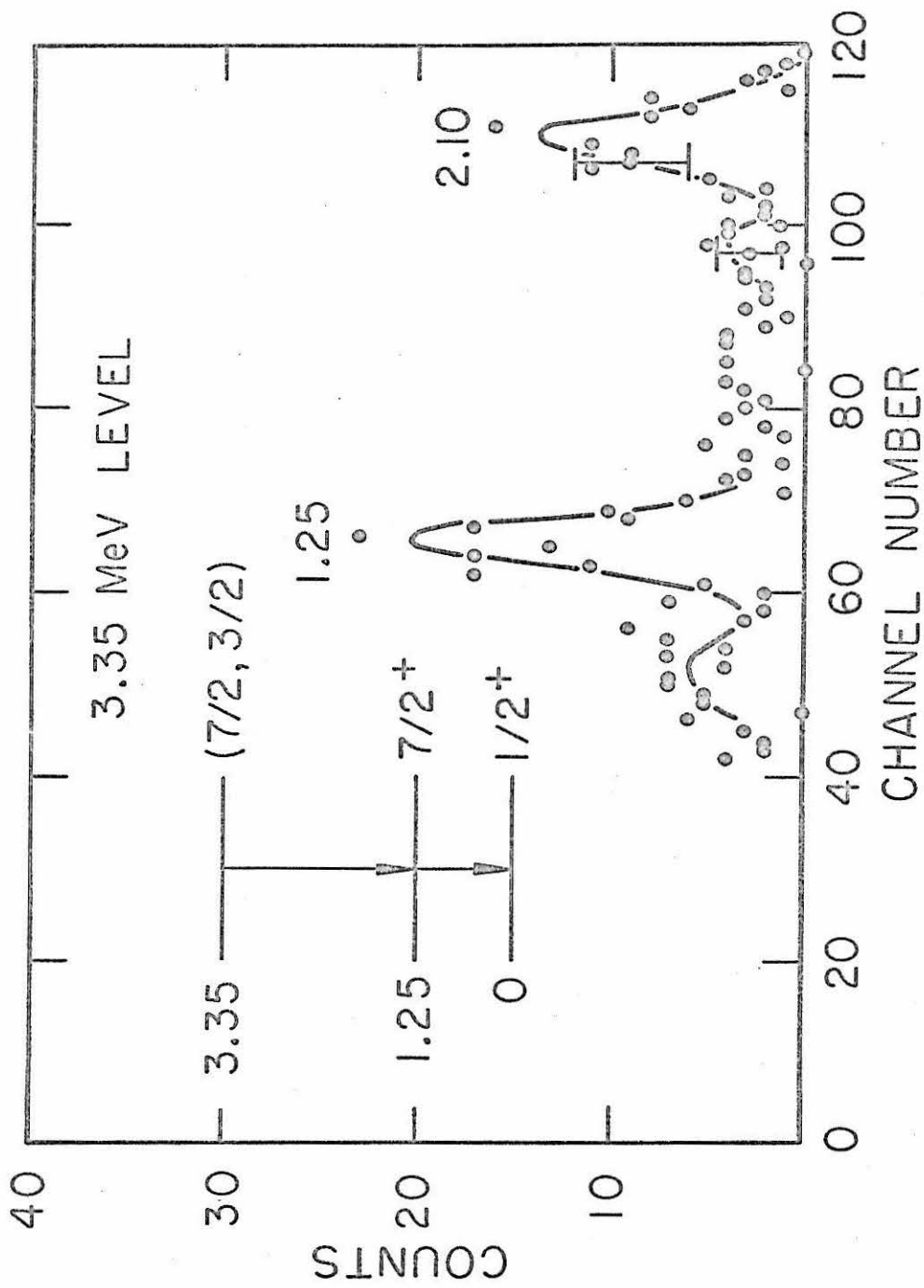
Figure 33

Angular Correlation of ^{31}S (2.23)

The angular correlation of the photopeak of the
2.23 MeV gamma rays detected in coincidence with the
alpha particles at 0° corresponding to ^{31}S (2.23) is shown.
The number of counts has been normalized to the number
of alpha particles detected. The error bars represent the
statistical uncertainties. The fit shown is for X = .053.
(See pages 42 and 49.)
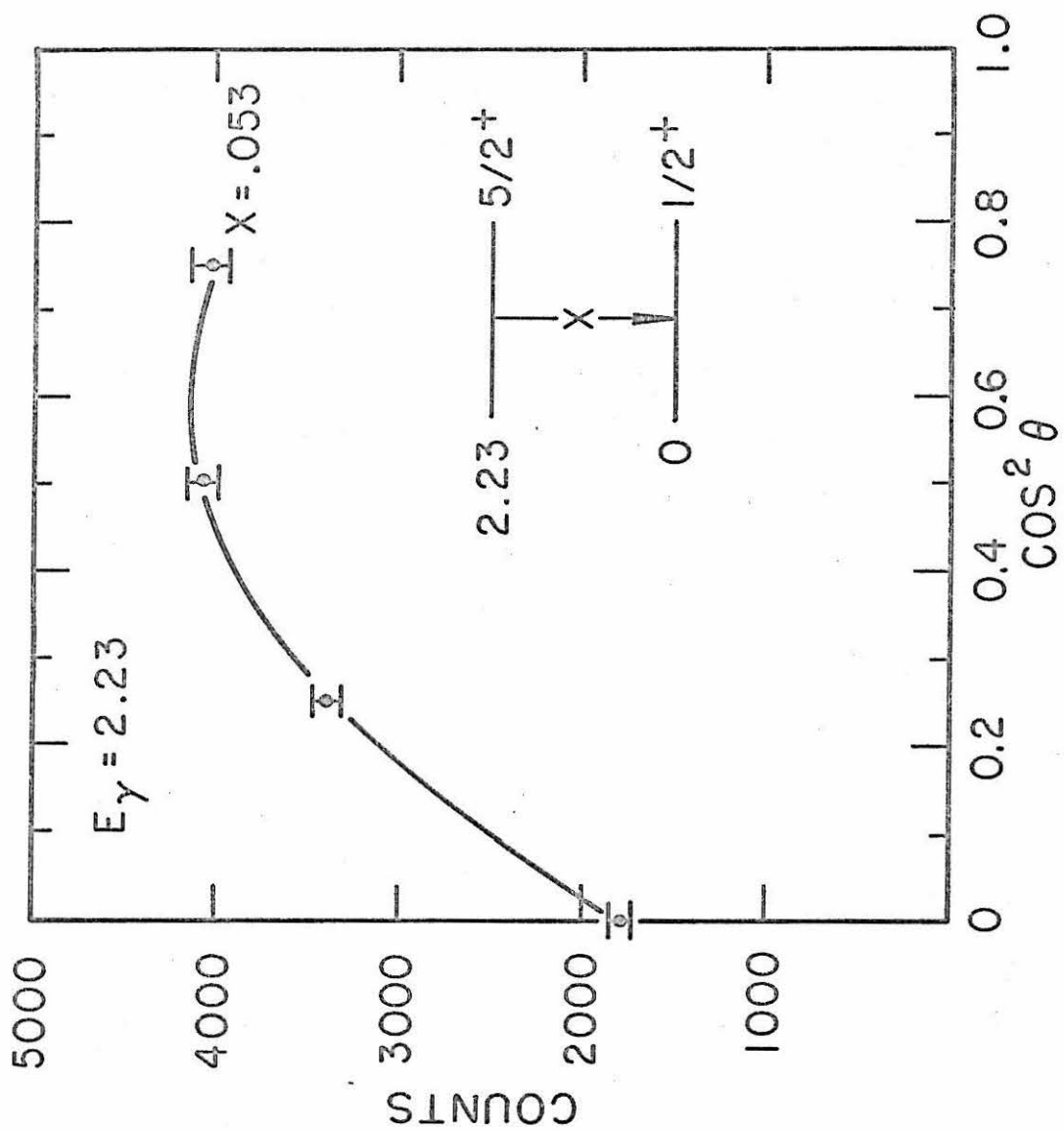
Figure 34

Gamma-Ray Spectrum from the Decay of ^{31}S (3.08)

The sum of the gamma-ray spectra obtained at $\theta_\gamma = 90^O$, 120°, 135°, and 150° from the decay of the level at 3.08 MeV excitation energy in ^{31}S is shown. The randoms spectra multiplied by the ratio $\frac{\text{number of reals}}{\text{number of randoms}}$ have already been subtracted. The gamma-ray energy calibration was established with gamma-ray sources.
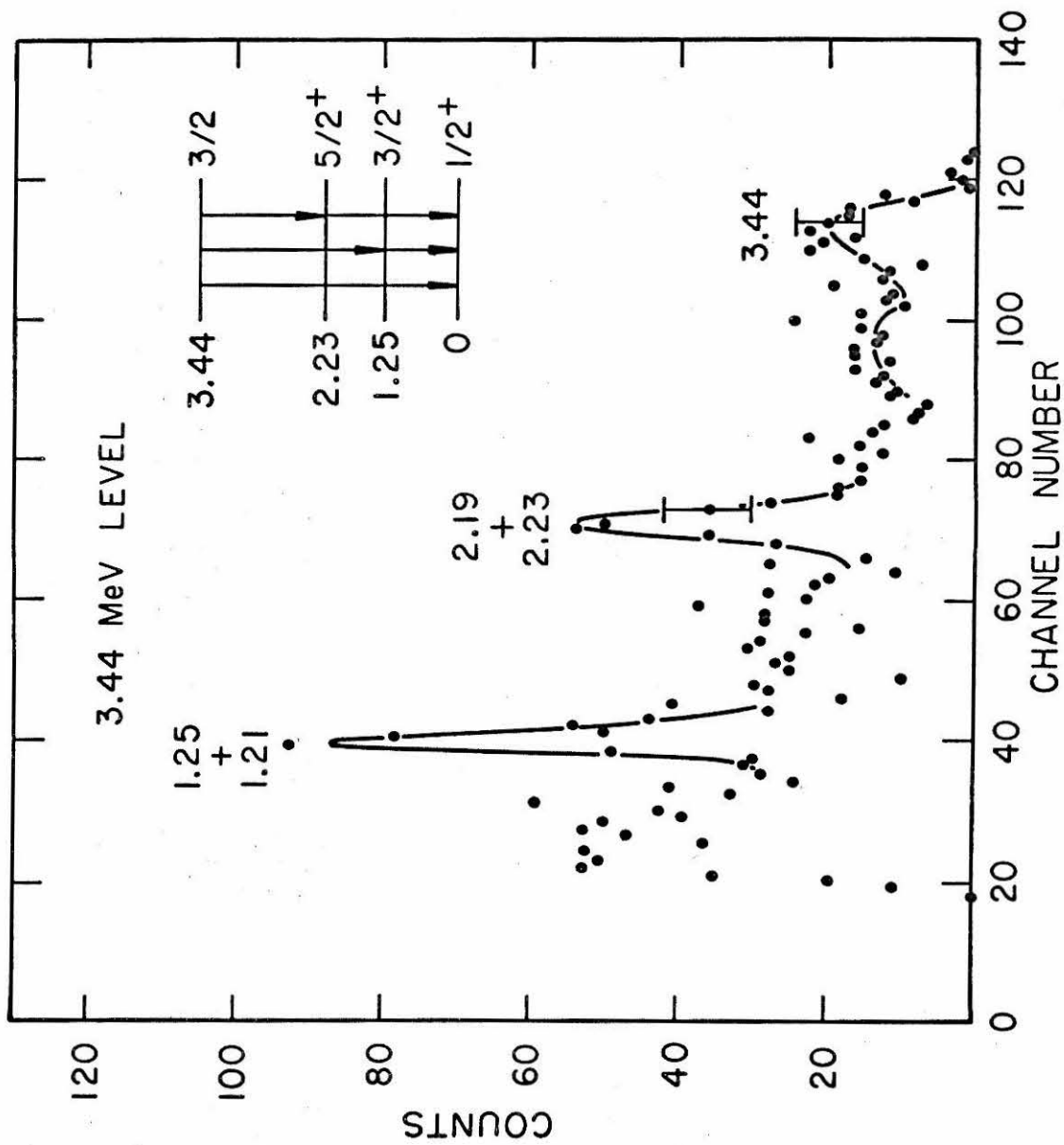
3.08 MeV LEVEL

3.08 ——————— 1/2⁺

0 ——————— 1/2⁺
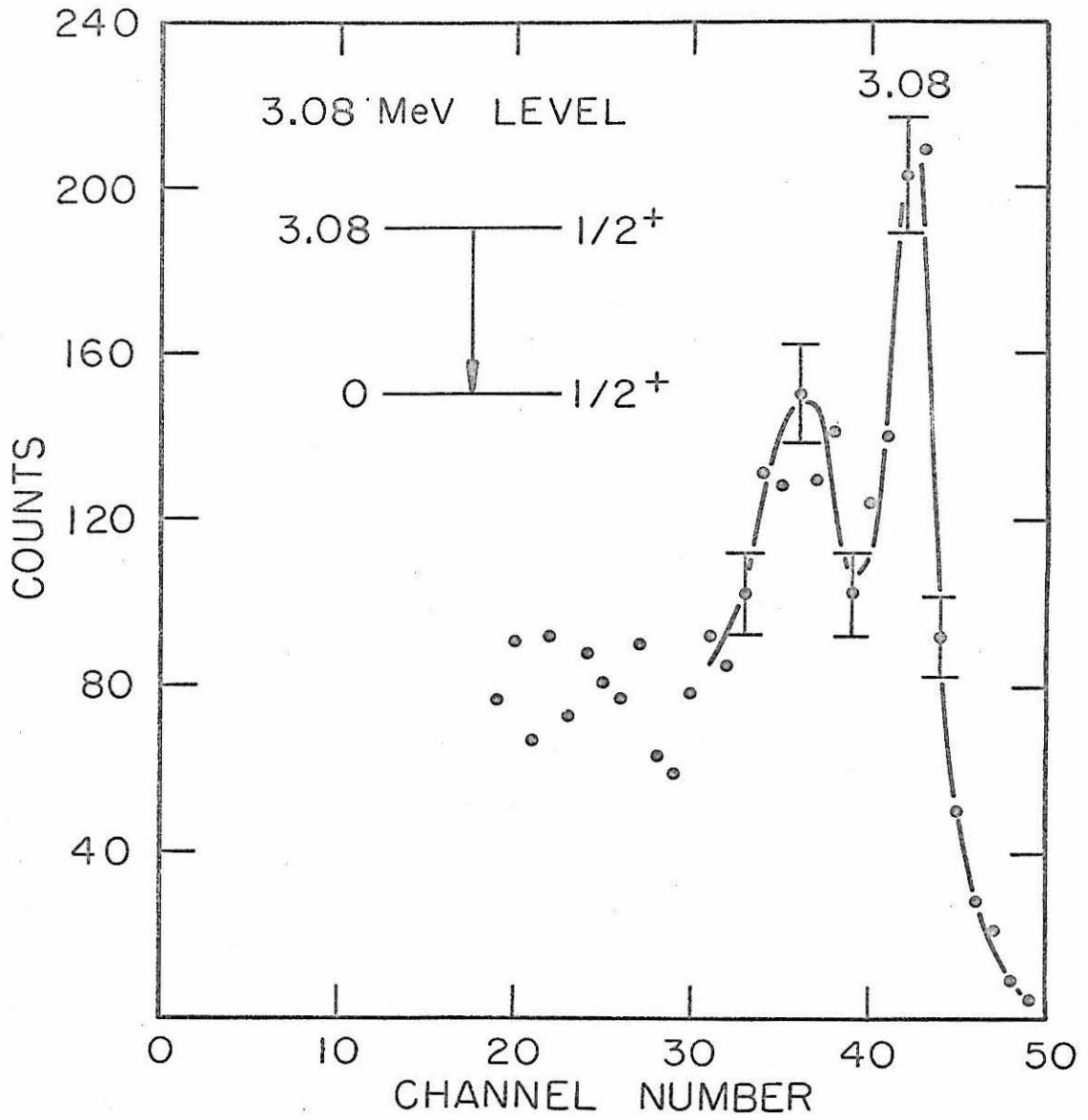
Figure 35

Angular Correlation of ^{31}S (3.08)

The angular correlation of the photopeak of the 3.08 MeV gamma rays detected in coincidence with the alpha particles at 0° corresponding to ^{31}S (3.08) is shown. The number of counts has been normalized to the number of alpha particles detected. The error bars represent statistical uncertainties. The theoretical fit is shown. (See pages 42 and 49.)

$E_\gamma = 3.08$

3.08 ——— $1/2^+$

0 ——— $1/2^+$
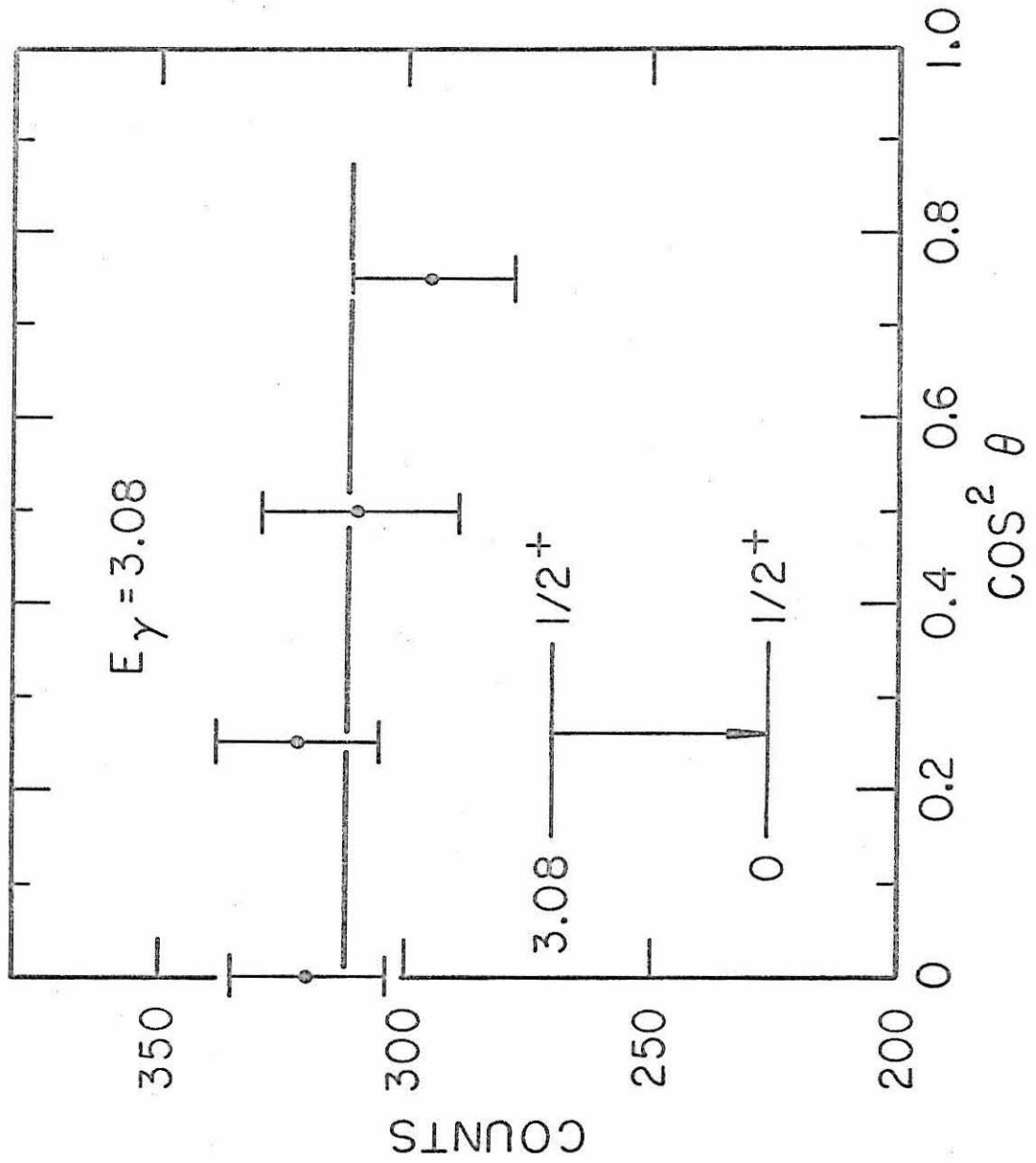
Figure 36

Gamma-Ray Spectrum from the Decay of ^{31}S (3.29)

The gamma-ray spectrum at $\theta_\gamma = 90^O$ from the decay of the level at 3.29 MeV excitation energy in ^{31}S is shown. The randoms spectrum multiplied by the ratio $\dfrac{\text{number of reals}}{\text{number of randoms}}$ has already been subtracted. The gamma-ray energy calibration was established with gamma-ray sources. (See page 42.)
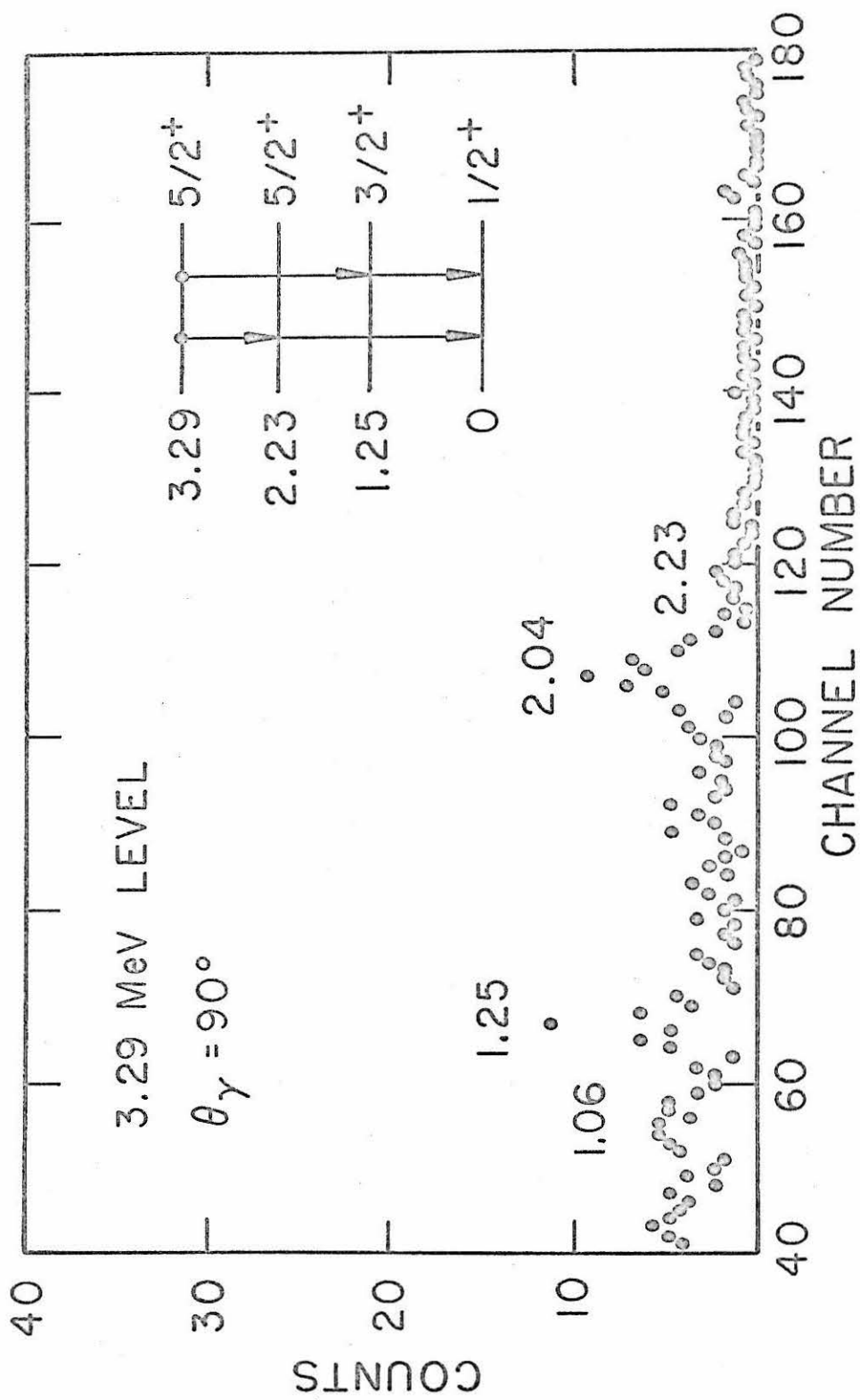
Figure 37

Angular Correlation of ^{31}S (3. 29)

The angular correlation of the photopeak of the 2. 04
MeV gamma rays detected in coincidence with the alpha
particles at 0° corresponding to ^{31}S (3. 29) is shown.   The
number of counts has been normalized to the number of
alpha particles detected.   The error bars represent the
statistical uncertainties.   The fits shown are for J = 5/2,
X = . 213, and J = 3/2, X = 1. 291.   (See pages 43 and 50.)
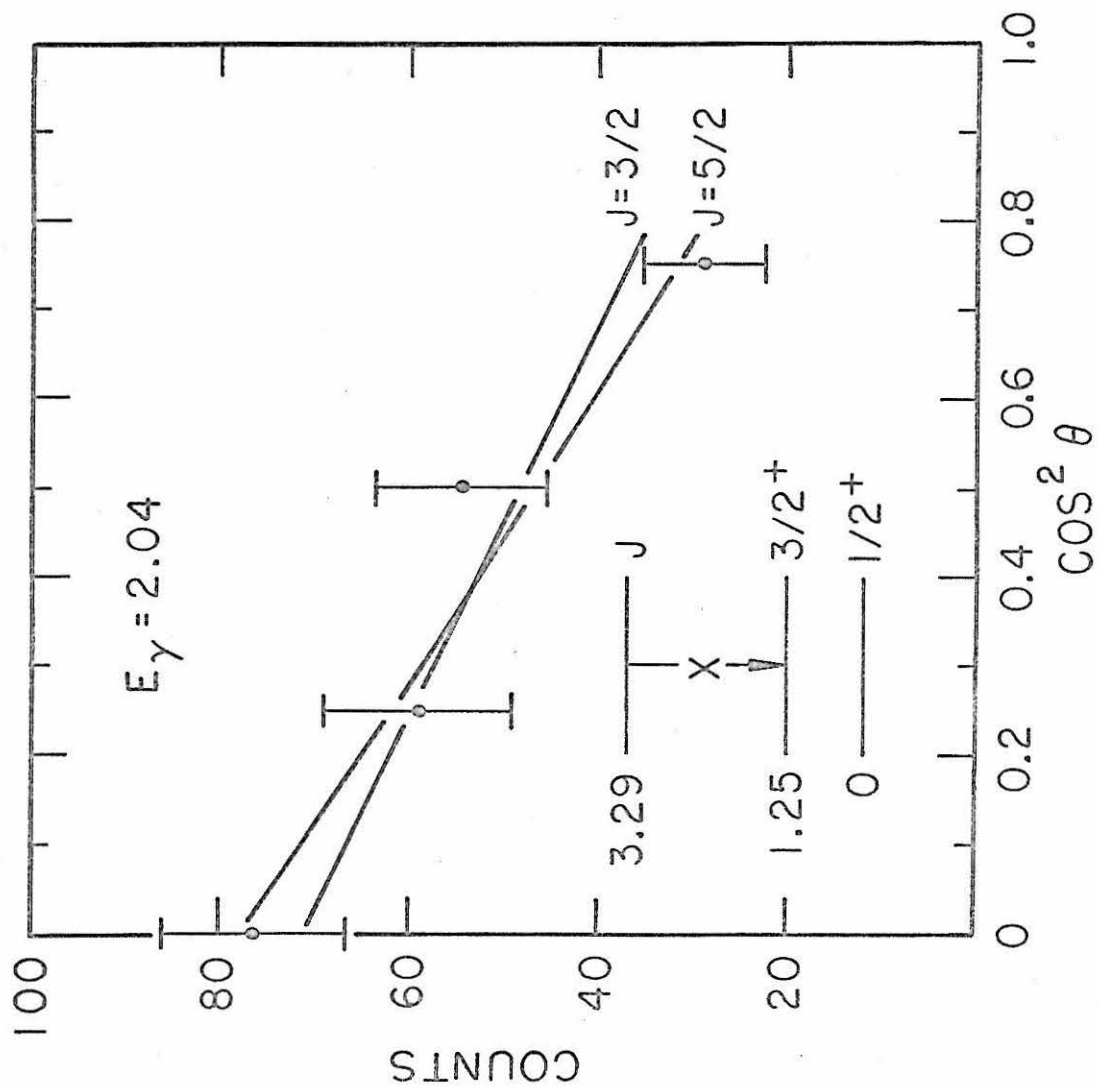
Figure 38

Gamma-Ray Spectrum from the Decay of ^{31}S (3.35)

The sum of the gamma-ray spectra obtained at $\theta_\gamma = 90^O$, 120°, 135°, and 150° from the decay of the level at 3.35 MeV excitation energy in ^{31}S is shown. The randoms spectra multiplied by the ratio $\frac{\text{number of reals}}{\text{number of randoms}}$ have already been subtracted. The gamma-ray energy calibration was established with gamma-ray sources. (See page 43.)

Figure 39

Angular Correlation of ^{31}S (3.35)

The angular correlation of the photopeak of the 2.10 MeV gamma rays detected in coincidence with the alpha particle at 0° corresponding to ^{31}S (3.35) is shown. The number of counts has been normalized to the number of alpha particles detected. The error bars represent the statistical uncertainties. The fits shown are for J = 7/2, X = -.467, and J = 3/2, X = -.775. (See pages 43 and 52.)

254
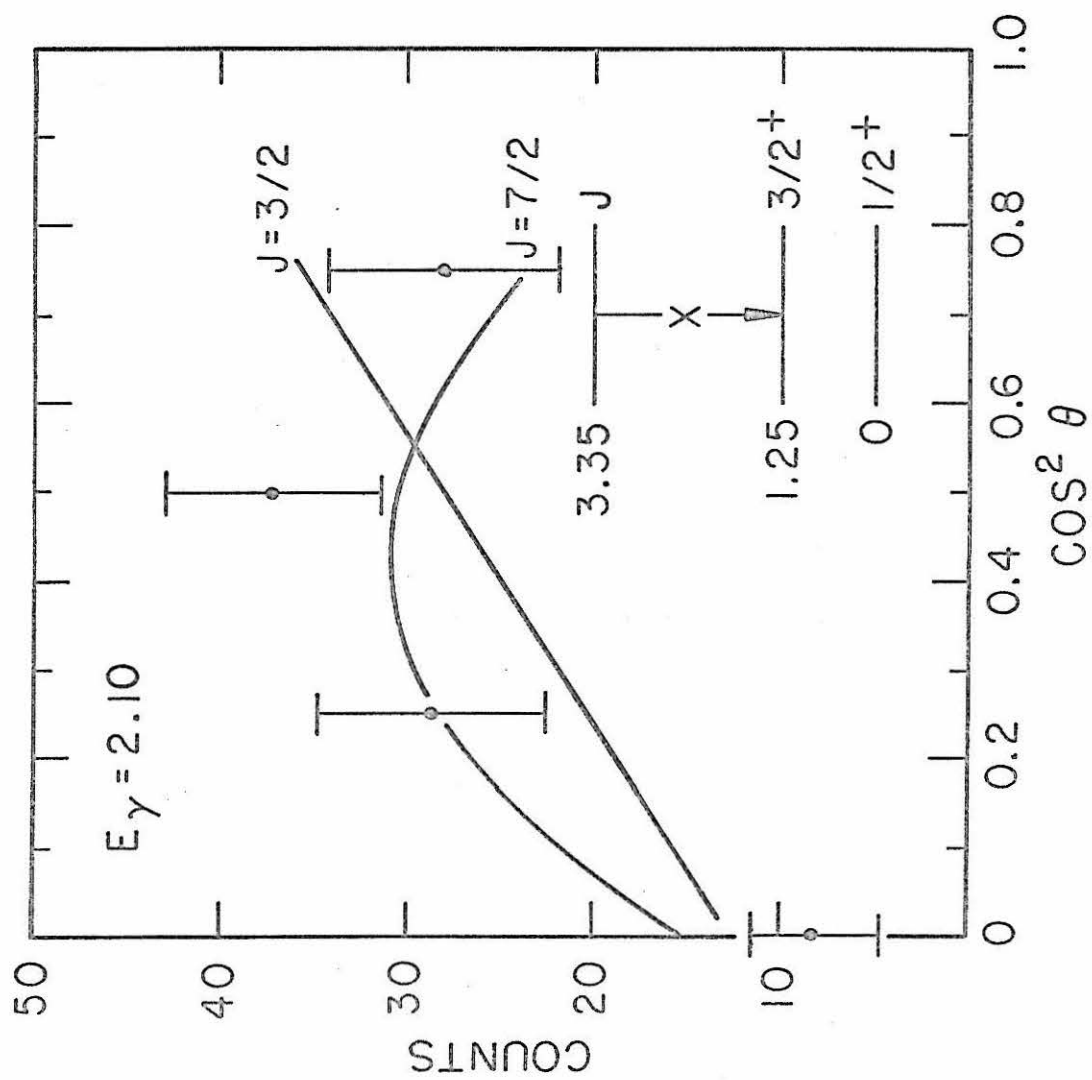
Figure 40

Gamma-Ray Spectrum from the Decay of ^{31}S (3.44)

The sum of the gamma-ray spectra obtained at $\theta_\gamma = 90^O$, 120°, 135°, and 150° from the decay of the level at 3.44 MeV excitation energy in ^{31}S is shown. The randoms spectra multiplied by the ratio $\dfrac{\text{number of reals}}{\text{number of randoms}}$ have already been subtracted. The gamma-ray energy calibration was established with gamma-ray sources. (See page 44.)

256

Figure 41

Angular Correlation of ^{31}S (3.44)

The angular correlation of the photopeak of the 3.44 MeV gamma rays detected in coincidence with the alpha particles at 0° corresponding to ^{31}S (3.44) is shown. The number of counts has been normalized to the number of alpha particles detected. The error bars represent the statistical uncertainties. The fits is for X = 0.577. (See pages 41 and 53.)
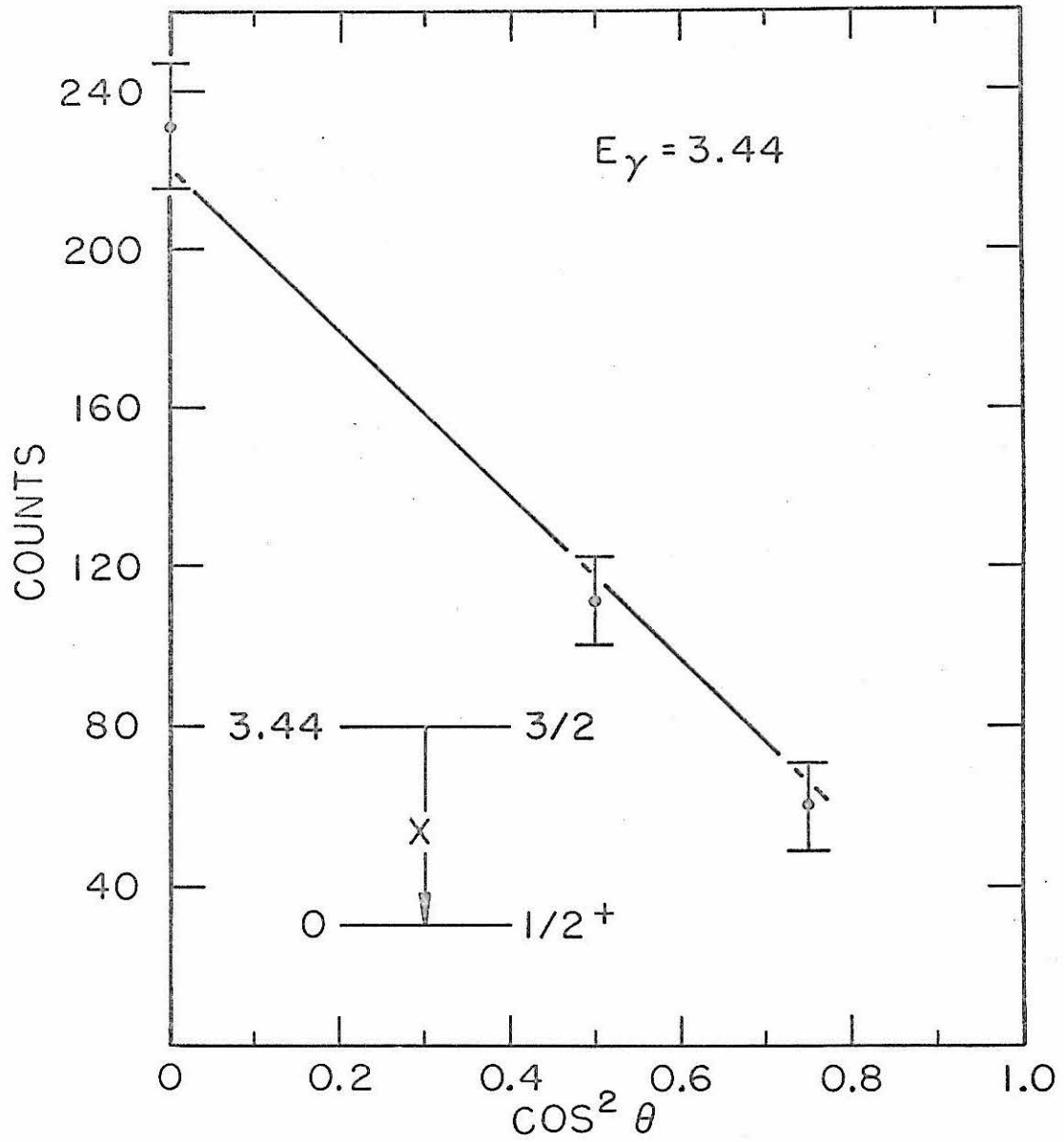
Figure 42

Notation for the Calculation of Q_k

The notation for the calculation of the attenuation factors Q_k is shown. (See page 45.)
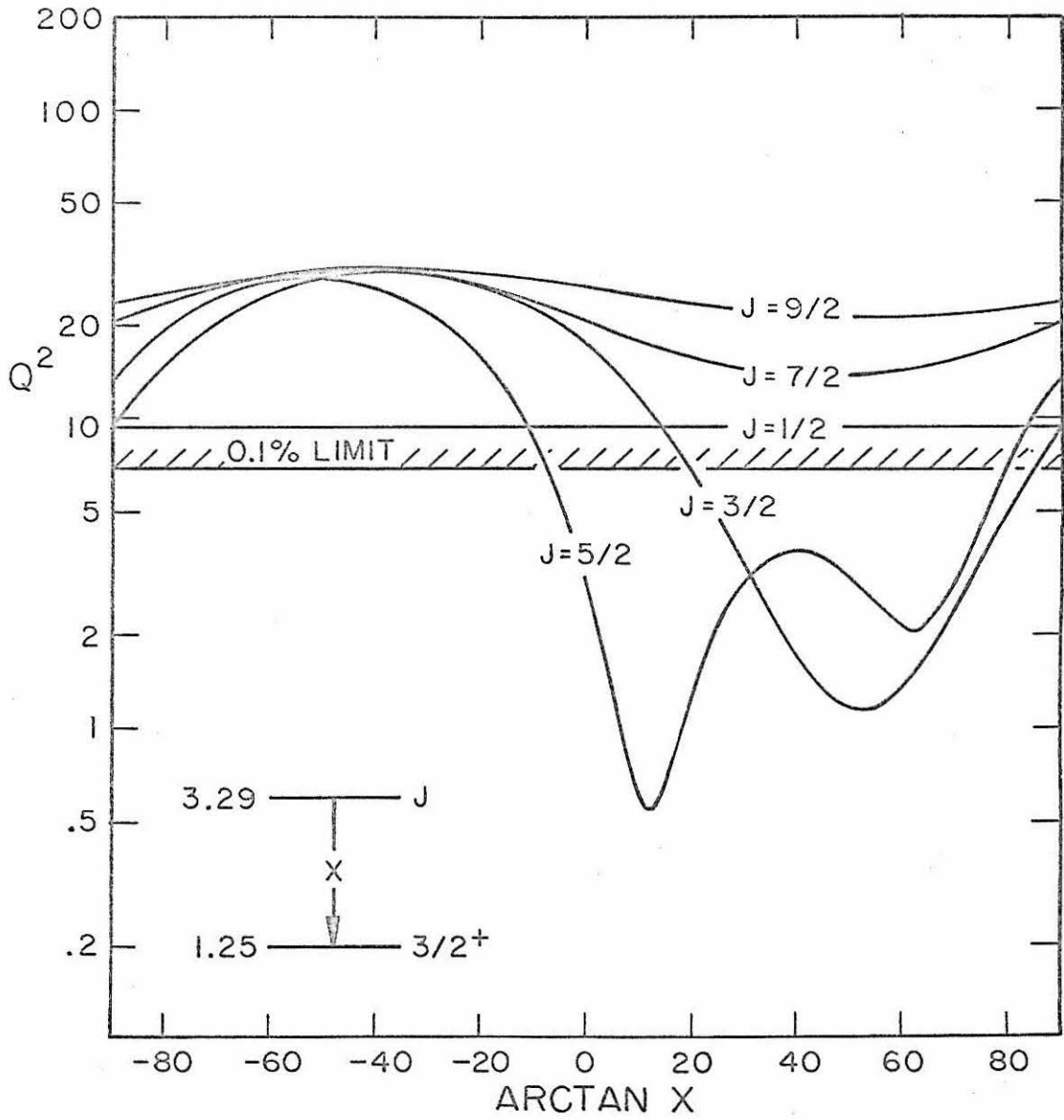
RADIUS R
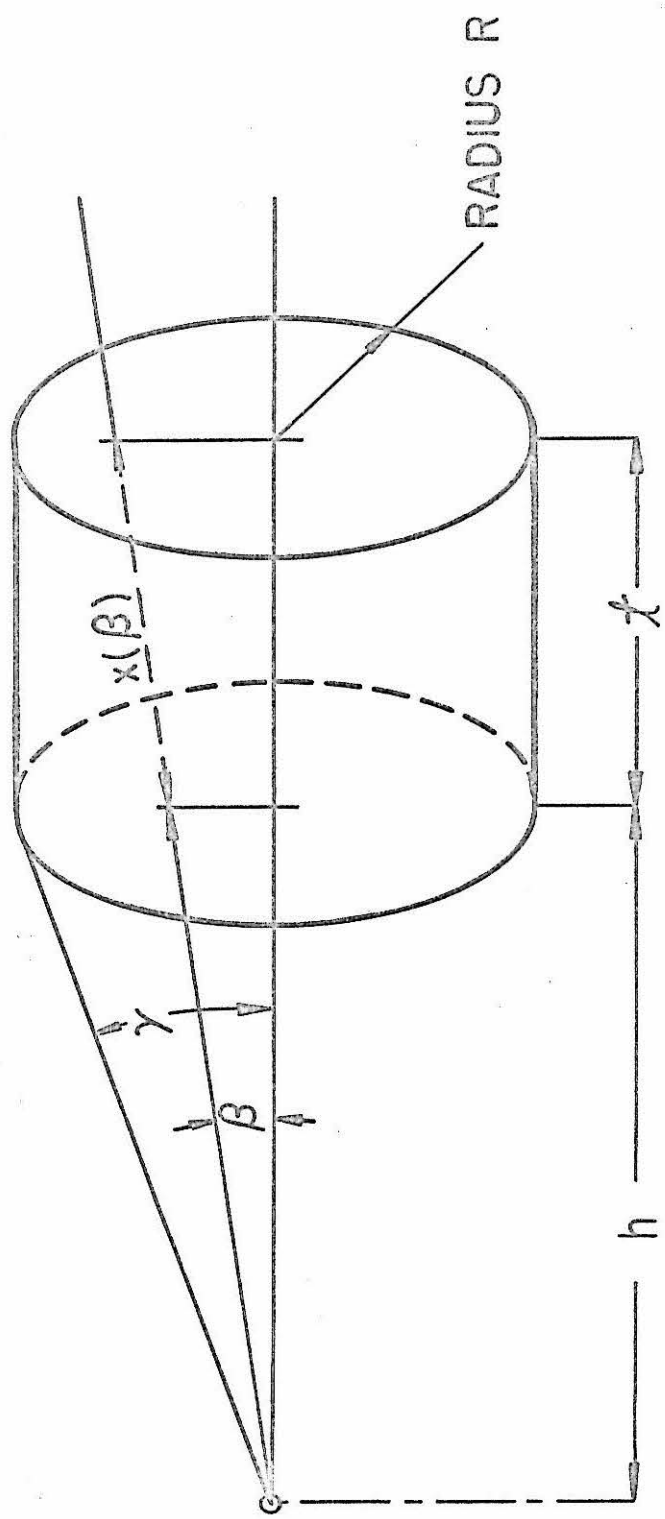
Figure 43

Q^2 Versus Arctan X for ^{31}S (1.25)

Plots of the minimum of Q^2 with respect to I(1/2) versus arctan X for various values of J for the transition ^{31}S (1.25) → ^{31}S (G.S.) are shown. For these plots, $\sigma = 0$ in Formula 4, Section III.B. The 0.1 percent confidence limit is shown, and all points on the curves which lie below this limit are assumed to be possible solutions. Only J = 3/2 gives a fit. (See page 47.)
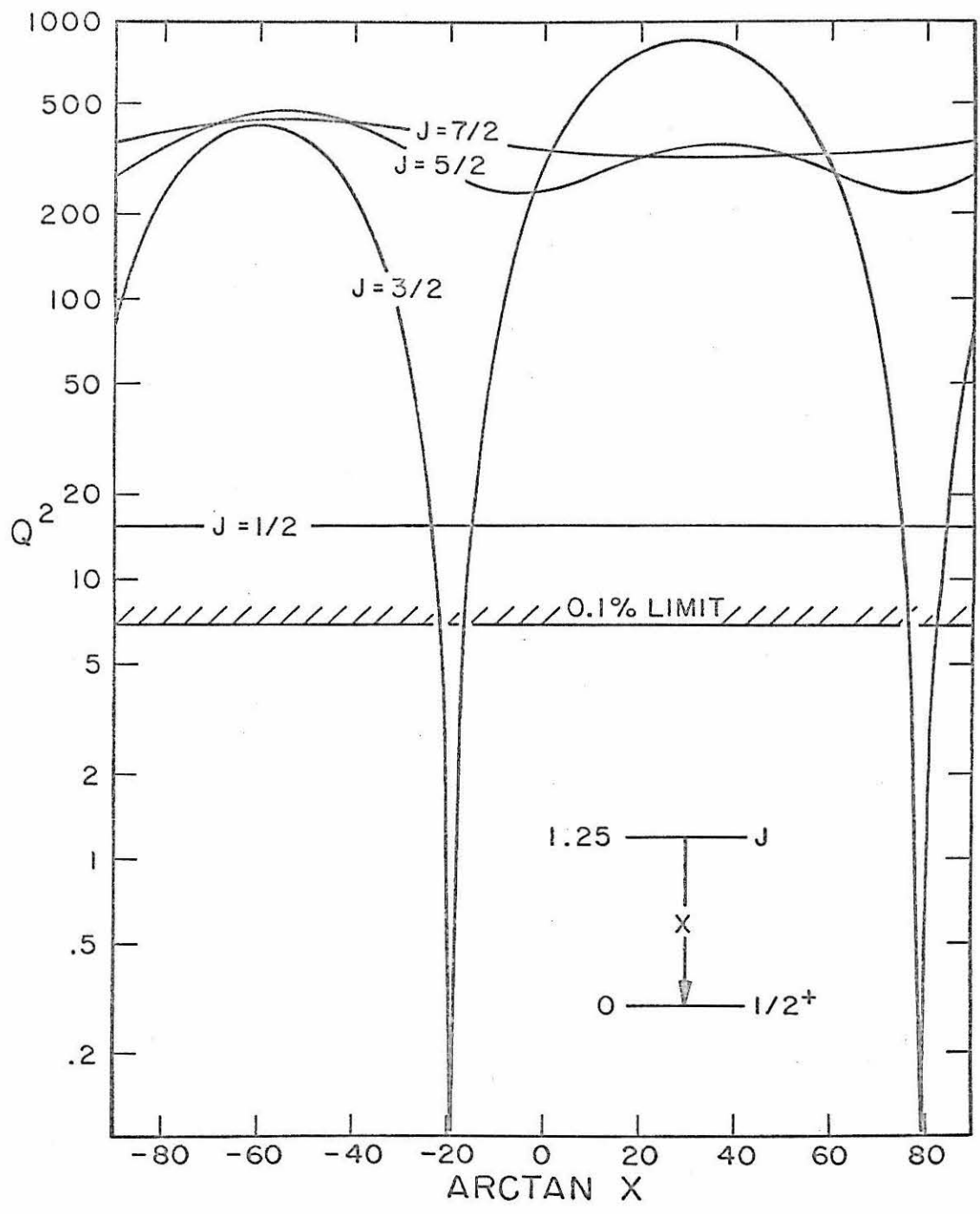
Figure 44

Q^2 Versus Arctan X for ^{31}S (2.23)

Plots of the minimum of Q^2 with respect to $I(1/2)$ versus arctan X for various values of J for the transition ^{31}S (2.23) → ^{31}S (G.S.) are shown. For these plots, $\sigma = 0$ in Formula 4, Section III. B. The 0.1 percent confidence limit is shown, and all points on the curves which lie below this limit are assumed to be possible solutions. Only J = 5/2 gives a fit. (See page 48.)
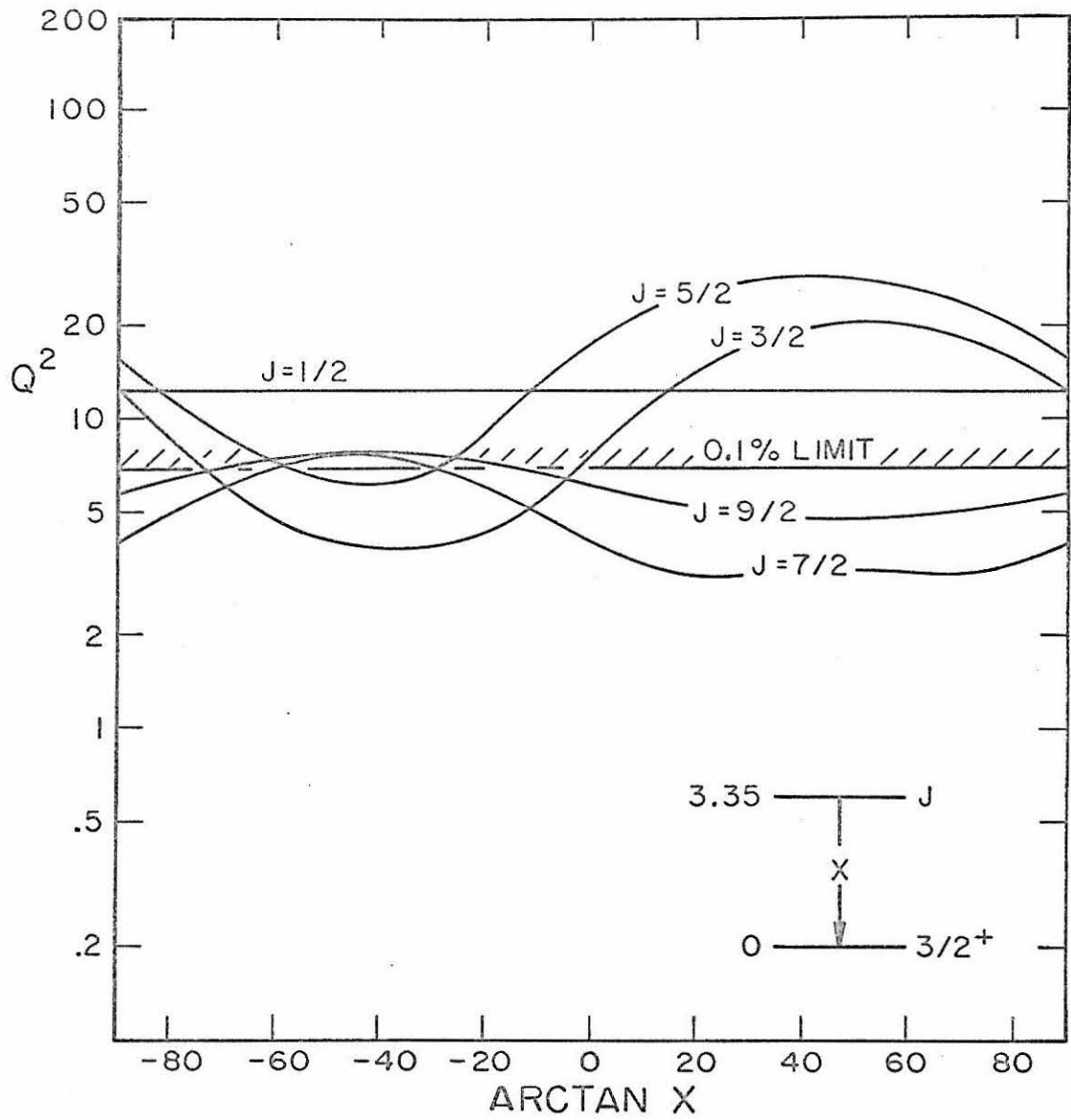
264
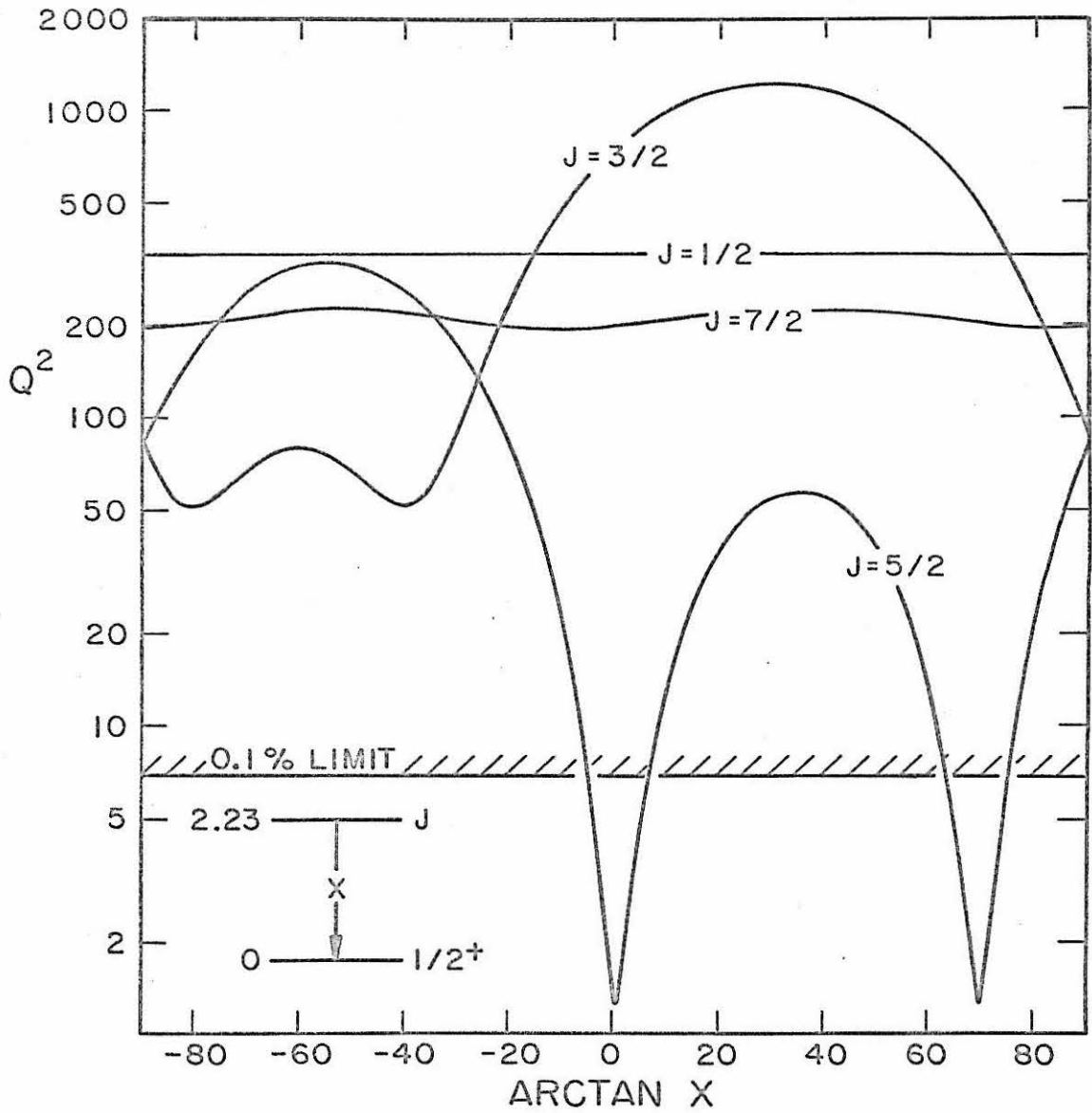
Figure 45

Q^2 Versus Arctan X for ^{31}S (3.08)

Plots of the minimum of Q^2 with respect to $I(1/2)$ versus arctan X for various values of J for the transition ^{31}S (3.08 → ^{31}S (G.S.) are shown. For these plots, $\sigma = 0$ in Formula 4, Section III. B. The 0.1 percent confidence limit is shown, and all points on the curves which lie below this limit are assumed to be possible solutions. Both J = 1/2 and 3/2 gives fits, but only J = 1/2 is allowed because $\ell_n = 0$.
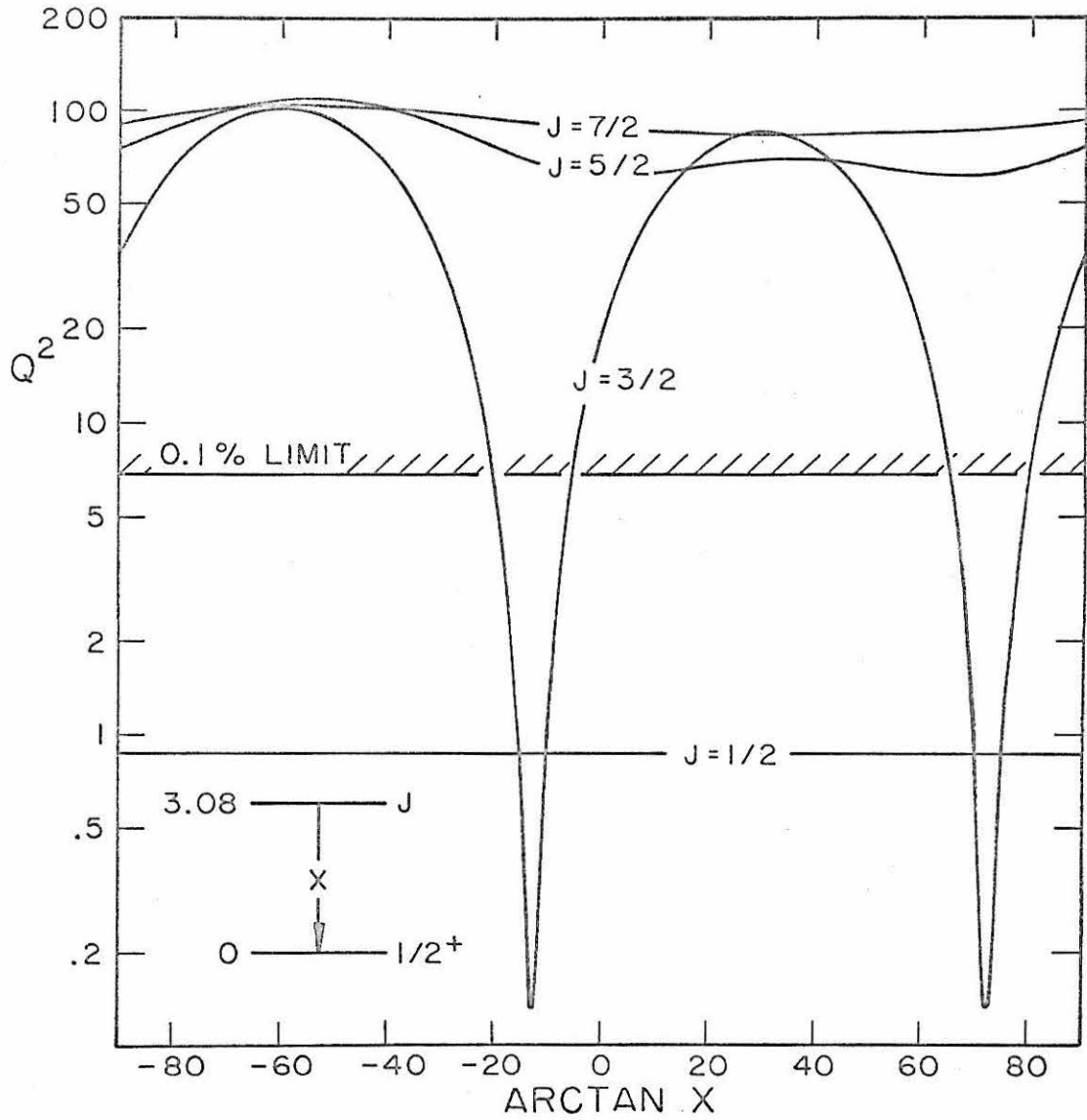
Figure 46

Q^2 Versus Arctan X for ^{31}S (3.29)

Plots of the minimum of Q^2 with respect to $I(1/2)$ versus arctan X for various values of J for the transition ^{31}S (3.29) → ^{31}S (1.25) are shown. For these plots, $\sigma = 0$ in Formula 4, Section III. B. The 0.1 percent confidence limit is shown, and all points on the curves which lie below this limit are assumed to be possible solutions. Both J = 5/2 and 3/2 give fits, but J = 5/2 is favored. (See page 50.)

Figure 47

Q^2 Versus Arctan X for ^{31}S (3.35)

Plots of the minimum of Q^2 with respect to $I(1/2)$ versus arctan X for various values of J for the transition ^{31}S (3.35) → ^{31}S (1.25) are shown. For these plots, $\sigma = 0$ in Formula 4, Section III. B. The 0.1 percent confidence limits are shown, and all points on the curves which lie below this limit are assumed to be possible solutions. In the order of preference, fits were obtained for J = 7/2, 3/2, 9/2, and 5/2. There is only a 1 percent probability that J_d = 9/2 is a fit and only a 0.3 percent probability that J_d = 5/2 is a fit. (See page 52.)

Figure 48

Q^2 Versus Arctan X for ^{31}S (3.44)

Plots of the minimum of Q^2 with respect to I(1/2) versus arctan X for various values of J for the transition ^{31}S (3.44) → ^{31}S (G.S.) are shown. For these plots, σ = 0 in Formula 4, Section III.B. The 0.1 percent confidence limit is shown, and all points on the curves which lie below this limit are assumed to be possible solutions. Only J = 3/2 gives a fit. (See page 53.)

272
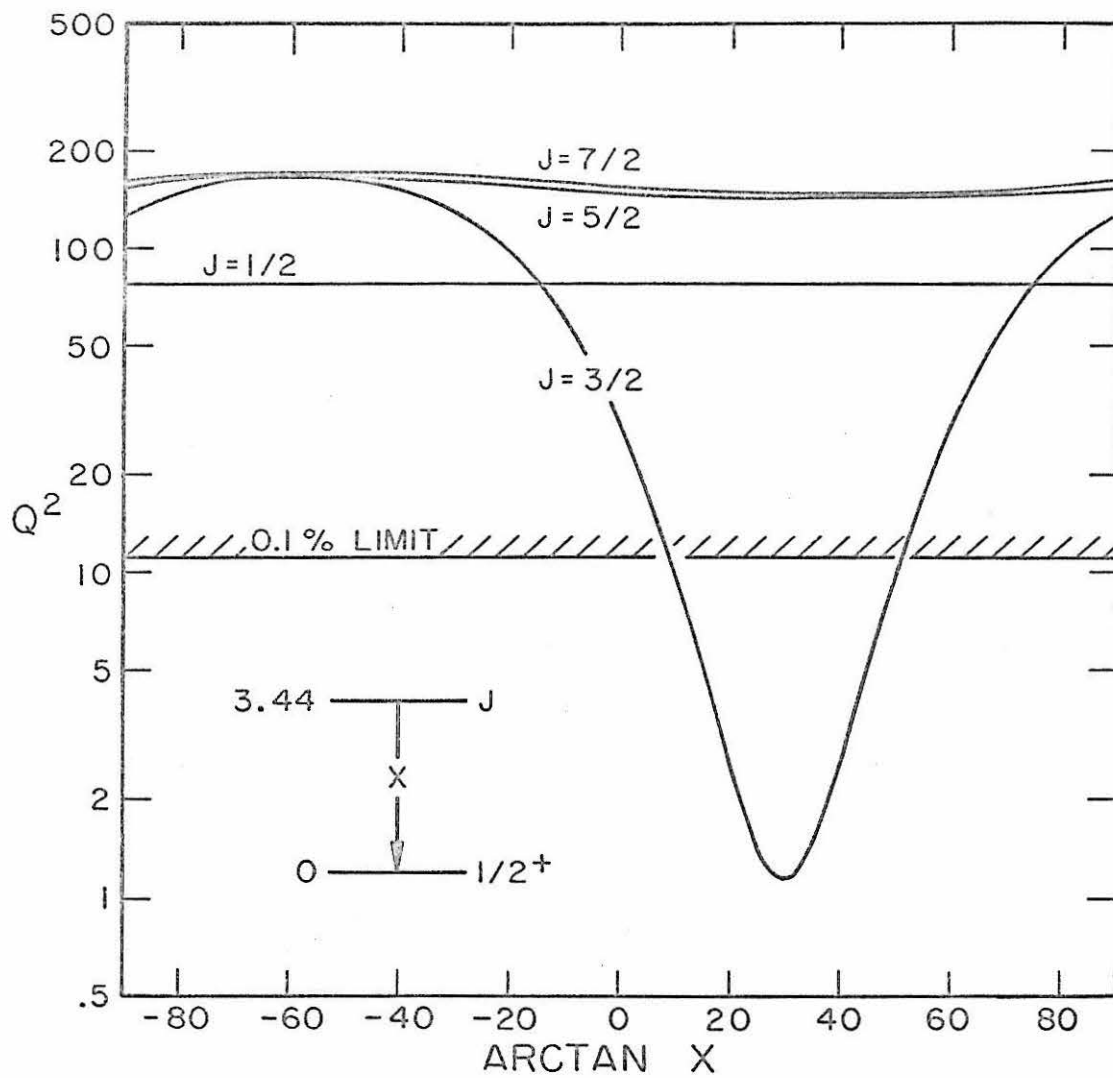
Figure 49

Schematic Diagram of Setup for Branching Ratio Measurements

A schematic diagram of the setup used for the branching ratio measurements in ^{31}S is shown. The front face of the 10.16 cm × 10.16 cm NaI(Tl) crystal was 3.556 cm from the center of the beam spot.
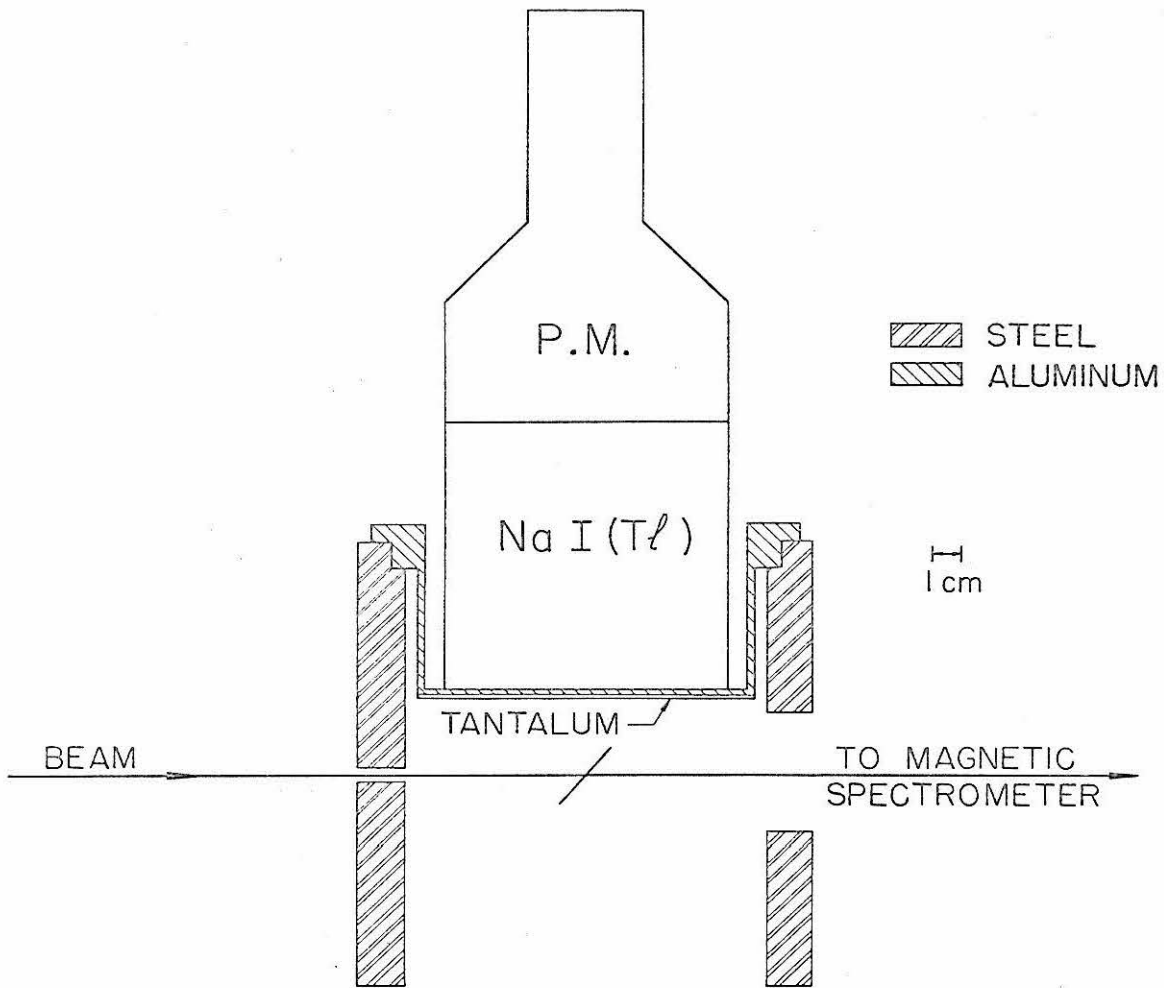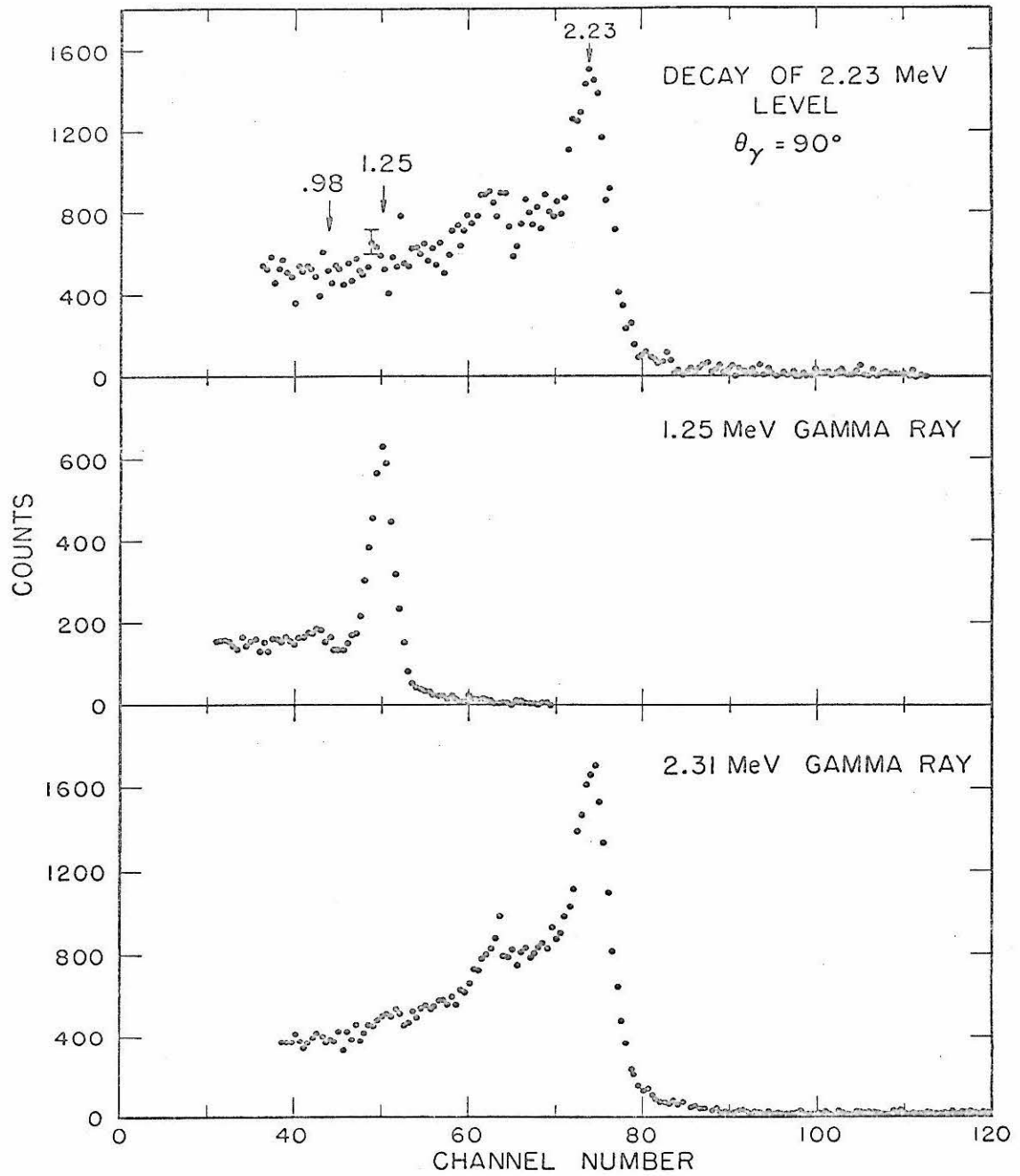
Figure 50

(a) Gamma-ray Decay Spectrum of the 2.23 MeV Level in ^{31}S

The gamma-ray decay spectrum taken with the aluminum cup (Figure 49) of the level at 2.23 MeV excitation energy in ^{31}S is shown. The positions of the 0.99 and 1.25 MeV gamma rays which would be emitted in a cascade through the 1.25 MeV level are indicated by arrows.

(b) 1.25 MeV Gamma-ray Line Shape

A line shape for a 1.25 MeV gamma ray obtained by observing the decay of ^{31}S (1.25) with the setup in Figure 49 is shown.

(c) 2.31 MeV Gamma-ray Line Shape

A line shape for a 2.31 MeV gamma ray obtained by observing the decay of ^{14}N (2.31) after formation by the reaction ^{12}C(^{3}He, p)^{14}N is shown. Again the setup in Figure 49 was used. This line shape was used as an approximation to the line shape of a 2.23 MeV gamma ray. (See page 54.)

Figure 51

Gamma-ray Decay Spectrum of the 3.35 MeV Level in ^{31}S

     The gamma-ray decay spectrum taken with the aluminum cup (Figure 49) of the level at 3.35 MeV excitation energy in ^{31}S is shown. (See page 60.)
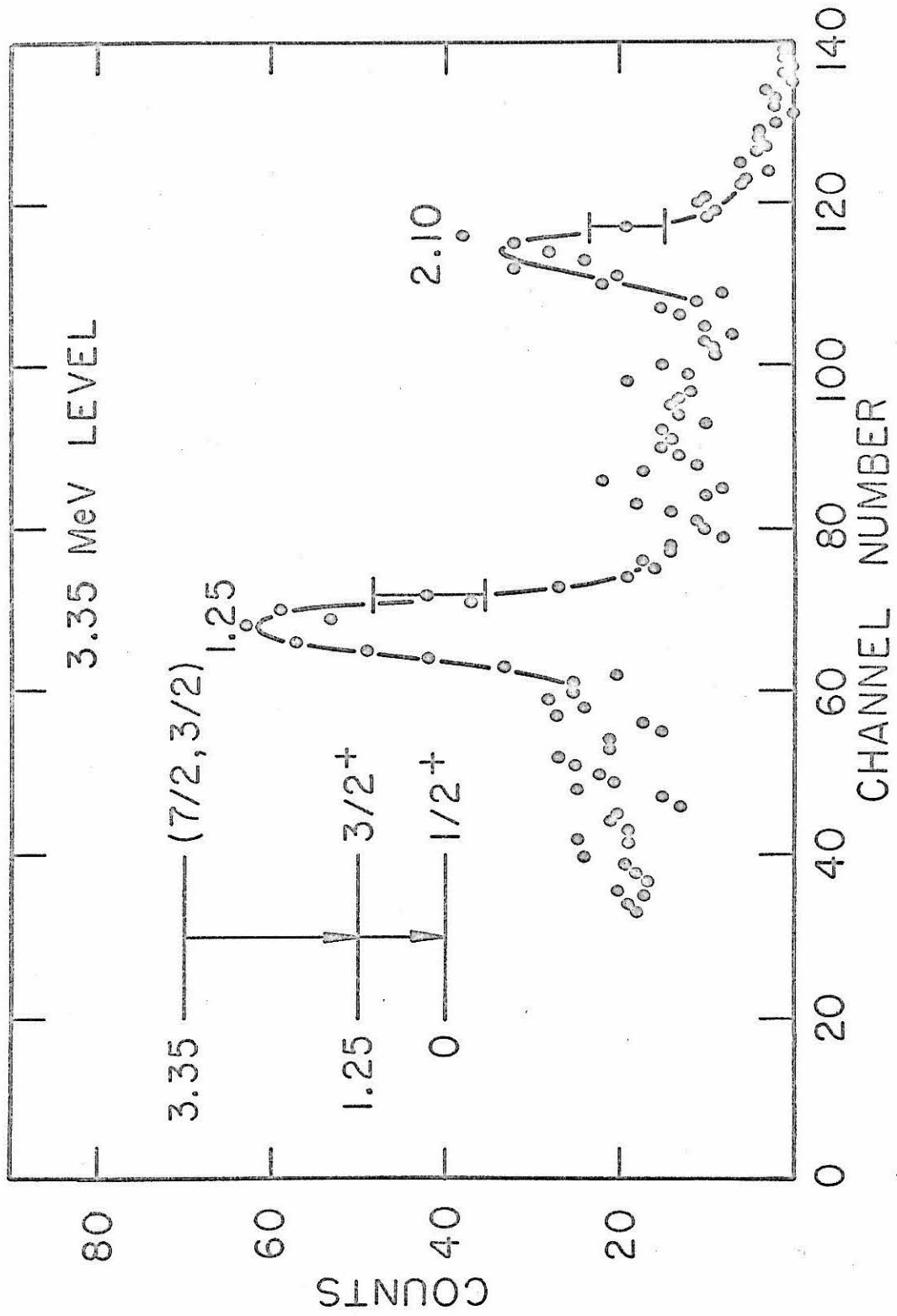
Figure 52

Energy Level Diagrams for ^{31}P and ^{31}S

The energy level diagrams for ^{31}P and ^{31}S are shown. The information on ^{31}P published since the compilation by Endt and van der Leun (1962) comes mainly from studies of the reactions ^{30}Si(p, γ)^{31}P and ^{30}Si(d, n)^{31}P. All of the information on ^{31}S was determined in the present experiment except the ℓ_n-values for the levels at 1.25, 2.23, and 7.04 (see Section II. C. 6). (See page 61.)

7.93 7.89 7.77 3/2+,1/2+
3/2+

7.15 1/2+

7.287
^{30}Si + p
T = 3/2

6.61 (1/2−,3/2−)
6.46 6.38 1/2− 3/2+ T = 3/2
6.24 6.18 6.05
5.89 5.77 5.66
5.53
5.25 5.12 5.01 (1/2+) 3/2−
4.78 5/2,(7/2)
4.63 4.59 3/2 5/2+
4.43 7/2−
4.26 4.19 3/2+ 5/2+

3.51 3.41 3/2+ 7/2+
3.29 5/2+
3.13 1/2+

2.23 5/2+

1.27 3/2+

$J^\pi = 1/2+$
β^+

^{31}P

7.73 ℓ_n

7.31 7.20 7.16
7.04 2

6.71 6.86 6.83 6.74
6.69 6.59 6.54
6.40 6.35 6.27
6.15 6.084
5.98 5.89 5.82 ^{30}P + p
5.78 5.68
5.44 5.41 5.52
5.30
5.15 1/2+ 0
5.03 4.97 1
4.87
4.72 (5/2+) (1)
4.58 2,(3)
4.52 4.45 2
3
4.21
4.08 (5/2+) (2)

3.44 3/2(+)
3.35 3.29 (3/2,7/2) 5/2+,(3/2)+ (2)
2
3.08 1/2+ 0

2.23 5/2+ 2

1.25 3/2+ 2

$J^\pi = 1/2+$ 0

^{31}S

15

5.538
^{32}S + ^{3}He − α

Figure 53

Decay Schemes for ^{31}P and ^{31}S

The gamma-ray decay schemes for the low-lying levels in ^{31}P and ^{31}S are shown. The decay schemes for ^{31}P is taken from references cited in the text. The decay scheme for ^{31}S was measured in the present experiment. (See pages 56 and 61.)
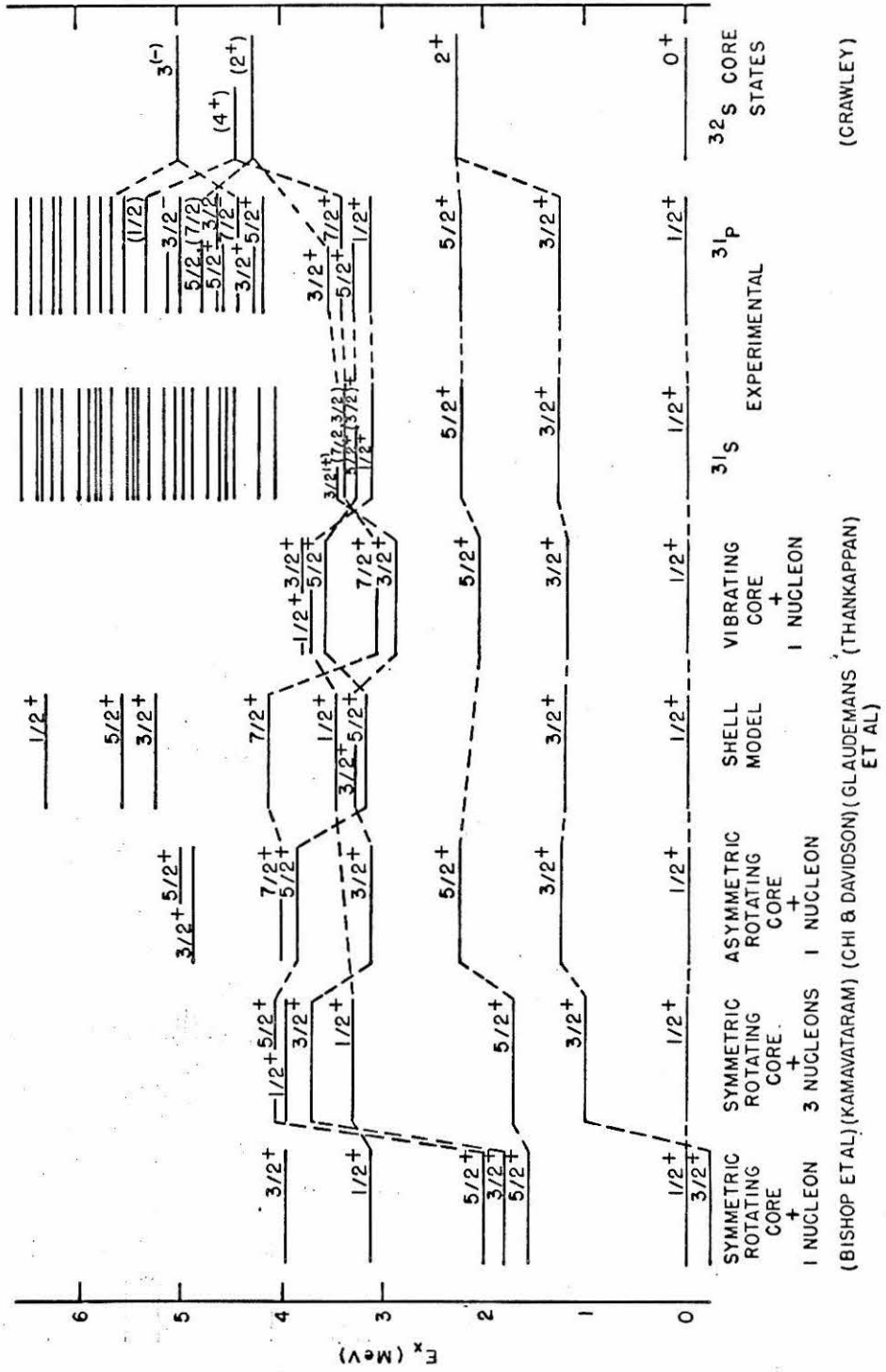
^{31}P

^{31}S
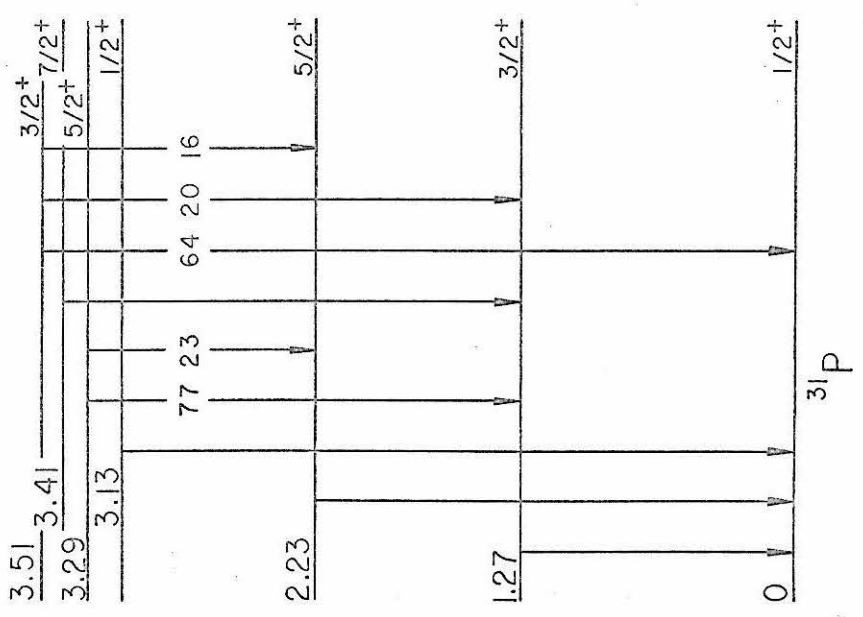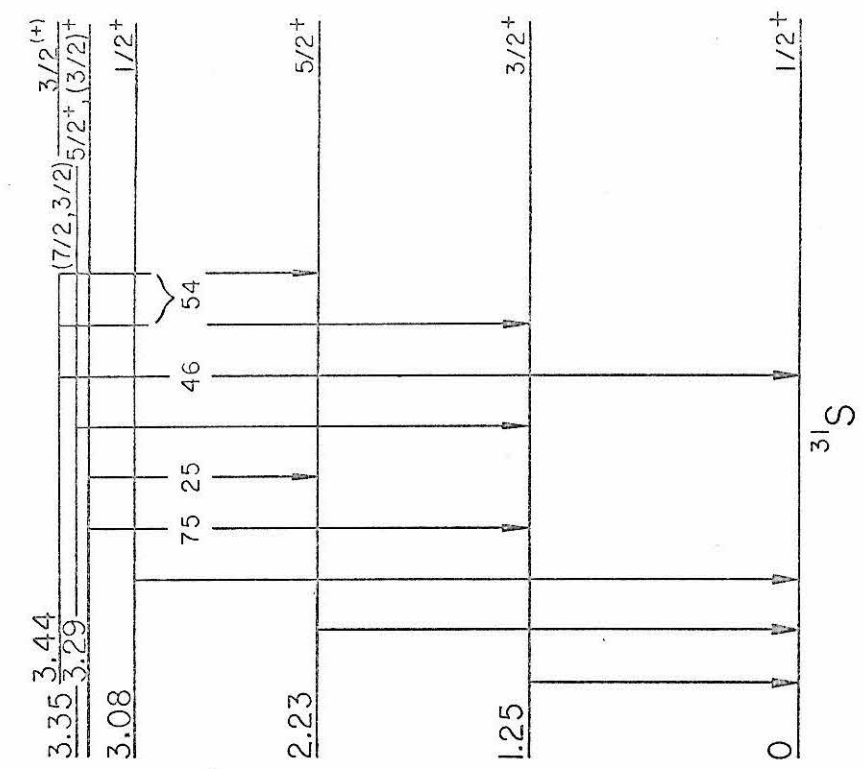
Figure 54

Models for A = 31

The predictions of several models for A = 31 are
compared with the experimental results. The models are
discussed in the text. (See page 63.)

Figure 55

16 Detector Array Spectra from the Reaction $^{32}S(^3He, d)^{33}Cl$
(This figure is in the rear pocket.)

a) A deuteron spectrum obtained at $\theta_{Lab} = 10^O$ from the bombardment of natural sulfur with 12.0 MeV $^3He^{++}$ particle is shown. Each point represents 150 µC of incident charge. The lower scale is the NMR magnetometer frequency for the magnetic spectrometer, and the upper scale is the corresponding deuteron energy. The levels are numbered as in Table XV.

b) A deuteron spectrum obtained at $\theta_{Lab} = 20^O$ from the bombardment of natural sulfur is shown. Each point above FREQUENCY = 33600 represents 150 µC of incident charge, and the scale on the right is to be used. Each point below FREQUENCY = 33600 represents 300 µC of incident charge, and the scale on the left is to be used.

c) A deuteron spectrum obtained at $\theta_{Lab} = 20^O$ from the bombardment of sulfur enriched to 98.1% ^{32}S (natural sulfur contains 95.0% ^{32}S) is shown. The scales are similar to those in b).

d) A deuteron spectrum obtained at $\theta_{Lab} = 45^O$ from the bombardment of natural sulfur is shown. Each point represents 300 µC of incident charge.

e) A deuteron spectrum obtained at $\theta_{Lab} = 45^O$ from the bombardment of sulfur enriched to 98.1% ^{32}S is shown. The scales are similar to those in d). (See page 71.)

Figure 56

Single Detector Spectra from the Reaction $^{32}S(^{3}He, d)^{33}Cl$

Deuteron spectra obtained at $\theta_{Lab} = 20^{O}$ in (a) and at $\theta_{Lab} = 45^{O}$ in (b) from the bombardment of natural sulfur with 12.0 MeV $^{3}He^{++}$ particles is shown. The lower scale is the NMR magnetometer frequency for the magnetic spectrometer and the upper scale is the corresponding deuteron energy. The levels are numbered as in Table XV. The gaps in the spectra correspond to regions of severe elastic scattering from the gold foil. (See page 75.)
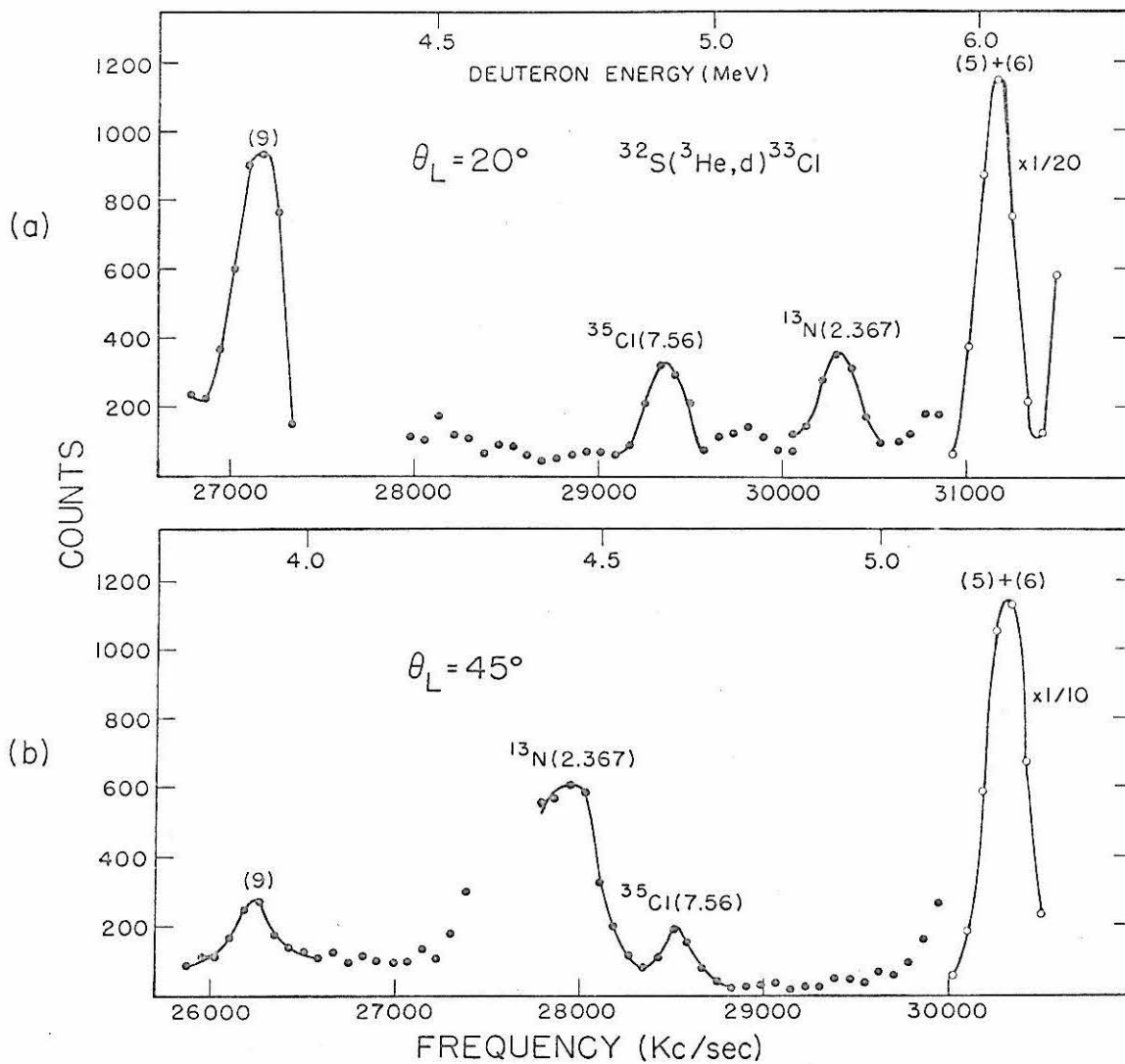
Figure 57

Angular Distribution for ^{33}Cl (G. S.)

The angular distribution of the deuterons from the reaction ^{32}S(^{3}He, d)^{33}Cl (G. S.) is shown. This distribution was obtained as a by-product of the angular distribution of the alpha particles from the reaction ^{32}S(^{3}He, α)^{31}S (G. S.) shown in Figure 13. The curve is a DWBA prediction. Level ^{33}Cl (G. S.) must have ℓ_p = 2 because for this level J^{π} = $3/2^+$. (See page 80.)
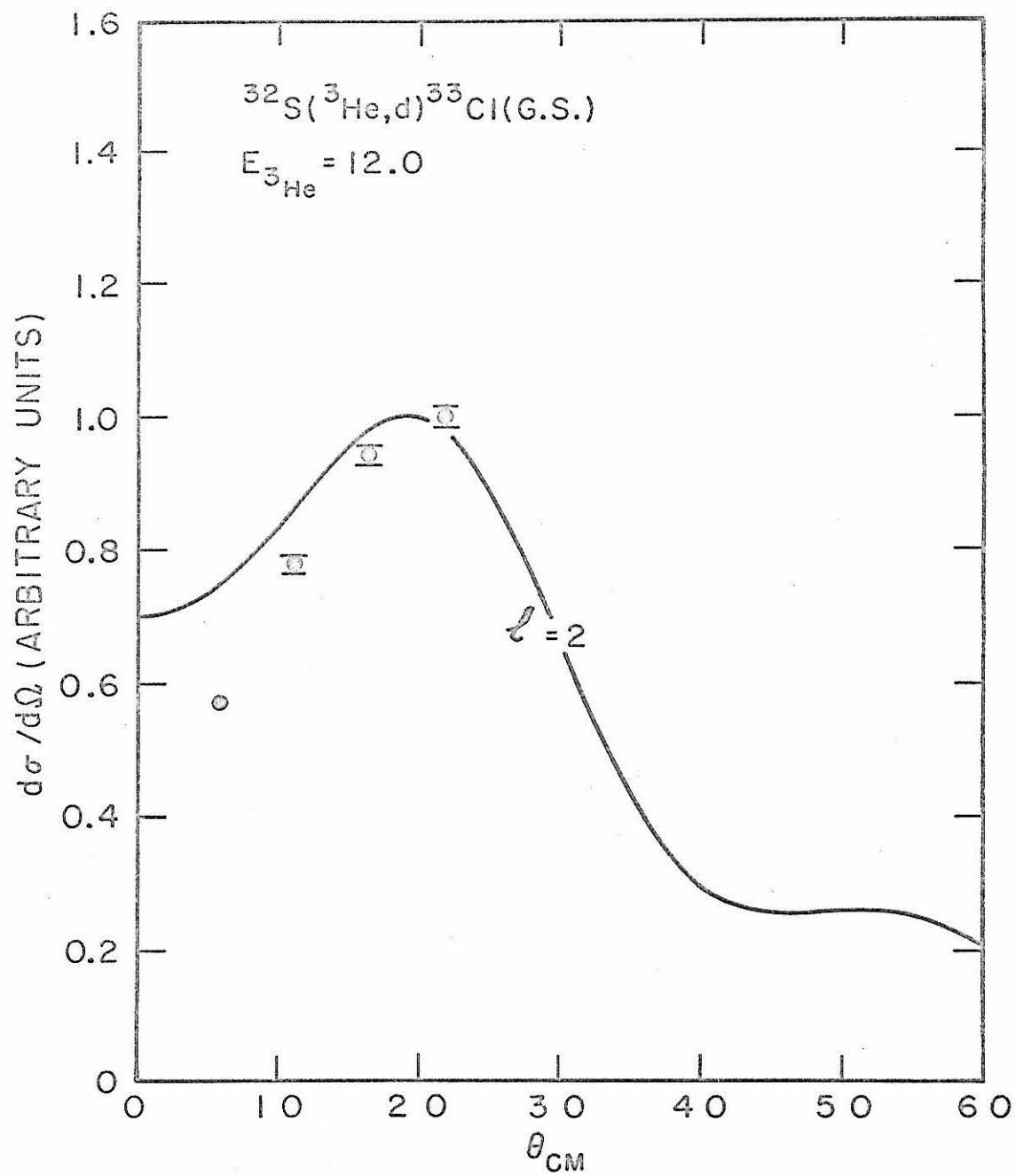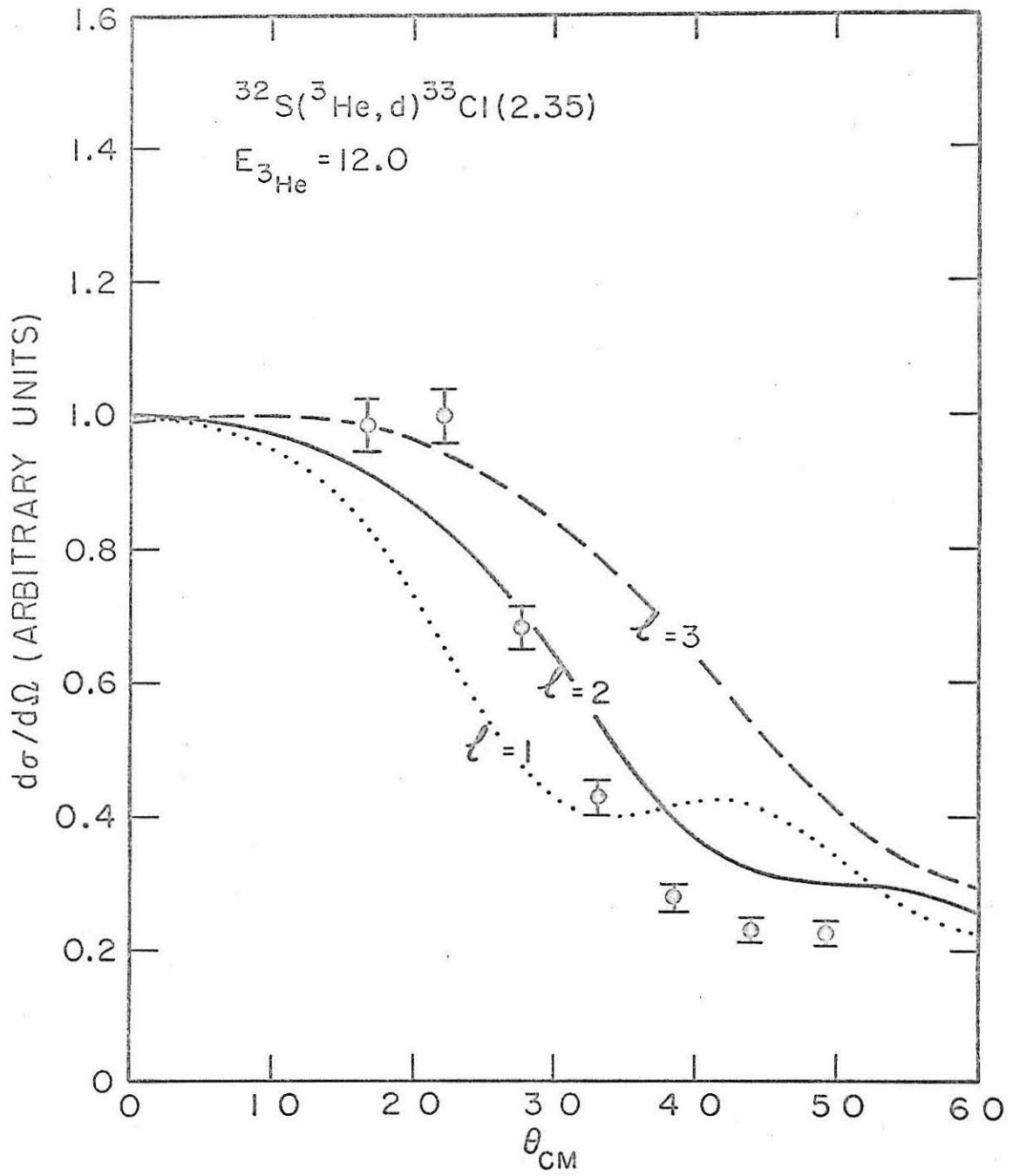
$^{32}S(^3He,d)^{33}Cl(G.S.)$

$E_{^3He} = 12.0$

$\ell = 2$

Figure 58

Angular Distribution for ^{33}Cl (2.35)

The angular distribution of the deuterons from the reaction ^{32}S(^{3}He, d)^{33}Cl (2.35) is shown. This distribution was obtained as a by-product of the angular distribution of the alpha particles from the reaction ^{32}S(^{3}He, α)^{31}S. The curves are DWBA predictions. Level ^{33}Cl (2.35) is assigned $\ell_p = (2)$. (See page 80.)

$^{32}S(^3He,d)^{33}Cl(2.35)$

$E_{3_{He}} = 12.0$

Figure 59

Angular Distribution for ^{33}Cl (2.69)

The angular distribution of the deuterons from the reaction ^{32}S(^{3}He, d)^{33}Cl (2.69) is shown. This distribution was obtained as a by-product of the angular distributions of the alpha particle from the reaction ^{32}S(^{3}He, α)^{31}S. The curves are DWBA predictions. The predictions for $\ell_p = 3$ agrees best with the experimental distribution, but no assignment is made. (See page 81.)
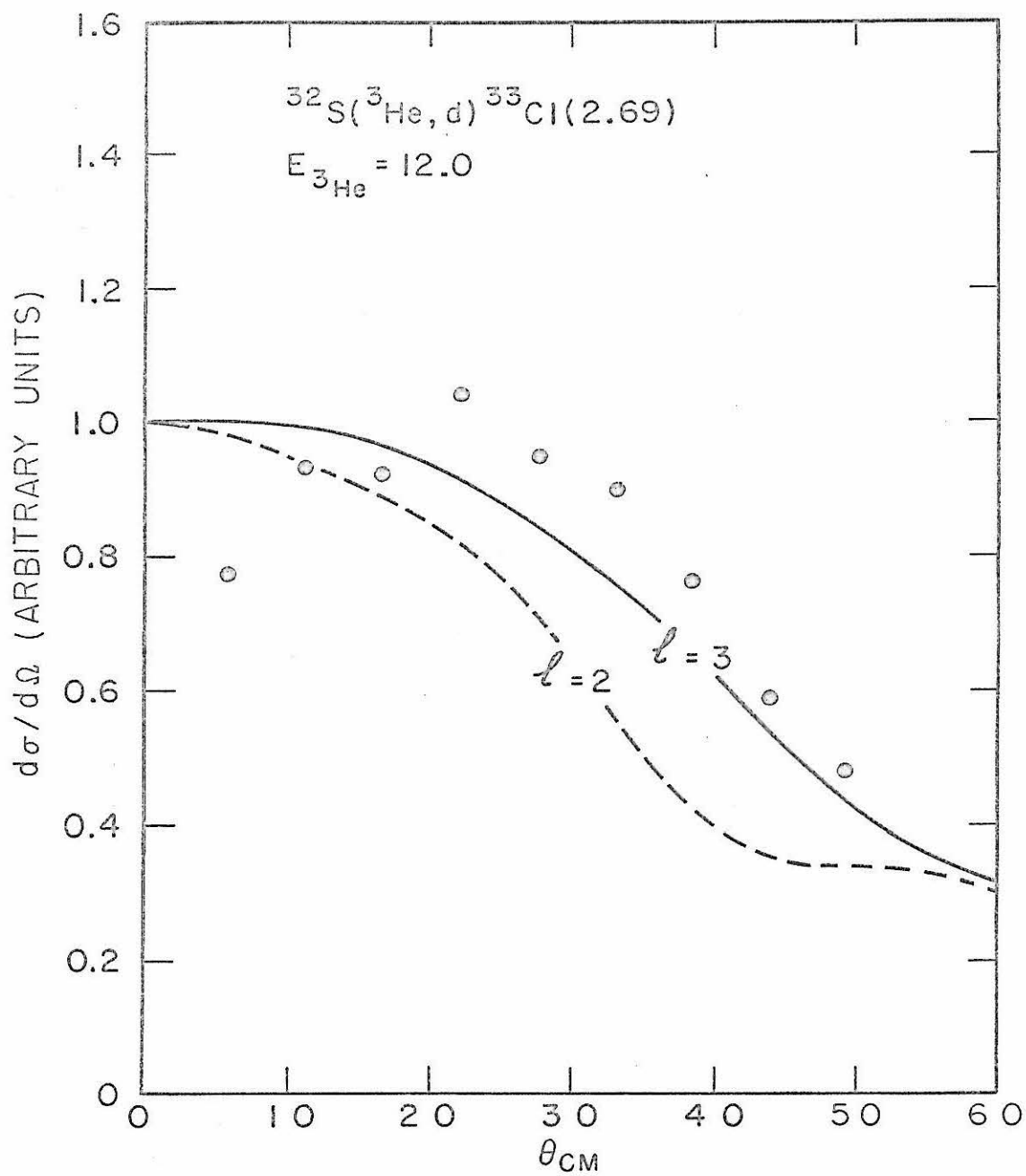
$^{32}S(^{3}He,d)^{33}Cl(2.69)$

$E_{3_{He}} = 12.0$

$\ell = 2$

$\ell = 3$

$d\sigma/d\Omega$ (ARBITRARY UNITS)

θ_{CM}

Figure 60

Gas Cell for the Reaction $^{36}Ar(p, \alpha)^{33}Cl$

The gas cell used in the magnetic spectrometer for the study of the reaction $^{36}Ar(p, \alpha)^{33}Cl$ is shown. Foil A was 5000 Å thick, and foil C was 10000 Å thick. Foil B and D were not used. (See page 82.)
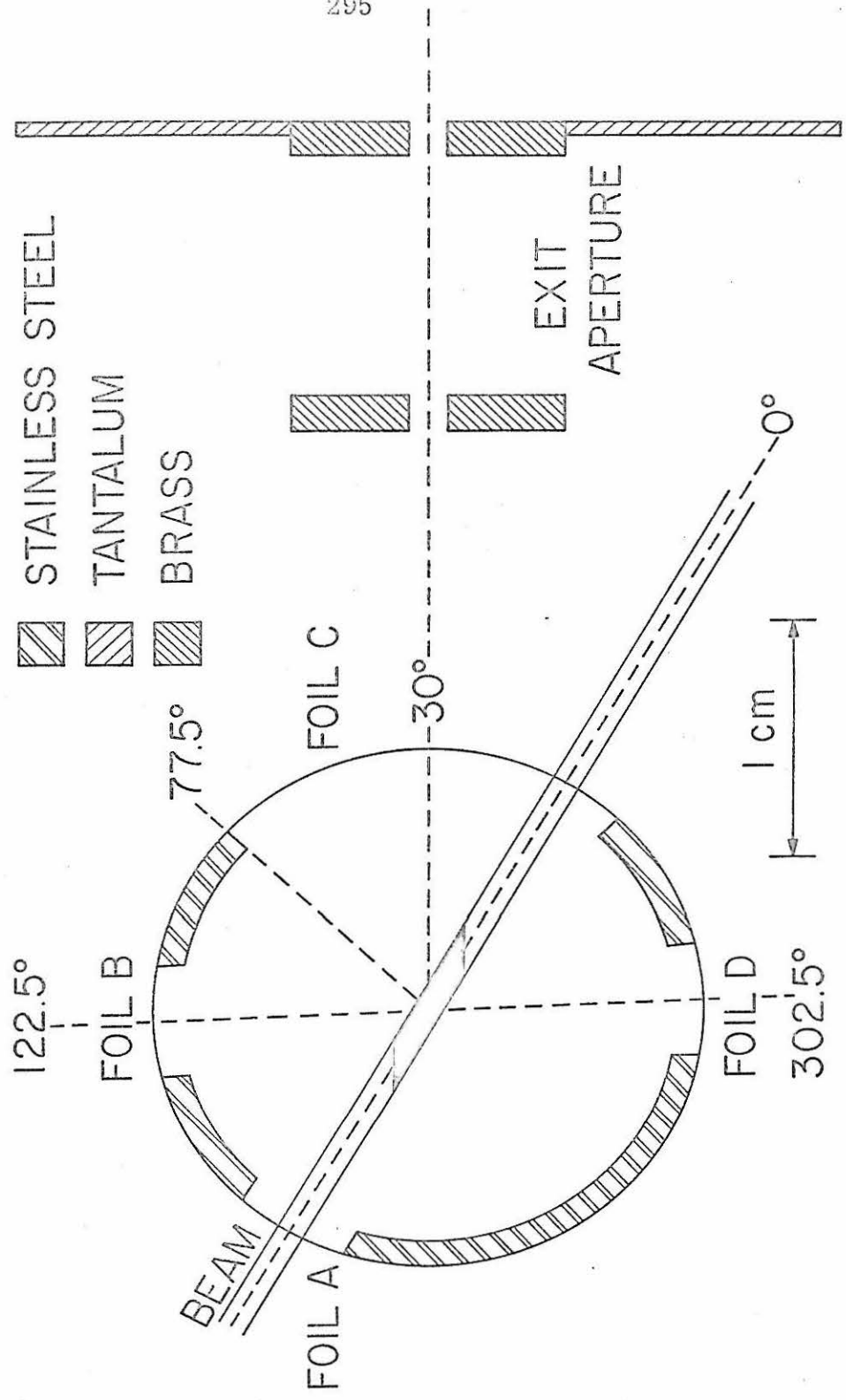
STAINLESS STEEL

TANTALUM

BRASS

FOIL C

77.5°

30°

122.5°

FOIL B

EXIT
APERTURE

0°

1 cm

FOIL D

302.5°

BEAM

FOIL A

Figure 61

16 Detector Array Spectra from the Reaction ^{36}Ar(p, α)^{33}Cl

The alpha particle spectra obtained at $\theta_{Lab} = 20^O$ in (a), 40° in (b), and 60° in (c) from the bombardment of ^{36}Ar with 12.0 MeV protons is shown. Each point presents 180 μC of incident charge. The lower scale is the NMR magnetometer frequency for the magnetic spectrometer and the upper scale is the corresponding alpha particle energy. The levels are numbered as in Table XV. (See page 85.)
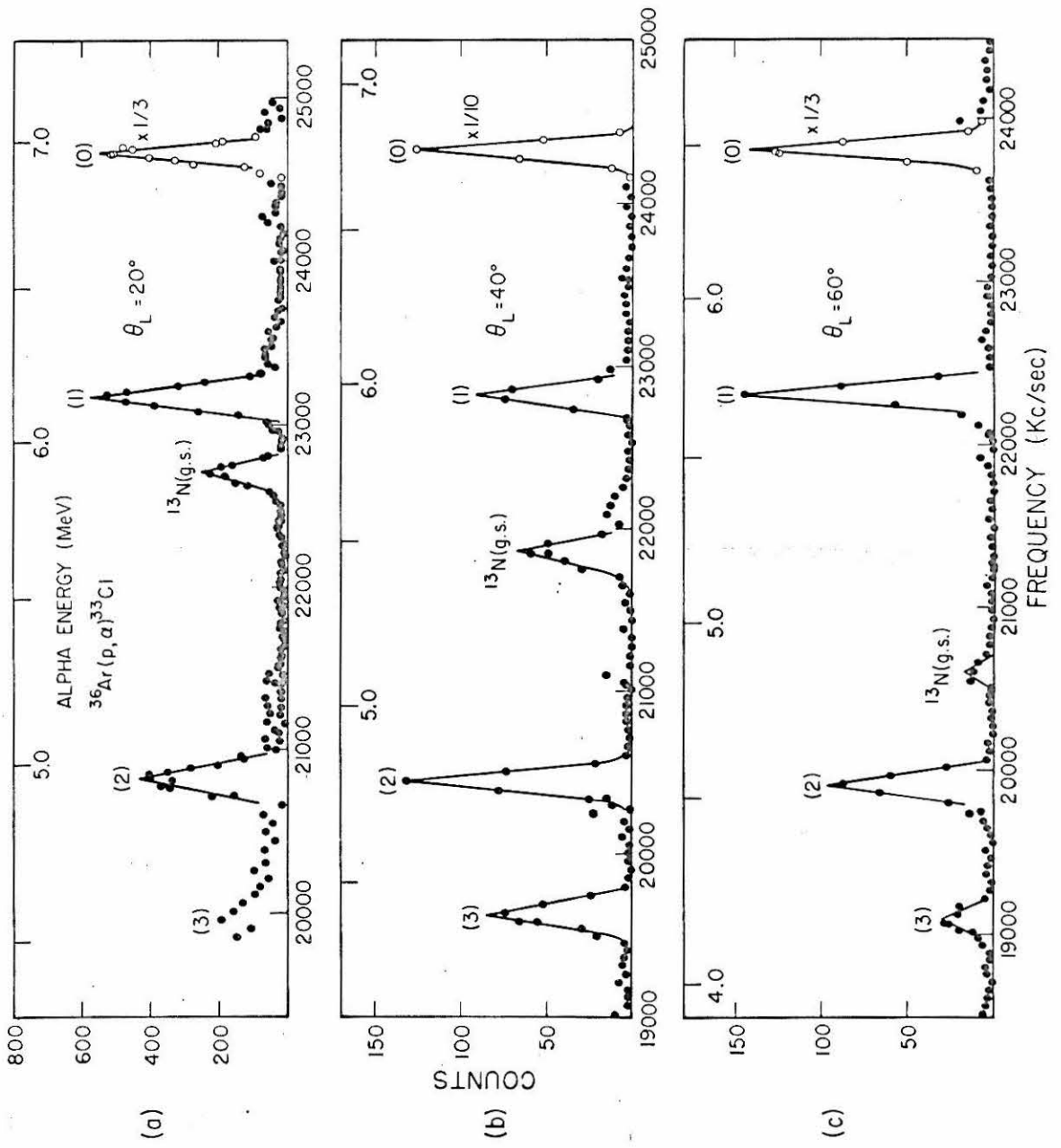
Figure 62

Energy Level Diagrams for ^{33}S and ^{33}Cl

The energy level diagrams for ^{33}S and ^{33}Cl are shown. The information on ^{33}S was taken from the compilation of Endt and van der Leun (1962) as well as from more recent work by Becker et al.(1966), O'Dell et al.(1966), and Moss (1967). (See Appendix G.) The information for ^{33}Cl was taken from Endt and van der Leun (1962) and the present work. The levels at 2.686 and 2.980 MeV in ^{33}Cl were located in the present work. (See page 86.)
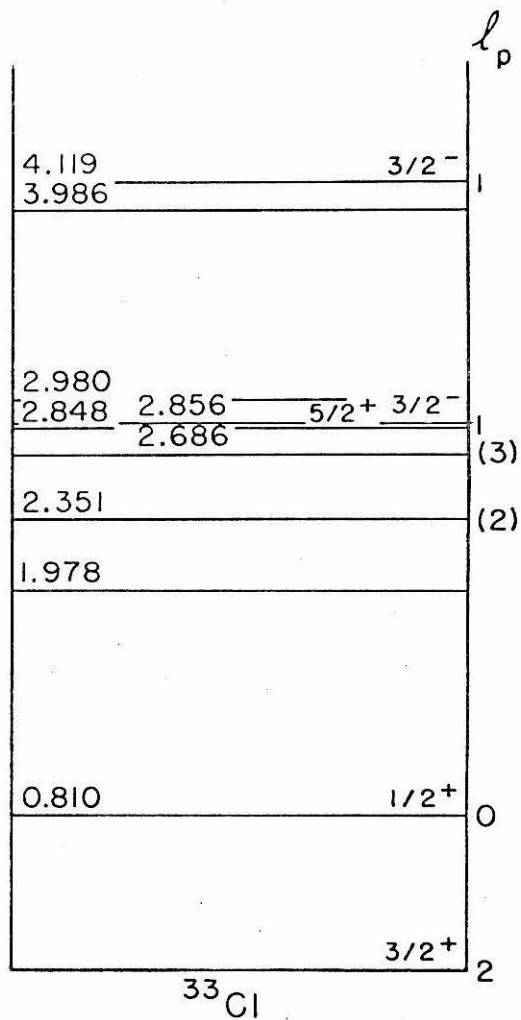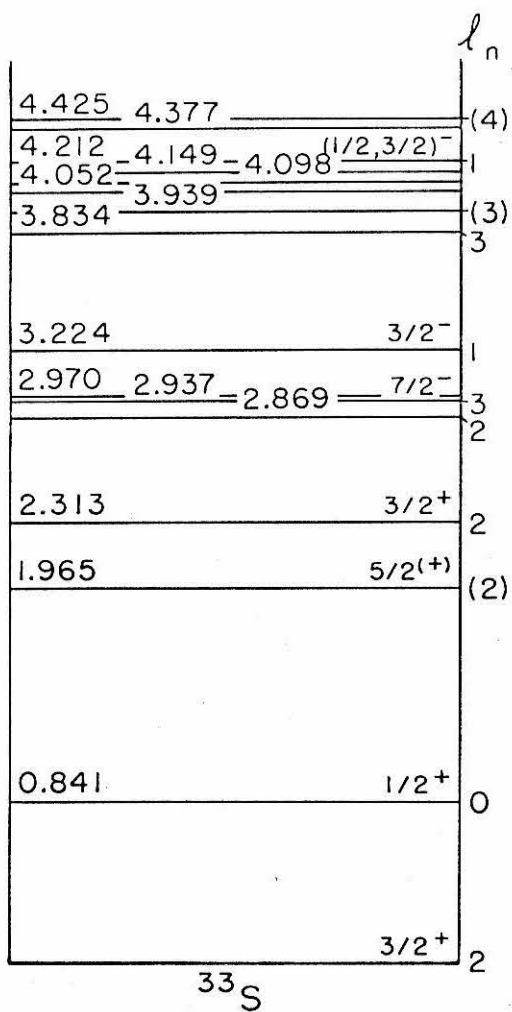
Energy level diagram comparing ^{33}S and ^{33}Cl.

^{33}S, ℓ_n:

Energy	J^π	ℓ_n
4.425		
4.377		(4)
4.212		
4.149		1
4.098	$(1/2, 3/2)^-$	
4.052		
3.939		
3.834		(3)
		3
3.224	$3/2^-$	1
2.970		
2.937		
2.869	$7/2^-$	3
		2
2.313	$3/2^+$	2
1.965	$5/2^{(+)}$	(2)
0.841	$1/2^+$	0
	$3/2^+$	2

^{33}Cl, ℓ_p:

Energy	J^π	ℓ_p
4.119	$3/2^-$	1
3.986		
2.980		
2.848		
2.856	$5/2^+$ $3/2^-$	1
2.686		(3)
2.351		(2)
1.978		
0.810	$1/2^+$	0
	$3/2^+$	2

Figure 63

Models for A = 33

The predictions of several models for A = 33 are compared with the experimental results.   The models are discussed in the text.   (See page 88.)
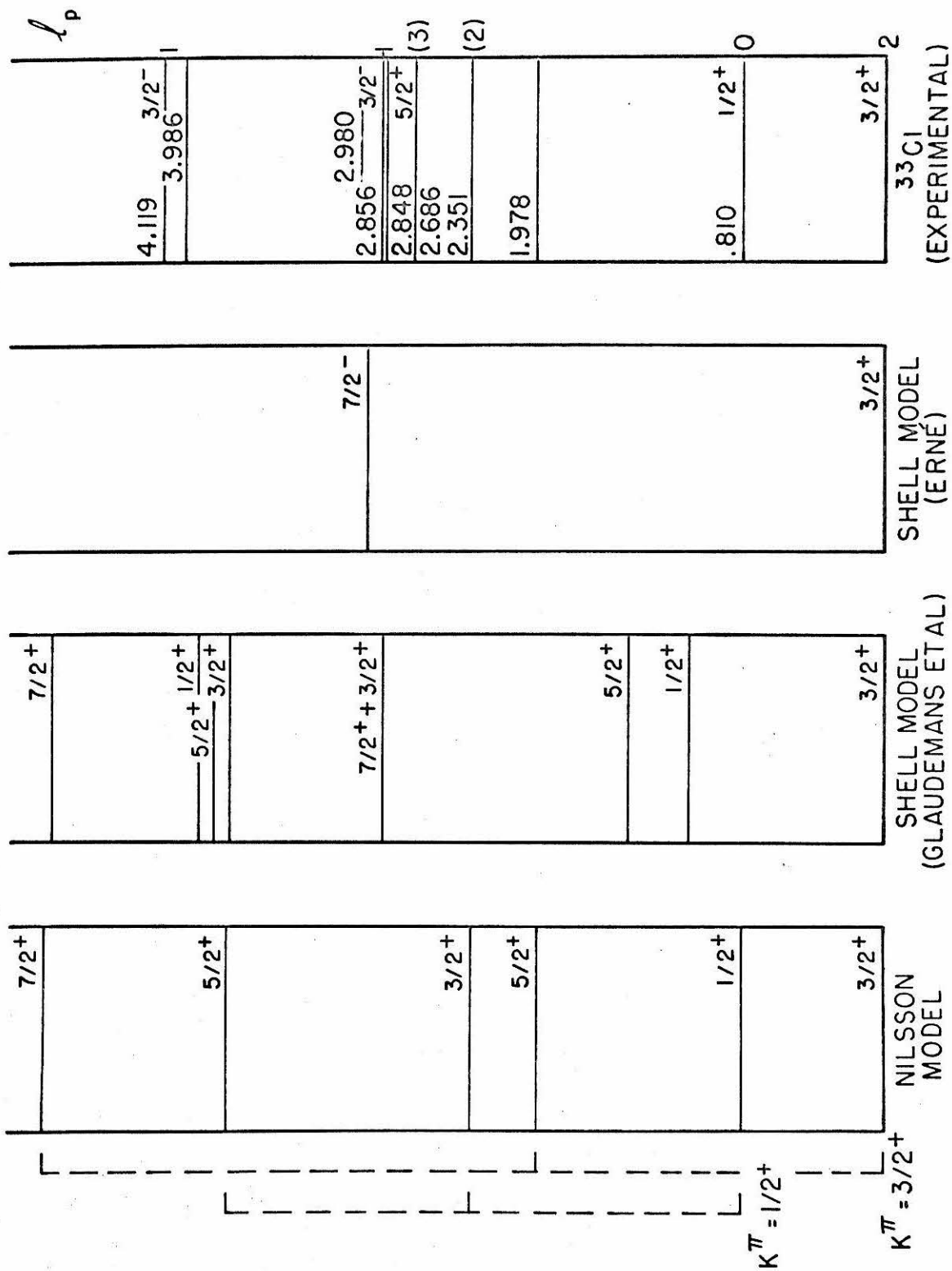
Figure 64

Notation for the Calculation of $\theta_{effective}$

The notation used in the calculation of the effective laboratory angle of the magnetic spectrometer is shown. The square represents the entrance to spectrometer. (See page 102.)
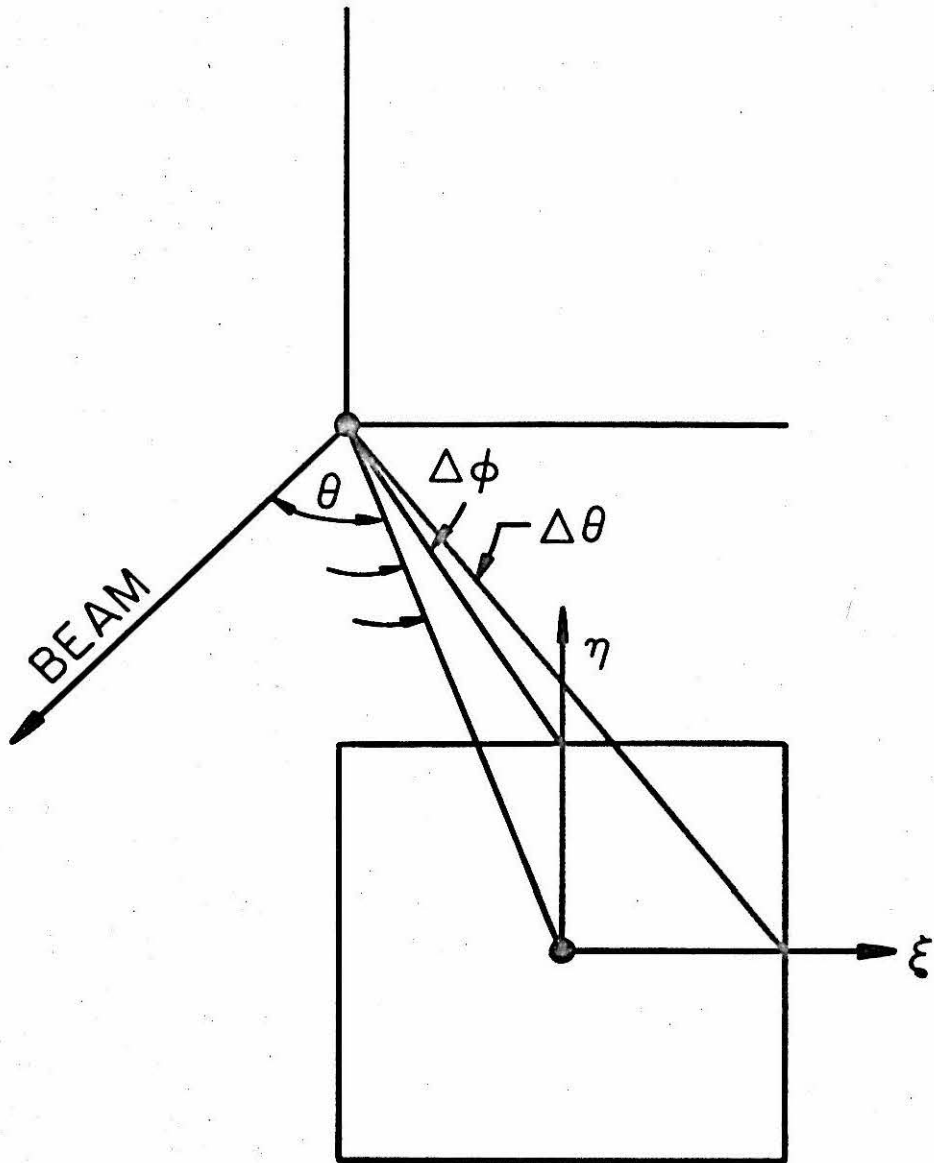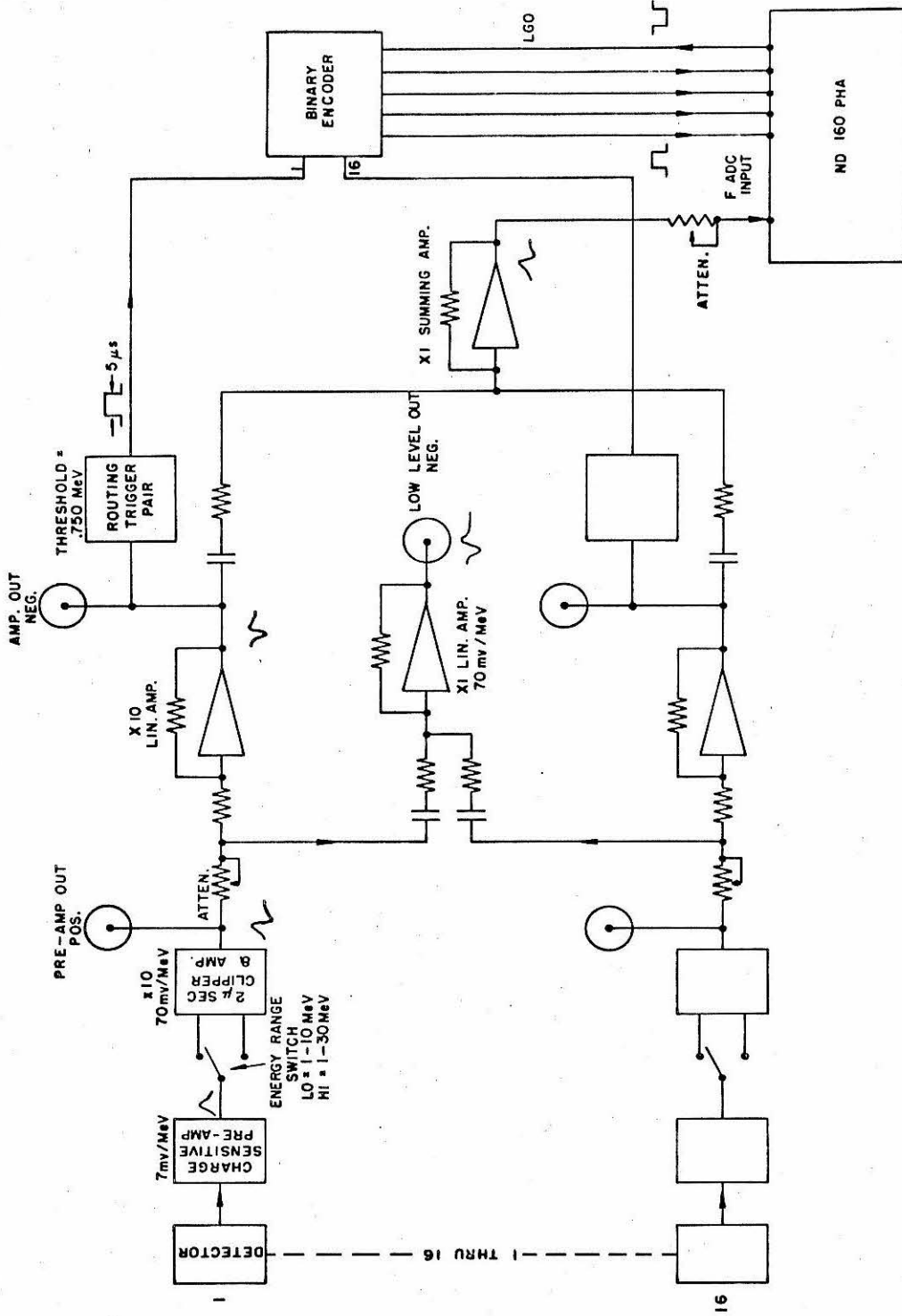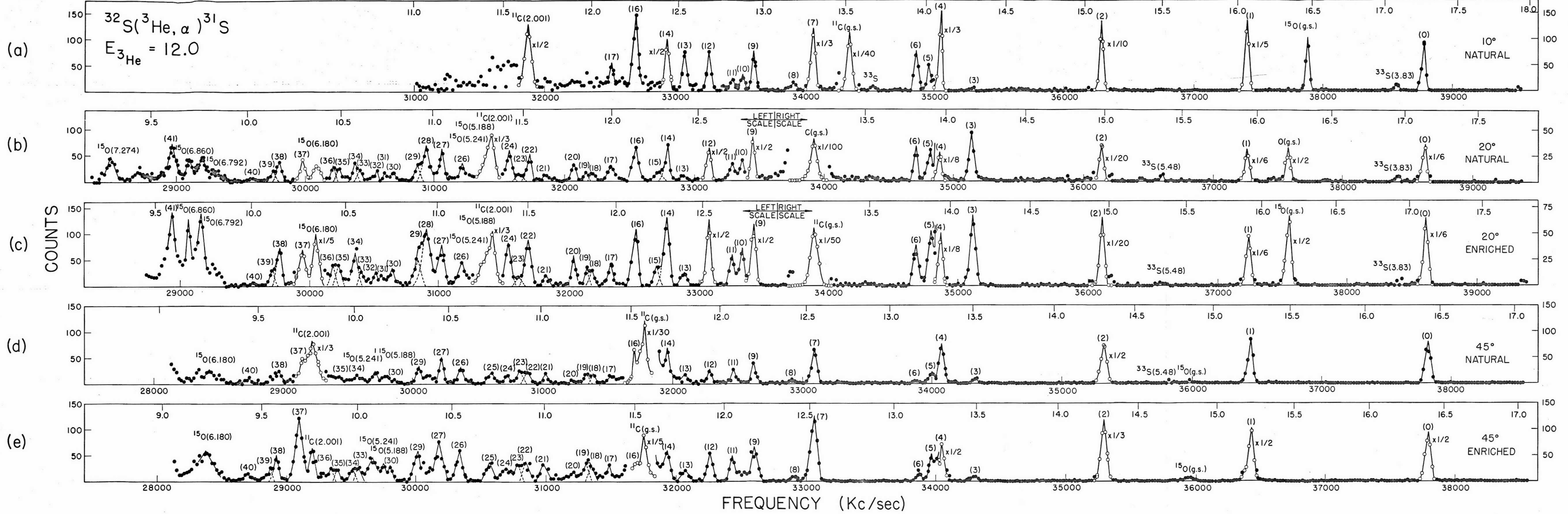
Figure 65

Array Electronics

A block diagram of the 16 detector array electronics is shown. Since all detectors have identical circuitry, only the circuitry for detector 1 is shown in detail. (See page 143.)

BLOCK DIAGRAM OF 16 CHANNEL ARRAY FOR 61 cm SPECTROMETER

$^{32}S(^3He, \alpha)^{31}S$
$E_{3_{He}} = 12.0$

Figure caption: $^{32}S(^3He,d)^{33}Cl$, $E_{^3He} = 12.0$